Sede Amministrativa: Università degli Studi di Padova

Dipartimento di Ingegneria Civile, Edile ed Ambientale

---

DOCTORAL COURSE IN SCIENCES OF CIVIL, ENVIRONMENTAL AND ARCHITECTURAL ENGINEERING
CURRICULUM: Rischio, vulnerabilità, ambiente, salute e territorio
SERIES: XXXIV

# NATURAL AND ANTHROPOGENIC DRIVERS OF EROSIONAL AND DEPOSITIONAL DYNAMICS IN SHALLOW TIDAL SYSTEMS

**Coordinator:** Prof. Carmelo Maiorana
**Supervisor**: Prof. Luca Carniello
**Co-Supervisor**: Prof. Andrea D'Alpaos

**PhD candidate**: Davide Tognin

**Università degli Studi di Padova**

Department of Civil, Environmental and Architectural Engineering

Ph.D. Course in Sciences of Civil, Environmental and Architectural Engineering

# Natural and anthropogenic drivers of erosional and depositional dynamics in shallow tidal systems

Advisor

**Prof. Luca Carniello**

Co-advisor

**Prof. Andrea D'Alpaos**

Ph.D. candidate

**Davide Tognin**

matr. 1203229

This dissertation is submitted for the degree of
*Doctor of Philosophy*

**January 2022**

*Tell her to find me an acre of land*
*Between the salt water and the sea strand*

— Scarborough Fair

# DECLARATION

I hereby declare that this submission is my own work and that, to the best of my knowledge and belief, it contains no material previously published or written by another person or material which has to a substantial extent been accepted for the award of any other degree or diploma at any university or other institute of higher learning, except where due acknowledgement has been made in the text.

*Padova, January 2022*

Davide Tognin

# ACKNOWLEDGEMENTS

I would like to express my sincere gratitude to my advisors Professor Luca Carniello and Professor Andrea D'Alpaos, who have guided and advised me with remarkable insight, extraordinary knowledge and constant patience. Their guidance and continued support, along with their contagious enthusiasm and motivation, helped me all the time and in the writing of this thesis, and made this PhD experience worthy, intellectually stimulating and exciting.

I would also like to extend my deepest gratitude to Professor Massimiliano Ghinassi, for having introduced me to the principles of sedimentology and offered a different and complementary point of view to tackle sediment transport processes. Thanks for sharing his extensive knowledge and always being willing to discuss scientific problems with me.

This work would not have been possible without the support and assistance of the amazing technical staff of the University of Padova. Special thanks to Dr. Cristina Breggion and Andrea Sambo of the Department of Biology for their help during fieldwork and for having driven me safely through the most remote parts of the Venice Lagoon. I owe much also to Dr. Daria Pasqual, Dr. Marco Favero, Dr. Carlotta Betto, Dr. Silvia Cattò and Dr. Lisa Santello of the Department of Geosciences: without their technical expertise and assistance, the measurements and laboratory analyses contained in this dissertation would not have been possible. Thanks also for the understanding and flexibility when I invaded their laboratory with hundreds of samples and for making the sample processing an engaging, riveting, sometimes explosive, but always safe, experience.

I would like to sincerely thank all my co-authors. In particular, I had the pleasure of working with Dr. Alvise Finotello. Besides having shared with him one of the luckiest sampling campaigns ever and discussed many promising ideas, his invaluable advice and meaningful suggestions were fundamental in conceiving, writing and improving the last chapter of this work. I would also like to thank Dr. Mattia Pivato, with whom I have had the privilege to share unique fieldwork days, attempts to run increasingly longer numerical simulations and funny convivial moments.

My sincere thanks also go to Professor Iris Möller, who provided me an incredible opportunity to join her team at the Trinity College Dublin as visiting student.

I would like to thank all my PhD colleagues. Particular mention must go to Dr. Alice Puppin and Dr. Elena Bellizia. Besides having spent long days with me in the laboratory and provided fruitful insights on multivariate analysis of grain size distribution, they contributed to making this PhD experience worthy and above all funny day by day. Many thanks also to Dr. Nicola Durighetto and Dr. Leonardo Costa, with whom I have had the pleasure to enjoy this PhD experience.

Most importantly, I am grateful for my family's unconditional and unequivocal support and encouragement, provided not only throughout the duration of this PhD journey.

Davide

# ABSTRACT

Coastal wetlands in shallow tidal systems are among the most valuable environments on Earth, as they provide a diverse range of ecosystem services. Nevertheless, their survival is questioned by increasing rates of sea-level rise and reduced fluvial sediment delivery to the coasts. Moreover, anthropogenic pressures are becoming increasingly significant, as densely populated coastal urban areas are adopting protection infrastructures to reduce flooding, such as storm-surge barriers, whose potential effects on the evolution of the surrounding coastal wetlands are still poorly investigated. Therefore, a better understanding of the effects of natural and anthropogenic processes affecting the morphological evolution of coastal wetlands is crucial to develop management strategies aiming at preserving and restoring these delicate environments and the precious ecosystem services they provide.

With this aim, in the present work we start considering sediment erosion and transport dynamics on tidal flats and test the possibility to develop a synthetic theoretical framework to realistically describe erosional and depositional processes in the long-term time scale. Beyond determining the evolution of tidal flats, sediment reworking is also a major mechanism controlling salt-marsh sedimentation, offsetting the negative effects of sea-level rise. This is particularly true in sediment starved systems. Hence, using field measurements from the Venice Lagoon (Italy), a representative case of sediment starved back-barrier system, we investigate the effects of continually varying influences of natural processes on temporal and spatial sedimentation patterns on salt marshes. Finally, combining field data and numerical modelling of the first-ever closures during Fall 2020 of the storm-surge barriers designed to protect Venice, we evaluate the impacts of anthropogenic flood regulation on salt-marsh sedimentation and on the

morphological evolution of the tidal basin as a whole.

The main results from this work highlight that: i) bottom shear stress and suspended sediment concentration dynamics can be modelled as marked Poisson processes, thus bearing important consequences for realistic, statistically-based analyses of the long-term biomorphodynamic evolution of tidal landscapes; ii) the high temporal variability in sediment reworking due to the combined action of tides, waves and storm surges affects salt-marsh sedimentation, with intense storm surges accounting for the large majority of sediment accumulation on salt marshes, despite their brief duration; iii) the combination of these varying hydrodynamic forcing factors also affect spatial sedimentation patterns, which thus cannot be interpreted solely as an essentially tide-driven process and sign the marsh topographic profile; iv) flood regulation, by modifying hydrodynamic and sediment transport processes during storm surges, which are largely responsible for sediment delivery in the upper intertidal frame, significantly reduces sedimentation on salt marshes thus affecting their resilience to sea-level rise; v) at the basin scale, even though storm-surge barrier operations can temporarily reduce the net sediment loss from the system, flood-regulation promotes a less-diverse geomorphological structure, rather than contributing to the preservation of tidal landforms.

# SOMMARIO


Le zone umide costiere sono tra gli ambienti più preziosi sulla Terra, poiché forniscono diversi servizi ecosistemici. Ciononostante, il loro futuro è messo in forte dubbio dall'aumento dei tassi di innalzamento del livello del mare e dal ridotto apporto di sedimenti alle zone costiere. Inoltre, gli interventi antropici stanno diventando sempre più pervasivi, dato che molte aree urbane densamente popolate per ridurre il rischio di allagamenti costieri stanno adottando infrastrutture, come ad esempio barriere di protezione, i cui effetti sull'evoluzione degli ambienti a marea circostanti sono però ancora poco noti. È pertanto di fondamentale importanza capire gli effetti dei processi naturali e antropici che influenzano l'evoluzione morfologica degli ambienti a marea, al fine di poter sviluppare strategie di gestione volte alla conservazione e al rispristino di questi delicati ambienti e dei preziosi servizi ecosistemici che forniscono.

Al fine di raggiungere questo obiettivo, il presente lavoro inizia considerando le dinamiche erosive e di trasporto di sedimenti sui bassifondali e verifica la possibilità di sviluppare un inquadramento teorico sintetico per descrivere in maniera realistica i processi erosivi e deposizionali sul lungo periodo. La risospensione dei sedimenti dai bassifondali, oltre a determinare l'evoluzione morfologica degli stessi, è anche uno dei principali meccanismi di approvigionamento per la sedimentazione sulle barene, che consente loro di compensare gli effetti negativi dell'innalzamento del livello del mare, soprattutto in contesti caratterizzati da scarso apporto di sedimenti. Avvalendosi di misure di campo condotte nella laguna di Venezia, utilizzata come caso studio rappresentativo dei sistemi con scarso apporto di sedimenti, sono stati studiati gli effetti della continua evoluzione dei procesi naturali sui pattern temporali e spaziali di sedimentazione sulle barene.

Infine, combinando dati di campo e modellazione numerica delle prime chiusure in assoluto delle barriere progettate per difesa di Venezia dalle acque alte avvenute nell'autunno 2020, sono stati valutati gli impatti che la regolazione antropica dei livelli per mezzo di barriere di protezione ha sulla sedimentazione sulle barene e sull'evoluzione morfologica del bacino a marea nel suo insieme.

I principali risultati di questo lavoro evidenziano che: i) lo sforzo al fondo e la concentrazione di sedimenti in sospensione possono essere descritti come processi di Poisson marcati, con importanti conseguenze per condurre un'analisi realistica dell'evoluzione biomorfodinamica a lungo termine degli ambienti a marea; ii) l'alta variabilità temporale della rielaborazione dei sedimenti a causa dell'azione combinata della marea, delle onde da vento e degli eventi di acqua alta influisce sulla sedimentazione sulle barene, alla quale gli eventi meteomarini più intensi contribuiscono in maniera sostanziale, nonostante la loro breve durata; iii) la variabilità di queste forzanti idrodinamiche e la loro combinazione hanno effetti rilevanti anche sulla dinamica spaziale della sedimentazione e marcano in maniera indelebile il profilo topografico delle barene; iv) la regolazione antropica dei livelli di marea finalizzata a mitigare il sempre più alto rischio di allagamento costiero, modificando i processi idrodinamici e di trasporto solido durante gli eventi meteomarini più intensi, che sono responsabili in larga parte dell'accumulo di sedimenti nella porzione superiore della fascia intertidale, riduce in modo significativo la sedimentazione sulle barene compromettendone la capacità di adattamento all'incremento del livello del mare; v) a scala di bacino, anche se l'attivazione delle barriere di protezione dagli allagamenti costieri può ridurre temporaneamente la perdita di sedimenti dal sistema, essa si dimostra favorire un appiattiamento generalizzato della morfologia degli ambienti a marea, piuttosto che contribuire al mantenimento della loro struttura morfologica.

# CONTENTS

# LIST OF FIGURES

# LIST OF TABLES

# 1

# INTRODUCTION

## 1.1 COASTAL WETLANDS IN SHALLOW TIDAL SYSTEMS

Coastal wetlands constitute the peculiar landscape of low-energy shallow transitional systems, generally sheltered from wave action and dominated by tides, such as deltaic, estuarine and lagoonal settings (Woodroffe, 2002; Masselink et al., 2014). In these environments, sediment deposits, composed predominantly of cohesive sediments, are shaped and reshaped by the complex interaction among different hydrodynamic forcing factors and are importantly affected by biotic components (A. D'Alpaos et al., 2007). The mutual co-adjustment of form and processes, known as morphodynamic feedback (Wright and Thom, 1977), leads to the self-organization of shallow tidal systems in distinctive landforms, namely channels, tidal flats and salt marshes (Figure 1.1, 1.2 and 1.3).

Tidal channels (Figure 1.1) are the preferential pathway by which the system is regularly flooded and drained and, thus, provide a pivotal control on fluxes of water, sediment, nutrients and biota (Coco et al., 2013). Unlike rivers, where flow is unidirectional and runoff-dependent, tidal channels are shaped by a bi-directional flow, primarily driven by the stage of the tide. Tidal currents are responsible for the erosion processes, which carve the intertidal landscape and generate incised channel cross sections (A. D'Alpaos et al., 2005; Finotello et al., 2018, 2020a). Although the intertidal morphology,

**Figure 1.1:** Tidal channel, northern Venice Lagoon, Italy. Photo: Davide Tognin

excluding the deep channel network, is relatively flat, a bimodal distribution of elevations can be observed in shallow tidal basins, differentiating tidal flats and salt marshes, as intermediate conditions are rare (Fagherazzi et al., 2006; Defina et al., 2007).

The peak of the distribution with elevation below mean sea level represents tidal flats. Tidal flats are low-gradient surfaces, that can be permanently submerged or temporarily exposed during low tide, depending on their relative elevation and local tidal range (Figure 1.2). They may experience periodic processes of erosion and deposition determined by the coupled action of tidal currents and wind waves and by sediment availability. When erosion is predominant, the overall elevation profile is concave upwards, whereas a convex profile occurs where there is a net depositional trend (Dyer, 1998). Though tidal flats are generally composed of a mixture of sand and mud (silt and clay), sediment has a sufficiently high mud content to exhibit cohesive properties and usually shows an important organic component. Tidal flats can be unvegetated or colonized by benthic vegetation, hosting faunal species that have developed various adaptation strategies to cope with drastic and cyclical changes in environmental conditions.

The upper intertidal zone, representing the second peak in the elevation distribution of shallow tidal systems, often supports halophytic vegetation.

**Figure 1.2:** Tidal flat during low tide in front of the Burano island, Venice Lagoon, Italy. Photo: Davide Tognin

Different annual and perennial species, adapted to the stresses of inundation and salinity, encroach the muddy substrate in temperate climates, giving rise to salt marshes (Figure 1.3 and 1.4; Chapman, 1974). In tropical climates, salt marshes are outcompeted by mangrove forests, thriving within the upper intertidal fringe.

**Figure 1.3:** Salt marsh at North Bull Island, Dublin, Ireland. Photo: Davide Tognin

**Figure 1.4:** Global distribution of salt marshes (Mcowen et al., 2017).

In temperate salt marshes, frequency and duration of flooding, whose combination is indicated as hydroperiod (French and Spencer, 1993) and depends on the relative elevation to the local mean sea level, primarily control vegetation type and distribution pattern, which is usually referred to as zonation (Bertness and Ellison, 1987; Adam, 1990). Hence, marshes are often classified into low marsh and high marsh on the basis of these parameters. The low marsh is downward bounded by the seaward margin of vegetation, whereas the landward upper limit of high marsh is commonly marked by a sharp elevation change with the hinterland or by artificial structures on developed coasts. The low marsh is subject to frequent inundation and salinity around seawater. Pioneer annual species, such as *Salicornia* spp. and *Spartina* spp., can withstand these harsh physical conditions and colonize the lower portion of salt marshes. Contrarily, greater oxygenation and less frequent flooding tend to characterize the high marsh, which usually exhibits more variable patterns in the composition of flora. The high marsh can contain diverse competing floral species, such as *Aster tripolium*, *Atriplex portulacoides*, *Juncus* spp., *Limonium* spp., *Plantago maritima*, *Puccinellia* spp., *Sarcocornia* spp., and *Suaeda maritima*.

Owing to the crucial control exerted by elevation, even subtle microtopographical differences can affect vegetation colonization. Slightly lower elevations and unfavourable drainage conditions can lead to water ponding on the marsh surface, thus making vegetation colonisation impossible and

Figure 1.5: Salt pan on the marsh surface, Conche salt marsh, Venice Lagoon, Italy. Photo: Davide Tognin

leading to the formation and maintenance of salt pans (Figure 1.5; Pethick, 1974).

## 1.2 ECOSYSTEM SERVICES

Coastal wetlands are of high environmental and societal importance, as they deliver vital ecosystem services (Costanza et al., 1997; Barbier et al., 2011). Firstly, salt marshes play a valuable function in the flood risk reduction of the coastal hinterland, dissipating wave energy and ameliorating the impact of storm surges (Möller et al., 1999, 2014). In particular, along estuaries and open coasts, salt marshes are considered effective nature-based solutions able to mitigate the effects of storm-driven flooding and to generate important damage savings (Temmerman et al., 2013; Spalding et al., 2014; Fairchild et al., 2021). Compared to engineered flood defences that fulfil only a coastal stabilizing function, coastal wetlands provide multiple ecosystem services, therefore allowing a much higher 'return on investment' than the construction of engineered defences alone (Möller et al., 2021).

Secondly, coastal wetlands act as natural filters that purify water, mediating pollutants fluxes and nutrient cycling (Mitsch and Gosselink, 2015).

Moreover, shallow intertidal areas are hot spots for biodiversity, providing peculiar habitats and performing a nursery role for a wide range of faunal species. Besides boosting the production of economically and ecologically important fishery species, such as shrimps, oysters, clams, and fishes (MacKenzie and Dionne, 2008), shallow tidal environments are a sanctuary for resident and migratory bird species, both overwintering and breeding.

One further key function of vegetated coastal environments is their role as carbon sinks. These ecosystems sequester carbon over decades within living biomass aboveground (leaves, stems) and belowground (roots), and within non-living biomass (litter). But carbon storage over centennial to millennial time scales in salt marshes is essentially linked to their ability to continuously bury carbon within the sediment as they accrete vertically (Chmura et al., 2003; Duarte et al., 2005; Mcleod et al., 2011). Carbon buried by deposited sediment is not limited to autochthonous sources but also comprises suspended allochthonous material, both terrestrial and marine, carried by currents and trapped by the marsh during flooding. Moreover, the low oxygen concentration in the sediments promotes a slow decay of organic carbon and the release of methane into the atmosphere is limited due to saline conditions.

Thanks to their efficiency in trapping carbon, the contribution of salt marshes per unit area to long-term carbon sequestration is much greater than that of terrestrial forests. Long-term rates of carbon accumulation in salt-marsh sediments range between 18 and 1713 $\mathrm{g\,C\,m^{-2}\,yr^{-1}}$ (Mcleod et al., 2011). By contrast, temperate, tropical, and boreal forests accumulate carbon at rates between 0.7 and 13.1 $\mathrm{g\,C\,m^{-2}\,yr^{-1}}$ (Schlesinger and Bernhardt, 2020). Thus, although salt-marsh global area is one to two orders of magnitude smaller, total carbon burial rates in salt marshes (5-87 $\mathrm{Tg\,C\,yr^{-1}}$) are comparable to those of terrestrial forest types (53.0 $\mathrm{Tg\,C\,yr^{-1}}$ for temperate, 78.5 $\mathrm{Tg\,C\,yr^{-1}}$ for tropical, and 49.3 $\mathrm{Tg\,C\,yr^{-1}}$ for boreal forests). Despite the small aboveground biomass and their limited areal coverage, salt marshes have hence the potential to contribute substantially to long-term carbon sequestration and to mitigate atmospheric carbon dioxide concentration.

## 1.3 HYDRO- AND MORPHODYNAMIC PROCESSES

The morphodynamics of shallow tidal environments is influenced by the complex interaction between hydrodynamic, sedimentological and biotic factors over a wide range of temporal and spatial scales. Among hydrodynamic factors, both tides and waves play a major control in erosion, transport and deposition processes of both cohesive and non-cohesive particles (Wang, 2012). The tide generates currents that preferentially propagate along the channel network (Hughes, 2012), typically transporting non-cohesive sediment as bedload and finer cohesive fraction as suspended load during the rising (flood) and falling (ebb) phases, with deposition occurring mostly during slack phases. As the tide overspills on the adjoining intertidal flats and salt marshes, it is strongly affected by shallower water and friction effects (Friedrichs and Madsen, 1992), so that its velocity and, hence, its transport capacity can diminish considerably, naturally promoting sediment accumulation in these zones.

Tide-induced water-level fluctuations also modulate wave action. While the tide floods tidal-flat areas, wind waves can propagate and generate bottom shear stresses capable of resuspending sediments (Anderson, 1972; Le Hir et al., 2000; Green and Coco, 2014). Because waves generated inside estuarine and lagoonal basins by winds have a typically short period, wave-orbital motions are likely not to be able to penetrate down to the bed of deep channels, where tidal currents tend to be predominant (A. D'Alpaos et al., 2013). By contrast, wind waves represent a key driver for sediment resuspension and transport on shallow tidal flats (Fagherazzi and Wiberg, 2009; Carniello et al., 2011; Green and Coco, 2014).

When the tidal level is high enough, wind waves can further propagate from tidal flats onto salt marshes. Once on the salt-marsh surface, waves energy is rapidly dissipated due to drag forces caused by the presence of dense vegetation canopy (Möller et al., 1996, 1999). Flow velocity reduction due to vegetation not only prevents salt-marsh surface erosion but also favours particle settling (Temmerman et al., 2003). However, wave-energy dissipation localized at the sharp transition between tidal flats and salt marshes enhances marsh margin lateral erosion (Feagin et al., 2009; Marani et al., 2011; Leonardi et al., 2016; Tommasini et al., 2019; Finotello et al., 2020b).

Owing to the continually varying influences of hydrodynamic drivers and sediment transport processes, coastal wetlands are exceptionally dynamic ecosystems, continuously changing due to erosion and sedimentation. Sedimentary processes may be dominated by either (or both) tides and waves depending on the specific location within the system as well as on the time scale of interest. For example, wind-wave resuspension on tidal flats results in important short-term bed-level variations that usually turn out in a tendency for erosion, but can be partially compensated in the longer time scale with deposition during periods dominated by the action of tidal currents (Wells et al., 1990; Lee et al., 2004; Friedrichs, 2011; Hu et al., 2017).

As far as these variations trigger negative feedback, coastal systems can cope with morphological changes, by adjusting to, or oscillating around, an equilibrium configuration (Zhou et al., 2017). But, when positive feedback intervenes and a threshold that marks different states is exceeded, coastal systems can experience fatal shifts (Marani et al., 2010). Thresholds can be particularly subtle in coastal wetlands, as these ecosystems are grounded on a delicate balance between hydrodynamic and sedimentary processes.

Salt marshes are a striking example of this fragile equilibrium. In the case of salt marshes, the threshold for their survival coincides with the physical threshold of a specific elevation range, because vegetation that characterizes these landforms is adapted to a determined relative elevation and, hence, hydroperiod. If marshes lose elevation with respect to mean sea level, increasing inundation frequency and duration challenge the persistence of halophytes, eventually paving the way to the transition to tidal flats. From this point of view, the maintenance of salt-marsh elevation with respect to sea level by sediment accumulation and subsequent vertical accretion appears to be integral to the long-term survival of these landforms and the ecosystem they support (Reed, 1995; J. R. L. Allen, 2000).

The salt-marsh surface acts as a topographic limit and only periodic flooding allows for mineral sediment to be deposited on the marsh (Figure 1.6; French and Stoddart, 1992). Sediment accumulation is generally regarded to be inversely proportional to hydroperiod. Thus, high marsh generally has a shorter hydroperiod and lower opportunity for accumulating sediment than does low marsh. Therefore, as a salt marsh accretes

**Figure 1.6:** Marsh flooded during high tide, San Felice salt marsh, Venice Lagoon, Italy. Photo: Davide Tognin

and increases its elevation, the hydroperiod decreases with a subsequent decrease in the rate of sediment accumulation (Figure 1.7; Pethick, 1981).

This simplified conceptual model is the starting point of many elaborations and refinements carried out in the following years, taking into account the effects of spatial and temporal variability of the process as well as the influence of the biotic component, on the basis of both empirical evidence and modelling studies.

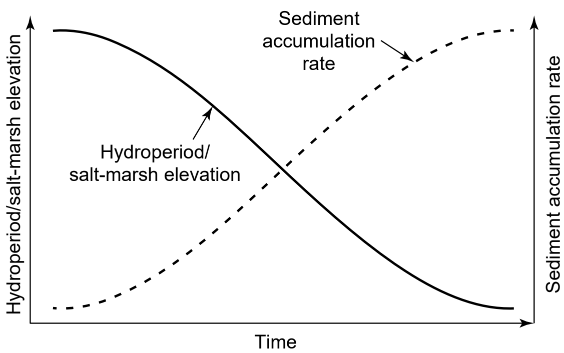


**Figure 1.7:** Simplified conceptual model of the relationship between hydroperiod, which generally correlates with salt-marsh elevation, and the rate of sediment accumulation. (Adapted from Rogers and Woodroffe, 2015)

**SPATIAL VARIABILITY** Besides the influence of elevation, salt-marsh sedimentation exhibits a strong relationship with the distance from the source of sediment at different spatial scales. At subcatchment scale, the tidal creek system dissecting the salt-marsh platform is generally regarded as the key driver of sediment redistribution and, hence, highly influences the spatial sedimentation pattern. As water flow overspills on the marsh and is dampened by the resistance offered by the vegetation canopy (Nepf, 1999), its transport capacity declines with increasing distance from the creek, favouring settling. Consequently, sedimentation generally shows a marked decrease away from the creek (Reed et al., 1999; Temmerman et al., 2003).

Although broadly replicating this process, the spatial sedimentation pattern at larger scales proves to be more variable (French et al., 1995). In many marshes, sedimentation typically follows an inverse relationship with the distance from the sediment source, showing a maximum at the seaward edge and a decrease landward (Carling, 1982; Oenema and DeLaune, 1988; Reed, 1988; Temmerman et al., 2005a). However, this spatial sedimentation distribution may considerably change and, in particular, marshes often display a wave-influenced sedimentation pattern in the most exposed portions. Especially in the zone extending for some distance back from the seaward marsh edge, a large proportion of water exchange may take place directly via the marsh boundary (French and Stoddart, 1992; Davidson-Arnott et al., 2002; Schuerch et al., 2019) and sedimentation is mainly influenced by waves (Duvall et al., 2019). The sedimentation pattern appears to be rather complex and space-dependent, so that a simplified model based solely on elevation may not completely portray the spatial variability.

**TEMPORAL VARIABILITY** The relative influence of tides and waves in affecting sediment transport onto salt marshes also varies in time. The periodic, low-magnitude tidal flooding is deemed to be the regular condition influencing marsh sedimentation. However, during episodic, high-magnitude events, such as storm surges, enhanced water levels can result in the deep flooding of the marshes and, usually, their exposure to more intense wave activity. Therefore, storm surges have long been recognized as events that can cause significant changes in the marsh morphology, despite their episodic nature (Cahoon, 2006; Leonardi et al., 2018), but a comprehensive quantification of their effect is still lacking.

Single surge events were found to be especially important in delivering sediment and supporting salt-marsh vertical accretion (Stumpf, 1983; Cahoon et al., 1995; Goodbred and Hine, 1995; Reed, 1995). Hence, salt marshes may be largely dependent on sediment inputs derived from storm-surge activities. This becomes particularly true for marshes that are very high in the tidal frame, making accretion increasingly dependent on infrequent high-deposition events as marsh platforms gain elevation (Goodwin and Mudd, 2019).

Thus, the morphological evolution of salt marshes need to be considered as affected by both "normal conditions" or "non-events" and "events", which are characterized by higher energy conditions, and sedimentation can be regarded as the cumulative product of numerous non-events and events.

**BIOTIC COMPONENT** Geomorphological processes on salt marshes are intimately connected with biological activity. Halophytes have long been recognized to exert a strong control on their substrate elevation, by affecting both above and below ground dynamics. Above ground, plant shoots protect sediment against erosion and influence mineral sediment deposition by slowing water velocities and by directly trapping inorganic sediment (Fagherazzi et al., 2012). Moreover, salt-marsh vegetation favours the accumulation of allochthonous plant litter during flooding. Below ground, plant roots affect soil resistance (Brooks et al., 2021; Chirol et al., 2021) and their growth and decay directly add organic matter to the soil profile, raising elevation by sub-surface expansion. Plant-litter accumulated on the surface and below-ground productivity, together with their subsequent decomposition, make a significant contribution to soil volume and relative elevation change (Morris et al., 2002, 2016; Roner et al., 2016).

Biota in tidal environments is not just passively adapting to morphological features prescribed by sediment transport, but rather play an active role as ecosystem engineers (Jones et al., 1994). Vegetation indeed tends to actively stabilize their relative elevation and seaward extent through feedback that varies with the depth and duration of flooding. So that vegetation acts as a "Secret Gardener", fundamentally constructing the tidal landscape (A. D'Alpaos et al., 2012; Da Lio et al., 2013; Marani et al., 2013).

All these fascinating interactions between plants and geomorphology allow salt marshes to actively adjust their position within the intertidal frame in ways that enhance ecosystem persistence (Kirwan and Megonigal, 2013).

## 1.4 CONSERVATION OF COASTAL WETLANDS

Thanks to the mutual adjustment among different ecomorphodynamic processes, coastal wetlands are deemed to be highly resilient ecosystems. However, persistent trends or sudden changes in the external constraints can challenge their resilience. In particular, salt marshes rely on their relative elevation with respect to mean sea level to preserve their morphological identity. Consequently, rising sea levels and reduced sediment availability cast doubt on their future survival (Kirwan and Megonigal, 2013; Schuerch et al., 2018).

It is important to recognise that human influence can modify rates of these natural changes, thus further exacerbating their negative effects. Both relative sea-level rise and changes in sediment availability can be considered indirect impacts of anthropogenic activities, that together with direct human actions, play a critical role in the long-term management of coastal wetlands.

### 1.4.1 Indirect human impacts

**SEA-LEVEL RISE** Climate-enhanced sea-level rise is a major consequence of global warming (Nicholls et al., 2007), and there has been considerable discussion as to how temperate coastal wetlands will respond in the future (Reed, 1995; A. D'Alpaos et al., 2011; Kirwan and Megonigal, 2013; FitzGerald and Hughes, 2019). A key determinant of salt-marsh vulnerability is whether its relative elevation can keep pace with rising sea levels. A change in relative sea level produces an alteration in the ecological state of salt marshes, and the different plant associations within the salt-marsh continuum are expected to migrate in response to different hydrologic conditions, as far as they can cope with increasing hydroperiods.

**SEDIMENT SCARCITY** Fluvial catchments have long been altered by humans with often inadvertent, but far-reaching consequences on sediment transport at the basin scale. Soil erosion enhanced by deforestation and land-use change can increase sediment loads in rivers and, hence, sediment delivery to the coasts. As an example, salt marshes in Plum Island Estuary (Massachusetts, United States) expanded rapidly during the 18$^{th}$ and 19$^{th}$ centuries due to increased rates of sediment delivery following deforestation associated with European settlement (Kirwan et al., 2011). On the contrary, the increasing freshwater requirements for human consumption and irrigation resulted in the widespread construction of dams, dikes, and canals. Sediments transported by rivers accumulate within reservoirs, reducing the amount of sediment reaching the coastal zone (Syvitski et al., 2005). The negative impacts of sediment input reduction are clearly visible in sinking riverine deltas (Blum and Roberts, 2009; Syvitski et al., 2009) and increased coastal erosion.

### 1.4.2 Direct human impacts

Direct human impacts on coastal wetlands aimed at both exploiting natural resources and controlling processes to stabilize coastal morphology. Salt marshes have been used for livestock grazing since the Neolithic (Meier, 2004), but large-scale wetland reclamation and diking has been mostly undertaken for agricultural purposes (Williams, 1990). Many areas that were originally reclaimed for agriculture were then transformed into urban and industrial areas. Coastal cities such as Amsterdam, Rotterdam, Boston, San Francisco, Tokyo and Venice expanded on former coastal wetlands (Pinder and Witherick, 1990). Engineering works, such as historical land reclamation and shoreline hard defences, are thus often present in urbanized coasts and estuaries, constituting an additional anthropogenic forcing providing further constraints on the morphological evolution of coastal wetlands.

Moreover, the high density of human population in coastal regions (Valiela, 2009) and the increasing flooding risk associated with rising sea levels call for further protective interventions. Nature-based solutions and management realignment of the coast, where feasible, can be seen as an opportunity for coastal wetland conservation and restoration (Temmerman et al., 2013; Fairchild et al., 2021). However, due to specific coastal settings and management strategies, especially on highly urbanized coasts, hard engineered defences are often preferred. As an example, storm-surge barriers to reduce flooding risk associated with enhanced water levels are increasingly more common worldwide (Figure 1.8; Mooyaart and Jonkman, 2017). However, the potential effects of coastal flooding protection infrastructures on the resilience of coastal environments are still largely unknown (Gedan et al., 2009; Rodríguez et al., 2017; Sandi et al., 2018; Silvestri et al., 2018).


Figure 1.8: **Examples of storm-surge barriers. a**, Inner Harbor Navigation Canal (IHNC) Lake Borgne Surge Barrier designed to protect New Orleans, Louisiana, US. Photo: engineering-channel.com. **b**, Barrier of the Mo.S.E. system at the Chioggia inlet, Venice Lagoon, Italy. Photo: mosevenezia.eu

## 1.5 GOALS OF THE STUDY

Towards the goal of improving the current understanding of erosional and depositional processes controlling the morphological evolution of coastal wetlands, the present work investigates the spatial and temporal dynamics of natural and anthropogenic drivers in shallow tidal environments. A multidisciplinary approach has been used, combining numerical modelling, statistical analyses, field observations and laboratory techniques.

In this framework, focuses and research questions of the present study can be listed as follows:

i. Sediment dynamics on tidal flats control key ecological and geomorphic processes that ultimately contribute to the long-term evolution of coastal and estuarine landscapes. Sediment erosion and transport on tidal flats are mainly driven by wind waves, modulated by periodic tidal currents.

   However, wind-wave forcing is often neglected in the long-term modelling of tidal-flat evolution.

   Can the stochastic effects of high-energy, wave-driven events on sediment erosion and transport be considered in a synthetic, but reliable, modelling framework for the long-term evolution of shallow tidal environments?

ii. Vertical accretion through sediment accumulation is necessary for salt marshes to keep pace with sea-level rise. Tidal flooding is generally considered the main mechanism controlling sediment accumulation.

   But, storm-surge events may also importantly affect sediment delivery and support vertical accretion of salt marshes.

   Which is the relative contribution of storm-dominated and fair-weather periods to salt-marsh sedimentation?

iii. Tidal exchange via the creek system has been traditionally considered the preferential mechanism for sediment supply and redistribution on salt marshes.

   However, sediment exchange may also take place directly across the marsh edge from the tidal flat, driven by the coupled action of flooding and waves.

How do tides and wind waves affect spatial sedimentation patterns on salt marshes?

iv. To protect coastal urban areas from increasing flooding risk associated with storm surges and rising sea levels, the adoption of storm-surge barriers is increasingly more common worldwide.

But, their effects on the morphological evolution of shallow tidal basins are still largely unknown.

How do storm-surge barriers affect sediment transport at the basin scale? In particular, how is salt-marsh sedimentation affected by flood regulation?

## 1.6 THESIS OUTLINE

This introductory chapter is followed by five main chapters.

Chapter 2 deals with the statistical characterization of erosion events on tidal flats aiming at testing the possibility to develop a synthetic theoretical framework to realistically describe erosional dynamics in the long-term time scale. Erosion dynamics and how they are affected by morphological changes are analysed in the study case of the Venice Lagoon, for which six historical configurations in the last four centuries are available.

Chapter 3 further develops this framework, investigating the dynamics of suspended sediment transport.

Chapter 4 focuses on the spatial pattern of salt-marsh sedimentation, evaluating the relative contribution of tide and waves to sediment supply and redistribution on salt marshes. Analyses are supported by both topographic data and field measurements of sedimentation carried out in the salt marshes of the Venice Lagoon between October 2018 and October 2021.

Chapter 5 considers the temporal variability of the sedimentation process on salt marshes. First, sedimentation measurements are used to understand the relative contribution of storm surges to sedimentation. Then, the effects of storm-surge barriers on salt-marsh resilience are evaluated and discussed by combining numerical modeling, and empirical evidence from field data.

Chapter 6 expands the analysis of the effects of storm-surge barriers at the basin scale using a numerical modelling approach. These analyses focus on the first-ever activations of the storm-surge barrier designed to protect Venice during Fall 2020.

A summary of the main results obtained in this thesis is finally traced in Chapter 7.

# 2

# EROSION DYNAMICS IN SHALLOW TIDAL SYSTEMS

This chapter is a manuscript ready to be submitted for publication and focuses on the statistical characterization of erosion dynamics. Sediment erosion plays a crucial role in the morphodynamic evolution of shallow tidal systems and is mainly driven by the bottom shear stress induced by wind waves. As wind waves have a stochastic nature, a statistical approach is necessary to properly account for their effects on morphology. Here we apply this approach to bottom shear stress time series computed with a numerical model considering six historical configurations of the Venice Lagoon along the last four centuries. Forcing different configurations with the same water-level and wind conditions allows us to understand the effects of morphological changes on erosional dynamics. The results are used to test the possibility to describe erosion dynamics as a Poisson process in a synthetic modeling framework able to reproduce the long-term evolution of shallow tidal environments.

# UNRAVELLING SEDIMENT EROSION DYNAMICS IN SHALLOW TIDAL BASINS: A STATISTICAL APPROACH APPLIED TO THE VENICE LAGOON IN THE LAST FOUR CENTURIES

**Davide Tognin[1,2], Andrea D'Alpaos[2,3], Laura Tommasini[3], Luigi D'Alpaos[1], Andrea Rinaldo[1,2,4], and Luca Carniello[1,2]**

[1]Department of Civil, Environmental, and Architectural Engineering, University of Padova, Padova, Italy

[2]Center for Lagoon Hydrodynamics and Morphodynamics, University of Padova, Padova, Italy

[3]Department of Geosciences, University of Padova, Padova, Italy

[4] Laboratory of Ecohydrology ECHO/IEE/ENAC, Ècole Polytechnique Fèdèrale de Lausanne, Lausanne, Switzerland

## 2.1 ABSTRACT

Wave-induced bottom shear stress is one of the leading processes that control sediment erosion dynamics in shallow tidal environments. Wave-generated erosion, in fact, is responsible for sediment resuspension on tidal flats and, jointly with tidal current, for sediment export to the open sea. Improving our knowledge on the characteristics of wave-induced erosion events is a key point to address issues of tidal-landscape long-term evolution, particularly through the use of effective, simplified theoretical frameworks. Here we adopted a fully-coupled bi-dimensional model to describe the spatial and temporal evolution of bottom shear stresses generated by both tidal currents and wind waves on six historical configuration of the Venice Lagoon. The one-year-long time series of the computed total bottom shear stresses were analysed on the basis of the peak over threshold theory, determining the statistical characteristics of events that exceed a given threshold. Our analysis suggests that erosion events can be modeled as a marked Poisson process in the intertidal zone for all of the considered historical configurations of the Venice Lagoon, being there

interarrival times, durations and intensities of the over-threshold exceedances exponentially distributed random variables. In addition, we find that intensity and duration of over-threshold events are temporally correlated, while almost no correlation exists between interarrival times and both durations and intensities. The resulting statistical characterization of erosion events is a tool of paramount importance to predict future scenarios for the Venice Lagoon, in particular, and to discuss implications for long-term morphodynamic modeling of tidal environments, in general. The estimate of the erosion work through the synthetic characterization of over-threshold events is consistent with field observations and provides interesting insights on the morphological evolution experienced by the Venice Lagoon along the past centuries and suggests a slow down of the ongoing erosion trend in the last few decades.

## 2.2 INTRODUCTION

Wind waves and bottom shear stresses play a cardinal role in the eco-morphological equilibrium of shallow tidal landscapes, strongly influencing sediment erosion and resuspension dynamics (e.g., Carniello et al., 2005; Fagherazzi and Wiberg, 2009). The equilibrium elevation of subtidal platforms and tidal flats in shallow tidal environments is mainly driven by sediment deposition, wave-induced erosion and by the rate of relative sea level rise (RSLR) (e.g., J. R. L. Allen and Duffy, 1998; Fagherazzi et al., 2006; Marani et al., 2010; A. D'Alpaos et al., 2012; Green and Coco, 2014; Hu et al., 2017; Belliard et al., 2019). Moreover, together with tidal currents, wind-wave erosion and resuspension regulate sediment exchanges with the sea and salt marshes. In fact, the action of wind waves is usually recognized as one of the main causes for the retreat of salt-marsh margins (Möller et al., 1999; Schwimmer, 2001; Mariotti and Fagherazzi, 2010; Marani et al., 2011; Bendoni et al., 2016; Leonardi et al., 2016; Tommasini et al., 2019; Finotello et al., 2020b). The temporal and spatial evolution of wave-induced bottom shear stresses (BSSs) has an important impact on sediment dynamics in the intertidal zone (Carniello et al., 2005; Fagherazzi and Wiberg, 2009; Mariotti et al., 2010a), ultimately influencing the morphological and biological processes responsible for the evolution of tidal systems (Masselink et al., 2014). For instance, large wave-induced BSSs can disrupt the polymeric biofilm built up by microphytobenthos (MPB), a microalgae typically colonizing the bed sediment in shallow tidal environments (Amos et al., 2004; Mariotti and Fagherazzi, 2012), and therefore promote erosion of tidal-flat surfaces. The related increase in suspended sediment concentration can trigger negative feedback by promoting the decrease of light availability in the water column and thus limiting the sea grass and MPB proliferation (Lawson et al., 2007; Carr et al., 2010; Chen et al., 2017; Pivato et al., 2019). Furthermore, influencing the equilibrium elevation of tidal flats, wind-wave induced erosion affects the tidal prism and, as a consequence, the related morphological features of tidal networks, such as channel cross-sectional area (e.g., A. D'Alpaos et al., 2009, 2010) and drainage density (Marani et al., 2003; Stefanon et al., 2012).

As an example, the Venice Lagoon (Figure 2.1) has experienced strong erosion processes in the last centuries, which progressively deepened the lagoonal bottoms, promoted the export of fine cohesive sediments through the inlets toward the sea after storms, and led to the loss of extensive salt-marsh areas (Carniello et al., 2009; L. D'Alpaos, 2010a,b; Tommasini et al., 2019). The hydrodynamic and wind-wave fields in shallow tidal basins can be provided by several numerical models (e.g., Umgiesser et al., 2004; Carniello et al., 2011), as well as their impact on the morphodynamic evolution of tidal landscapes (e.g., Marani et al., 2010; A. D'Alpaos et al., 2012; Mariotti and Fagherazzi, 2013). However, modeling the morphodynamic evolution over time scales of centuries using fully-fledged models is a difficult task due to the numerical burdens involved and, therefore, simplified approaches are more and more frequently adopted (Murray, 2007). Towards the goal of developing a synthetic theoretical framework to represent wind-wave induced erosion events and accounting for

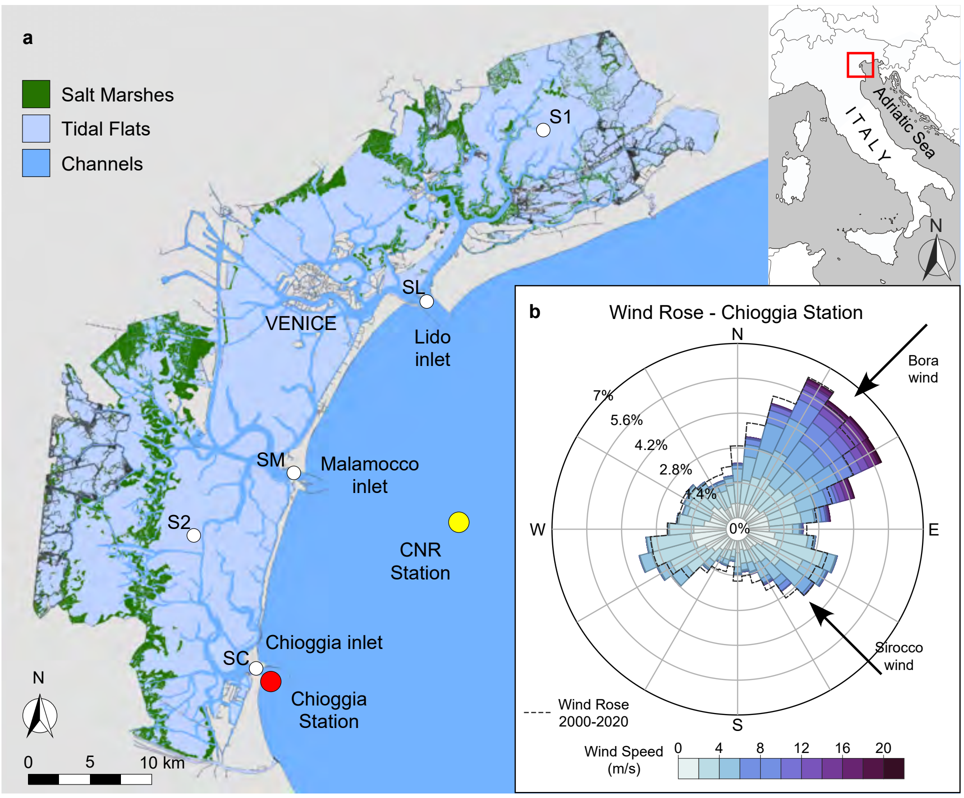


Figure 2.1: **Morphological features and wind conditions characterizing the Venice Lagoon.** **a**, Spatial distribution of the morphological features characterizing the the Venice Lagoon. The locations of the anemometric (Chioggia) and oceanographic (CNR Oceanographic Platform) stations are also shown, together with the locations of the three stations at the inlets (SL, SM and SC) and two stations (S1 and S2) for which we provide detailed statistical characterization of over threshold events. **b**, Wind rose for the data recorded at the Chioggia station in 2005. Dashed line shows the wind rose for the period 2000-2020.

their influence on the long-term morphodynamic evolution of tidal systems, we applied a two dimensional finite element model for reproducing and analysing the combined effect of wind-waves and tidal currents in generating the bed shear stresses in several historical configurations of the Venice Lagoon. More precisely, in the present study, we used the fully coupled Wind Wave-Tidal Model (WWTM) (Carniello et al., 2005; L. D'Alpaos and Defina, 2007; Carniello et al., 2011) to investigate the hydrodynamic behaviour of the following six configurations of the Venice Lagoon: 1611, 1810, 1901, 1932, 1970, and 2012. For each configuration, we run a one-year-long simulation considering representative tidal and meteorological boundary conditions. The resulting spatial and temporal dynamics of BSSs for the six configurations have been analysed on the basis of the peak over threshold (POT) theory once a critical shear stress for bed sediment erosion was chosen. We performed the analysis following the same framework adopted by A. D'Alpaos et al. (2013) and Carniello et al. (2016) for analysing, in the present configuration of the Venice Lagoon, the wave-induced BSSs and the suspended sediment concentrations, respectively.

The main goal of the present analysis is to find whether, in line with previous results, wave-induced erosion events can be modeled as marked Poisson processes also in the historical configurations of the Venice Lagoon. The relevance of this result lies in the possibility of describing those erosion processes as a Poisson process, which represents a promising framework for long-term studies. Indeed, the analytical characterization of the long-term behaviour of geophysical processes is becoming increasingly popular in hydrology and geomorphology (e.g., Rodriguez-Iturbe et al., 1987; D'Odorico and Fagherazzi, 2003; Botter et al., 2007; Park et al., 2014), although the applications to tidal landscapes are still quite rare (A. D'Alpaos et al., 2013; Carniello et al., 2016). Our analysis provide a temporally and spatially explicit characterization of wind-induced erosion events for the Venice Lagoon starting from the beginning of the seventeenth century, thus allowing us to investigate and understand the main features of the erosive trends the lagoon has been experiencing and to provide predictions on future scenarios.

## 2.3 MATERIALS AND METHODS

We considered six different configurations of the Venice Lagoon (Figure 2.2), covering a time span of four centuries, in order to assess the evolution through time of the feedback mechanisms between morphology and wave-induced erosion. The oldest three configurations

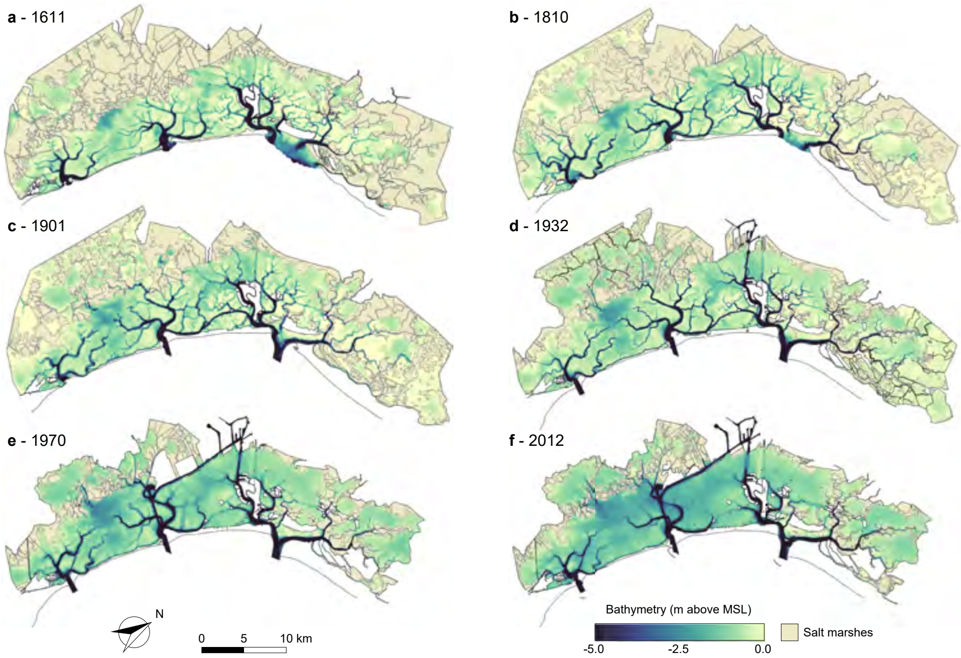


Figure 2.2: **Historical bathymetries of the Venice Lagoon.** Bathymetries of the six different configurations of the Venice Lagoon: 1611 (**a**), 1810 (**b**), 1901 (**c**), 1932 (**d**), 1970 (**e**), and 2012 (**f**).

(1611, 1810, and 1901) were reconstructed by using historical maps, while the more recent ones make use of the topographic surveys carried out by the Venice Water Authority (Magistrato alle Acque di Venezia) in 1932, 1970, and 2003. The updated description of the more recent morphological modifications, mainly occurred at the three inlets in the context of the Mo.S.E. project for the safeguard of the city of Venice by high tides (almost completed in 2012), was included in the 2003 configuration, so that we refer to this configuration as the 2012 configuration.

We refer the reader to Tommasini et al. (2019) for a detailed description of the methodology adopted to reconstruct the historical configurations and for information on the bathymetric data of the Venice Lagoon. The computational grids reproducing all the six configurations of the Lagoon have been presented and used in previous studies, namely: the 1611 by Tommasini et al. (2017); the 1810 by L.

D'Alpaos and Martini (2005) and L. D'Alpaos (2010b); the 1901, 1932, 1970 and 2012 by Carniello et al. (2009) and L. D'Alpaos (2010b).

During the last four centuries, the morphology of Venice Lagoon deeply changed in particular due to anthropogenic modifications. To prevent the Lagoon from silting up, the main rivers (Brenta, Piave, and Sile) were gradually diverted directly into the sea from the beginning of the fifteenth century. Meanwhile, during the last century, jetties were built at the inlets and navigation channels were excavated to connect the inner harbour with the sea (L. D'Alpaos, 2010b; Sarretta et al., 2010). The jetties deeply changed the hydrodynamics at the inlets and established a net export of sediment toward the sea, especially after storm events (Carniello et al., 2012). Globally speaking, these modifications enhanced erosion processes and triggered a net export of sediment toward the sea, resulting in a generalized deepening of tidal flats and subtidal platforms as well as the reduction of salt-marsh area. Indeed, in the last century, the average tidal-flat bottom elevation lowered from -0.51 m above mean sea level (a.m.s.l.) to -1.49 m a.m.s.l., while the salt-marsh area progressively shrank from 164.36 km$^2$ to 42.99 km$^2$ (Tommasini et al., 2019).

### 2.3.1 Numerical Model and Simulations

To compute the hydrodynamic and the wind-wave fields in the six selected configurations of the Venice Lagoon, we used the two-dimensional (2-D) fully coupled WWTM (Carniello et al., 2005, 2011). The numerical model, coupling a hydrodynamic module and a wind-wave module, describes the hydrodynamic flow field together with the generation and propagation of wind waves using the same computational grid.

The hydrodynamic module uses a semi-implicit staggered finite element method based on Galerkin's approach to solve the 2-D shallow water equations suitably rewritten in order to deal with partially wet and morphologically irregular domains (Defina, 2000; Martini et al., 2004; L. D'Alpaos and Defina, 2007). The bottom shear stress induced by currents, $\tau_{tc}$, is evaluated using the Strickler equation considering the case of a turbulent flow over a rough wall. The hydrodynamic module thus provides the water levels that are used by the wind-wave module to assess the wave group celerity and the bottom influence on wind-wave propagation.

For the wind-wave module (Carniello et al., 2005, 2011), the wave action conservation equation is parameterized using the zero-order moment of the wave action spectrum in the frequency domain (Holthuijsen et al., 1989). An empirical correlation function relating the peak wave period to the local wind speed and water depth determines the spatial and temporal distribution of the wave period (Young and Verhagen, 1996; Breugem and Holthuijsen, 2007; Carniello et al., 2011). The wind-wave module computes the bottom shear stress induced by wind waves, $\tau_{ww}$, as a function of the maximum horizontal orbital velocity at the bottom, which is related to the significant wave height through the linear theory.

The total bottom shear stress, $\tau_{wc}$, resulting from the combined effect of tidal currents and wind waves, is enhanced beyond the sum of the two contributions, because of the non-linear interaction between the wave and the current boundary layer. In the WWTM this is accounted for by using the empirical formulation suggested by Soulsby (1995, 1997):

$$\tau_{wc} = \tau_{tc} + \tau_{ww}\left[1 + 1.2\left(\frac{\tau_{ww}}{\tau_{ww} + \tau_{tc}}\right)\right] \tag{2.1}$$

Even if BSSs induced by the tidal currents are smaller than those produced by wind waves, they are of fundamental importance in modulating the temporal evolution of the total BSSs and can increase the peak BSS values by up to 30% (Mariotti et al., 2010a; A. D'Alpaos et al., 2013).

The WWTM has been widely tested against field observations not only in the Venice Lagoon (e.g., Carniello et al., 2005; L. D'Alpaos and Defina, 2007; Carniello et al., 2011) but also in other shallow microtidal environments worldwide, for example in the back-barrier lagoons of the Virginia Coast Reserve (Mariotti et al., 2010a) and the Cádiz Bay (Zarzuelo et al., 2018, 2019).

We applied the numerical model to the six computational domains representing the Venice Lagoon and a portion of the Adriatic Sea in front of it in order to perform one-year-long simulations. The boundary conditions of the model are the hourly tidal levels measured at the Consiglio Nazionale delle Ricerche (CNR) Oceanographic Platform, located in the Adriatic Sea offshore of the lagoon, and wind velocities and directions recorded at the Chioggia anemometric station, for which a quite long data set was available (Figure 2.1a). We forced the model with the time series recorded in 2005, being the probability distribution of wind speeds in 2005 the closest to the mean annual probability distribution in the period 2000-2020 and therefore a representative year for the wind characteristics in the Venice Lagoon (Figure 2.1b). By considering the same wind and tidal forcing for each historical configuration of the Venice Lagoon, we isolate the effects on the wind-wave fields and on the hydrodynamics owing to the changes in the lagoon morphology.

### 2.3.2 Peak Over Threshold Analysis

The morphodynamic evolution of tidal environments is controlled by the complex interaction between hydrodynamic, biologic and geomorphologic processes, which include both deterministic and stochastic components. As an example, it was shown that sediment transport dynamics in the Venice Lagoon is mostly linked to some limited and severe events induced by wind-waves (Carniello et al., 2011), whose dynamics are markedly stochastic in the present configuration (A. D'Alpaos et al., 2013; Venier et al., 2014; Carniello et al., 2016). In this work, at any location within each considered configuration of the Venice Lagoon, we used the peak over threshold theory (POT) (Balkema and Haan, 1974) to analyse the temporal and spatial evolution of the total BSS, $\tau_{wc}$. The threshold value of the BSS, $\tau_c$, was set equal to 0.4 Pa (Amos et al., 2004). The POT method allowed us to identify:

i. the interarrival time of over-threshold events, defined as the time between two consecutive upcrossings of the threshold;

ii. the duration of over-threshold events, that is the time elapsed between any upcrossing and the subsequent downcrossing of the threshold;

iii. its intensity, calculated as the largest exceedance of the threshold in the time elapsed between an upcrossing and the following downcrossing.

Once defined the probability density functions and the corresponding moments of these variables, a statistical analysis was performed for each location in all the considered configurations of the Venice Lagoon, in order to provide an accurate description of the BSS evolution through the last four centuries. This will allow us to take into account particular morphological trends over long-term time scales.

We performed the non-parametric Kolmogorov-Smirnov (KS) goodness of fit test to verify the hypothesis that the interarrival time of over-threshold events is an exponentially distributed random variable. The interarrival probability distribution plays an important role because, if interarrival times between subsequent exceedances of the threshold $\tau_c$ are independent and exponentially distributed random variables, the mechanics of erosion events can be mathematically described as a 1-D marked Poisson process, characterized by a vector of random marks (intensity and duration of each over-threshold event) associated to a sequence of random events along the time axis. The memorylessness is one of the most interesting mathematical features of Poisson processes since it allows to set the probability of observing a certain number of events in a pre-established time interval dependent only on its duration, regardless of its position along the time series. Therefore, the description of overthreshold BSS events as a Poisson process will allow one to immediately identify the probabilities of observing a certain number of resuspension events in a year or during a season, because all the sources of stochasticity in the physical drivers are described by a single parameter (i.e. the mean frequency of the process). Hence, it would be possible to set up a synthetic theoretical framework to model the wave-induced events through the use of Monte-Carlo realizations, bearing important consequences for the long-term evolution of tidal landscapes.

## 2.4 RESULTS AND DISCUSSION

We analysed the time series of computed total BSSs, $\tau_{wc}$, on the basis of a POT method, in order to provide a statistical characterization of wave-induced erosion events. For all the six configurations we set the critical shear stress, $\tau_c$, equal to 0.4 Pa (Amos et al., 2004; A. D'Alpaos et al., 2013) thus neglecting important effects related to modifications in bed composition. In order to eliminate spurius upcrossing and downcrossing of the prescribed threshold, the time series of BSSs were previously processed by applying a moving average filter. This low-pass filtering with a time window of 6 hours removes short-term fluctuation, preserving the modulation given by the semidiurnal tidal oscillation. Thanks to this procedure, over-threshold events satisfy the independence assumption required by the statistical analysis applied. Repeating this analysis for all the location within the computational domains, we characterized the spatial variability of mean interarrival times (Figure 2.3), peak excesses (Figure 2.4) and duration of over-threshold events (Figure 2.5) in the six selected configurations of the Venice Lagoon.

Wind-wave generation is determined by energy transfer from the wind to the water surface and, thus, clearly depends on wind characteristics, namely wind intensity and duration, as well as on fetch length and water depth (Fagherazzi and Wiberg, 2009). As a consequence, the morphological distribution of channels, tidal flats, and, more importantly, salt marshes and islands strongly influences the response of a shallow tidal basin to wind forcing and the resulting distribution of BSSs (Fagherazzi et al., 2006; Defina et al., 2007). Large portions in the ancient configurations were occupied by salt-marsh areas, interrupting again and again the fetch and thus reducing exceedances of the critical threshold. As a result, in the four more

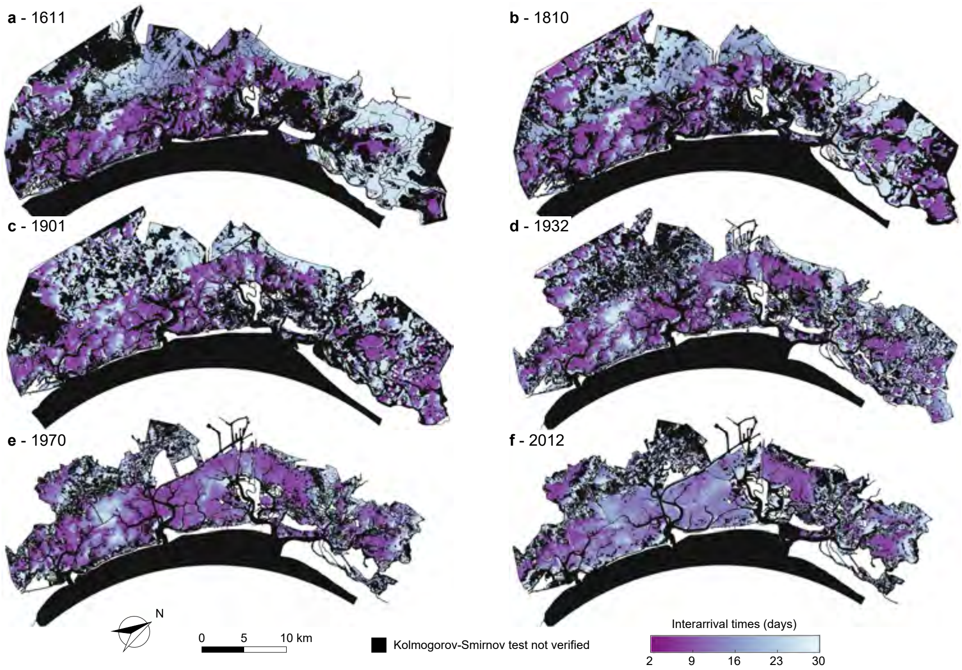


Figure 2.3: **Mean interarrival time of overthreshold erosion events.** Spatial distribution of mean interarrival times of over threshold exceedances, at sites where bed shear stress can be modeled as a marked Poisson process, as confirmed by the KS test ($\alpha = 0.05$) for the six different configurations of the Venice Lagoon: 1611 (**a**), 1810 (**b**), 1901 (**c**), 1932 (**d**), 1970 (**e**), and 2012 (**f**).

ancient configurations the characteristics of erosion events globally display a more complex spatial pattern, which conversely tends to be more uniform in the more recent configurations, due to the reduction of salt-marsh areas and to the deepening of tidal flats.

For each configuration, mean interarrival time, peak excess and duration of over-threshold events are shown at any location within the Venice Lagoon where the KS test, performed in order to verify that these variables are exponentially distributed, is satisfied at significance level $\alpha = 0.05$. Figure 2.6 shows the spatial distribution of the results of the KS test. In particular, we distinguished:

i. the dark blue area, where the KS test is not verified for the interarrival time, i.e. wave-induced erosion events can not be described as a Poisson process;

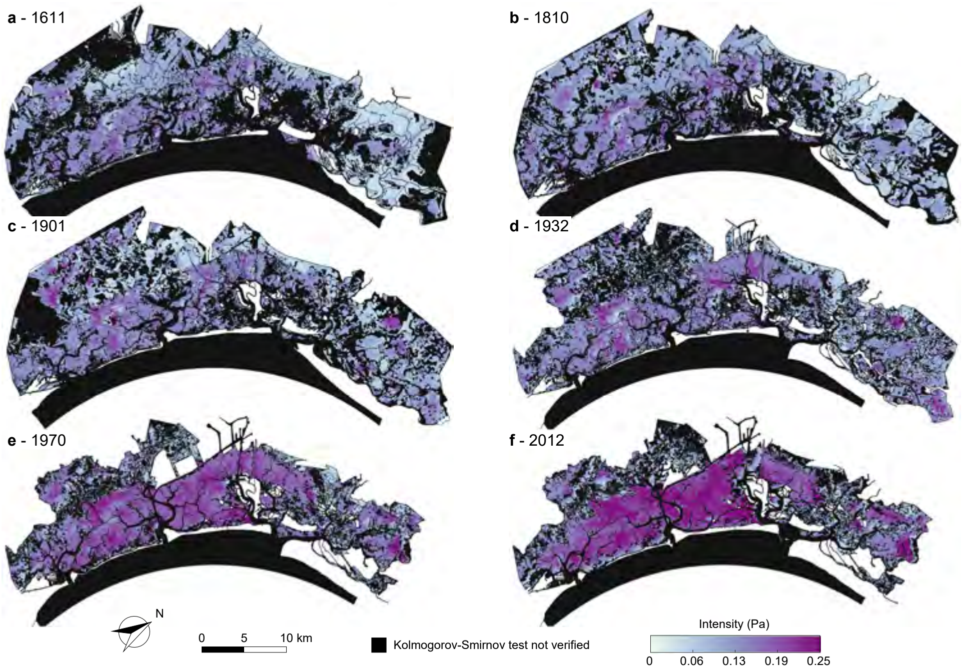


Figure 2.4: **Mean intensity of overthreshold erosion events.** Spatial distribution of mean intensity of peak excesses of over threshold exceedances, at sites where bed shear stress can be modeled as a marked Poisson process, as confirmed by the KS test ($\alpha = 0.05$) for the six different configurations of the Venice Lagoon: 1611 (**a**), 1810 (**b**), 1901 (**c**), 1932 (**d**), 1970 (**e**), and 2012 (**f**).

ii. the red area, where the KS test is verified for all the three stochastic variables we considered, namely interarrival times, intensity, and duration, i.e. wave-induced erosion events are indeed a marked Poisson process where also intensity and duration are exponentially distributed random variables;

iii. the yellow area, where the KS test is verified for the interarrival time but not for the intensity and/or duration, i.e. wave-induced erosion events are a marked Poisson process but at least one between intensity and duration is not an exponentially distributed random variable.

In all the selected configurations, salt marshes and tidal channel networks mostly represent the portion of the lagoon where wave-induced erosion events cannot be modeled as a Poisson process (dark

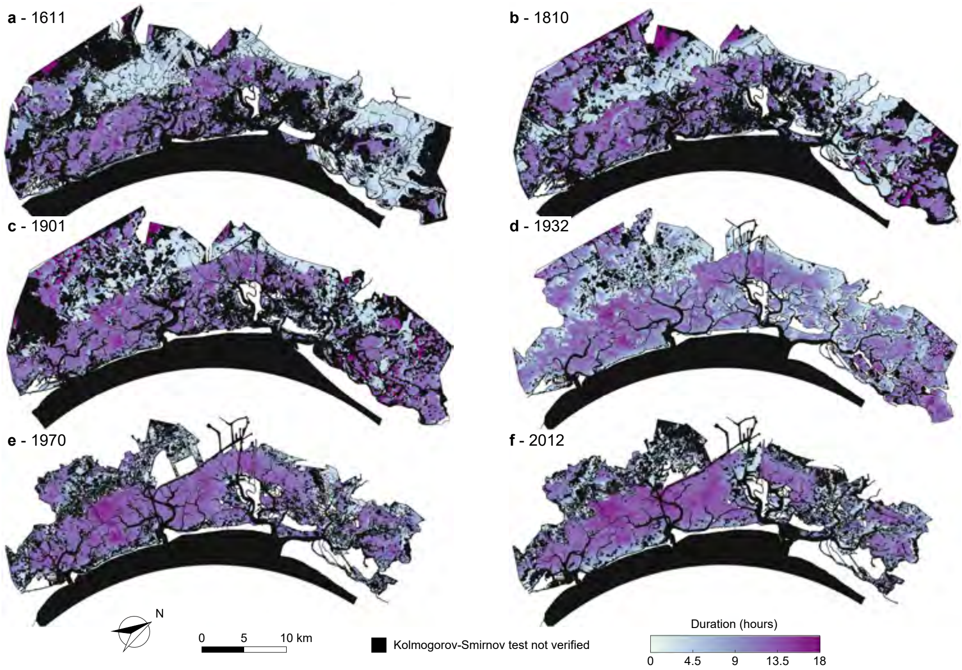


Figure 2.5: **Mean durations of overthreshold erosion events.** Spatial distribution of mean durations of over threshold exceedances, at sites where bed shear stress can be modeled as a marked Poisson process, as confirmed by the KS test ($\alpha = 0.05$) for the six different configurations of the Venice Lagoon: 1611 (**a**), 1810 (**b**), 1901 (**c**), 1932 (**d**), 1970 (**e**), and 2012 (**f**).

blue area in Figure 2.6). Over salt-marsh platforms almost no exceedances of the prescribed threshold, $\tau_c$, tend to occur (Figure 2.9) because of the low water depth that prevent the formation of significant waves (e.g., Möller et al., 1999). May we add that colonization of the salt-marsh surface by halophytic vegetation almost completely prevent any vertical erosion (Christiansen et al., 2000; Temmerman et al., 2005a). On the contrary, exceedances of the threshold are detected along the channel network and at the three inlets (Figure 2.9), but these are mostly associated with shear stresses produced by tidal currents, especially after the construction of the jetties at the inlets. Consequently, at these points the KS test is not satisfied and erosion events cannot be modeled as a Poisson process because of the strictly deterministic nature of tide-induced shear stress.

As an example, Figure 2.16 shows the time series and the prob-

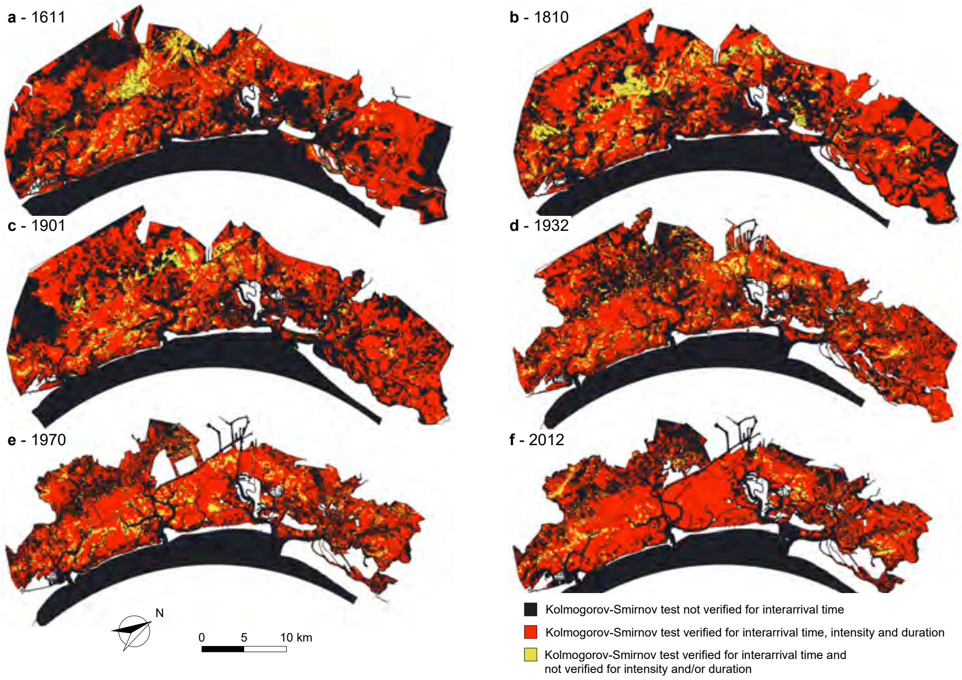


Figure 2.6: **Kolmogorov-Smirnov test for overthreshold erosion events.** Spatial distribution of Kolmogorov-Smirnov (KS) test at significance level ($\alpha = 0.05$) for the six different configurations of the Venice Lagoon: 1611 (**a**), 1810 (**b**), 1901 (**c**), 1932 (**d**), 1970 (**e**), and 2012 (**f**). In the maps we can distinguish areas where the KS test is: not verified (dark blue); verified for all the considered stochastic variables (interarrival time, intensity over the threshold and duration) (red); verified for the interarrival time and not for intensity and/or duration (yellow).

ability distribution at the SM station in the Malamocco inlet (see Figure 2.1a for the location). In the 1611 and 1810 simulations, owing to the configuration of the inlet, the BSS was very small such that almost no exceedances of the threshold occured. After the construction of the jetties at the Malamocco inlet in 1872, erosion mechanics abruptly changed: BSS considerably increased but it was driven by tidal forcing and, thus, interarrival times were not exponentially distributed, since the erosion threshold was exceeded once per day because of tidal fluxes (Figure 2.16c,d). The BSS analysis at the SL station in the Lido inlet, where the construction of the jetties ended in 1892, provides analogous results (Figure 2.15), meanwhile at the SC station in the Chioggia inlet BSS still does not systematically exceed the threshold also in the 1901 configuration, since the construction of the jetties at the Chioggia inlet took place in between 1930 and 1934 (L. D'Alpaos, 2010a) (Figure 2.17).

The KS test is verified over subtidal platforms and tidal flats, where current-induced BSSs are typically below the critical value, but wave-induced BSSs mainly contribute to the total BSS. Locations where interarrival time, duration and intensity follow an exponential distribution (see red areas in Figure 2.6) remain the vast majority of the tidal basin in all the configurations. As a result, a synthetic framework that model erosion as a Poisson process is deemed to be suitable for wide tidal-flat areas.

Almost in all configurations, large interarrival times (Figure 2.3) are essentially found in sheltered areas, where only particularly intense events are able to generate BSSs large enough to exceed $\tau_c$. A clear example is provided by the area protected by marsh platforms and by the mainland in the northeastern and in the western portion of the lagoon, sheltered from the north-easterly Bora wind, which is the main morphologically significant wind in the Venice Lagoon (Figure 2.1b). This pattern becomes even more evident in the configurations of 1611, 1810, and 1901 where larger portions of the lagoon were occupied by salt marshes and present interarrival times greater than 30 days. Large interarrival times can also be observed close to the three inlets where the water depth is such that only during intense events the bottom can be affected by wave oscillations and the total BSSs can exceed the threshold. Globally speaking, in the four oldest configurations we found relatively short (about 5 days) interarrival times spread all around the lagoon basin, while the present configuration, characterized by a more constant and larger water depth (in some areas greater than 1.5 m), displays longer interarrival times, e.g. between 10 and 15 days for the tidal flats located in the central-southern portion of the lagoon (Figure 2.3). This is mainly due to the relationship existing between $\tau_{ww}$ and water depth that, for a prescribed wind velocity, decreases as the water depth increases (Defina et al., 2007). Indeed, in the historical configurations large areas occupied by tidal flats are characterized by lower water depth ($\leq 0.5$ m), as a result $\tau_{ww}$ is higher also for weak wind speeds, thus increasing the number of exceedances of the threshold.

As an example, Figure 2.7a shows the probability distributions of the interarrival times for the S1 station (location shown in Figure 2.1a), named "Palude Maggiore", which maintained the same morphological features through the last four centuries. In this point, as in most areas of the lagoon, the mean interarrival time $\overline{\lambda}_t$ between two subsequent over-threshold events increases through time. On the contrary, the watershed divide area between the Chioggia and the Malamocco inlets, named "Fondo dei Sette Morti" (see point S2 in Figure 2.1a), shows a reverse trend: the interarrival times decreases from the past to the present (i.e. wave-induced erosion events are more frequent). Although the almost constant, relatively deep bottom elevation that this area maintained through centuries (Carniello et al., 2009; L. D'Alpaos, 2010b) prevent the exceedance of the threshold $\tau_c$ during less intense erosion events, the generalized deepening experienced by the surrounding portion of the lagoon in the most recent configurations allows more frequent and less intense events reaching this area and, therefore, a decrease of the interarrival times.

The over-threshold peak intensities generally strongly increased during the last four centuries (Figure 2.4 and 2.10b). For all the selected configurations, intensities are lower in the more pristine northern part of the lagoon, which is sheltered from the dominant Bora wind by the mainland and by preserved salt-marsh areas, interrupting the fetch. Meanwhile the central and southern portions of the lagoon are characterized by much larger intensity values, which more rapidly increased along the last few decades. In particular, in the central part of the lagoon the mean intensities increased from around 0.13 Pa to 0.25 Pa over the threshold, due to the flattening and deepening of this area. A quite similar situation characterizes also the southern part of the Venice Lagoon, between the Malamocco and Chioggia inlets.

For all the configurations, the durations of over threshold events

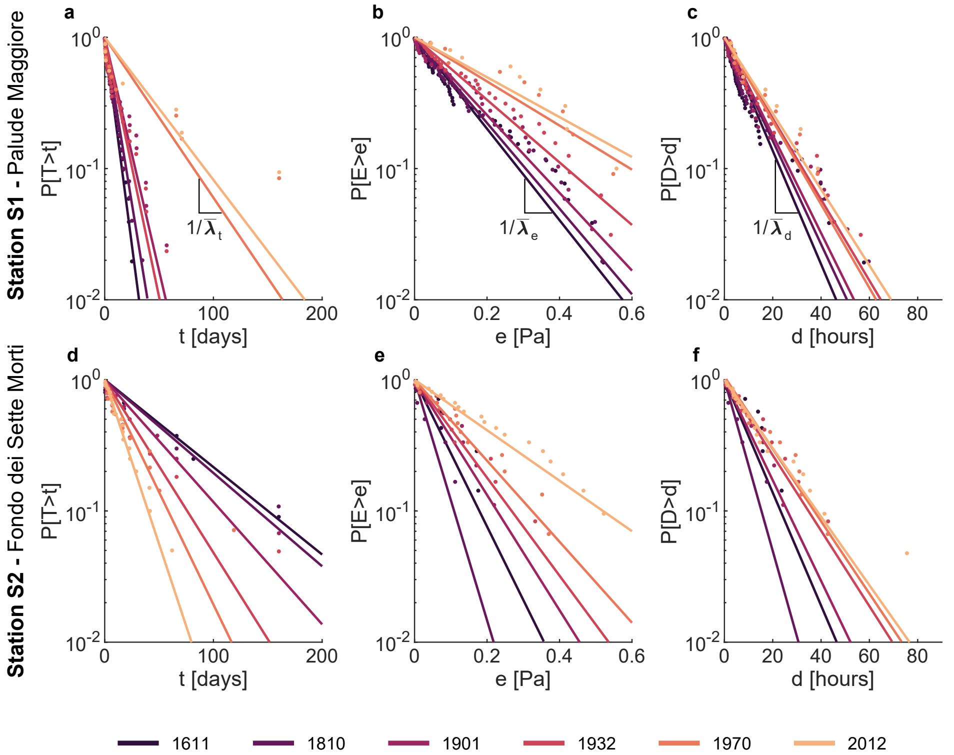


Figure 2.7: **Overthreshold erosion events at stations S1 and S2.** Statistical characterizations of over threshold events at two stations S1 "Palude Maggiore" and S2 "Fondo dei Sette Morti" (see Figure 2.1a for locations) in the six configurations of the Venice Lagoon. Probability distributions of (**a-b**) interarrival times, $t$; (**c-d**) intensities of peak excesses of over threshold exceedances, $e$; and (**e-f**) durations of over threshold event, $d$. $\overline{\lambda}_t$ mean interarrival time, $\overline{\lambda}_e$ mean peak excess intensity, and $\overline{\lambda}_d$ mean duration.

(Figure 2.5 and 2.10c), likewise intensities, present much lower values in the areas sheltered by salt marshes (i.e. the northern lagoon and the western portion of the southern lagoon) than in the fetch-unlimited central-southern portion of the lagoon. In the latter area, in fact, over-threshold events last more than 15 hours, compared to a duration of about 5 hours in the salt-marsh areas. The increase over time of peak intensities and durations of erosion events are clearly shown also by the probability distributions computed for points S1 and S2 (Figure 2.7).

The larger over threshold peak intensities, as well as the longer durations characterizing the central-southern portion of the lagoon and increasing from the past to the present, are in agreement with recent observations highlighting a critical erosive trend for the tidal flats and subtidal platforms in this area (e.g., Day et al., 1999; Carniello et al., 2009; Molinaroli et al., 2009; L. D'Alpaos, 2010b; Defendi et al., 2010; Sarretta et al., 2010).

Figures 2.11, 2.12 and 2.13 show the temporal cross-correlation between the three random variables, computed for each location and for all the six configurations. In particular the temporal cross-correlation between intensity of peak excesses and duration of over threshold exceedances display values very close to 1 for all the lagoon morphologies, thus suggesting a pseudo-deterministic link between peak intensities and the corresponding durations (Figure 2.11 and 2.14a). On the other hand, almost no correlation exists between durations and interarrival times (Figure 2.12 and 2.14b), as well as between intensities and interarrival times (Figure 2.13 and 2.14c). These results, in line with the temporal cross-correlation obtained for the statistical analysis of suspended sediment concentration for the present lagoon by Carniello et al. (2016), suggest that resuspension events can be modeled as a 3-D Poisson process in which the marks (duration and intensity) are mutually dependent but independent from the interarrival time between two subsequent over-threshold events.

In order to provide a more quantitative estimation of the spatial heterogeneity of interarrival times, duration and intensities of the critical BSS exceedances, we computed the erosion work (geomorphic work *sensu* Wolman and J. P. Miller, 1960, see also Mariotti and Fagherazzi, 2013). The erosion work $[E_w]$ experienced by a single point during the time interval $(t_2 - t_1)$ can be computed as:

$$[E_w] = \int_{t_1}^{t_2} \frac{e}{\rho_b} \left( \frac{\tau_{wc} - \tau_c}{\tau_c} \right) \mathrm{d}t. \tag{2.2}$$

where $e$ is the value of the erosion coefficient which depends on the sediment properties and $\rho_b = \rho_s(1-n)$ is the sediment bulk density, being $n$ the porosity. We set $e$ equal to $5 \cdot 10^{-5}$ kg m$^{-2}$ s$^{-1}$, as suggested for sand-mud mixtures (van Ledden et al., 2004; Le Hir et al., 2007) and in agreement with Carniello et al. (2012), $\rho_s = 2650$ kg m$^{-3}$ and $n = 0.4$.

Using the mean values of the stochastic variables we computed for characterizing erosion events (i.e. interarrival time, intensity and duration), once verified they can be modeled as a Poisson precess, we can simplify Eq. 2.2 as follows:

$$[E_w^*] = \frac{e}{\rho_b}\left(\frac{\tau_{wc} - \tau_c}{\tau_c}\right)(t_2 - t_1) \tag{2.3}$$

where we assume $(t_2 - t_1)$ to be the mean duration of over-threshold events and $(\tau_{wc} - \tau_c)$ their mean intensity. In order to estimate the erosion work for one year, $E_w$, we multiplied the result obtained with the Eq. 2.3 for the number of events computed as 365 (days per year) divided by the mean interarrival time in each point within the lagoon.

Figure 2.8 provides the spatial distribution of the annual erosion work, $E_w$, for the six configurations of the Venice Lagoon. We computed the erosion work also according to Eq. 2.2, in order to compare differences between the complete formulation based on the computed BSS time records and the synthetic approach exploiting the possibility of describing resuspension events as marked Poisson precesses (Figure 2.18). The erosion work computed following the two approaches is quite similar, as shown by the map of the relative error (Figure 2.19) and by the computed values of the spatially averaged relative error that varies between 10% and 14% considering all the analysed configurations of the lagoon (Table 2.1). Such an agreement between the two estimation of the erosion work support the validity of the provided statistical characterization of resuspension events.

The erosion work is almost constant between 1611 and 1932, it reaches its maximum in the 1970 and then it decreases in the present configuration (Figure 2.8). The ancient configurations (i.e. 1611, 1810, 1901 and 1932) display a more complex spatial pattern of the computed erosion work because of the wider presence of salt marshes and islands distributed throughout the basin and because of the shallower and more irregular bathymetry characterizing the tidal flats. This morphology is such that the fetch is continuously interrupted

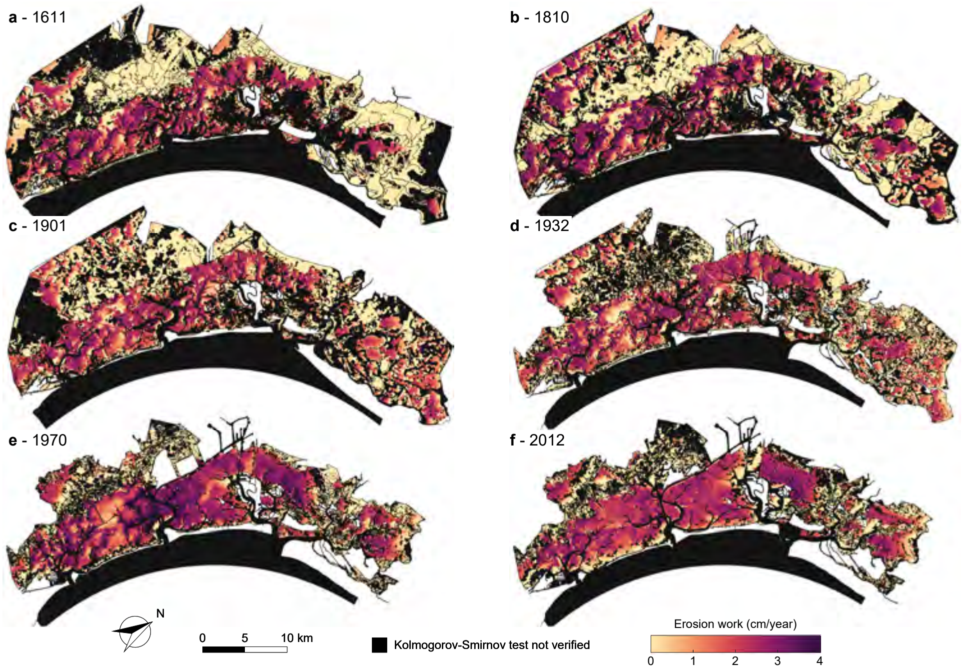


Figure 2.8: **Erosion work.** Spatial distribution of erosion work for the six different configurations of the Venice Lagoon: 1611 (**a**), 1810 (**b**), 1901 (**c**), 1932 (**d**), 1970 (**e**), and 2012 (**f**). Black identifies sites where the bottom shear stress cannot be modeled as a marked Poisson process (i.e. the KS test is not verified for the interarrival time).

and wind-waves are prevented from fully developing while generating and propagating over areas whose bathymetry is continuously varying. This indeed prevent a more uniform erosion of the lagoonal bottom. Interestingly, even if the present configuration of the lagoon displays larger mean intensities and longer mean durations than in 1970 (see Figure 2.4 and Figure 2.5), the combination with generally longer mean interarrival times (Figure 2.3) affects the erosion work. In fact, the erosion work is maximum in the 1970 configuration when it reaches a peak of more than 4.0 cm/year. This promoted an intense and uniform erosion of the lagoon, thus leading to the present morphology and bathymetry characterized by less complex erosion pattern and a roughly constant erosion rate of the tidal flats in the central southern lagoon of about 2.5 cm/year. Our results are in good agreement with previous studies (e.g., Carniello et al., 2009; Moli-

**Table 2.1:** Spatially averaged relative error between erosion work computed with Eq. 2.2 and 2.3

| Configuration | $r_e$ [-] |
|---|---|
| 1611 | 0.140 |
| 1810 | 0.108 |
| 1901 | 0.135 |
| 1932 | 0.131 |
| 1970 | 0.133 |
| 2012 | 0.112 |

naroli et al., 2009) that identified two different evolutionary trend in the northern lagoon and in the central-souther part, the northern lagoon displaying, on average, much lower erosion rate.

## 2.5 CONCLUSIONS

Our results provide a statistical characterization of sediment erosion in shallow tidal environments, aimed at testing the possibility to describe erosion dynamics as a Poisson process in a synthetic modeling framework able to reproduce the long-term evolution of shallow tidal environments. The approach is applied to the specific case of the Venice Lagoon, for which six configurations along the last four centuries are available.

In the present study, we applied the extensively calibrated and tested Wind Wave-Tidal Model to the six historical configurations of the Venice Lagoon, in order to perform a spatially-explicit analysis of the BSS time series under the same wind and water level forcing. We analysed the computed BSS temporal evolution following the Peak Over Threshold theory. We verified whether wind-wave erosion events could be modeled as a marked Poisson processes, by performing the non-parametric Kolmogorov-Smirnov goodness of fit test to confirm the hypothesis that the interarrival time of over threshold BSS events together with their durations and intensities are exponentially distributed random variables.

Statistical analyses of the wave-driven erosion processes suggest that interarrival times between two consecutive over threshold events, their durations and intensities can be described as exponentially distributed random variables over wide areas in all the selected configurations of the Venice Lagoon. As a consequence, the wave-induced erosion can be represented by a marked Poisson process through centuries.

Furthermore, we observed that durations and intensities of over-threshold BSS exceedances are highly correlated, while almost no correlation exists between duration and interarrival time, as well as between intensity and interarrival time. These observations indicate that a 3-D Poisson process, in which the marks (duration and intensity of the over-threshold events) are mutually dependent but independent from the interarrival time, is a suitable description of the wave-induced erosion processes.

Moreover, we showed that along the last four centuries the interarrival times of erosion events generally increased throughout the lagoon, as well as their intensities and durations, thus leading to less frequent but more intense wave-induced erosion events.

These modifications in the bottom shear stress field are generated by, but at the same time they are also responsible for, the morphological modifications of the Venice Lagoon, in particular the generalized deepening of tidal flats and reduction of salt marsh area. Only in the "Fondo dei Sette Morti", located close to the watershed divide between the Malamocco and the Chioggia inlets, interarrival times decreases along the last four centuries. Such an opposite trend is associated to the relatively deep and constant bottom elevation characterizing this area combined with the generalized deepening experienced by the surrounding areas that allows more frequent events reaching the "Fondo dei Sette Morti".

The erosion work, computed as combination of interarrival times, durations and intensities, remained almost constant and characterized by an irregular spatial pattern until the beginning of the twentieth century, when it rapidly increased reaching a peak in 1970. In the last few decades, the erosion work decreased, presenting a more uniform pattern suggesting that the quite intense erosive trend the Venice Lagoon has been experiencing since the beginning of the last century is, at present, slowing down as a consequence of the generalized deepening and flattening of the lagoonal bed. Owing to the choice of forcing the domain with the same conditions, these changes in the erosive trend are, in fact, only due to morphological modification experienced by the tidal basin.

The present findings represent an additional step towards the set up of a synthetic, statistically-based framework which can be used to model the long-term morphodynamic evolution of tidal systems through the use of Monte Carlo realizations.

## 2.6 SUPPORTING INFORMATION

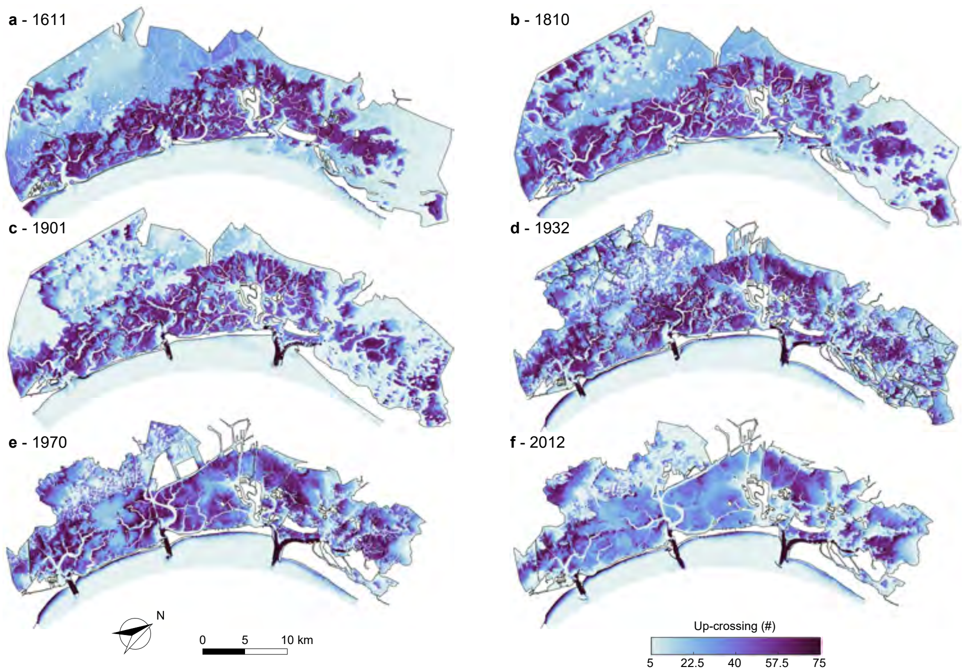


Figure 2.9: **Number of upcrossings of the erosion threshold.** Spatial distribution of the number of upcrossings of the threshold for erosion $\tau_c = 0.4$ Pa, for the six different configurations of the Venice Lagoon: 1611 (**a**), 1810 (**b**), 1901 (**c**), 1932 (**d**), 1970 (**e**), and 2012 (**f**).

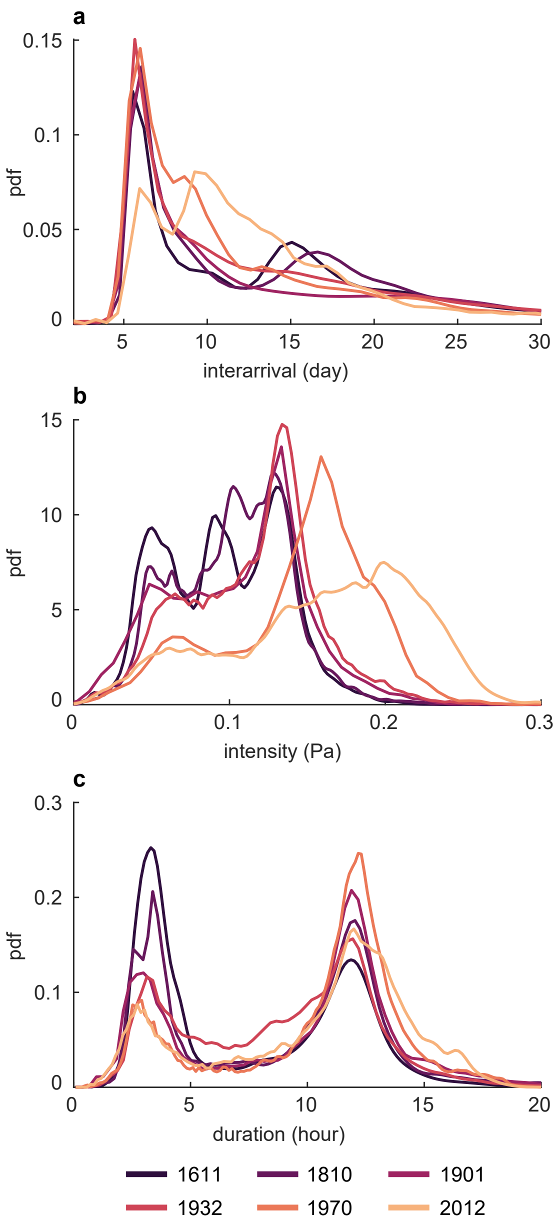


| Year | $t$ [day] (mean $\pm$ std) | (median) |
|---|---|---|
| 1611 | $45.27 \pm 76.56$ | 16.29 |
| 1810 | $34.30 \pm 61.99$ | 15.69 |
| 1901 | $48.35 \pm 80.10$ | 15.14 |
| 1932 | $26.09 \pm 40.21$ | 13.17 |
| 1970 | $20.35 \pm 32.07$ | 10.07 |
| 2012 | $26.13 \pm 42.83$ | 12.67 |

| Year | $e$ [Pa] (mean $\pm$ std) | (median) |
|---|---|---|
| 1611 | $0.09 \pm 0.03$ | 0.09 |
| 1810 | $0.10 \pm 0.03$ | 0.10 |
| 1901 | $0.10 \pm 0.04$ | 0.11 |
| 1932 | $0.11 \pm 0.04$ | 0.12 |
| 1970 | $0.14 \pm 0.04$ | 0.15 |
| 2012 | $0.16 \pm 0.06$ | 0.16 |

| Year | $d$ [hour] (mean $\pm$ std) | (median) |
|---|---|---|
| 1611 | $7.54 \pm 4.32$ | 6.47 |
| 1810 | $8.84 \pm 4.76$ | 10.18 |
| 1901 | $9.67 \pm 5.06$ | 11.12 |
| 1932 | $8.95 \pm 4.02$ | 9.75 |
| 1970 | $10.36 \pm 3.92$ | 11.64 |
| 2012 | $10.27 \pm 4.24$ | 11.57 |

Figure 2.10: **Spatial probability density function of interarrival time, intensity and duration of BSS overthreshold events.** Probability density function (left), mean (mean $\pm$ standard deviation) and median value (right) of interarrival times $t$ (**a**), intensity $e$ (**b**) and duration $d$ (**c**) of BSS overthreshold events.

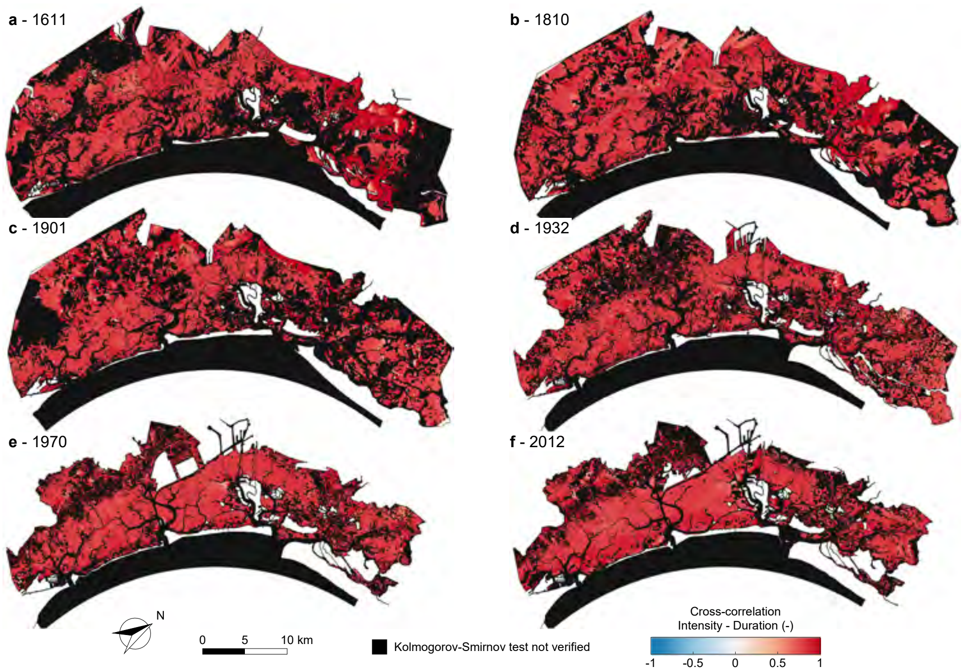


Figure 2.11: **Cross-correlation between intensity and duration of overthreshold BSS events.** Spatial distribution of temporal cross-correlation between intensity of peak-excesses and duration of over threshold exceedances for the six different configurations of the Venice Lagoon: 1611 (**a**), 1810 (**b**), 1901 (**c**), 1932 (**d**), 1970 (**e**), and 2012 (**f**). Black identifies sites where the bottom shear stress cannot be modeled as a marked Poisson process (i.e. the KS test is not verified for the interarrival time) .

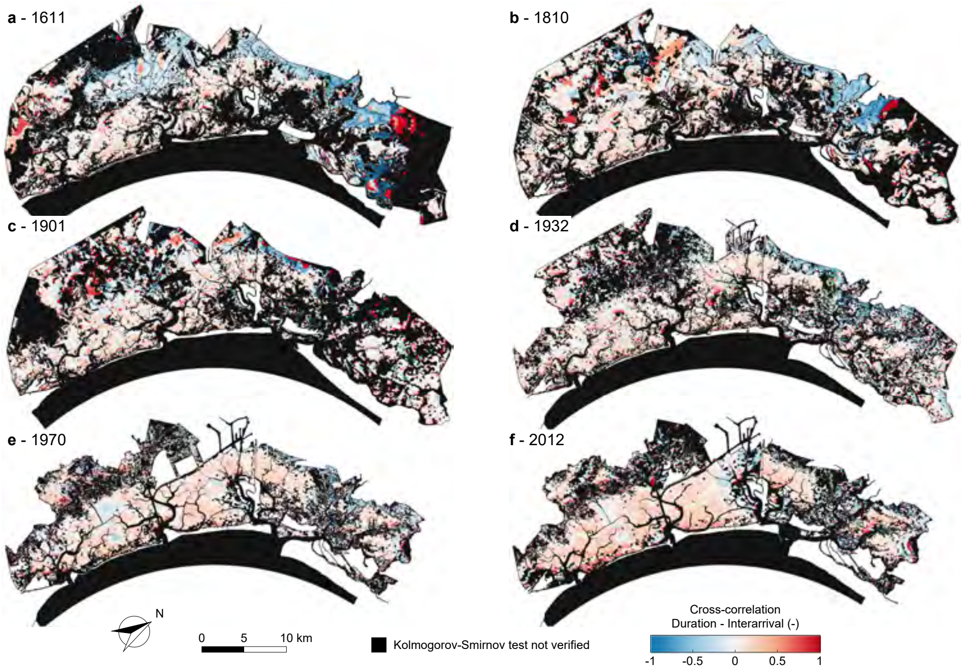


Figure 2.12: **Cross-correlation between duration and interarrival times of overthreshold BSS events.** Spatial distribution of temporal cross-correlation between duration and interarrival times of over threshold exceedances for the six different configurations of the Venice Lagoon: 1611 (**a**), 1810 (**b**), 1901 (**c**), 1932 (**d**), 1970 (**e**), and 2012 (**f**). Black identifies sites where the bottom shear stress cannot be modeled as a marked Poisson process (i.e. the KS test is not verified for the interarrival time).

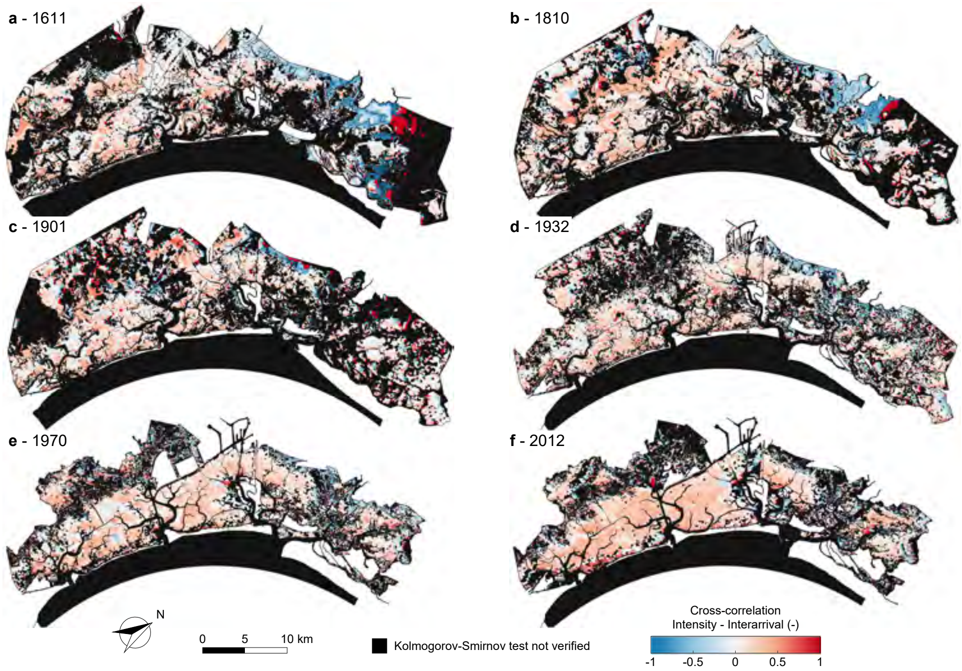


Figure 2.13: **Cross-correlation between intensity and interarrival times of overthreshold BSS events.** Spatial distribution of temporal cross-correlation between intensity of peak-excesses and interarrival times of over threshold exceedances for the six different configurations of the Venice Lagoon: 1611 (**a**), 1810 (**b**), 1901 (**c**), 1932 (**d**), 1970 (**e**), and 2012 (**f**). Black identifies sites where the bottom shear stress cannot be modeled as a marked Poisson process (i.e. the KS test is not verified for the interarrival time) .

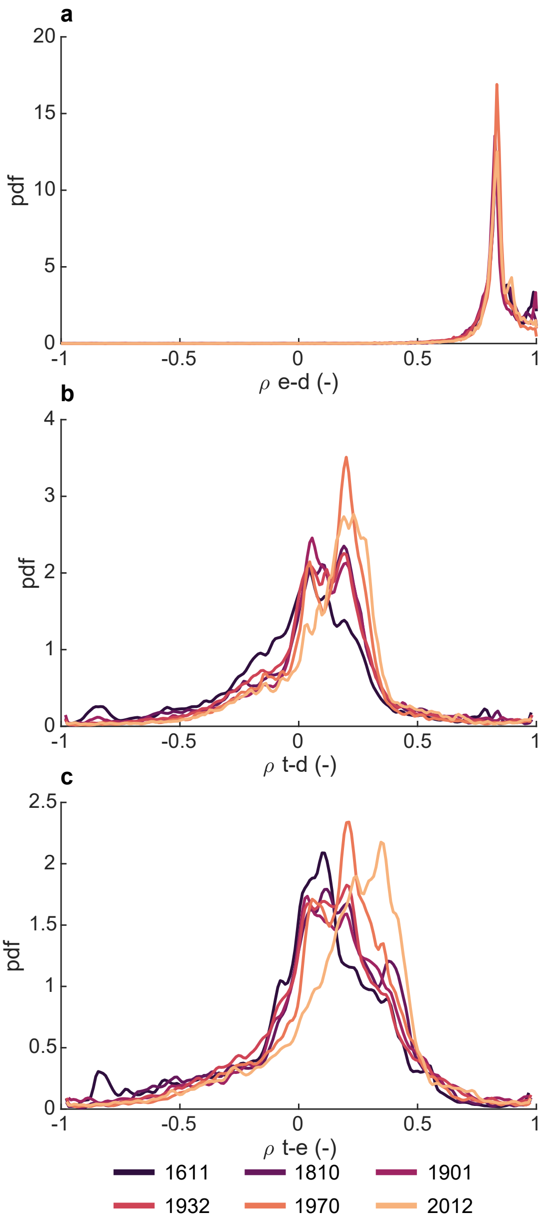


| Year | $\rho(e-d)$ [-] (mean $\pm$ std) |
|---|---|
| 1611 | $0.84 \pm 0.09$ |
| 1810 | $0.83 \pm 0.09$ |
| 1901 | $0.82 \pm 0.11$ |
| 1932 | $0.82 \pm 0.11$ |
| 1970 | $0.83 \pm 0.08$ |
| 2012 | $0.83 \pm 0.09$ |

| Year | $\rho(t-d)$ [-] (mean $\pm$ std) |
|---|---|
| 1611 | $0.005 \pm 0.365$ |
| 1810 | $0.069 \pm 0.318$ |
| 1901 | $0.078 \pm 0.356$ |
| 1932 | $0.070 \pm 0.312$ |
| 1970 | $0.105 \pm 0.277$ |
| 2012 | $0.130 \pm 0.308$ |

| Year | $\rho(t-e)$ [-] (mean $\pm$ std) |
|---|---|
| 1611 | $0.05 \pm 0.37$ |
| 1810 | $0.10 \pm 0.33$ |
| 1901 | $0.11 \pm 0.37$ |
| 1932 | $0.10 \pm 0.33$ |
| 1970 | $0.14 \pm 0.30$ |
| 2012 | $0.18 \pm 0.33$ |

Figure 2.14: **Spatial probability density function of cross-correlation between interarrival time, intensity and duration of BSS overthreshold events.** Probability density function (left) and mean value (mean $\pm$ standard deviation, right) of cross-correlation between intesity and duration $\rho(e-d)$ (**a**), interarrival time and duration $\rho(t-d)$ (**b**) and interarrival time and intensity $\rho(t-e)$ (**c**).

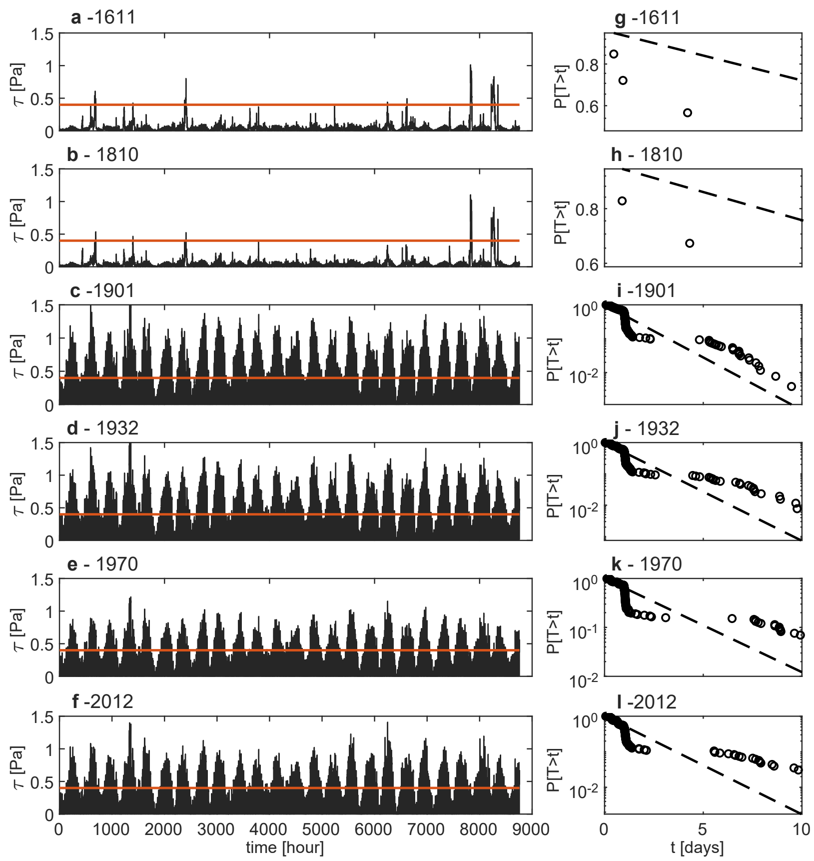


**Figure 2.15: Overthreshold BSS events at the Lido inlet.** Statistical analysis at SL station in the Lido inlet: time series of the computed BSS (**a-f**); probability distributions of the interarrival times (circles) and exponential distributions (dashed lines) (**g-l**).

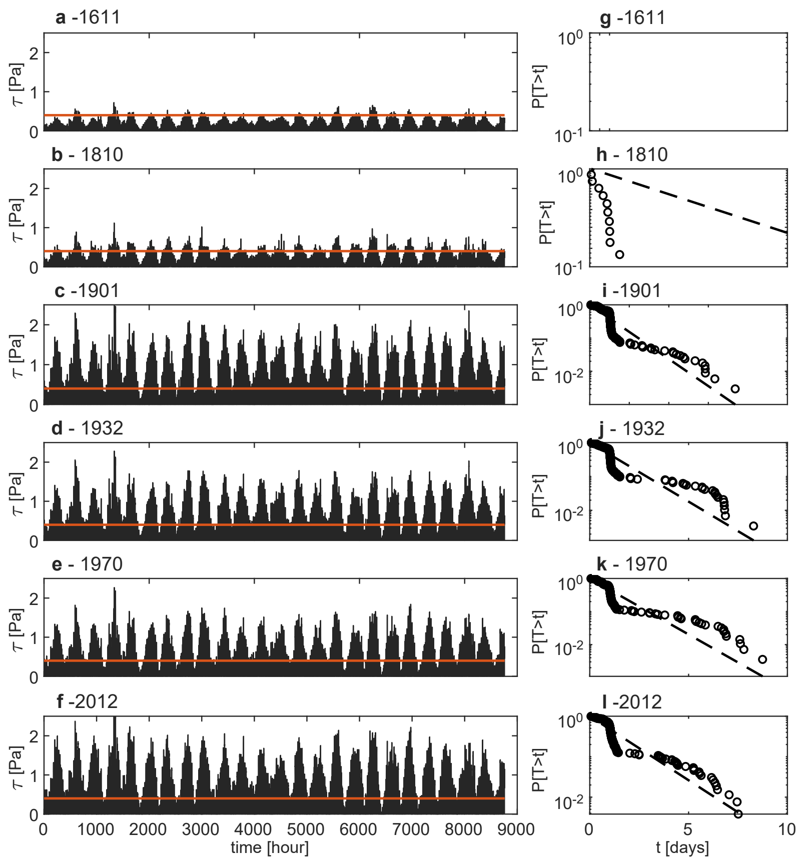


**Figure 2.16: Overthreshold BSS events at the Malamocco inlet.** Statistical analysis at SM station in the Malamocco inlet: time series of the computed BSS (**a-f**); probability distributions of the interarrival times (circles) and exponential distributions (dashed lines) (**g-l**).

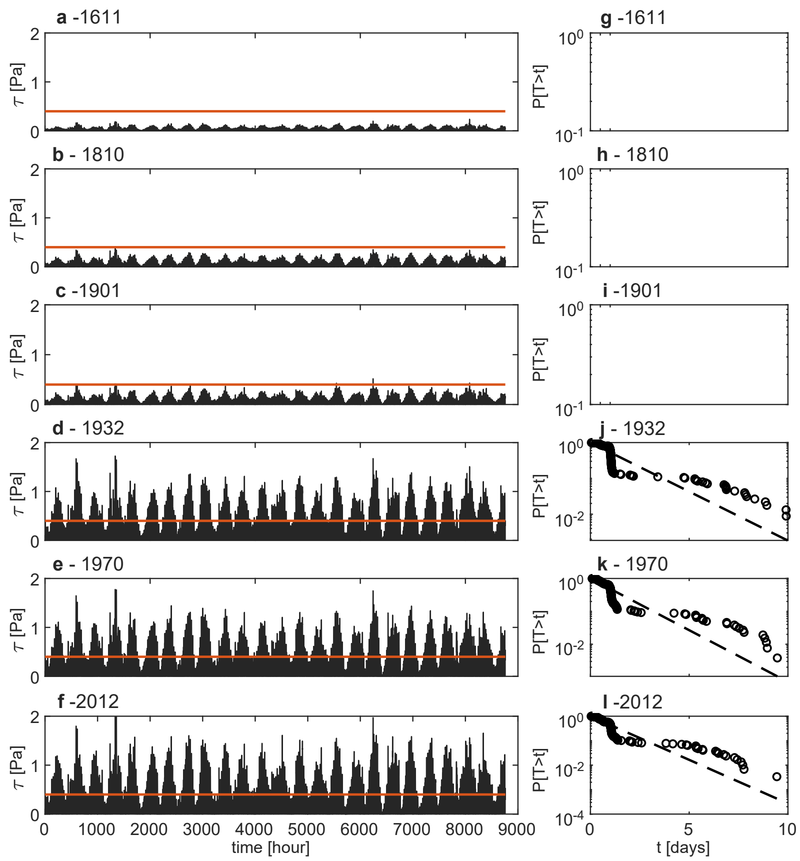


**Figure 2.17: Overthreshold BSS events at the Chioggia inlet.** Statistical analysis at SC station in the Chioggia inlet: time series of the computed BSS (**a-f**); probability distributions of the interarrival times (circles) and exponential distributions (dashed lines) (**g-l**).

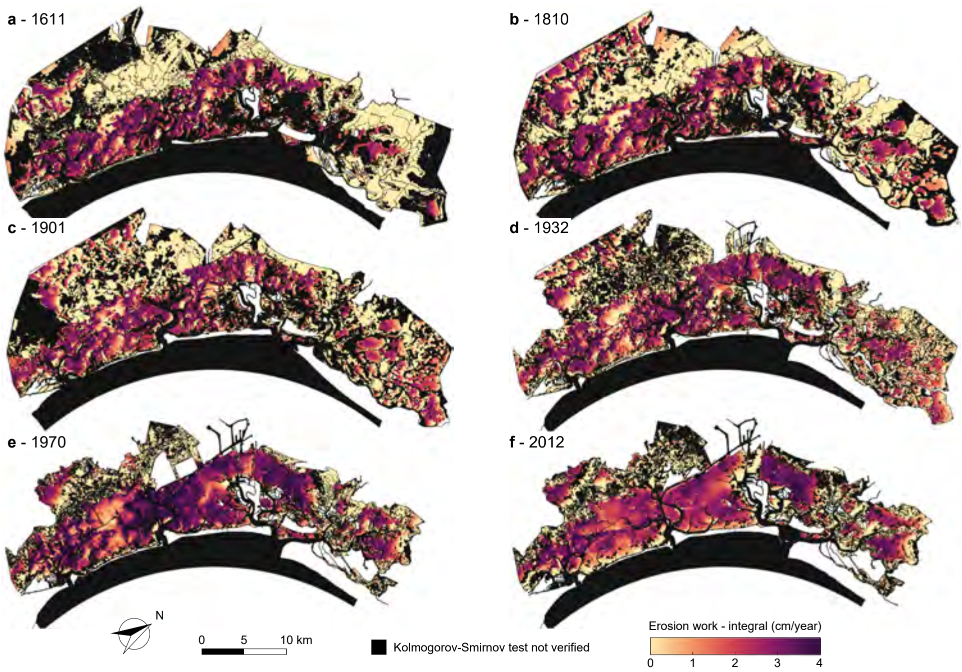


Figure 2.18: **Erosion work computed as integral of overthreshold BSS events.** Spatial distribution of erosion work computed with Eq. 2.2 for the six different configurations of the Venice Lagoon: 1611 (**a**), 1810 (**b**), 1901 (**c**), 1932 (**d**), 1970 (**e**), and 2012 (**f**). Black identifies sites where the bottom shear stress cannot be modeled as a marked Poisson process (i.e. the KS test is not verified for the interarrival time).

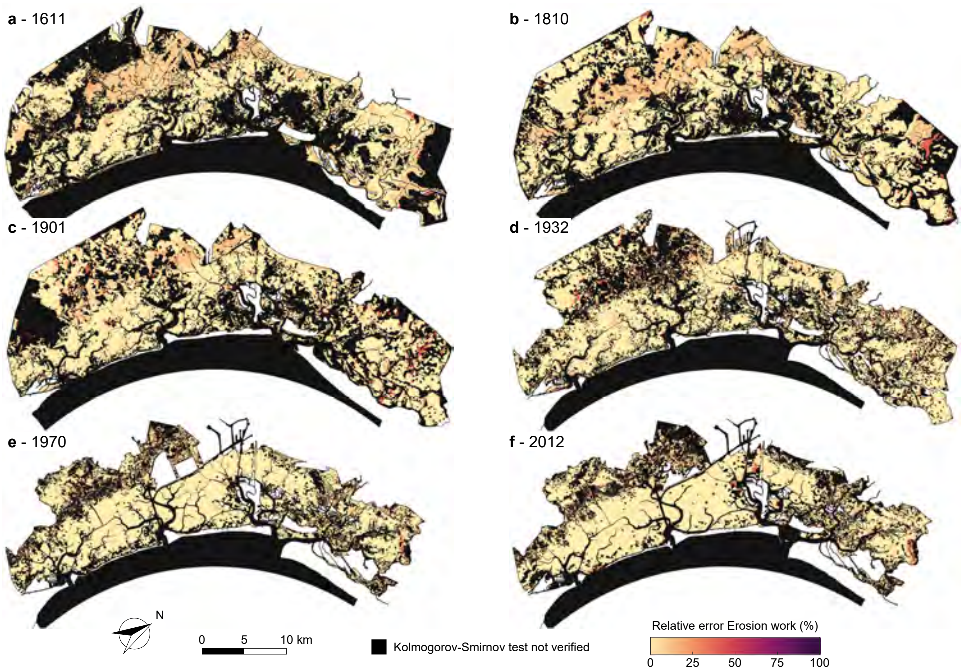


**Figure 2.19: Relative error of synthetic erosion work.** Spatial distribution of the relative error between the erosion work calculated with the integral formulation (Eq. 2.2) and synthetic (2.3) for the six different configurations of the Venice Lagoon: 1611 (**a**), 1810 (**b**), 1901 (**c**), 1932 (**d**), 1970 (**e**), and 2012 (**f**). Black identifies sites where the bottom shear stress cannot be modeled as a marked Poisson process (i.e. the KS test is not verified for the interarrival time).

# 3

# SEDIMENT TRANSPORT DYNAMICS IN SHALLOW TIDAL SYSTEMS

This chapter is a manuscript ready to be submitted for publication and focuses on the statistical characterization of sediment transport dynamics in shallow tidal systems. Suspended sediment dynamics influence numerous ecological and geomorphic processes that affect the morphological evolution of tidal environments. Transport of sediment in suspension is intimately related to resuspension dynamics, thus here we adopted the same approach used in Chapter 2 to analyse suspended sediment concentration time series in the same historical configurations of the Venice Lagoon. Despite the cause-effect relationship between erosion and suspended sediment transport, their dynamics are not identical because of the role of advection and dispersion processes affecting local sediment transport processes. Therefore, the results of this chapter are complementary to the analysis of erosion dynamics discussed in Chapter 2 and together complete the synthetic modeling framework aimed at describing the morphodynamic evolution of tidal systems on the long-term time scale.

## SEDIMENT TRANSPORT DYNAMICS IN THE VENICE LAGOON: A STATISTICAL CHARACTERIZATION OVER FOUR CENTURIES

**Davide Tognin[1,2], Luca Carniello[1,2], Luigi D'Alpaos[1], Andrea Rinaldo[1,2,4], and Andrea D'Alpaos[2,3]**

[1]Department of Civil, Environmental, and Architectural Engineering, University of Padova, Padova, Italy

[2]Center for Lagoon Hydrodynamics and Morphodynamics, University of Padova, Padova, Italy

[3]Department of Geosciences, University of Padova, Padova, Italy

[4] Laboratory of Ecohydrology ECHO/IEE/ENAC, Ècole Polytechnique Fèdèrale de Lausanne, Lausanne, Switzerland

### 3.1 ABSTRACT

Understanding suspended sediment dynamics is of fundamental importance to comprehend the long-term evolution of tidal environments. A complete spatial and temporal coverage of suspended sediment dynamics required to statistically characterize resuspension events are hardly available through observations alone, not even combining point measurements and satellite images, but it can be retrieved by calibrated and tested numerical models. Here we used a fully-coupled bi-dimensional numerical model to compute the spatial and temporal evolution of suspended sediment concentration induced by both wind waves and tidal currents on six historical configurations of the Venice Lagoon in the last four centuries. We analyzed computed one-year-long time series of suspended sediment concentration on the basis of the peak over threshold theory to obtain a statistically-based characterization of intense suspended sediment concentration (SSC) events. Our results suggest that SSC can be modeled as a marked Poisson process in the intertidal flats and subtidal platforms for all the considered historical configurations of the Venice Lagoon, since interarrival times of over-threshold events are exponen-

tially distributed. A poor correlation exists between interarrival times and both durations and intensities of over-threshold events, while intensity and duration are strongly correlated. Moreover, we find that statistical characteristics describing local erosion and over-threshold SSC events are highly related, although not identical because of the non-local dynamics of suspended sediment transport related to advection and dispersion processes. Thanks to this statistical characterization of SSC events, it is possible to generate synthetic, but realistic, time series of suspended sediment concentration for the long-term modeling of tidal environments.

## 3.2 INTRODUCTION

Suspended sediment dynamics in shallow tidal systems play a significant role as they influence geomorphic and ecological processes, that ultimately determine the long-term morphodynamic evolution of coastal, estuarine and lagoonal landscapes (Woodroffe, 2002; Masselink et al., 2014). Physical processes that drive sediment resuspension and transport in tidal environments are influenced by different hydrodynamic and sedimentological factors over a wide range of spatial and temporal scales.

Both tide and waves represent key drivers controlling sediment entrainment and transport in shallow tidal environments (Wang, 2012). The tide rise and fall generate currents that propagate along the preferential pathways provided by the channel network (Hughes, 2012) but, as the tide overspills on the adjoining intertidal flats, it is strongly affected by shallower water and friction effects (Friedrichs and Madsen, 1992), so that its velocity and, hence, its resuspension capacity can diminish considerably. On the other hand, wind waves with a typically short period can generate wave-orbital motions capable of resuspending intertidal-flat sediments (Anderson, 1972; Dyer et al., 2000; Carniello et al., 2005; Green, 2011). Therefore, stochastic wave-forced resuspension can increase locally, mainly under storm conditions, and can be particularly significant compared to the periodic resuspension by tidal currents (Sanford, 1994; Green et al., 1997; Ralston and Stacey, 2007). Wave-driven resuspension and erosion together with tide- and wave-driven sediment transport give rise to mechanisms leading to basin-wide sediment movement, which strongly shape the morphodynamic evolution of shallow tidal systems (e.g., Nichols and Boon, 1994; Green and Coco, 2007; Carniello et al., 2011; Green and Coco, 2014). The repeated cycles of erosion, resuspension and deposition, that sediments may undergo, winnow fine particles from coarser ones and, thus, modify sediment distribution and textural properties of intertidal flats and subtidal platforms, influencing physical and biological processes (Dyer, 1989), light climate (Moore and Wetzel, 2000) and ecosystem productivity (Lawson et al., 2007; Carr et al., 2010, 2016; McSweeney et al., 2017).

Moreover, resuspension dynamics are mutually linked to numerous biological and ecological processes (A. D'Alpaos et al., 2007; Kirwan and Murray, 2007; Temmerman et al., 2007; A. D'Alpaos et al., 2011; Marani et al., 2013). Benthic vegetation and algae play a key role in increasing sediment stability of subtidal platforms (e.g., Nepf, 1999; Venier et al., 2014; Tambroni et al., 2016). In fact, the interaction of flexible vegetation and bedforms can reduce the effective bed shear stress and, consequently, sediment mobility. Similarly, the action of halophytic vegetation over salt marshes has a significant impact on landscape development, enhancing accretion, both by directly trapping inorganic sediment and by producing organic matter (Da Lio et al., 2013; Marani et al., 2013; A. D'Alpaos and Marani, 2016). However, some studies have also suggested that, although vegetation anchors sediment through rooting and by slowing water flows, erosion and scour of the proximal sediments can also be enhanced (Temmerman et al., 2007; Tinoco and Coco, 2016). Microalgae, although small, may also heavily impact sediment erodability. Indeed, extracellular polymeric secretions (EPS) of microphytobenthos can increase grain adhesion and consequently erosion threshold of the sedimentary substrate (Le Hir et al., 2007; Parsons et al., 2016; Chen et al., 2019). As a result, sediment resuspension decreases in the presence of EPS, which affects light availability and, in turn, microalgae proliferation, thus triggering positive feedback (Pivato et al., 2019). Benthic fauna can further modify the bed sediment by changing its geotechnical properties and erosion resistance (Widdows and Brinsley, 2002; Vu et al., 2017).

Owing to the complexity of the underlying processes and the interplay between physical and biological drivers, sediment dynamics in shallow tidal systems are rather entangled. Therefore, observation-based approaches have been widely adopted to investigate the suspended sediment concentration (hereafter SSC), using either in situ point measurements (e.g., Wren et al., 2000; Gartner, 2004; Brand et al., 2020) or remote sensing and satellite image analysis (Ruhl et al., 2001; R. L. Miller and McKee, 2004; Volpe et al., 2011). However, both these techniques have some drawbacks. In situ measurements can provide an accurate description of the temporal dynamics of SSC, but lacks information on its spatial heterogeneity. Moreover, acoustic and optical sensors installed in point turbidity stations require periodic cleaning to prevent failure due to biofouling. Whereas, satellite-based data can supply instantaneous information on SSC spatial variability, but are barely informative on its temporal dynamics. Indeed, SSC events can hardly be fully captured by satellites with fixed and often long revisit periods. Furthermore, intense SSC typically occurs during severe storms, frequently characterized by clouds, which make satellite data useless. As a matter of fact, reliable long-term SSC time-series at basin scale, required for the statistical analysis performed herein, are seldom available.

In order to overcome these shortcomings and to exploit measurements of in situ point observations and satellite images, these data can be combined to calibrate and test numerical models (Ouillon et al., 2004; Carniello et al., 2014; Maciel et al., 2021), thereby, using them as physically-based "interpolators" to compute temporal and spatial SSC dynamics. However, computing SSC dynamics over time scales of centuries in order to model the morphodynamic evolution of tidal environments through fully-fledged numerical models is rather difficult owing to the computational burden involved. Therefore, modeling the long-term evolution of tidal systems requires simplified approaches (Murray, 2007).

Pointing to the development of a synthetic theoretical framework to represent intense SSC events and to account for their landscape-forming action on tidal basin morphology, we applied a two-dimensional finite element model to simulate the interaction among wind-waves, tidal current and sediment transport in several historical configurations of the Venice Lagoon. In particular, we used a previously-tested Wind Wave-Tidal Model (WWTM) (Carniello et al., 2005, 2011) coupled with a sediment transport model (Carniello et al., 2012) to investigate hydrodynamics and suspended sediment dynamics in the following six historical configurations of the Venice Lagoon: 1611, 1810, 1901, 1932, 1970, and 2012. For each of them, we run a one-year-long simulation forced with representative tidal and meteorological boundary conditions. The computed SSC time-series have been analyzed on the basis of the peak over threshold (POT) theory, following the approach introduced by A. D'Alpaos et al. (2013) and expanding the analysis performed by Carniello et al. (2016) to study the statistics of SSC in the present configuration of the Venice Lagoon.

This chapter aims to expand this analysis to other historical configurations of the Venice Lagoon in order to unravel the effects on sediment transport of the morphological and anthropogenic modifications experienced by the lagoon in the last four centuries and to test whether SSC dynamics can be modeled as a marked Poisson process also when accounting for the morphological evolution of the lagoon. The latter represents an interesting goal, being the use of stochastic frameworks particularly promising for long-term studies, as pointed out by their increasing popularity in hydrology and geomorphology to describe long-term behaviour of geophysical processes (e.g., Rodriguez-Iturbe et al., 1987; D'Odorico and Fagherazzi, 2003; Botter et al., 2013; Park et al., 2014; Bertassello et al., 2018). Nonetheless, applications to tidal systems are still quite uncommon (A. D'Alpaos et al., 2013; Carniello et al., 2016). Our analysis provides a spatial and temporal characterization of resuspension events for the Venice Lagoon from the beginning of the seventeenth century to present, in order to show how morphological modification affected sediment transport and to set a framework to forecast future scenarios.

## 3.3 MATERIAL AND METHODS

To study the influence of the morphological changes on suspended sediment dynamics, we considered six different historical configurations of the Venice lagoon, ranging from the beginning of the seventeenth century to today (Figure 3.1). The three ancient most configurations (i.e. 1611, 1810, and 1901) were remodeled relying on historical maps, whereas the topographic surveys carried out by the Venice Water Authority (Magistrato alle Acque di Venezia) in 1932, 1970, and 2003 were used for the more recent ones. Due to some morphological modifications at the three inlets associated with the Mo.S.E. project for the safeguard of the city of Venice from flooding (almost completed in 2012), the 2003 configuration was updated, so we will refer to this configuration as the 2012 configuration. For a detailed description of the methodology applied for the reconstruction of the historical configurations of the Venice Lagoon and additional information on the more recent bathymetric data, we refer the reader to Tommasini et al. (2019).

The morphology of the Venice Lagoon, which faces the Adriatic Sea along the northeastern coast of Italy, deeply changed through the last four centuries, especially owing to anthropogenic modifications. From the beginning of the fifteenth century, the main rivers (Brenta, Piave, and Sile) were gradually diverted in order to flow directly into the sea and prevent the lagoon from silting up. Later, during the last century, the inlets were provided with jetties and deep navigation channels were excavated to connect the inner harbour with the sea (L. D'Alpaos, 2010a; Sarretta et al., 2010). The jetties deeply changed the hydrodynamics at the inlets establishing an asymmetric hydrodynamic behaviour responsible for a net export of sediment

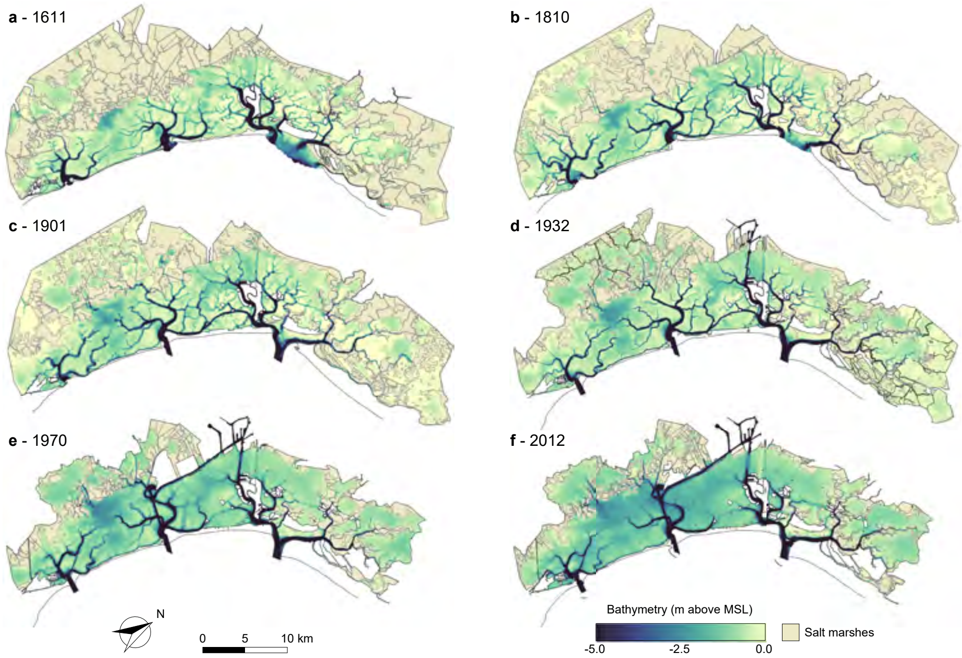


Figure 3.1: **Historical bathymetries of the Venice Lagoon.** Bathymetries of the six different configurations of the Venice Lagoon: 1611 (**a**), 1810 (**b**), 1901 (**c**), 1932 (**d**), 1970 (**e**), and 2012 (**f**).

toward the sea especially during severe storm events, able to resuspend large amounts of sediments (Carniello et al., 2012). In general, these modifications heavily influenced sediment transport triggering strong erosion processes that were further aggravated by sea-level rise. The net sediment loss clearly emerges from the morphological modifications of the Venice Lagoon, in particular, the generalized deepening of tidal flats and subtidal platforms as well as the reduction of salt-marsh area (Carniello et al., 2009). Indeed, in the last century, the average tidal-flat bottom elevation lowered from -0.51 m to -1.49 m above mean sea level (a.m.s.l.), while the salt-marsh area progressively shrank from 164.36 km$^2$ to 42.99 km$^2$ (Tommasini et al., 2019).

### 3.3.1 Numerical Model and Simulations

The flow field and sediment transport in the six configurations of the Venice Lagoon are computed by using a numerical model, consisting of three modules. The coupling of the hydrodynamic module with the wind-wave module (WWTM) describes the hydrodynamic flow field together with the generation and propagation of wind waves (Carniello et al., 2005, 2011), and the sediment transport and the bed evolution module (STABEM) evaluates the effect on the morphology (Carniello et al., 2012). All modules share the same computational grid.

The hydrodynamic module solves the 2-D shallow water equations using a semi-implicit staggered finite element method based on Galerkin's approach (Defina, 2000; Martini et al., 2004; L. D'Alpaos and Defina, 2007). The equations are suitably rewritten in order to deal with flooding and drying processes in morphologically irregular domains. The Strickler equation is used to evaluate the bottom shear stress induced by currents, $\tau_c$ , considering the case of turbulent flow over a rough wall. Further, the hydrodynamic module provides the flow field characteristic requested by the wind-wave module to simulate the generation and propagation of wind waves.

The wind-wave module (Carniello et al., 2011) solves the wave action conservation equation parametrized using the zero-order moment of the wave action spectrum in the frequency domain (Holthuijsen et al., 1989). The peak wave period is related to the local wind speed and water depth, and this empirical correlation function is used to determine the spatial and temporal distribution of the wave period (Young and Verhagen, 1996; Breugem and Holthuijsen, 2007; Carniello et al., 2011). The bottom shear stress induced by wind waves, $\tau_{ww}$, is computed as a function of the maximum horizontal orbital velocity at the bottom, which is related to the significant wave height through the linear theory. Owing to the non-linear interaction between the wave and current boundary layers, the maximum bottom shear stress, $\tau_{wc}$, is enhanced beyond the linear addition of the wave-alone and current-alone stresses: in the WWTM this is considered adopting the empirical formulation suggested by Soulsby (1995, 1997).

The sediment transport and bed evolution module (STABEM) is based on the solution of the advection-diffusion equation and Exner's equation (Carniello et al., 2012). This module uses two size classes of sediments to describe the bed composition (i.e. non-cohesive sand and cohesive mud), in order to consider the simultaneous presence of cohesive and non-cohesive sediment typically characterizing tidal lagoons (van Ledden et al., 2004). The local mud content, which varies both in space and time, marks off the transition between the cohesive and non-cohesive behaviour of a mixture, and, consequently, determines the critical value for bottom shear stress, based on the critical values assumed for pure sand and pure mud. However, this task is tough and site-specific, and, moreover, field data are often limited compared to the spatial variability of bed composition. To address this issue, field surveys in the Venice Lagoon have been used to identify an empirical relationship between the local bed composition and both the local bottom elevation and the distance from the inlets. We refer to Carniello et al. (2012) for further details.

Another peculiarity of the sediment transport module is the stochastic approach chosen to model the near-threshold conditions for sediment entrainment. Indeed, in shallow tidal basins, resuspension events are periodically driven by bottom shear stresses that slightly exceed the erosion threshold. The bottom shear stress, as well as the critical shear stress, is very unsteady owing to the non-uniform flow velocity, wave characteristics and small-scale bottom topography. Hence, following the stochastic approach suggested by Grass (1970), both the total bottom shear stress, $\tau_{wc}$, and the critical shear stress for erosion, $\tau_c$, are treated as random variables ($\tau'_{wc}$, and $\tau'_c$, respectively) with lognormal distributions, and their expected values are those calculated by WWTM and STABEM. Consequently, the erosion rate depends on the probability that $\tau_{wc}$, exceeds $\tau'_c$.

This numerical model was used to perform one-year-long simulations within the six different computational grids representing the historical configuration of the Venice Lagoon and the portion of the Adriatic Sea in front of it. Hourly tidal level gauged at the Consiglio Nazionale delle Ricerche (CNR) Oceanographic Platform, located in the Adriatic Sea offshore of the lagoon, and wind velocities and directions recorded at the Chioggia anemometric station are imposed as boundary conditions (Figure 2.1a).

All configurations are forced with the time records of tidal level and wind velocity and directions measured during the whole year 2005, as this year was selected as a representative year, being the probability distribution of wind speed at the Chioggia Station in 2005 the closest to the mean annual probability distribution in the period 2000-2020 (Figure 2.1b). Forcing all the historical configurations of the Venice Lagoon with the same wind and tidal conditions enables us to pinpoint the effects of the morphological modifications on the wind-wave field, hydrodynamics and sediment dynamics.

### 3.3.2 Peak Over Threshold Analysis

Sediment transport dynamics in tidal environments are the results of the complex interplay between hydrodynamic, biologic, and geomorphologic processes. This interplay between different factors can be fully framed only by taking into account both its deterministic and stochastic components. As an example, Carniello et al. (2011) argued that morphological dynamics in the Venice Lagoon is mostly linked to a few severe resuspension events induced by wind waves, whose dynamics are markedly stochastic in the present configurations (A. D'Alpaos et al., 2013; Venier et al., 2014; Carniello et al., 2016). In the present work, we used the peak over threshold theory (POT) (Balkema and Haan, 1974) to analyze temporal and spatial dynamics of the total SSC at any location within each configuration of the Venice lagoon. First, a minimum-intensity threshold, $C_0$, is chosen to identify the set of events from the modeled SSC record, then a statistical analysis of interarrival times, durations and intensities of the exceedances of the threshold is carried out. The interarrival time is defined as the time between two consecutive upcrossings of the threshold, the duration of the events is the time elapsed between any upcrossing and the subsequent downcrossing of the threshold, and, finally, the intensity is calculated as the largest exceedance of the threshold in the time-lapse between an upcrossing and the subsequent downcrossing. These three variables are characterized by means of their probability density functions and the corresponding moments for any location in all the considered configurations of the Venice Lagoon, in order to provide a complete description of the SSC pattern. The nature of the stochastic processes can be determined by the analysis of the interarrival times distribution. Indeed, resuspension events can be mathematically modeled as a marked Poisson process if the interarrival times between subsequent exceedances of the threshold, $C_0$, are independent and exponentially distributed random variables. In order to assess that over-treshold SSC events can be modeled as a Poisson process, we performed the Kolmogorov-Smirnov (KS) goodness of fit test on interarrival times distribution. In our case, the sequence of random events that define a 1-D Poisson process along the time axis is associated with a vector of random marks that defines the duration and intensity of each over-threshold event. Memorylessness is one of the most interesting features of Poisson processes because it states that the number of events observed in disjoint subperiods is an independent, Poisson-distributed random variable. According to the extreme value theory, a Poisson process emerges from a stochastic signal whenever enough high censoring threshold is chosen (Cramér and Leadbetter, 1967). However, as this present analysis is designed to remove only the weak resuspension events induced by periodic tidal currents, the critical threshold is well below the maximum observed values. As a consequence, the aim of the proposed analysis is to characterize the bulk effect of morphologically meaningful SSC events, rather than to describe the extreme events.

Notwithstanding the increasing popularity of Poisson processes for the analytical modeling of the long-term evolution of geophysical processes controlled by stochastic drivers in hydrological and geomorphological sciences (e.g., Rodriguez-Iturbe et al., 1987; D'Odorico and Fagherazzi, 2003; Botter et al., 2013; Park et al., 2014; Bertassello et al., 2018), only in the last few years this approach has been adopted for tidal systems (A. D'Alpaos et al., 2013; Carniello et al., 2016) and the applications portray an encouraging framework.

## 3.4 RESULTS AND DISCUSSION

The statistical characterization of suspended sediment dynamics is provided through the analysis of the one-year-long time series of the computed SSC on the basis of the POT method. The choice of the threshold value, $C_0$, that identifies significant over-threshold SSC events, has to consider two contrary requirements. On the one hand, stochastic sediment concentration generated by storm-induced wind waves can be distinguished from tide-modulated daily concentration only if $C_0$ is large enough. On the other hand, too high values of $C_0$ can lead to a non-informative analysis, being several events neglected. In the following, we used a constant threshold, $C_0$, equal to $40\,\mathrm{mg\,l^{-1}}$, as suggested by Carniello et al. (2016), performing a sensitivity analysis for the statistical analysis of SSC events in the present configuration of the Venice Lagoon. As a first step, the SSC time series provided by the numerical simulations were low-pass filtered by applying a moving average procedure with a time window of 6 hours, in order to preserve the tide-induced modulation of the signal but, at the same time, removing artificial upcrossing and downcrossing of the threshold, generated by short-term fluctuations. We replicate the analysis for all the points within the computational domain of each configuration and obtain the spatial distribution of the mean interarrival times (Figure 3.2), mean intensities of peak excesses (Figure 3.3), and mean durations (Figure 3.4) of over-threshold resuspension events.

SSC dynamics at any location are affected by local entrainment and advection/dispersion processes from and toward the surrounding areas. Furthermore, the local resuspension is highly influenced by the combined effect of tidal currents and wind waves, thus de-

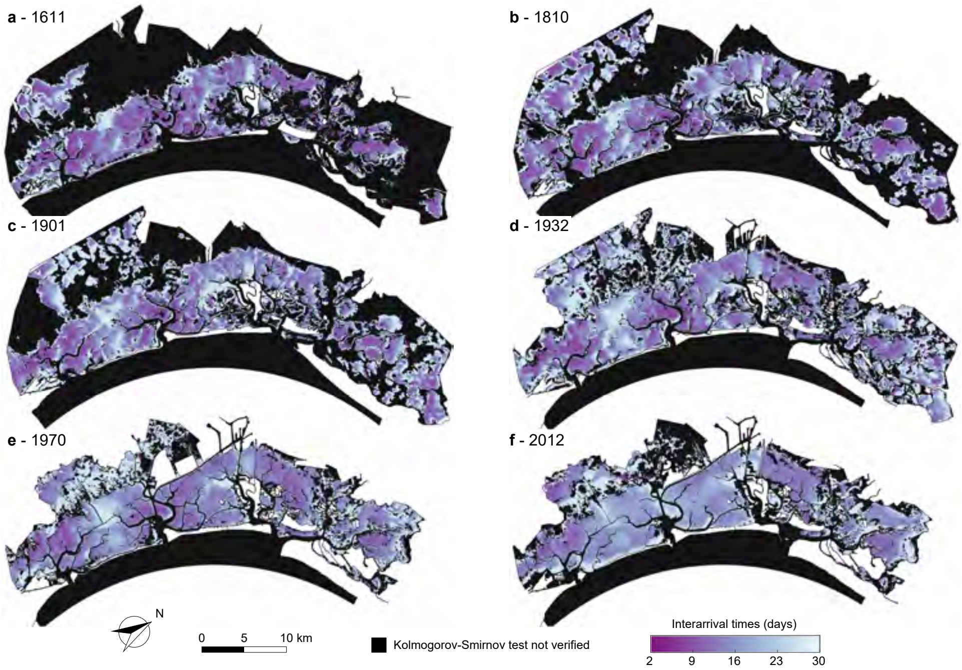


Figure 3.2: **Mean interarrival time of overthreshold SSC events.** Spatial distribution of mean interarrival times of over threshold exceedances, at sites where SSC events can be modeled as a marked Poisson process, as confirmed by the KS test ($\alpha = 0.05$) for the six different configurations of the Venice Lagoon: 1611 (**a**), 1810 (**b**), 1901 (**c**), 1932 (**d**), 1970 (**e**), and 2012 (**f**).

pending on current velocity, water depth, fetch, wind intensity and duration (Fagherazzi and Wiberg, 2009; Carniello et al., 2016). As a consequence, the mean values of the random variables characterizing resuspension events present highly heterogeneous spatial patterns in the more ancient configurations due to their morphological complexity.

Another important issue to consider when studying SSC dynamics in shallow tidal environments is the presence of benthic and halophytic vegetation, which both shelters the bed against the hydrodynamic action and increases the local critical shear stress for erosion because of the presence of roots. While the presence of halophytic vegetation over salt marshes is almost ubiquitous, reconstructing the presence of benthic vegetation on the tidal flats is much more difficult even for the present configuration of the lagoon and practically

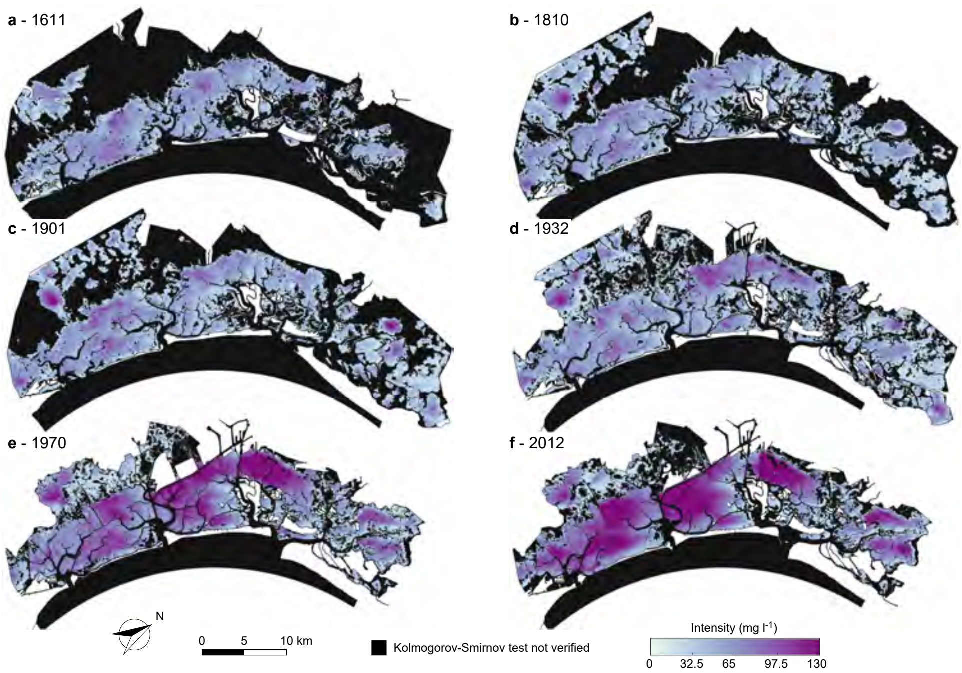


Figure 3.3: **Mean intensity of overthreshold SSC events.** Spatial distribution of mean intensity of peak excesses of over threshold exceedances, at sites where SSC events can be modeled as a marked Poisson process, as confirmed by the KS test ($\alpha = 0.05$) for the six different configurations of the Venice Lagoon: 1611 (**a**), 1810 (**b**), 1901 (**c**), 1932 (**d**), 1970 (**e**), and 2012 (**f**).

impossible for the ancient configurations (Goodwin et al., 2021). For the above reasons and for the sake of homogeneity, the simulations of the present study neglect the presence of benthic vegetation on the tidal flat and assume all salt-marsh platform to be completely vegetated in each configuration of the lagoon, thus neglecting sediment resuspension over them (Christiansen et al., 2000; Temmerman et al., 2005a).

The spatial distribution of mean interarrival times, peak excesses and durations are shown at any location within each of the six historical configurations where SSC events can be modeled as a Poisson process (i.e., the KS test is verified for interarrival times at significance level $\alpha = 0.05$). The results of the KS test, performed for each element of the domains, are shown in Figure 3.5. In particular, we can identify three different situations:

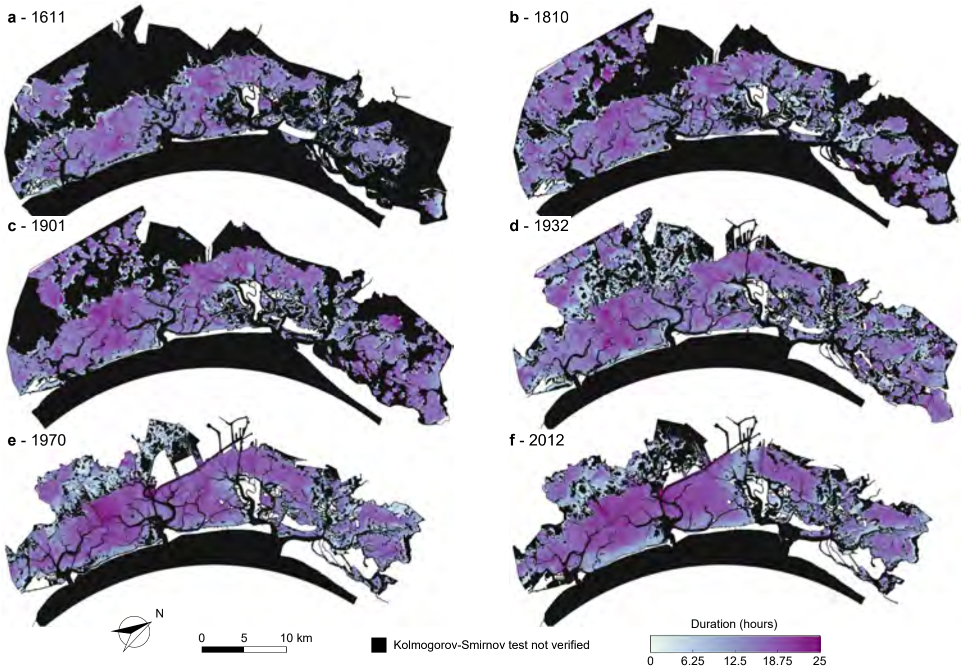


Figure 3.4: **Mean durations of overthreshold SSC events.** Spatial distribution of mean durations of over threshold exceedances, at sites where SSC events can be modeled as a marked Poisson process, as confirmed by the KS test ($\alpha = 0.05$) for the six different configurations of the Venice Lagoon: 1611 (**a**), 1810 (**b**), 1901 (**c**), 1932 (**d**), 1970 (**e**), and 2012 (**f**).

i. SSC events cannot be described as a Poisson process, i.e. the KS test is not satisfied for interarrival times, in the dark blue areas;

ii. SSC events are indeed a marked Poisson process, because interarrival times, peak excesses and durations satisfy the KS test, and, thus, are exponentially distributed random variables, in the red areas;

iii. SSC events still are a marked Poisson process but at least one between intensity and duration does not satisfy the KS test, i.e. although interarrival times follow an exponential distribution, at least one between intensity and duration does not, in the yellow areas.

Similarly to the results for erosion events (BSS) presented in Chapter 2, the area of the lagoon where over-thresholds SSC events cannot

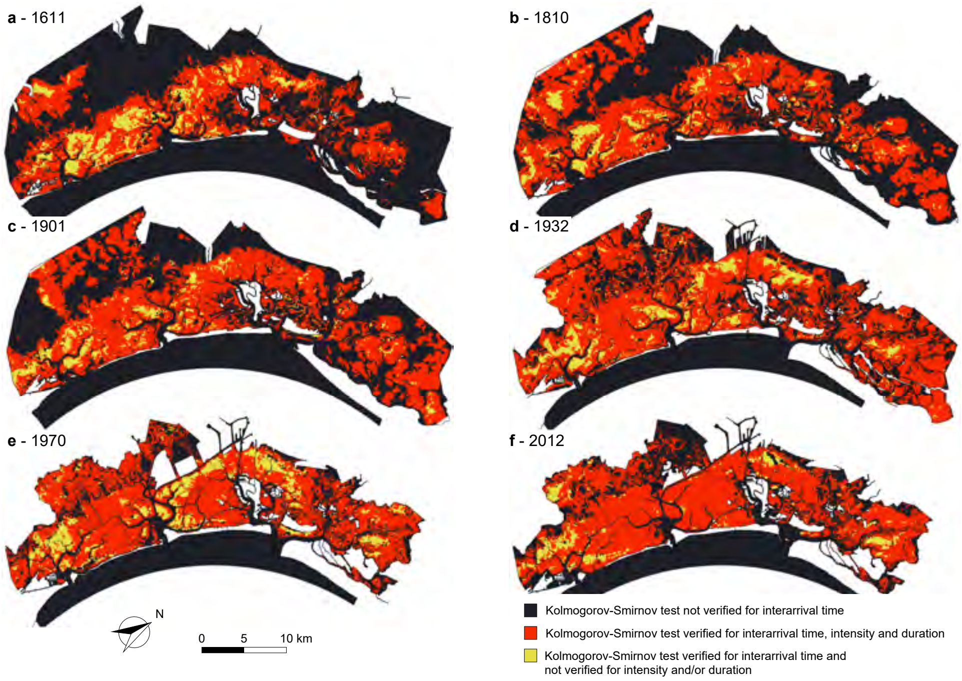


Figure 3.5: **Kolmogorov-Smirnov test for overthreshold SSC events.** Spatial distribution of Kolmogorov-Smirnov (KS) test at significance level ($\alpha = 0.05$) for the six different configurations of the Venice Lagoon: 1611 (**a**), 1810 (**b**), 1901 (**c**), 1932 (**d**), 1970 (**e**), and 2012 (**f**). In the maps we can distinguish areas where the KS test is: not verified (dark blue); verified for all the considered stochastic variables (interarrival time, intensity over the threshold and duration) (red); verified for the interarrival time and not for intensity and/or duration (yellow).

be modeled as Poisson processes are mostly represented by salt marshes and tidal channels in all configurations (see dark blue areas in Figure 3.5). On salt-marsh areas, both BSS and SSC thresholds ($\tau_C$ and $C_0$ respectively) are seldom exceeded (Figure 2.9 and 3.7), because the reduced water depth over the marsh prevents the propagation of large wind waves and the presence of halophytic vegetation limits sediment advection by promoting deposition and stabilizes the bottom preventing erosion (e.g., Möller et al., 1999; Carniello et al., 2005; Temmerman et al., 2005a). Within the main tidal channels and at the three inlets, as happens for BSS, SSC dynamics are not Poissonian, but the reason why interarrival times of erosion and resuspension events are not exponentially distributed are slightly different. In the main channel network and at the inlets, SSC exceeds the threshold value, $C_0$, very few times or it does not exceed the threshold at all, due to vertical dispersion mechanisms that decrease the local concentration of sediment in suspension in deeper areas (Figure 3.7). Conversely, BSS typically exceeds the threshold $\tau_c$ twice or four time a day mainly because of the tide action (Figure 2.15,2.16 and 2.17), which cannot be modeled as a stochastic process (Figure 2.9), as confirmed by the KS test on interarrival times of over-threshold BSS events.

However, SSC events can be modeled as a Poisson process over wide areas of the six configurations of the Venice Lagoon, in particular over tidal flats and subtidal platforms (see red and yellow areas in Figure 3.5). As a consequence, SSC dynamics can be effectively modeled by using a synthetic framework based on Poisson processes over widespread portions of the different morphological configurations experienced by the Venice Lagoon in the last four centuries.

Large interarrival times (i.e., larger than 30 days, Figure 3.2) are observed on tidal flats close to the main channel network because dilution processes within higher water depth, enhanced by the higher velocities in these sites, reduce sediment concentration, and hence only severe, but infrequent, events can lead to an exceedance of the threshold. Sheltered areas are also characterized by large interarrival times as represented by the northern portion of the lagoon, which is protected by the mainland from the north-easterly Bora wind, which is the most intense and morphologically significant wind in the Venice Lagoon (Figure 2.1b), and where the presence of extensive salt-marsh areas continuously interrupt the propagation of wind waves. In this case, the reduced number of upcrossing events, and, consequently, for large interarrival times is due to the protective action of salt marshes and islands in reducing wind-wave resuspension action. SSC events over the marsh platform slightly changed through centuries. In the three oldest configurations (i.e., 1611, 1810 and 1901) mainly because of the wide extent of salt marshes, resuspension events over salt marshes do not even reach the threshold, as shown by the number of upcrossing (Figure 3.7). In the more recent ones, where salt-marsh extent importanly decreases, marshes start experiencing some over-threshold SSC events because of advection of sediment from the adjacent areas, but the lower number of upcrossing let the mean interarrival time assume large values.

Over wide tidal flat areas, where the threshold is exceeded in all the considered configurations, the mean interarrival time generally slightly increases through centuries (Figure 3.8a). This trend is more evident in the central and southern parts of the lagoon, where, because of the deepening experienced in the last century, the number of events able to resuspend sediments from the bottom decreased, hence increasing the mean interarrival time of significant SSC events. In fact, over the central-southern shallow tidal flats of the four ancient most configurations, interarrival times present relatively low values (about 10 days), meanwhile they generally become longer (between 20 and 25 days) on the same areas in the more recent configurations. On the contrary, in the well-preserved, northern portion of the lagoon, where the fetch is continuously interrupted by islands, spits, and salt marshes also in the more recent configurations, the mean interarrival times barely changed through centuries. As an example, Figure 3.6a shows the mean interarrival times experienced by the "Palude Maggiore" tidal flat (station S1 in Figure 2.1a). Interestingly, the subtidal flat at the watershed divide between the Chioggia and Malamocco inlets, known as “Fondo dei Sette Morti” (station S2 in Figure 2.1a), display decreasing interarrival times through centuries (Figure 3.6d). In the more ancient configurations, thanks to its relatively lower depth and its position sheltered by shallower tidal flats, "Fondo dei Sette Morti" experienced over-threshold events only during severe events. In the more recent configurations, over-threshold events become more frequent due to the deepening of the surrounding tidal flats, thus allowing larger waves to propagate in this area and enhancing resuspension.

The intensity of over-threshold events abruptly increases between 1932 and 1970 (Figure 3.3 and 3.8b). Indeed, SSC exceedance intensity maintains low mean values, generally below $60\,\mathrm{mg\,l^{-1}}$, in all the

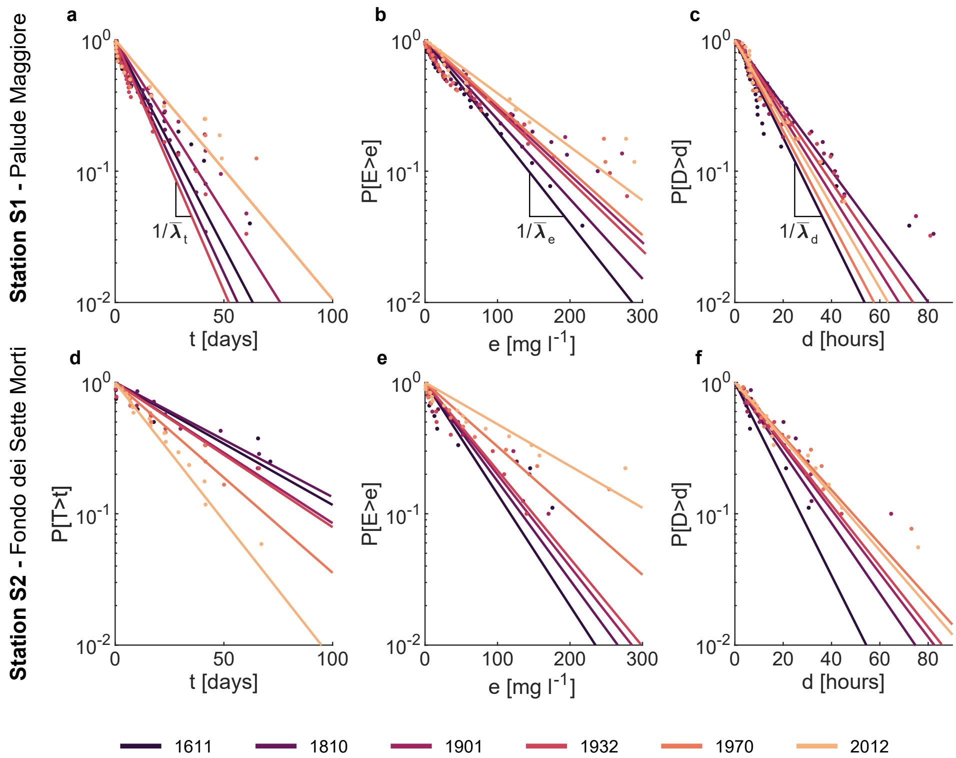


**Figure 3.6: Overthreshold SSC events at stations S1 and S2.** Statistical characterizations of over threshold events at two stations S1 "Palude Maggiore" and S2 "Fondo dei Sette Morti" (see Figure 2.1a for locations) in the six configurations of the Venice Lagoon. Probability distributions of (**a-b**) interarrival times, $t$; (**c-d**) intensities of peak excesses of over threshold exceedances, $e$; and (**e-f**) durations of over threshold event, $d$. $\overline{\lambda}_t$ mean interarrival time, $\overline{\lambda}_e$ mean peak excess intensity, and $\overline{\lambda}_d$ mean duration.

configurations until 1932, thereafter it doubles on wide tidal flat areas, especially in the central-southern lagoon and northwest of the city of Venice, where the action of wind waves can be stronger. The punctual analysis confirms that intensity increase is much more important in the central lagoon (station S2, Figure 3.6e) rather than in the northern part (station S1, Figure 3.6b).

Overall, over-threshold event durations slightly increase through centuries (Figure 3.4 and 3.8c). However, two different trends can be distinguished in different portions of the lagoon, likewise interarrival times and intensities. The duration increase in the pristine, northern portion of the basin is much lower than in the central and southern lagoon due to the heavier morphological modifications these areas experienced (Figure 3.6c and f).

The temporal cross-correlation between interarrival times, durations and intensities computed for each point within the six configurations of the Venice Lagoon confirms the results obtained for the 2012 configuration (Figure 3.9,3.10 and 3.11). Duration of over threshold exceedances and intensity of peak excesses are highly correlated in all the six considered configurations, suggesting that longer events are linked to more intense ones (Figure 3.9 and 3.12a). Contrarily, durations and interarrival times, as well as intensities and interarrival times display almost no correlation (Figure 3.10, 3.11 and 3.12b,c). These relations between interarrival time, intensity and duration back up the idea that, as for BSS dynamics (Chapter 2), over-threshold SSC events can be modeled as a 3-D Poisson process in which the marks (intensity and duration of over threshold events) are mutually dependent but independent on interarrival times.

As a result of the cause-effect relationship between the BSS (cause) and SSC (effect), their spatial and temporal dynamics show a high cross-correlation between interarrival times (Figure 3.13), intensity (Figure 3.14) and duration (Figure 3.15) of BSS and SSC over-threshold events. Remebering the absence of correlation between interarrival times and both intensities and durations for both BSS and SSC events, we can conclude that, when generating synthetic time series, interarrival times of BSS and SSC events are mutually dependent but not related to their intensity and duration. Intensities and durations of SSC are instead strongly correlated with the corresponding properties of BSS events.

Despite showing high similarity and correlation, erosion and resuspension events are not identical. The BSS ultimately depends on the local hydrodynamics (tidal currents and wind waves). On the contrary, the SSC is not only a function of the local entrainment but also of the suspended sediment flux from and towards the surrounding areas. As a result of the advection/dispersion processes, the spatial pattern of SSC is smoother than that of BSS.

The statistical characterization of overthreshold SSC events using their mean interarrival times, intensity and duration can be useful to estimate the total amount of reworked sediments. Although different portions of the lagoon experience different trends in these parameters depending on specific morphological modifications, a spatial average over the whole area where overthreshold SSC events can be described as Poisson processes shows that globally mean interarrival times and duration remain almost constant and equal to about 30 days and 13 hours, respectively (Figure 3.8a and c). By contrast, intensity of the peak excess abruptly changes between 1932 and 1970. Between 1611 and 1932 the mean intensity maintains a value lower than 45 $\mathrm{mg\,l^{-1}}$, but increases to 64 $\mathrm{mg\,l^{-1}}$ in 1970 and further to 73 $\mathrm{mg\,l^{-1}}$ in 2012 (Figure 3.8b).

This increase in the intensity of overthreshold SSC events, together with the generalized deepening of the tidal flat area, generates an increase in the amount of reworked sediments. This means that on average every month, for 13 hours, the amount of sediment mobilized within the basin increases from about $2 \cdot 10^6$ kg in the three most ancient configurations to more than $6.8 \cdot 10^6$ kg in the 2012 configuration (Table 3.1). Besides directly boosting the amount of sediment available for export toward the open sea given the ebb-dominated character of the Venice Lagoon (Ferrarin et al., 2015; Finotello et al., 2019), the increase of suspended sediment also affects numerous biological and ecological processes that in turns influence the morphological evolution of the tidal system (Venier et al., 2014; Pivato et al., 2019).

Modeling the morphodynamic evolution of tidal landscapes over long timescales (decades or centuries) necessarily requires the use of simplified approaches. However, the classical assumption of long-term evolution models is that the sediment supply is constant or monotonically related to mean water depth. The results presented in this chapter, together with those obtained in Chapter 2 on erosion events, demonstrate that the time series of both BSS and SSC can be described as marked Poisson processes with exponentially dis-

Table 3.1: **Sediment reworking in the historical configurations of the Venice Lagoon.** *area* ($km^2$): area of the lagoon where KS is verified; $h$ (m): mean water depth of the area; $V_w$ ($10^6$ $m^3$): mean volume of water, obtained as product of area and water depth; $e$ (mg $l^{-1}$): mean intensity of overthreshold SSC events; $S_{mob}$ ($10^6$ kg): sediment mobilized, assuming a triangular-shaped temporal evolution of overthreshold SSC events, with peak excess $e$.

| Year | area ($km^2$) | h (m) | $V_w$ ($10^6$ $m^3$) | $e$ (mg $l^{-1}$) | $S_{mob}$ ($10^6$ kg) |
|---|---|---|---|---|---|
| 1611 | 226.882 | 0.59 | 134.403 | 44.20 | 1.980 |
| 1810 | 294.649 | 0.43 | 127.022 | 40.84 | 1.729 |
| 1901 | 307.951 | 0.47 | 143.985 | 42.66 | 2.047 |
| 1932 | 350.166 | 0.54 | 188.661 | 43.49 | 2.734 |
| 1970 | 283.196 | 0.77 | 217.863 | 64.16 | 4.659 |
| 2012 | 270.022 | 1.04 | 279.969 | 73.21 | 6.832 |

tributed interarrival times, intensities, and durations, thereby setting a framework for the synthetic generation of statistically significant external forcing factors (shear stress at the bottom and suspended sediment available in the water column) that should improve the reliability of long-term biomorphodynamic models with a limited increase in the number of parameters.

## 3.5 CONCLUSIONS

SSC dynamics in shallow tidal environments are usually investigated by means of field measurements or remote sensing analysis. However, due to the limited spatial and temporal resolution of measurements and satellite images respectively, long-term SSC dynamics at basin scale are seldom available. Numerical models, once properly calibrated and tested, can provide reliable long SSC time series which can be used to statistically characterize the spatial and temporal variability of intense SSC events.

In the present study, we applied a custom-built, extensively tested, 2-D finite-element numerical model to reproduce SSC dynamics at basin scale in six historical configurations of the Venice Lagoon, covering a time span of four centuries. The computed SSC time series were analysed on the basis of the Peak Over Threshold theory. Statistical analyses suggest that over-threshold SSC events can be modelled as a marked Poisson process over wide areas of all the selected configurations of the Venice Lagoon.

Due to the morphological evolution experienced by the lagoon in the last four centuries, mean interarrival time, intensity and duration of over-threshold events generally increase through centuries, generating less frequent, but stronger and longer, resuspension events.

Furthermore, almost no correlation exists between durations and interarrival times of over-threshold exceedances and between intensities and interarrival times, whereas the intensity of peak excesses and duration are highly correlated. This confirms that resuspension events can be modeled as a 3-D marked Poisson process with marks (intensity and duration) mutually dependent but independent on the interarrival times in all the historical configurations of the Venice Lagoon. Moreover, a comparison with the analysis of over-threshold BSS events shows that interarrival times, intensities and durations of both BSS and SSC events are mutually related.

These findings provide the basis to develop a theoretical framework for generating synthetic, but statistically realistic, forcings to be used in the long-term morphodynamic modeling of shallow tidal environments.

## 3.6 SUPPORTING INFORMATION

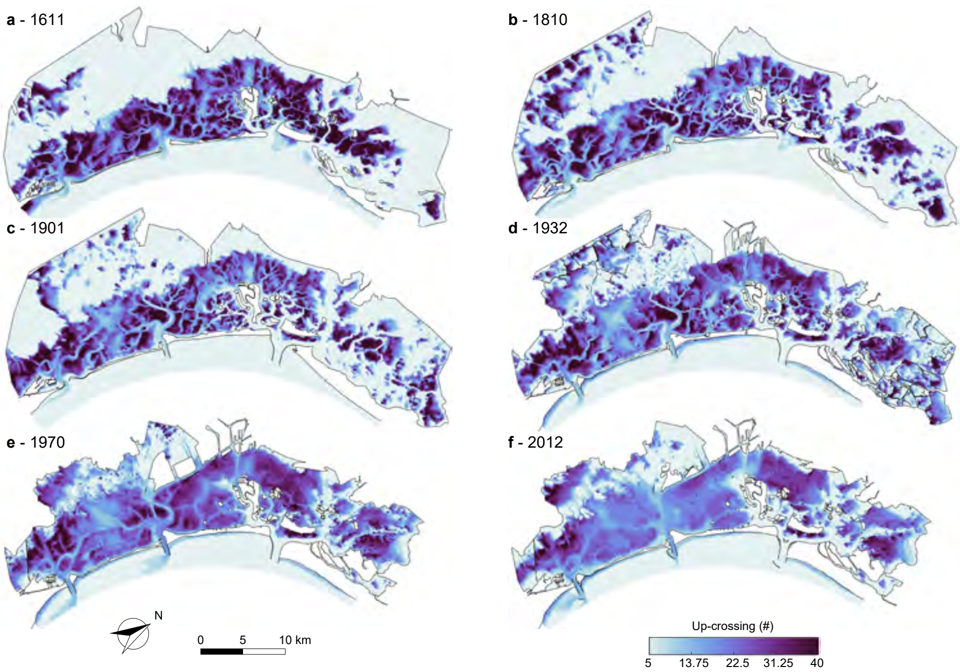


**Figure 3.7: Number of upcrossings of the SSC threshold.** Spatial distribution of the number of upcrossing of the threshold for suspended sediment concentration $C_0 = 40$ mg $l^{-1}$, for the six different configurations of the Venice Lagoon: 1611 (**a**), 1810 (**b**), 1901 (**c**), 1932 (**d**), 1970 (**e**), and 2012 (**f**).

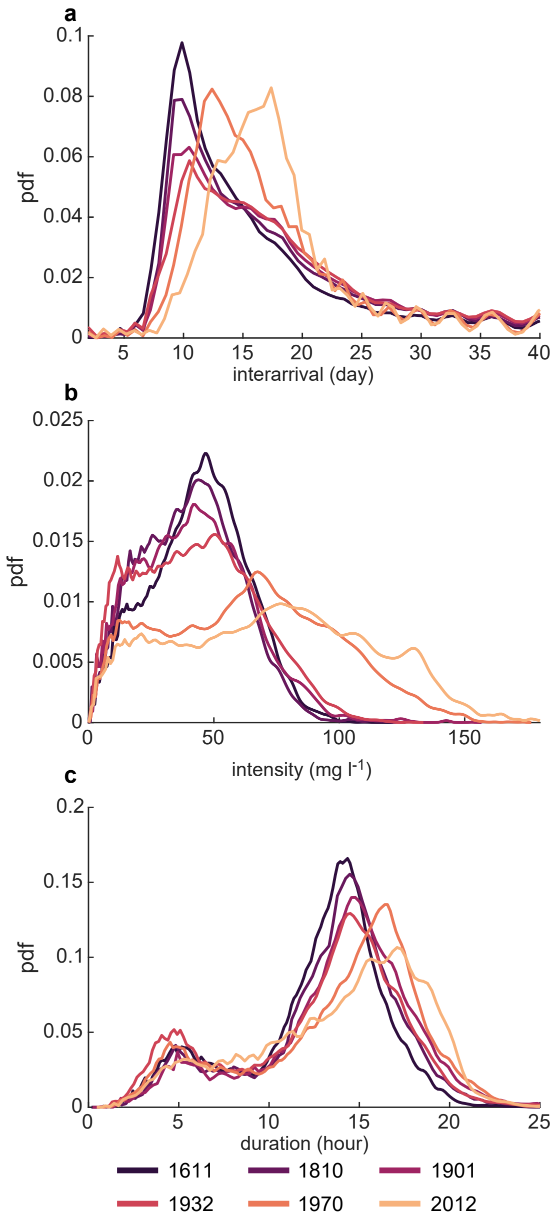


| Year | $t$ [day] (mean ± std) | (median) |
|---|---|---|
| 1611 | 27.49 ± 36.45 | 14.96 |
| 1810 | 29.35 ± 36.32 | 16.47 |
| 1901 | 32.47 ± 40.30 | 17.93 |
| 1932 | 33.59 ± 41.09 | 18.31 |
| 1970 | 27.87 ± 32.87 | 16.47 |
| 2012 | 29.24 ± 32.25 | 17.95 |

| Year | $e$ [mg l$^{-1}$] (mean ± std) | (median) |
|---|---|---|
| 1611 | 44.20 ± 19.00 | 44.99 |
| 1810 | 40.84 ± 19.17 | 41.05 |
| 1901 | 42.66 ± 21.80 | 41.96 |
| 1932 | 43.49 ± 23.36 | 42.95 |
| 1970 | 64.16 ± 33.86 | 65.02 |
| 2012 | 73.21 ± 38.85 | 74.68 |

| Year | $d$ [hour] (mean ± std) | (median) |
|---|---|---|
| 1611 | 12.58 ± 3.91 | 13.50 |
| 1810 | 13.23 ± 4.12 | 14.02 |
| 1901 | 13.78 ± 4.27 | 14.46 |
| 1932 | 12.71 ± 4.71 | 13.85 |
| 1970 | 13.76 ± 4.73 | 14.98 |
| 2012 | 13.96 ± 4.70 | 14.96 |

Figure 3.8: **Spatial probability density function of interarrival time, intensity and duration of SSC overthreshold events.** Probability density function (left), mean (mean ± standard deviation) and median value (right) of interarrival times $t$ (**a**), intensity $e$ (**b**) and duration $d$ (**c**) of SSC overthreshold events.

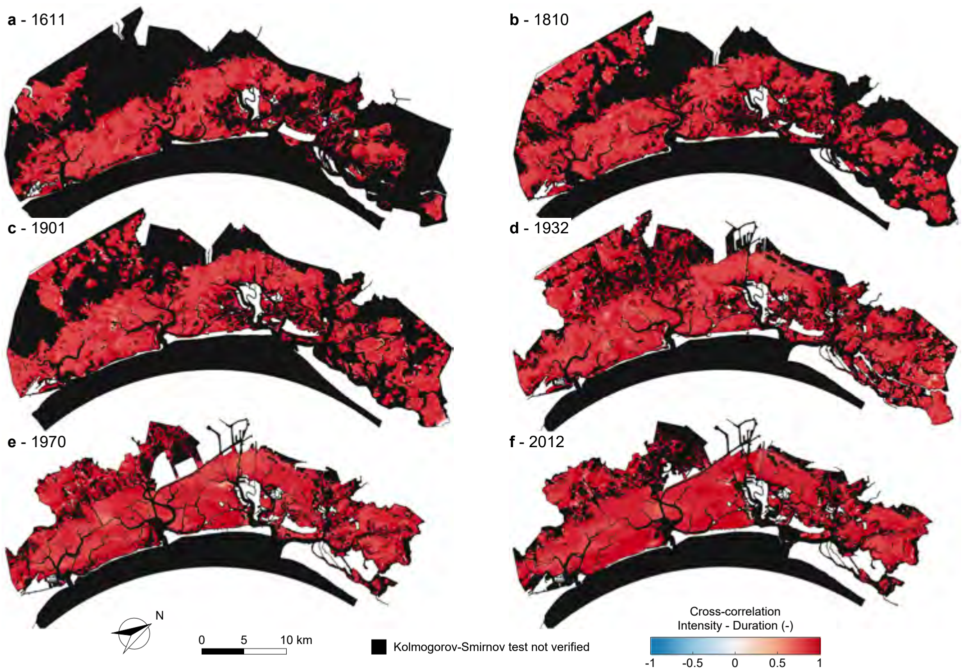


Figure 3.9: **Cross-correlation between intensity and duration overthreshold SSC events.** Spatial distribution of temporal cross-correlation between intensity of peak-excesses and duration of over threshold exceedances for the six different configurations of the Venice Lagoon: 1611 (**a**), 1810 (**b**), 1901 (**c**), 1932 (**d**), 1970 (**e**), and 2012 (**f**). Black identifies sites where overthreshold SSC events cannot be modeled as a marked Poisson process (i.e. the KS test is not verified for the interarrival time).

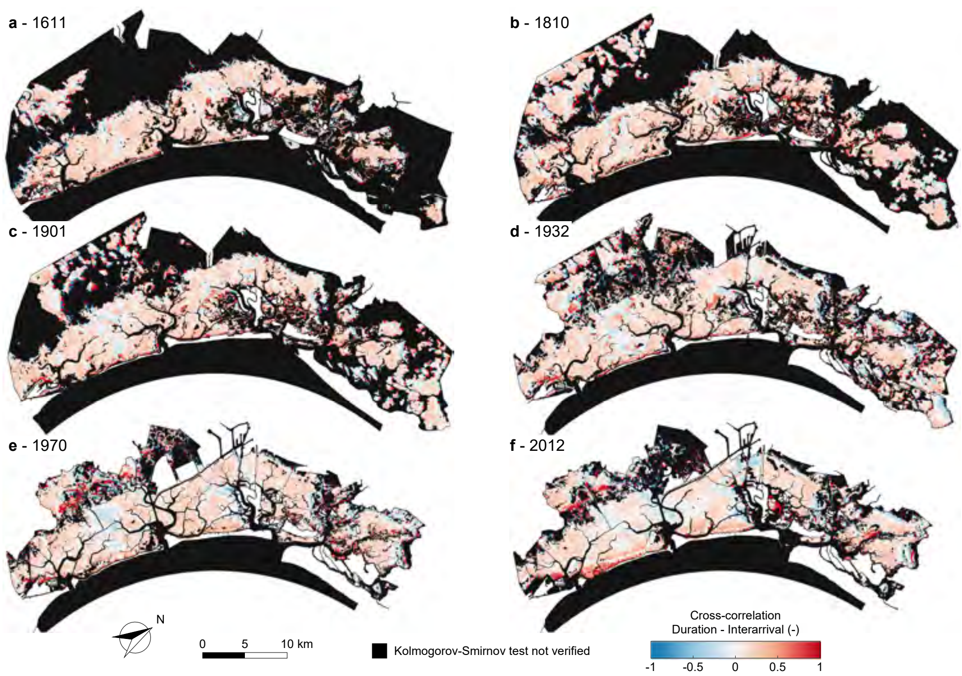


Figure 3.10: **Cross-correlation between duration and interarrival times overthreshold SSC events.** Spatial distribution of temporal cross-correlation between duration and interarrival times of over threshold exceedances for the six different configurations of the Venice Lagoon: 1611 (**a**), 1810 (**b**), 1901 (**c**), 1932 (**d**), 1970 (**e**), and 2012 (**f**). Black identifies sites where overthreshold SSC events cannot be modeled as a marked Poisson process (i.e. the KS test is not verified for the interarrival time).

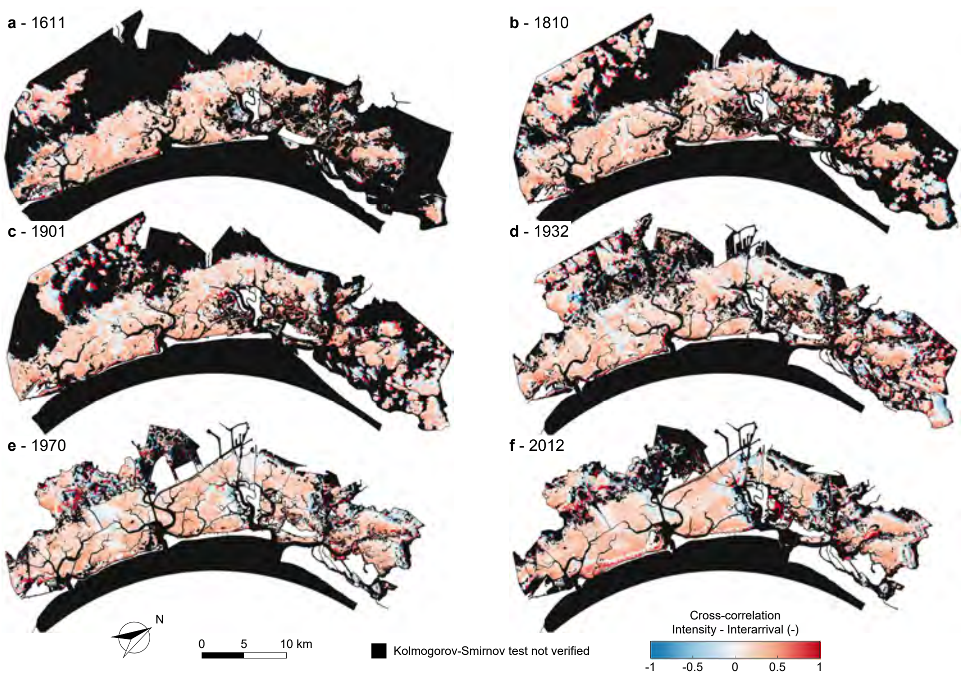


Figure 3.11: **Cross-correlation between intensity and interarrival times of overthreshold SSC events.** Spatial distribution of temporal cross-correlation between intensity of peak-excesses and interarrival times of over threshold exceedances for the six different configurations of the Venice Lagoon: 1611 (**a**), 1810 (**b**), 1901 (**c**), 1932 (**d**), 1970 (**e**), and 2012 (**f**). Black identifies sites where overthreshold SSC events cannot be modeled as a marked Poisson process (i.e. the KS test is not verified for the interarrival time).

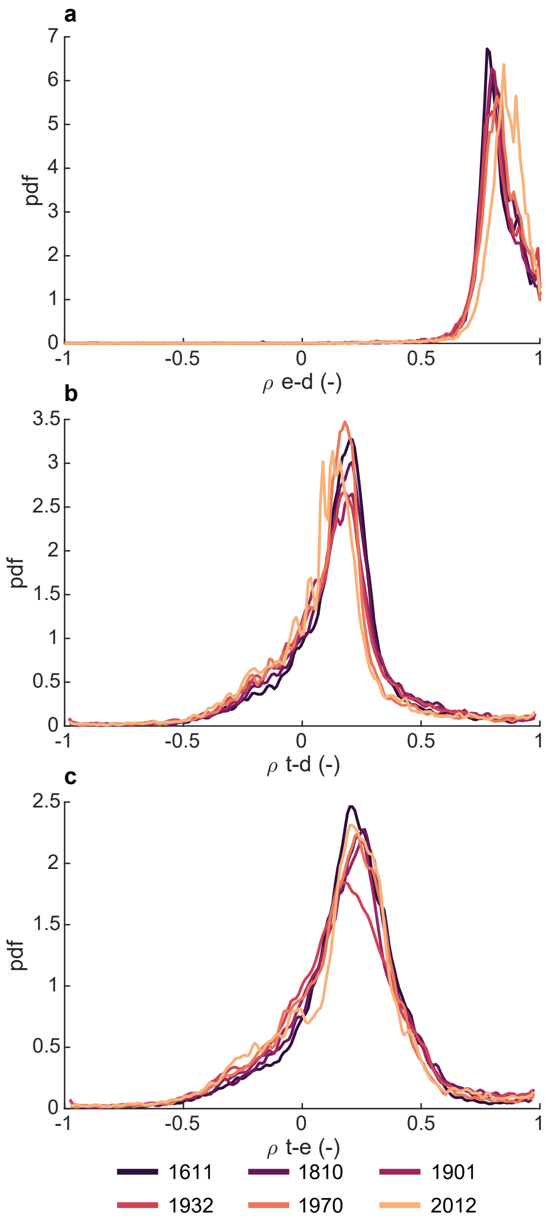


| Year | $\rho(e-d)$ [-] (mean $\pm$ std) |
|---|---|
| 1611 | $0.81 \pm 0.10$ |
| 1810 | $0.82 \pm 0.11$ |
| 1901 | $0.81 \pm 0.11$ |
| 1932 | $0.81 \pm 0.12$ |
| 1970 | $0.83 \pm 0.10$ |
| 2012 | $0.85 \pm 0.10$ |

| Year | $\rho(t-d)$ [-] (mean $\pm$ std) |
|---|---|
| 1611 | $0.14 \pm 0.30$ |
| 1810 | $0.15 \pm 0.30$ |
| 1901 | $0.13 \pm 0.32$ |
| 1932 | $0.12 \pm 0.33$ |
| 1970 | $0.11 \pm 0.29$ |
| 2012 | $0.10 \pm 0.31$ |

| Year | $\rho(t-e)$ [-] (mean $\pm$ std) |
|---|---|
| 1611 | $0.18 \pm 0.30$ |
| 1810 | $0.19 \pm 0.31$ |
| 1901 | $0.18 \pm 0.33$ |
| 1932 | $0.16 \pm 0.34$ |
| 1970 | $0.16 \pm 0.30$ |
| 2012 | $0.16 \pm 0.32$ |

Figure 3.12: **Spatial probability density function of cross-correlation between interarrival time, intensity and duration of SSC overthreshold events.** Probability density function (left) and mean value (mean $\pm$ standard deviation, right) of cross-correlation between intesity and duration $\rho(e-d)$ (**a**), interarrival time and duration $\rho(t-d)$ (**b**) and interarrival time and intensity $\rho(t-e)$ (**c**).

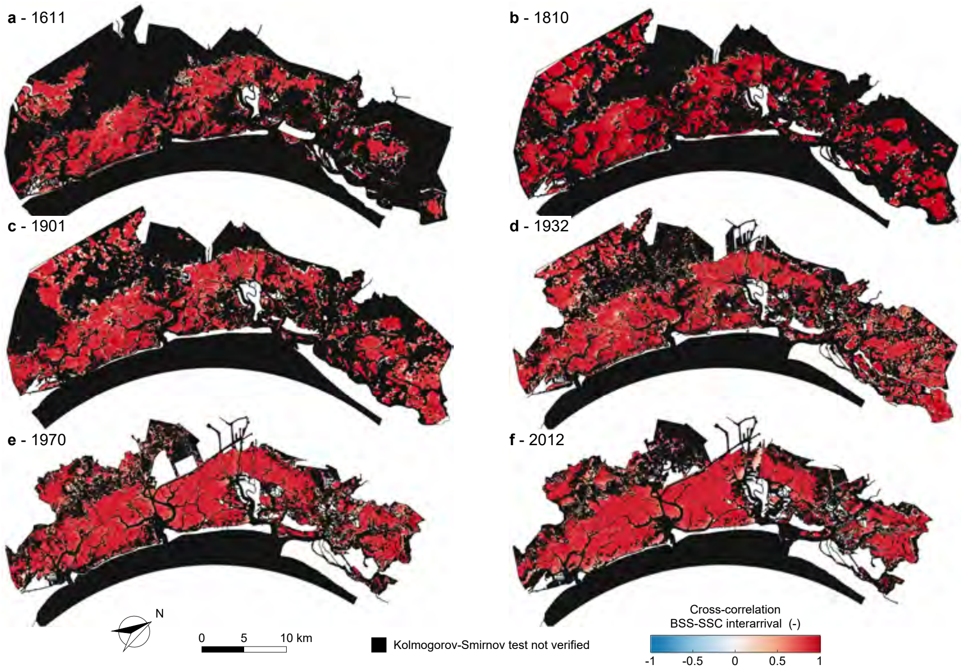


Figure 3.13: **Cross-correlation between interarrival times of overthreshold BSS and SSC events.** Spatial distribution of the cross-correlation between interarrival times of overthreshold BSS and SSC exceedances for the six different configurations of the Venice Lagoon: 1611 (**a**), 1810 (**b**), 1901 (**c**), 1932 (**d**), 1970 (**e**), and 2012 (**f**). Black identifies sites where overthreshold BSS and SSC events cannot be modeled as a marked Poisson process (i.e. the KS test is not verified for the interarrival time).

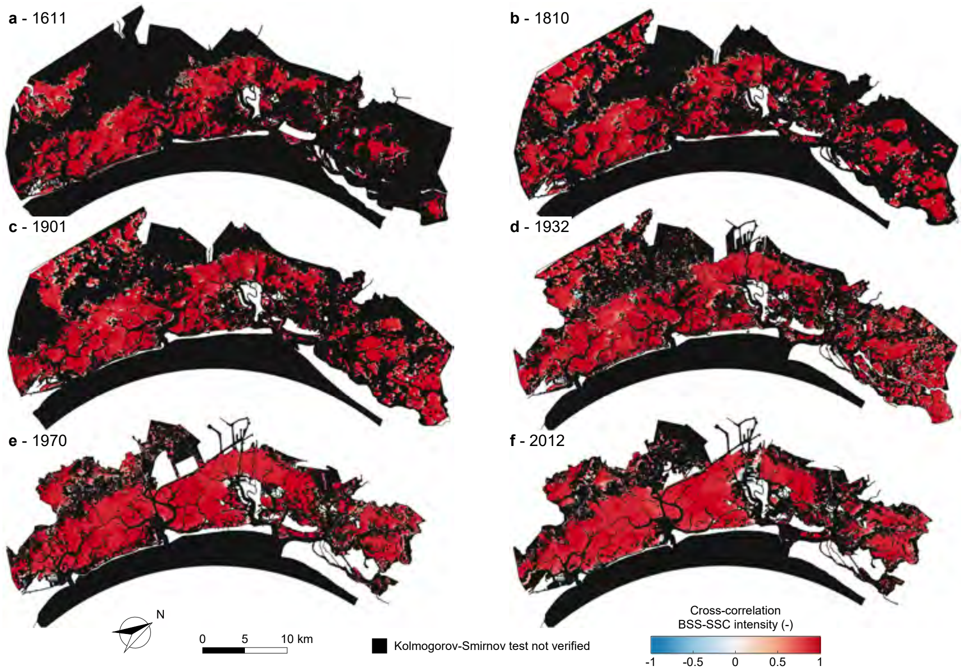


**Figure 3.14: Cross-correlation between intensities of overthreshold BSS and SSC events.** Spatial distribution of the cross-correlation between intesities of over threshold exceedances BSS and SSC for the six different configurations of the Venice Lagoon: 1611 (**a**), 1810 (**b**), 1901 (**c**), 1932 (**d**), 1970 (**e**), and 2012 (**f**). Black identifies sites where overthreshold BSS and SSC events cannot be modeled as a marked Poisson process (i.e. the KS test is not verified for the interarrival time).

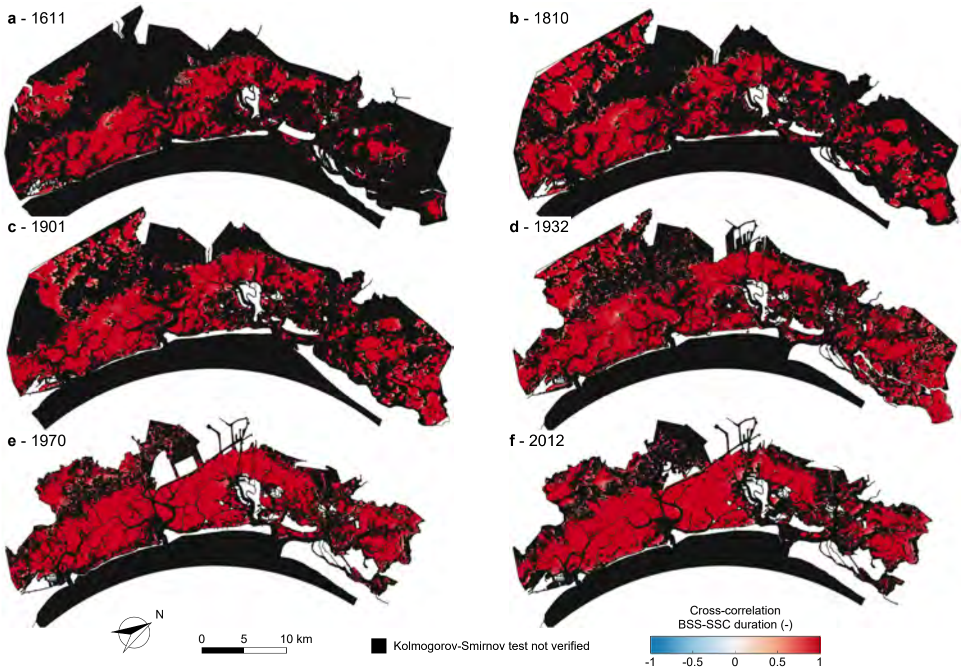


**Figure 3.15: Cross-correlation between durations of overthreshold BSS and SSC events.** Spatial distribution of the cross-correlation between durations of over threshold exceedances BSS and SSC for the six different configurations of the Venice Lagoon: 1611 (**a**), 1810 (**b**), 1901 (**c**), 1932 (**d**), 1970 (**e**), and 2012 (**f**). Black identifies sites where overthreshold BSS and SSC events cannot be modeled as a marked Poisson process (i.e. the KS test is not verified for the interarrival time).

# 4

# SPATIAL PATTERNS OF STORM-DRIVEN SEDIMENTATION ON SALT MARSHES

This chapter is a manuscript ready to be submitted for publication and its primary goal is to understand how spatial sedimentation patterns on salt marshes are affected by tide and wind waves. Inorganic sediment redistributed during flooding supports marsh vertical accretion and, especially in sediment-starved systems, is mainly driven by resuspension events on tidal flats, whose dynamics are markedly stochastic as shown in Chapter 2 and 3. The non-linearity of suspended sediment available for deposition over the marsh surface and the relative importance of tidal flooding and wind waves during storm surges and fair-weather conditions can importantly affect the spatial pattern of salt-marsh sedimentation. Here we use sedimentation measurements from different salt marshes of the Venice Lagoon to analyse the relative importance of these different hydrodynamic processes in affecting the spatial pattern of sedimentation. Moreover, by comparing topographic profiles of salt marshes in different tidal systems worldwide, we show that marsh topography reveals the signature of the different physical processes driving their vertical accretion.

# MARSH TOPOGRAPHY REVEALS THE SIGNATURE OF STORM-DRIVEN SEDIMENTATION

**Davide Tognin[1,2], Andrea D'Alpaos[2,3], Massimiliano Ghinassi[2,3], and Luca Carniello[1,2]**

[1]Department of Civil, Environmental, and Architectural Engineering, University of Padova, Padova, Italy

[2]Center for Lagoon Hydrodynamics and Morphodynamics, University of Padova, Padova, Italy

[3]Department of Geosciences, University of Padova, Padova, Italy

## 4.1 ABSTRACT

Salt marshes are precious tidal landforms threatened by drowning due to increasing sea levels. Sediment settling during repeated flooding contributes to vertical accretion, offsetting relative elevation loss. Tidal flooding is commonly depicted as the main sediment supplier to marsh platforms. However, storm surges and waves may deeply impact tidal flow conditions and sediment reworking, thus raising questions on the relative contribution of these processes to salt-marsh sediment supply. Here we show, through a 3-year-long measurement record, that storm surges substantially sustain marsh sediment budget and critically influence deposition patterns. Surge-enhanced water levels promote wind-wave driven sediment fluxes directly across the tidal flat-marsh transition, altering tidal sedimentation patterns and, thus, affecting marsh topographic elevation and morphology. By comparing sedimentation patterns and topographic profiles, we show that the signature of tides, wind waves and storm surges can be read in marsh topography, which we suggest therefore as an easily detectable indicator of the physical processes driving marsh vertical evolution. Our results challenge the conventional view of salt-marsh sedimentation as an essentially tide-driven process and

provide further insight into the relative importance of different sedimentary processes, which is key to understanding the future of salt marshes and indicating preservation and restoration strategies.

## 4.2 INTRODUCTION

Salt marshes rim low-lying, sheltered coastlines in extratropical climate, occupying the transition zone between land and sea. This border situation makes them simultaneously one of the most productive and precarious ecosystems on Earth (Kirwan and Megonigal, 2013; Schuerch et al., 2018). Thus, the alarming loss of marshes under increasing natural and human-induced pressures threatens numerous benefits they provide, extending to carbon sequestration, water quality enhancement, biodiversity conservation, wildlife habitat provision, and shoreline protection (Chmura et al., 2003; Barbier et al., 2011; Kirwan and Mudd, 2012; Möller et al., 2014). Understanding sedimentation processes that counteract salt-marsh drowning is therefore crucial to the preservation and restoration of these precious habitats and the ecosystem services they provide.

As the marsh elevation acts as a topographic threshold (French and Stoddart, 1992), only flooding allows for mineral sediment to be deposited on the marsh. While tides control marsh inundation, wind-waves control suspended sediment availability for sedimentation, episodically reworking sediment on tidal flats by increasing bottom shear stress (Fagherazzi and Wiberg, 2009; Carniello et al., 2011; A. D'Alpaos et al., 2013; Green and Coco, 2014; Carniello et al., 2016). The mutual combination of tidal oscillation and wind waves is deeply affected by meteorological conditions, especially during storm surges, when enhanced water levels are typically associated with strong winds.

Tidal exchange via the channel and creek system has been traditionally considered the preferential mechanism (herein *tide-driven*) for sediment supply and redistribution on salt marshes (Reed et al., 1999; Friedrichs and Perry, 2001; Kirwan et al., 2010; Hughes, 2012).

However, in salt marshes with a limited tidal exchange, prolonged high water levels associated with storm surges can sustain sediment accumulation, substantially affecting the marsh sediment budget (Stumpf, 1983; Reed, 1989; Goodbred and Hine, 1995 and Chapter 5). Beyond changing sedimentation rate and timing, storm surges may also affect spatial depositional patterns, owing to the different sediment transport mechanisms involved. Enhanced storm-driven water levels activate usually inaccessible flow paths, so that wind waves, can propagate on the marshland via the tidal flat-marsh interface (Möller et al., 2014). Following these occasional flow paths, sediment exchange may also take place directly across the marsh edge from the tidal flat (French and Stoddart, 1992; Davidson-Arnott et al., 2002; Duvall et al., 2019; Schuerch et al., 2019), driven by the coupled action of storm-induced flooding and waves (herein *wave-driven*).

Here we evaluate the relative importance of *tide-* and *wave-driven* processes and their combination during storm surges and fair-weather periods by analyzing short-term sedimentation data and topographic profiles of salt marshes in the Venice Lagoon, Italy (Figure 4.1a and Supporting Information), and we furthermore highlight their signature in the topography of other salt-marsh environments worldwide.

Due to the negligible marine and fluvial sediment input, the morphological evolution of the Venice Lagoon, as in many other coastal settings (Syvitski et al., 2005), is mainly controlled by the reworking of sediment resuspended and transported by tidal currents and wind waves (Figure 4.1a and Material and Methods). To assess the relative contribution of tide- and wave-driven processes to salt-marsh sedimentation, we measured sediment accumulation at four sites (SF, SE, CO and PA, Fig 4.1b-e). These sites include both marshes facing channels, where tide contribution is expected to be preeminent, and marshes facing tidal flats, potentially more exposed to wind-wave action. Sedimentation data were collected continuously over a 3-year-long period from October 2018 to October 2021 with a monthly frequency or immediately after severe storm-surge events (see Material and Methods).

While demonstrating that salt-marsh sediment accumulation is essentially a storm-driven process, we show how local tide or wave dominance can profoundly impact spatial sedimentary dynamics. Assuming the existence of a relationship between form and physical process, the signature of different land-shaping processes can be read in marsh topographic profiles. Therefore, marsh topography provides an easily detectable and broadly applicable indicator of the mechanisms that control sediment supply and redistribution, which is a crucial piece of information for protection and restoration management policies.

## 4.3 RESULT AND DISCUSSION

Sediment accumulation measurements carried out in the Venice Lagoon (Figure 4.1a and 4.2) reveal that the contribution of fair-weather and storm-dominated periods to marsh accretion varies depending on marsh topography and location. Overall, storm-driven deposition accounts for 70% on average of the total sediment accumulation (Figure 4.1f-q), despite the brief duration of storm-dominated periods (Supporting Information, Table 4.1), highlighting the strong temporal variability of the depositional processes. Among the different sites, slightly lower, but still substantial, contributions of storm-surge conditions are observed also in more sheltered areas, such as the site SF4, facing a very shallow, small tidal flat (Figure 4.1i), and the site PA, where salt marshes are less exposed to dominant winds (especially PA1 and PA3, Figure 4.1o and q) and high-water levels are attenuated due to the location in the innermost portion of the lagoon.

Although sedimentation is generally controlled by storm-surge events, its spatial patterns differ on salt marshes facing channels or tidal flats. Along channel-facing transects (i.e., SF1, SF2, and SF3), sedimentation shows a rapidly decreasing trend with the distance from the marsh margin (Figure 4.4a) with storm-dominated periods providing between 73 and 90% of the total observed sedimentation and mostly boosting accumulation on the margin (Figure 4.1f-h). Con-

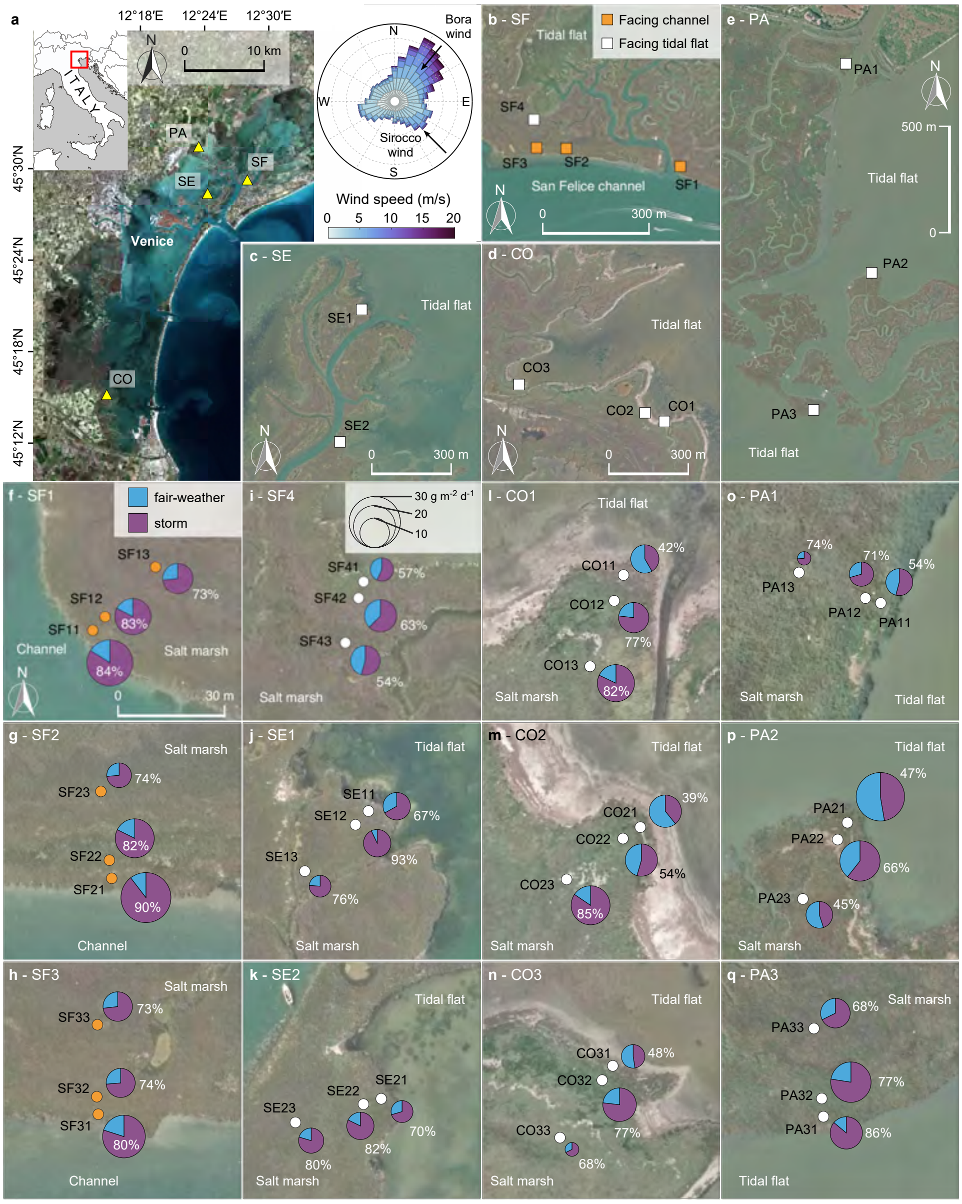


Figure 4.1: **Sedimentation in the salt marshes of the Venice Lagoon, Italy. a**, Location of the study areas within the Venice Lagoon. Inset shows the wind statistics for the period 2000-2019. Position of the transects within each study area: SF (**b**), SE (**c**), CO (**d**), and PA (**e**). Orange squares indicate channel-facing transects; white squares indicate transects facing tidal flats. Storm-dominated (purple) and fair-weather (blue) relative contribution to sedimentation for each transect: SF1 (**f**), SF2 (**g**), SF3 (**h**), SF4 (**i**), SE1 (**j**), SE2 (**k**), CO1 (**l**), CO2 (**m**), CO3 (**n**), PA1 (**o**), PA2 (**p**), and PA3 (**q**). Pie-chart dimension represents the mean sediment accumulation rate per unit area (in $g\,m^{-2}$) per day) for the period October 2018-October 2021, numbers show the percentage of sedimentation related to storm-dominated periods.

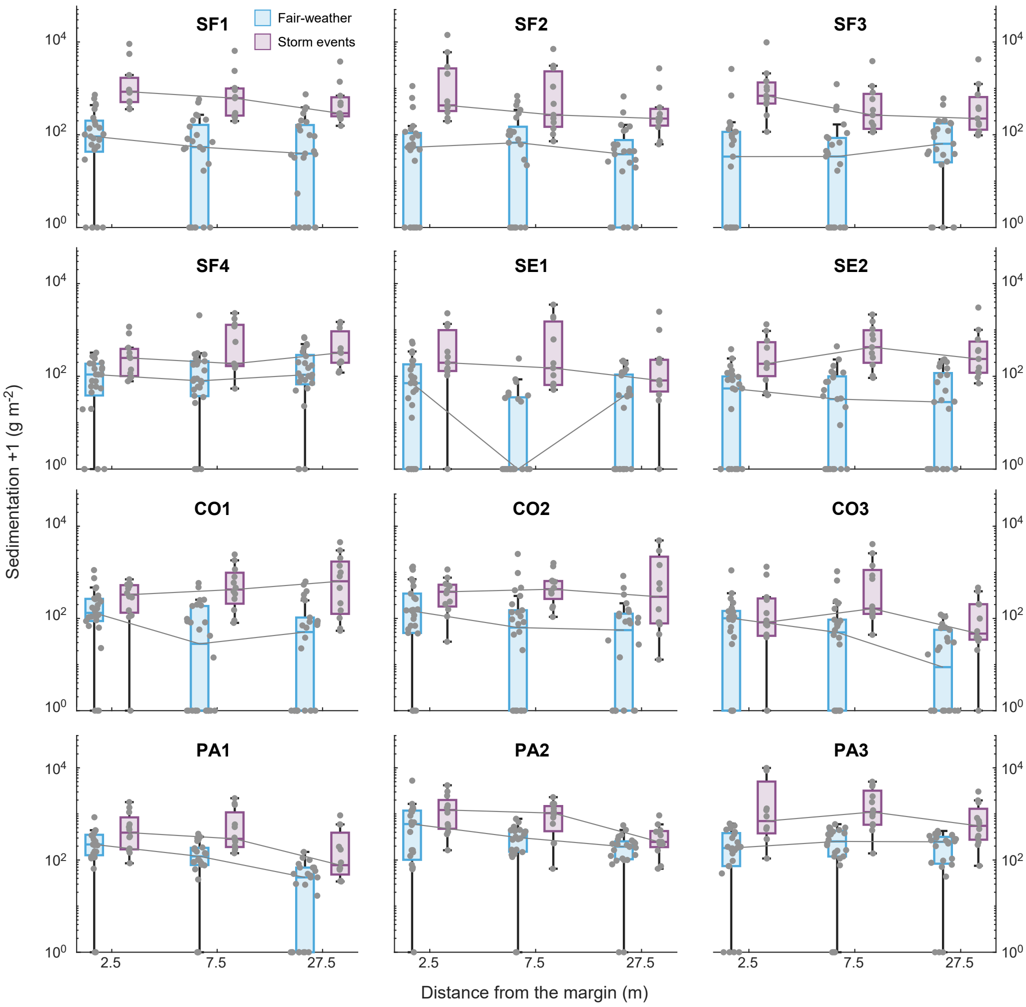


**Figure 4.2: Sedimentation along transects.** Sedimentation (in $g\,m^{-2}$) related to fair-weather conditions (blue) and storm-dominated periods (purple), for each transect. Box plots show median and quartiles, swarm plots show single values.

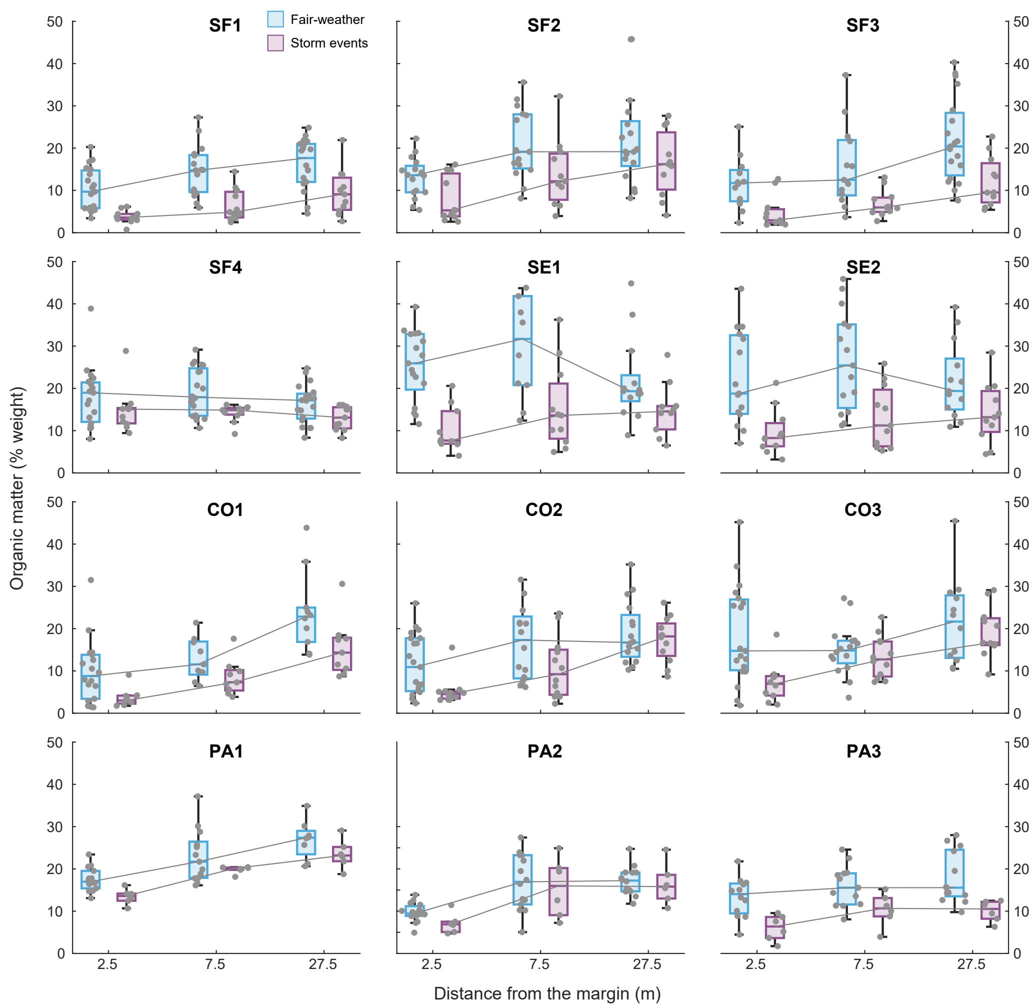


**Figure 4.3: Organic matter content along transects.** Organic matter as percentage in weight, related to fair-weather conditions (blue) and storm-dominated periods (purple), for each transect. Box plots show median and quartiles, swarm plots show single values.

versely, the spatial sedimentation pattern in marshes facing tidal flats (i.e., SF4. SE, CO, and PA) generally shows maximum sedimentation at inner marsh locations (Figure 4.4b), also in this case primarily due to storm-surge contribution which range between 54 and 93% of the total observed sedimentation (Figure 4.1i-q).

Enhanced sedimentation in preferential zones yields higher elevations, thus sediment deposition patterns signs marsh topographic profile (Figure 4.4a-b). Channel-facing marshes display the classical levee profile, which is the signature of sedimentation that rapidly diminishes away from the channel (Figure 4.4a, 4.2 and Supporting Information). By contrast, marshes facing tidal flats show more gently sloping profiles, with no marked levees at the margin owing to the more extensive sedimentation pattern (Figure 4.4b, 4.2 and Supporting Information).

Different depositional patterns and, hence, morphologies documented on channel- and tidal flat-facing marshes arise from the different combinations of tide and wave-driven depositional processes. Along channels, high tide overspills and propagates on the adjacent marshes, where the halophytic vegetation dissipates flow energy and favors a rapid sediment settling (Leonard and Luther, 1995; Nepf, 1999). Even during storm surges and with strong winds, waves can hardly be directly generated across marsh-bordered channels due to the limited fetch. Therefore, sediment transport on channel-facing marshes is always primarily controlled by tidal exchange rather than by wind waves. Thus, sedimentation peaks at the marsh margin and declines toward the inner marsh, creating a levee-shaped profile.

Contrarily, on tidal flats, velocities generated by tidal currents alone under fair-weather conditions are often insufficient to resuspend and transport sediment. Larger bottom shear stresses able to rework tidal flat sediment are generated by wind waves (Carniello et al., 2011; A. D'Alpaos et al., 2013) and typically are associated with storm conditions, sustaining also higher water level. Enhanced water levels during storm surges allow for resuspended sediment to be directly delivered across the marsh edge by wind waves (Duvall

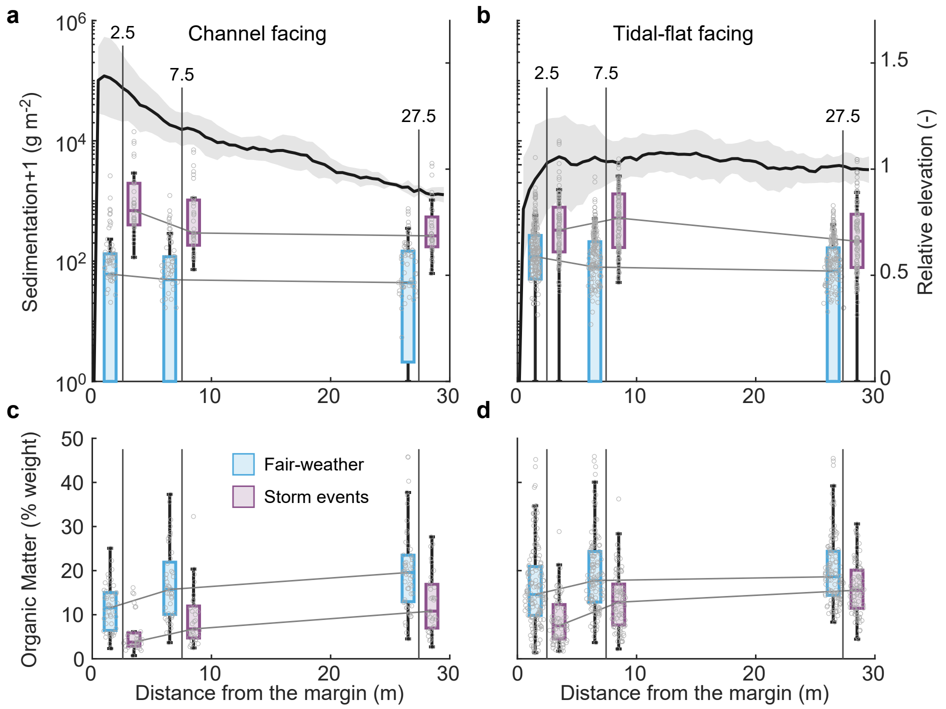


Figure 4.4: **Comparison between sedimentation and topographic profiles.** Sedimentation (in g m$^{-2}$, on the left axis) related to fair-weather conditions (blue) and storm-dominated periods (purple), for transects facing channels (**a**) and facing tidal flats (**b**). Box plots show median and quartiles, swarm plots show single values. y-axis is in logarithmic scale. The relative elevation (elevation divided by the mean profile elevation, on the right axes) is indicated by the black lines; gray shaded areas show the interval between minimum and maximum values. Organic matter content as percentage in weight for fair-weather conditions (blue) and storm dominated periods (purple), for transect facing channels (**c**) and facing tidal flats (g m$^{-2}$). Measurement station position along transects (i.e., 2.5, 7.5, and 27.5 m) is indicated by vertical lines.

et al., 2019; Lacy et al., 2020), causing an inland displacement of the maximum accumulation zone rather than close to the margin (Figure 4.4b). The sedimentation processes affected by the more dynamic action of wind waves result in gently sloped topographic profiles not displaying a marked levee.

Besides inorganic sediments, plant productivity contributes to the sedimentary fabric through the accumulation of refractory organic particles from the aboveground biomass, in addition to root and rhizome tissue (Morris et al., 2016). Due to its low density, aboveground litter can be easily mobilized also by the everyday tidal flow and can accumulate during the ebb phase in the lowest portions of the marsh drained by the inner creek system. As a result, organic matter content is low at the margin and gradually increases toward the inner portion of the marsh both for marshes facing channels and tidal flats interface (Figure 4.4c-d, 4.3 and Supporting Information). Storm-related deposits have a relatively greater inorganic content due to higher resuspension of clastic sediment from tidal flats (A. D'Alpaos et al., 2013; Carniello et al., 2016) and therefore it contributes to a greater long-term accretion owing to the lower decomposition and compressibility (Morris et al., 2016). As a result of the notably greater sedimentation and lower organic matter content, the marsh topographic profiles closely resemble the spatial sedimentation patterns of storm-dominated periods both on marshes facing channels and tidal flats.

The dichotomy between levee-shaped and gently-sloped marsh margins is a recurrent feature across different tidal ranges worldwide, so that we suggest marsh topography to represent an easily detectable, but simultaneously broadly applicable, indicator of land-forming processes that drive salt-marsh morphological evolution. To prove the consistency of this indicator, we considered both channel and tidal-flat facing marsh profiles in five coastal transitional systems with different tidal ranges (Figure 4.5). The Virginia Coastal Reserve (Figure 4.6), located on the Atlantic coast of the Delmarva Peninsula, USA, is a microtidal system, with a spring tidal range of 1.2 m (Mariotti et al., 2010b). San Pablo Bay (Figure 4.7) is located in the northern part of San Francisco Bay, on the Pacific coast of the USA, where the spring tidal range is about 2.5 m (Lacy et al., 2020). In the open-coast marshes fringing the Dengie Peninsula (Figure 4.8) and the Wash (Figure 4.9) (UK), the spring tidal range is 4.8 m and 6.5 m, respectively (Evans et al., 2019; Schuerch et al., 2019). Finally, marshes in the Cobequid Bay (Figure 4.10) are located at the head of the Bay of Fundy, on the Atlantic coast of Canada, where the spring tidal range can exceed 12 m (Davidson-Arnott et al., 2002).

Consistently with the topographic profiles detected in the Venice lagoon, in all the above tidal systems, regardless of the tidal range, marshes along channel borders show a cliff margin with a levee, which is diagnostic of the sediment flux controlled by the gradual tidal flooding. Contrarily, a higher dissipative margin characterized by a more extensive, gently-sloped ramp (Evans et al., 2019) characterizes marshes facing tidal flats, where wave-driven transport becomes more important. As the tidal range increases, the levee at the marsh-channel interface becomes less pronounced (Figure 4.5a-e), because higher tidal excursions generate stronger currents that can propagate inland with higher velocities, thus distributing sediment along longer paths rather than close to the marsh margin. Similarly, the gently-sloped profiles characterizing microtidal marsh margins facing tidal flats display a decreasing slope gradient as the tidal range increases (Figure 4.5f-j). During normal spring high tide, because the water depth over the marsh in macrotidal system is notably higher than in microtidal ones, vegetation-induced attenuation offered becomes less effective (Davidson-Arnott et al., 2002), allowing the sediment flux to propagate further landward and contribute to more extensive sedimentation than in microtidal systems.

In conclusion, the high temporal and spatial sedimentation variability suggests that the common depiction of sedimentation on salt marshes as a processes mainly driven by tidal flooding and concentrated close to the marsh margin is somewhat incomplete because it neglects the relative contribution of storm-driven sediment supply. Marsh topography provides undeniable evidence of the relative importance of these different land-forming processes that control the spatial sedimentation pattern over salt marshes.

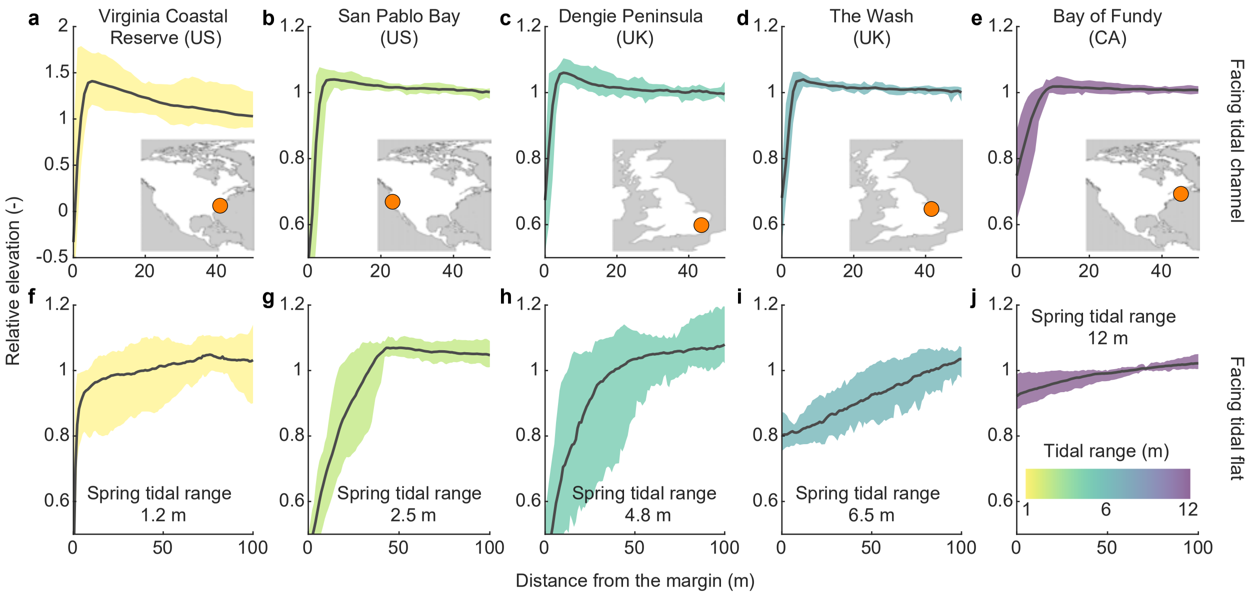


**Figure 4.5: Marsh topographic profiles for different tidal ranges and exposure.** Marsh profile relative elevation in the Virginia Coastal Reserve, US (**a, f**); San Pablo Bay, US (**b, g**); Dengie Peninsula, UK (**c, h**); the Wash, UK (**d, i**); and the Bay of Fundy, CA (**e, j**), for both transects facing channels (**a-e**) and tidal flats (**f-j**). Color scale displays the tidal range.

## 4.4 MATERIAL AND METHODS

### 4.4.1 Geomorphological setting

The Venice Lagoon, Italy, formed over the last 7500 years and is the largest Mediterranean brackish semi-enclosed basin extending over an area of about 550 $km^2$ (Figure 4.1a). Owing to the tidal exchange with the Adriatic Sea through the three inlets (Lido, Malamocco and Chioggia), the Lagoon has a semidiurnal microtidal regime, with a spring tidal range of about 1 m (A. D'Alpaos et al., 2013). The Venice Lagoon is also highly influenced by meteorological forcings, such as severe storm surges (up to 2 m) driven by the southeasterly Sirocco wind blowing along the Adriatic Sea and relatively large wind waves ($>$ 1 m) and wind setup generated by the northeasterly Bora wind within the Lagoon, due to its NE-SW elongated shape (Carniello et al., 2011). Wind waves enhance sediment resuspension and, thus, the erosion of tidal flats, whose deepening, in turn, favours larger waves and higher bottom shear stresses (A. D'Alpaos et al., 2013; Carniello et al., 2016), triggering positive feedback. The artificial diversion of the major rivers between the $15^{th}$ and $17^{th}$ centuries stopped any fluvial sediment input from the inland watershed and the construction of jetties at the three inlets between 1872 and 1934 hindered almost any marine source of sediment, worsening the lagoon sediment-starved condition (Carniello et al., 2012).

To measure spatial dynamics of sediment accumulation on salt marshes, we selected 12 margin-perpendicular transects each made up of three aligned measurement stations at increasing distance from the marsh edge (i.e., 2.5, 7.5 and 27.5 m) and grouped in four study sites: San Felice (SF, 4 transects, 12 stations, Figure 4.1b), Sant'Erasmo (SE, 2 transects, 6 stations, Figure 4.1c), and Pagliaga (PA, 3 transects, 9 stations, Figure 4.1e) in the northern Lagoon, and Conche (CO, 3 transects, 9 stations, Figure 4.1d) in the southern Lagoon. In the SF salt marsh, we deployed three transects (SF1, SF2 and SF3, Figure 4.1f-h) on the southern edge, bordered by one of the main channels cutting through the northern lagoon, and one (SF4, Figure 4.1i) facing the relatively small tidal flat on the northeastern edge. The SE marsh is close to the Sant'Erasmo island, and both transects (SE1 and SE2, Figure 4.1j-k) northeasterly faces a shallow tidal flat. The PA (Figure 4.1o-q) salt marsh sits between two tidal flats, thus PA1 and PA2 face the northeastern one and PA3 the southern one. The CO salt marsh rims the mainland and northeasterly faces toward the wide subtidal flat that occupies the central-southern Venice Lagoon so that all transects (CO1, CO2 and CO3, Figure 4.1l-n) are exposed to wind waves generated by the northeasterly Bora wind.

Measurement stations were surveyed with a total station Wild T2002 with a precision of $\pm 0.01$ m. The elevation was referred to the Italian Geographic Military Institute (IGM) reference datum.

### 4.4.2 Storm-dominated period classification

Using water level and wind conditions measured close to each study area by the monitoring network of the Italian Institute for Environmental Protection and Research (ISPRA), we classify the climatology of each observation period. After computing Mean Higher High Water (MHHW) as the arithmetic mean of the higher high water level over a specific 19-year cycle, we define periods for which the measured water level is above MHHW for more than the average over 19 years as "storm-dominated". We implicitly account for the different effects contributing to surges (i.e., wind and barometric pressure) by using measured water levels. More details can be found in Methods section of Chapter 5.

### 4.4.3 Sediment sampling and analysis

Two circular sediment traps (diameter 0.18 m) in each station were deployed to sample sediment accumulation on salt marshes with a monthly frequency or immediately after severe storm-surge events, consistently with sediment trap temporal resolution (i.e., from weekly to monthly sampling frequency) (Temmerman et al., 2003; Nolte et al., 2013). From October 2018 to October 2021 we collected and analyzed $n = 2628$ samples.

Sediment accumulation was determined by rinsing samples with deionized water and oven-drying them at 40°C for 48 hours or till no change in weight occurs. Organic matter content was estimated as the difference in weight after Loss-on-Ignition (LOI) treatment, combusting 2 g of crumbled sediment in a muffle furnace at 375°C for 16 hours (Ball, 1964; Roner et al., 2016).

### 4.4.4 Topographic profiles

The five salt-marsh systems of the Virginia Coastal Reserve (US), San Pablo Bay (US), Dengie Peninsula (UK), the Wash (UK), and the Bay of Fundy (CA) are selected to cover different tidal ranges worldwide, where LiDAR surveys with a resolution of 1 m are available. In each study area, 10 locations facing channels and 10 locations facing tidal flats were selected. At each location of both marsh types, a first profile perpendicular to the marsh margin, identified as the transition between vegetated and unvegetated area, was chosen and it was then replicated with 10 parallel, equally-spaced profiles. The average elevation profile was then obtained as the mean of the 10 parallel profiles, to avoid being influences by local heterogeneities. To highlight the shape of the profile, its relative elevation was calculated by making the marsh topographic profile dimensionless with its mean elevation.

## 4.5 SUPPORTING INFORMATION

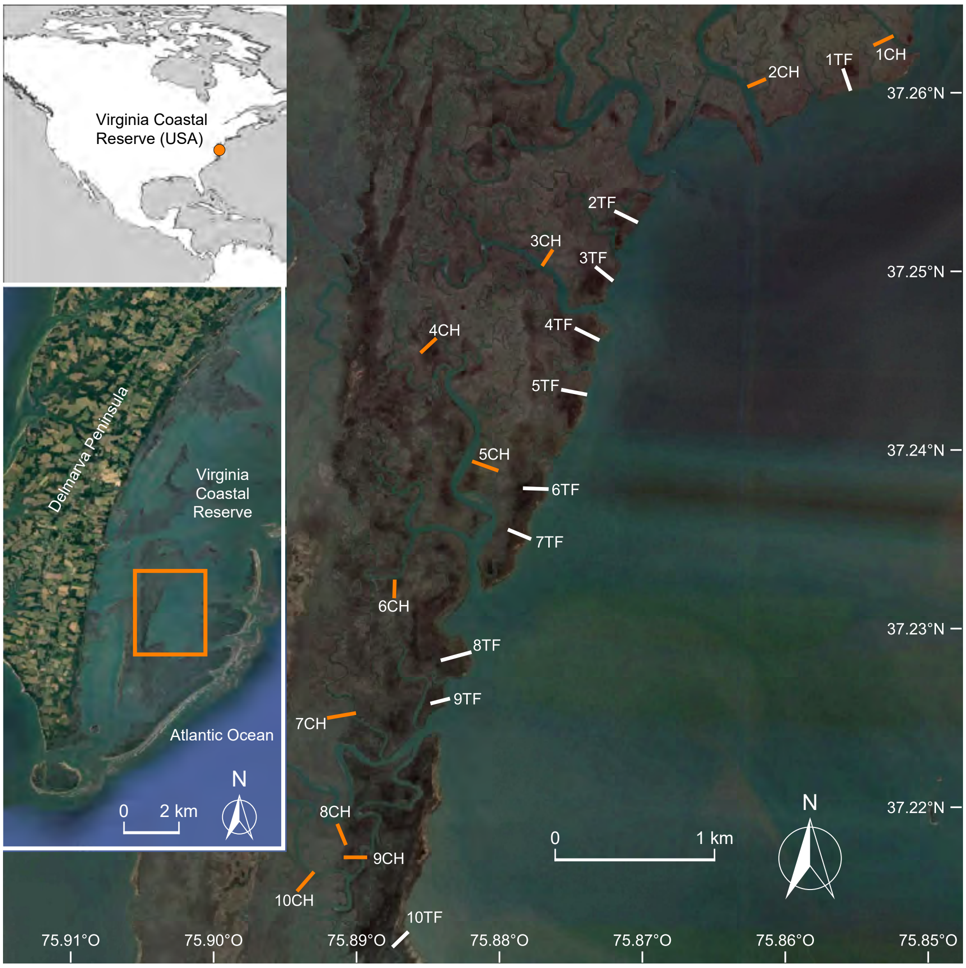


**Figure 4.6: Virginia Coastal Reserve, USA.** Position of the selected channel-facing (orange) and tidal-flat facing (orange) transects in the Virginia Coastal Reserve marshes.

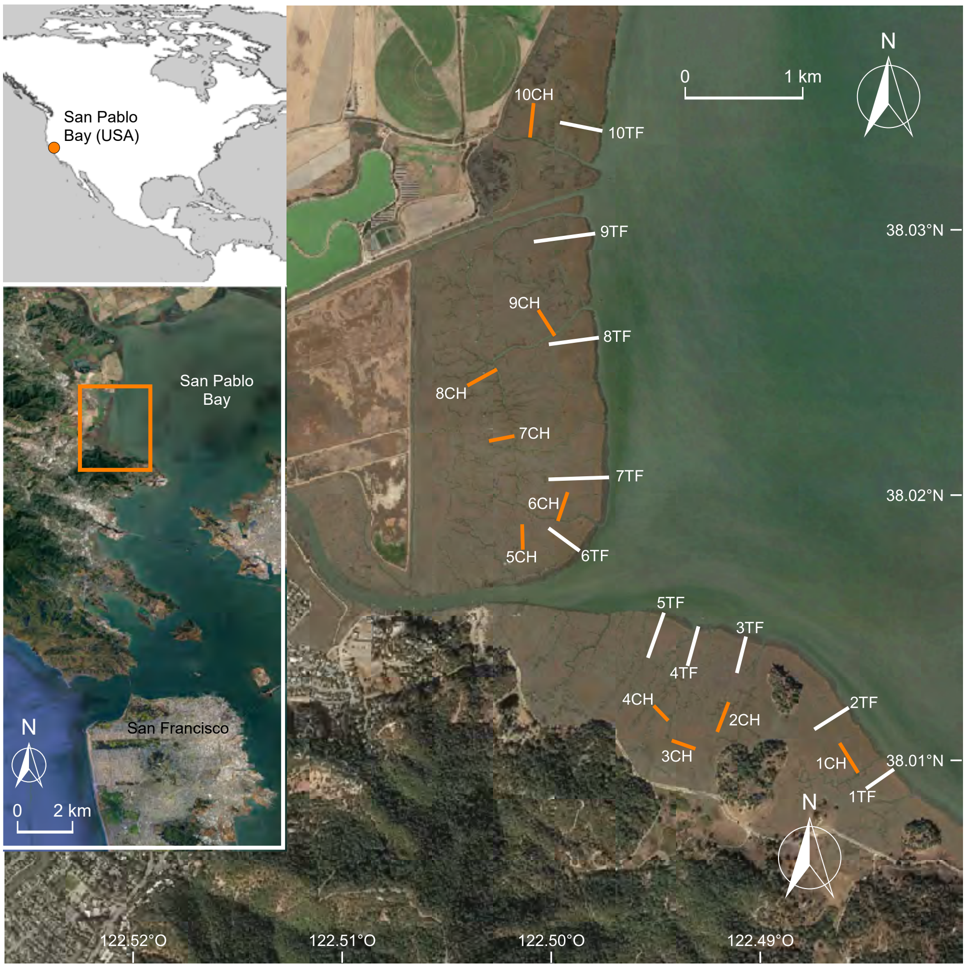


**Figure 4.7: San Pablo Bay, USA.** Position of the selected channel-facing (orange) and tidal-flat facing (orange) transects in the San Pablo Bay marshes.

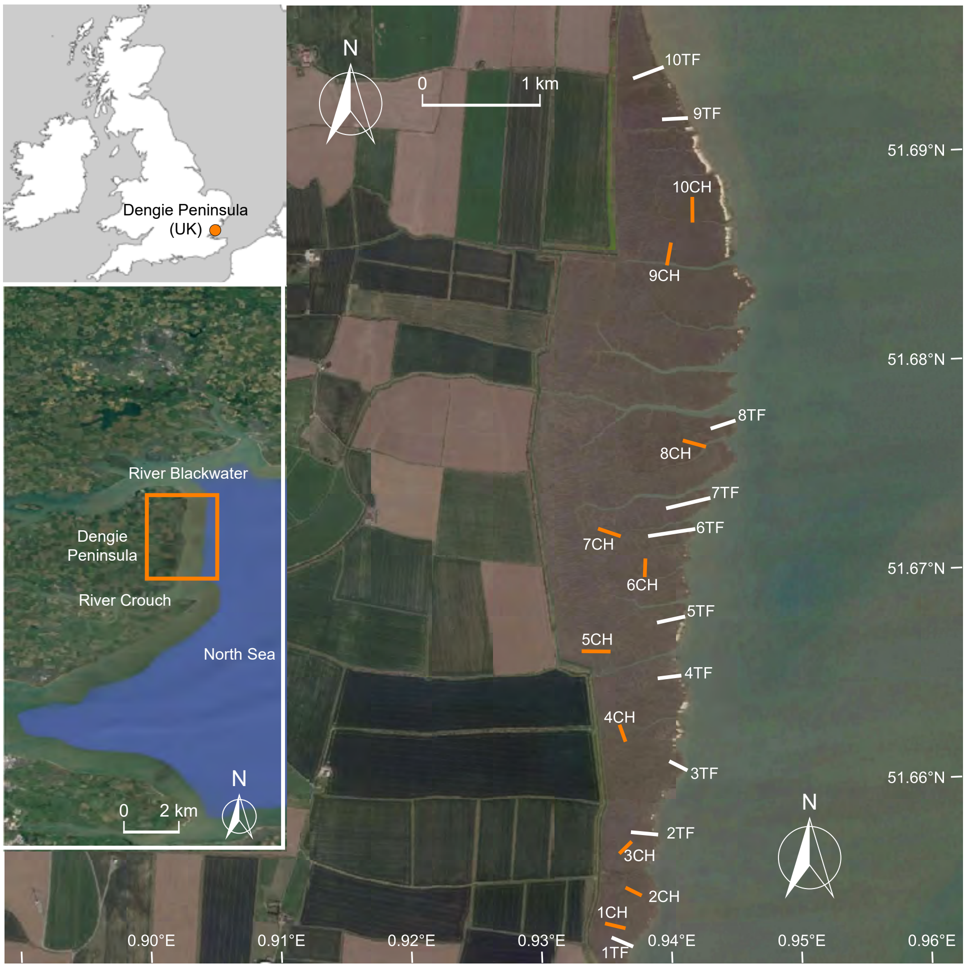


Figure 4.8: **Dengie Peninsula, UK.** Position of the selected channel-facing (orange) and tidal-flat facing (orange) transects in the Dengie Peninsula marshes.

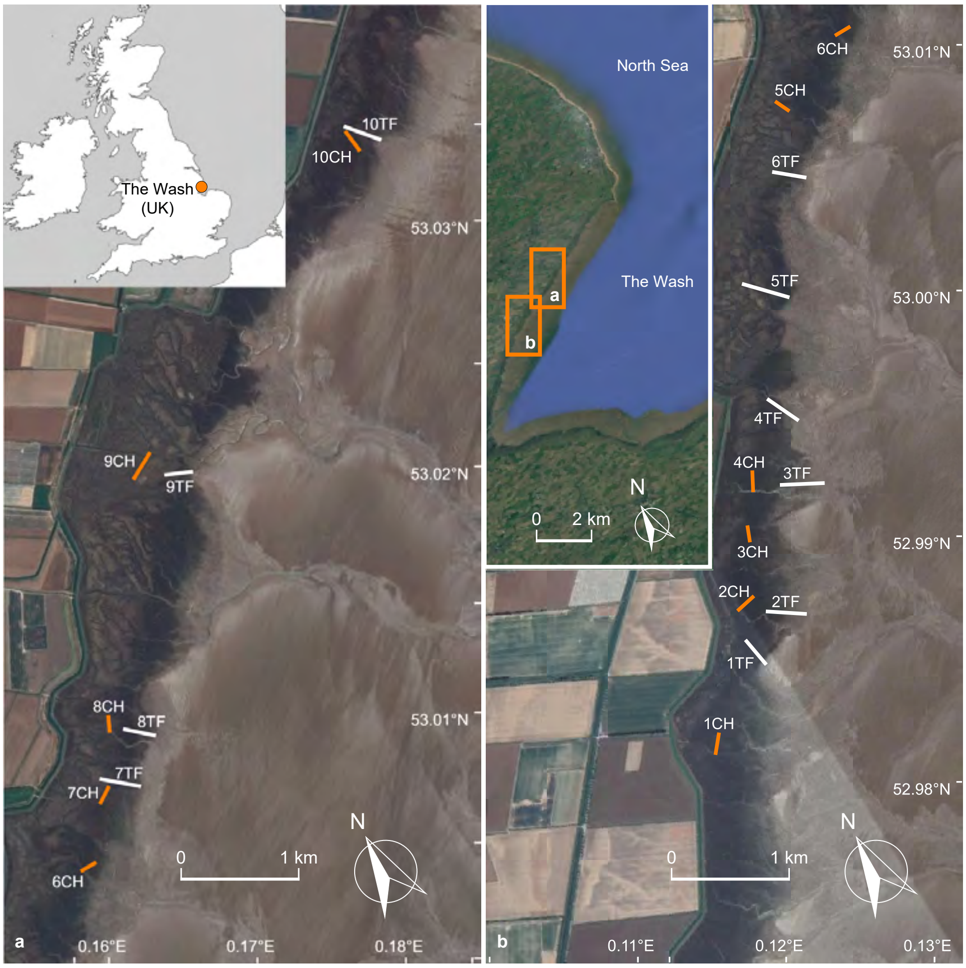


Figure 4.9: **The Wash, USA.** Position of the selected channel-facing (orange) and tidal-flat facing (orange) transects in the Wash marshes.

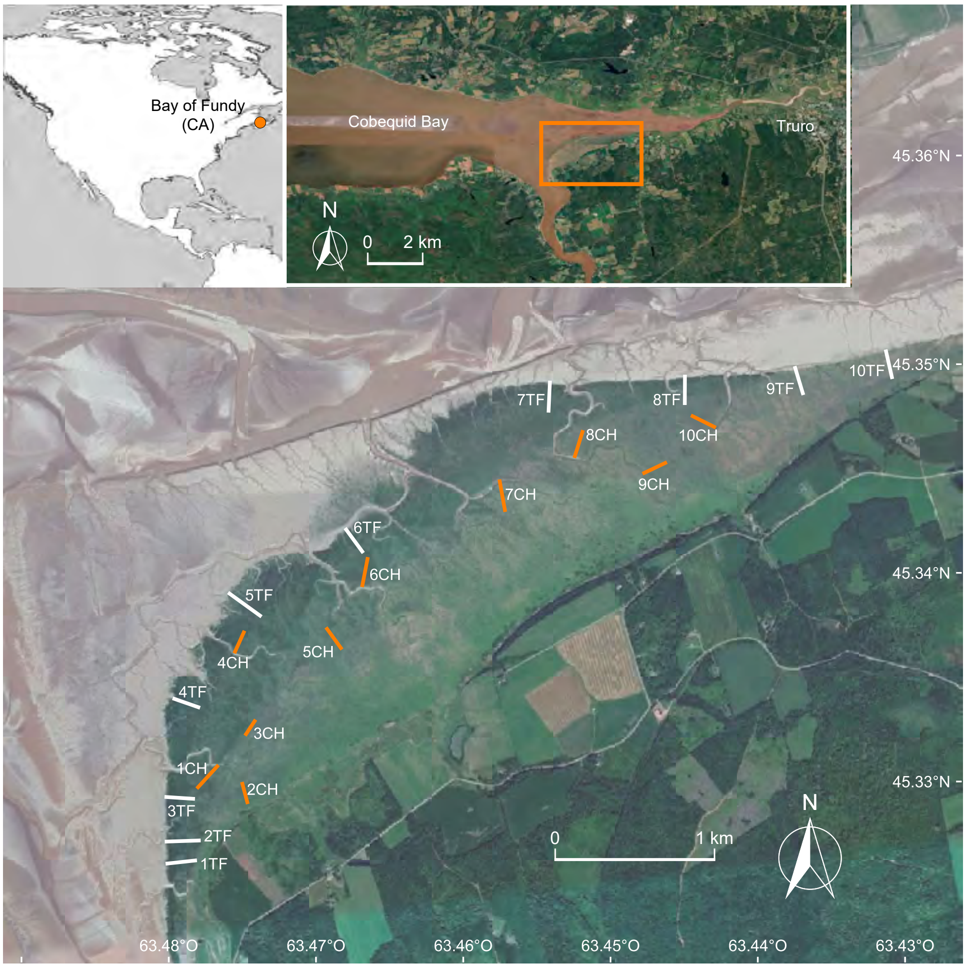


**Figure 4.10: Bay of Fundy, USA.** Position of the selected channel-facing (orange) and tidal-flat facing (orange) transects in the Bay of Fundy marshes.

**Table 4.1: Storm-related sedimentation.** Relative contribution of storm-dominated and fair-weather periods in terms of duration and sedimentation (mean (min – max) in the study area).

| Study area | Storm duration (%) | Fair-weather duration (%) | Storm sedimentation (%) | Fair-weather sedimentation (%) |
|---|---|---|---|---|
| SF | 28.27 | 71.73 | 73.86 (54.46 - 89.58) | 26.14 (10.42 - 45.54) |
| SE | 27.85 | 72.15 | 78.05 (66.86 - 92.99) | 21.95 (7.01 - 33.14) |
| CO | 29.36 | 70.64 | 63.42 (39.21 - 84.46) | 36.58 (15.54 - 60.79) |
| PA | 31.14 | 68.86 | 64.77 (45.01 - 86.07) | 35.23 (13.93 - 54.99) |
| Mean | 29.15 | 70.85 | 70.03 | 29.97 |

# 5

# EFFECTS OF STORM-SURGE BARRIERS ON SALT-MARSH ACCRETION

This chapter is a manuscript published in *Nature Geoscience* (Tognin et al., 2021) and further analyses the intrinsic variability of the sedimentation processes and its implications on the future of salt marshes within artificially flood-regulated shallow tidal embayments. Firstly, we focus on the temporal variations of salt-marsh sedimentation analysing measurements carried out in the Venice Lagoon to unravel the relative contribution of storm surges and fair-weather periods to salt-marsh sediment accumulation. We further assess the impacts of storm-surge barriers on salt-marsh sedimentation and, hence, on their resilience to increasing rates of sea-level rise.

# MARSH RESILIENCE TO SEA-LEVEL RISE REDUCED BY STORM SURGE BARRIERS IN THE VENICE LAGOON

**Davide Tognin[1,2], Andrea D'Alpaos[2,3], Marco Marani[1,2], and Luca Carniello[1,2]**

[1]Department of Civil, Environmental, and Architectural Engineering, University of Padova, Padova, Italy

[2]Center for Lagoon Hydrodynamics and Morphodynamics, University of Padova, Padova, Italy

[3]Department of Geosciences, University of Padova, Padova, Italy

## 5.1 ABSTRACT

Salt marshes are important coastal habitats and provide ecosystem services to surrounding communities. They are, however, threatened by accelerating sea-level rise and sediment deprivation due to human activity within upstream catchments, which result in their drowning and a reduction in their extent. Rising seas are also leading to an expansion of coastal flooding protection infrastructures, which might also represent another serious if poorly understood threat to salt marshes due to effects on the resuspension and accumulation of sediment during storms. Here, we use observations from the Venice Lagoon (Italy), a back-barrier system with no fluvial sediment input recently protected by storm-surge barriers, to show that most of the salt-marsh sedimentation - more than 70% in this case - occurs due to sediment reworking during storm surges. We also prove that the large, yet episodic, storm-driven sediment supply is seriously reduced by operations of storm-surge barriers, revealing a critical competition between the objectives of coastal flooding protection and natural ecosystems preservation. Without complementary interventions and management policies that reduce barrier activations, the survival of coastal wetlands is even more uncertain.

## 5.2 INTRODUCTION

Coastal wetlands represent some of the most valuable and vulnerable ecosystems globally. They mitigate coastal flooding by buffering storm surges, mediate nutrient and pollutant fluxes, uptake atmospheric carbon, and constitute a sanctuary for endangered species (Costanza et al., 1997; Chmura et al., 2003; Barbier et al., 2011; Kirwan and Mudd, 2012; Möller et al., 2014). Increasing rates of sea-level rise, together with reduced fluvial sediment delivery to the coasts (Syvitski et al., 2005) and increasing anthropogenic pressures, are questioning the very survival of coastal wetlands at the global scale (Marani et al., 2010; A. D'Alpaos et al., 2011; Kirwan and Megonigal, 2013; Schuerch et al., 2018; FitzGerald and Hughes, 2019), worsening drowning (Reed, 1995; Morris et al., 2002; Carniello et al., 2009) and lateral erosion mechanisms (Marani et al., 2011; Mariotti and Fagherazzi, 2013; Mariotti and Carr, 2014; Tommasini et al., 2019; Finotello et al., 2020b). Although these processes are mediated by feedbacks between geomorphology and organic production (Morris et al., 2002; Marani et al., 2007; Fagherazzi et al., 2012; Kirwan and Megonigal, 2013; Marani et al., 2013), the key component to both vertical and lateral accretion/erosion dynamics is minerogenic sediment supply from upland, interior, and oceanic sources, driven by wind waves and tidal currents and distributed during wetland flooding (Mariotti and Fagherazzi, 2013; Carniello et al., 2014; Green and Coco, 2014).

Hence, by increasing wave resuspension and promoting flooding by sediment-laden waters, storm surges may represent an important geomorphic driver of salt-marsh evolution. Although they were found to contribute only marginally to marsh lateral erosion in the long term (Leonardi et al., 2018), it is still unclear whether storm surges play a major role in vertical accretionary dynamics of salt marshes in extratropical areas (Reed, 1995; Castagno et al., 2018; Goodwin and Mudd, 2019), unaffected by the influence of tropical cyclones mobilizing large amounts of sediment (Cahoon et al., 1995; Tweel and Turner, 2014; Du et al., 2019).

Far less understood are the potential effects of coastal flooding protection infrastructures on the resilience of coastal environments (Gedan et al., 2009; Temmerman et al., 2013; Rodríguez et al., 2017; Sandi et al., 2018; Silvestri et al., 2018). The large share of the global population living near the coast and the presence of some of the largest and socio-economically important cities in many estuaries and deltas are making the adoption of storm-surge barriers increasingly more common (Mooyaart and Jonkman, 2017). Important examples include barriers that have already been completed, such as those in the river Scheldt Estuary (The Netherlands), St. Petersburg (Russia), the river Thames (UK), New Orleans (USA), and Venice (Italy), and others that are being proposed or planned, such as those in Shanghai (China) and Galveston Bay (USA). The operation of movable gates under storm-surge conditions, particularly in view of increased sea level in the medium and long term, could lower sediment supply to coastal wetlands, by reducing wetland flooding duration and water depth. An important question, that still awaits a quantitative answer, is whether such a reduction will significantly affect the resilience of coastal wetlands and whether the safeguarding of coastal cities worldwide is in contrast with the preservation of the natural environments around them.

Here, through observations and modelling in the Venice Lagoon (Italy), but with wide implications for similar coastal systems worldwide, we find that storm surges are essential suppliers of sediment to the marshes and, consequently, storm-surge barrier operations seriously affect sediment accumulation on the marsh platforms. Hence, the reduction of water levels associated with flood barriers is likely to be a leading morphodynamic factor in many coastal transitional areas in the present century. Our results point to a fundamental divergence of the conservation needs of the built and the natural coastal environments, which compete for the same “short blanket”, and highlight that “engineered” wetland environments are more fragile than previously thought.

## 5.3 RESULTS

### 5.3.1 Sedimentation dynamics in the Venice Lagoon

The Venice Lagoon is a shallow tidal basin characterized by negligible riverine and marine sediment inputs. Therefore, its morphological evolution is primarily driven by the redistribution of sediment resuspended from within the lagoon (Figure 5.1a-c and Methods). In October 2020 the storm-surge barriers known as Mo.S.E. system (Eprim, 2005) (the Italian acronym for *Experimental Electromechanical Module*), designed to stop increasingly frequent city flooding by temporarily closing the lagoon inlets, became operational. By reducing water levels within the lagoon, the operation of the flood barriers is likely to affect the redistribution of reworked sediment which crucially contributes to marsh accretion.

We measured sediment accumulation at three different salt-marsh sites with monthly frequency or immediately after significant storm-surge events for a total of $n = 1446$ samples from October 2018 to January 2021, thus including both non-regulated conditions and 15 closures of the flood barriers that occurred between October 2020 and January 2021. Site-averaged sediment accumulation varies between 0 and 5500 $\mathrm{g\,m^{-2}}$ and the maximum observed sedimentation rate is 155 $\mathrm{g\,m^{-2}\,d^{-1}}$ (Figure 5.1d-f). The variability in sedimentation rate, extending for more than two orders of magnitude, signals the importance of pulsing events, such as intense storm surges, in conveying sediment over salt marshes. Under fair-weather conditions, sedimentation rates barely reach 20 $\mathrm{g\,m^{-2}d^{-1}}$ and are largely constituted by halophytes' organic production, representing up to 40% in weight of the sediment deposited in summer and early autumn (Morris et al., 2002; Kirwan and Megonigal, 2013; Marani et al., 2013; Morris et al., 2016) (Figure 5.2). During storm surges, on the contrary, the organic contribution to overall soil accumulation decreases to around 10% (Figure 5.2). This characteristic behaviour confirms that, especially in microtidal coastal wetlands, everyday tidal inundation hardly pro-

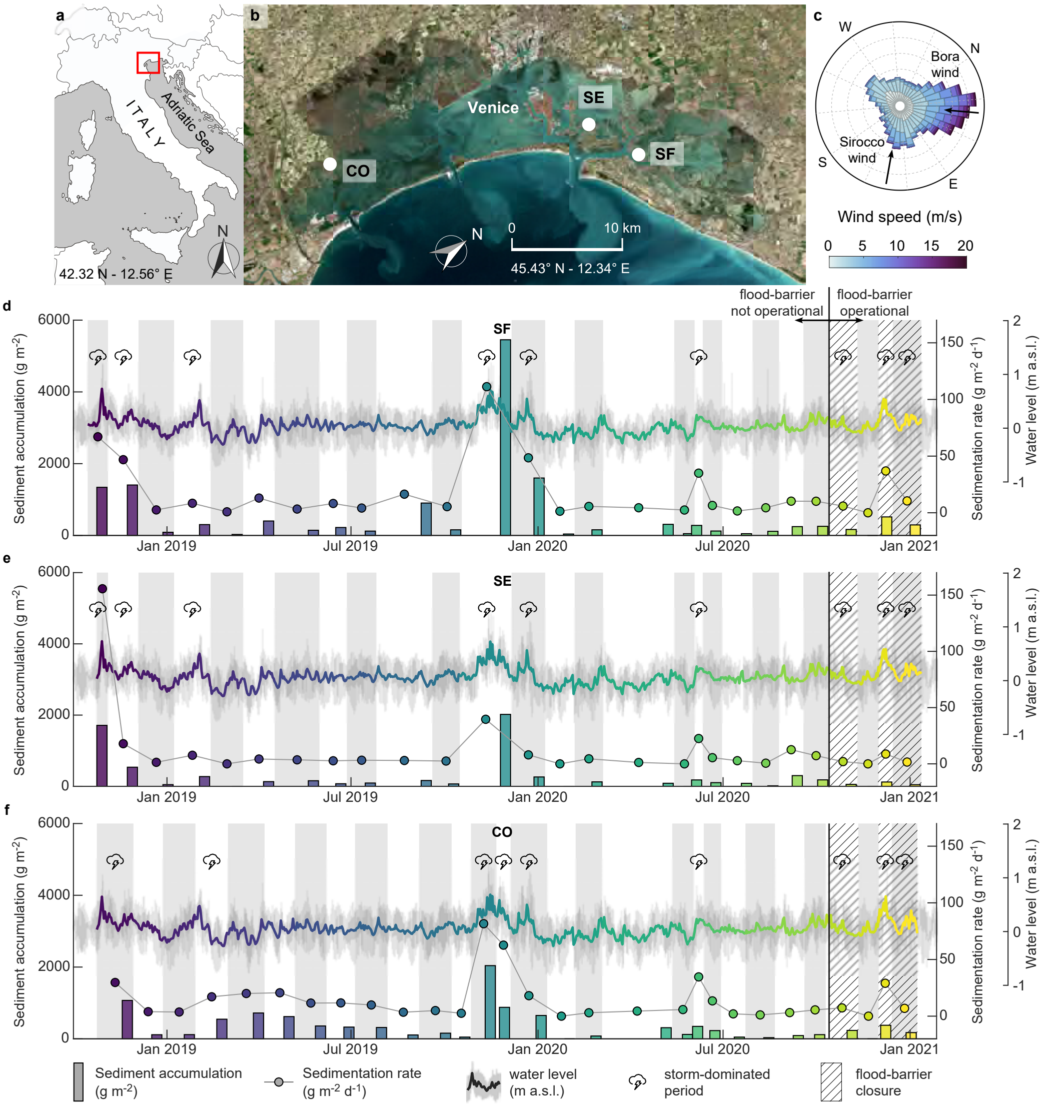


Figure 5.1: **Site location and sedimentation characteristics. a**, Location of Venice Lagoon, Italy. **b**, Location of the three study sites: SF, SE and CO. **c**, Wind statistics for the period 2000–2019, highlighting the two morphologically relevant wind conditions (north-easterly Bora wind and south-easterly Sirocco wind). **d-f**, Mean sediment accumulation, mean sedimentation rate and water level at study site SF (**d**), SE (**e**) and CO (**f**). The thick line (coloured according to observation period) represents the daily mean water level, the thin grey line represents the hourly water level referred to local mean sea level, bars indicate site-averaged sediment accumulation, solid circles show site-averaged sedimentation rates and the cloud symbol identifies storm-dominated periods. Alternate white and grey background indicates different observation periods, and hatched background indicates periods with actual closures of the flood barrier.

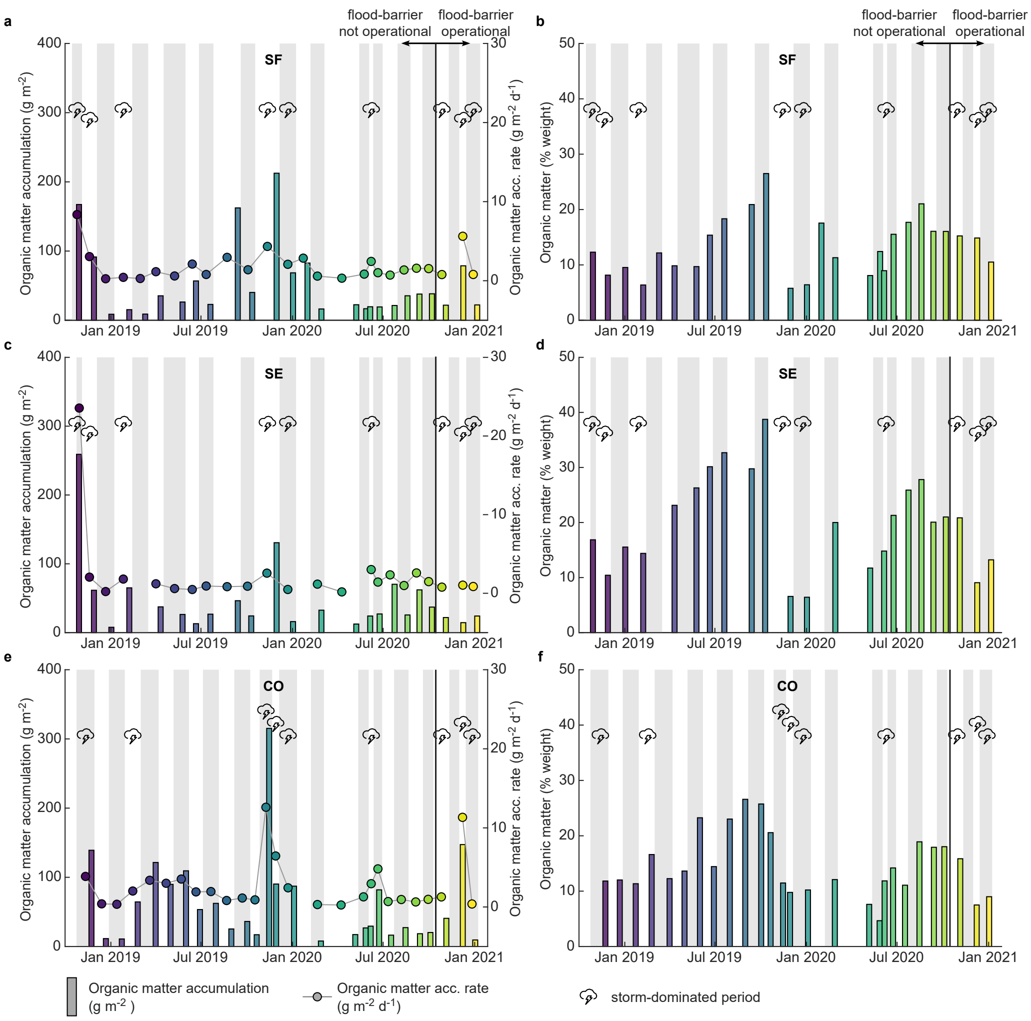


Figure 5.2: **Organic matter content. a,c,e**, Organic matter accumulation (bars) and organic matter accumulation rate (solid circles); (**b,d,f**) organic matter as percentage of weight. The cloud symbol indicates storm periods. Data are grouped for study area: SF (**a-b**), SE (**c-d**) and CO (**e-f**). Alternate white and grey background indicates different observation periods.

vides sediment necessary for marsh survival and only storm surges can mobilize sand and silt from the adjacent tidal flats and deliver them onto the salt-marsh surface (Stumpf, 1983; Cahoon et al., 1995; Reed, 1995). The signature of such severe storm surges appears in the sedimentary record as sub-millimetric sandy laminae interbedded within muddy deposits, generated by the settling around periodic high-water slack and supported by organic production (Roner et al., 2017). Sediment accumulation measured from October 2020 to January 2021, under flood-regulated conditions, is much lower than that observed in the corresponding months of the previous two years (Figure 5.1d-f).

Based on deposition measurements in non-regulated conditions and concurrent water-level and meteorological observations (see Methods), we find that storm-driven contribution accounts for more than 70% of the yearly total sediment accumulation on the marsh surface (Figure 5.3a), even though just 25% of the observational period is storm-dominated (Figure 5.3b and 5.9). Hence, sediment accumulation on salt marshes is supplied by intense, episodic storm surges, rather than the mild, rhythmic tidal flooding, also in extratropical areas, where extreme meteorological phenomena such as tropical cyclones are absent.

### 5.3.2 Relationship with geomorphological drivers

Sediment deposition is often related to the duration, intensity or frequency of marsh inundation (French and Spencer, 1993; J. R. L. Allen, 1995; Morris et al., 2002). To outline this dependence, we explore here a relationship between sedimentation rate and Mean Inundation Depth (MID), which is the mean water depth over the marsh during the observation period. This relationship is conceptually justified, representing MID a natural proxy for sediment contained in the water column during wetland flooding (Methods). We find the sedimentation rate to increase exponentially with MID, similar to previous findings in macrotidal systems (Temmerman et al., 2003) (Figure 5.4a).

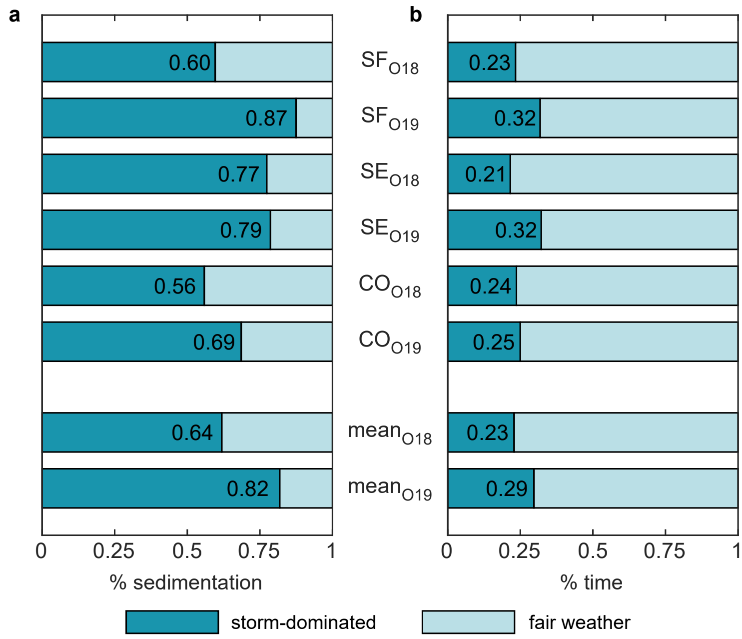


Figure 5.3: **Storm-related sedimentation. a,b**, Percentage of sedimentation (**a**) and percentage of time (**b**) related to storm-dominated periods and to fair-weather conditions. Categories refer to the study areas (SF, SE and CO) and their mean; subscripts indicate the beginning of the grouping period: *O*18, from October 2018 to October 2019, *O*19 from October 2019 to October 2020.

The empirical exponential model captures deposition dependence on MID both under storm and fair-weather conditions, as an exponential regression on storm data only does not significantly differ from the global one (Figure 5.4b). Data scatter around the exponential model is somewhat more relevant for fair-weather observations, especially for summer, when organic sediment accounts for a greater proportion of accumulation, which is thus less tightly related to MID (Figure 5.2). However, the contribution to the global accumulation of largely organic material associated with fair-weather conditions is generally much smaller (up to two orders of magnitude smaller) than that occurring during storm-dominated periods so that the effect of this uncertainty under fair-weather conditions is deemed negligible. Moreover, the empirical model calibrated with data collected under non-regulated conditions well represents also sedimentation

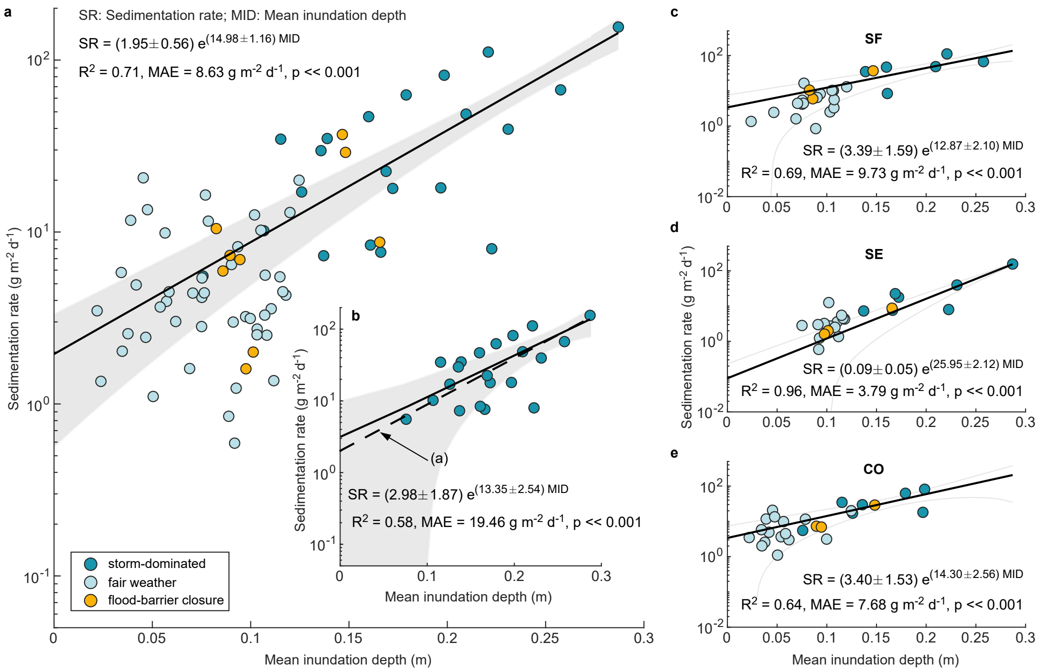


Figure 5.4: **Sedimentation rate increases exponentially with tidal inundation. a**, Exponential relationship between sedimentation rate (SR) and MID for Venice Lagoon. **b**, Exponential relationship fitted considering data relative to storm events only compared with the model in a (dashed line). **c-e**, Relationships between SR and MID for study area SF (**c**), SE (**d**) and CO (**e**). Models calibrated by a standard bootstrap technique (Methods), showing 95% CI (shaded areas), $R^2$, mean absolute error ($MAE$) and $p$-value. Yellow circles represent data from flood-regulated periods. All $y$ axes are on a logarithmic scale.

rates measured when the inlets are closed (yellow dots in Figure 5.4), confirming that the model can be applied to both non-regulated and flood-regulated scenarios. Finally, marsh-specific models are also fitted to gauge the influence of spatially variable factors and to better reproduce local sediment transport processes (Figure 5.4c-e). Overall, local exponential models show modest deviations from the global one (Methods).

The exponential nature of the relationship between sedimentation rate and MID highlights the non-linear effect of intense pulsing events, due to the simultaneous increase in both water levels and suspended sediment concentrations associated with storm-surge conditions (A.

D'Alpaos et al., 2013; Carniello et al., 2016). In turn, the non-linearly large contribution of storm-driven accumulation, in spite of the brief duration of storm-dominated vs. non-storm conditions, points to their crucial contribution to marsh ability to withstand increased rates of sea-level rise and the potentially significant effects of its reduction associated with the operation of storm-surge barriers.

### 5.3.3 The effect of storm-surge barrier operation

The operation of storm-surge barriers, by design, aims to reduce water levels in a tidal basin below a prescribed safety threshold, thereby affecting the wetland flooding (i.e., MID value) and, hence, sediment accumulation on marshes (Figure 5.5a and b).

Here we quantify the effects of operating the storm-surge barrier system built to protect the city of Venice on the ability of marshes to keep up with a rising sea level. The Mo.S.E. system is designed to close the three inlets connecting the Venice Lagoon to the Adriatic Sea when the level of the latter is expected to exceed about 80 cm above the current mean sea level (the official activation level is 110 cm above the traditional datum of Punta della Salute, now approximately 30 cm below mean sea level) to prevent widespread flooding of the city (Eprim, 2005). We first compute water levels in the lagoon together with the corresponding MID as they would have been modified by Mo.S.E. operations during the observational period using a numerical hydrodynamic model (Carniello et al., 2011; Mel et al., 2019) (Methods and Supporting Information). We then apply the site-specific exponential relationships (Figure 5.4c-e) to calculate the modified sediment accumulation and vertical accretion rate at our study sites (Figure 5.6, 5.10 and 5.11). In the flood-regulated scenario, high water levels are capped by the closing of the Mo.S.E. system only for about 70 hours/year (namely 40 hours between October 2018 and October 2019, and 100 hours between October 2019 and October 2020): surprisingly, such a temporally limited reduction in water levels suffices to reduce the yearly sediment accumulation by more than 25% on average (Figure 5.6b and 5.12). This occurs because MID,

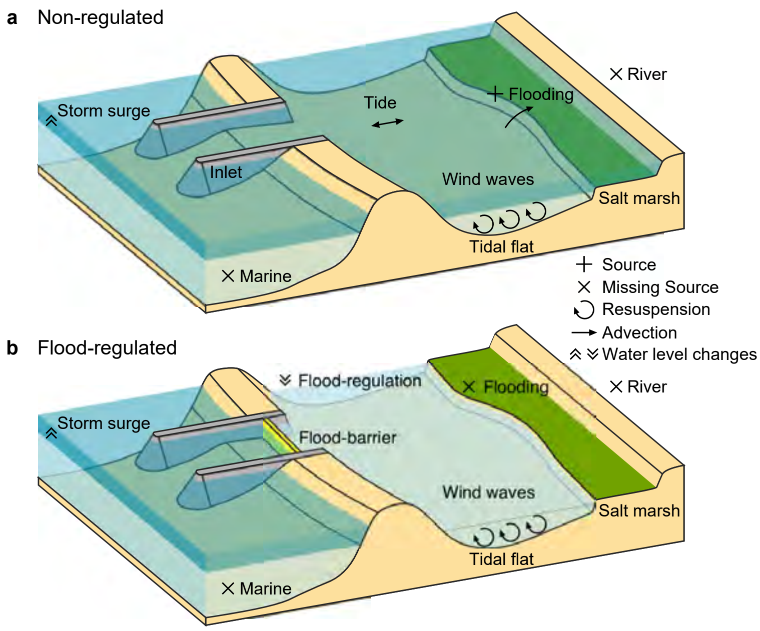


Figure 5.5: **Changes of the physical processes driving sedimentation in the flood-regulated scenario. a,b**, Sediment dynamics in a non-regulated (**a**) and flood-regulated (**b**) system.

and hence sediment delivery to the marshes, is much reduced by the barrier operations. The monitored salt marshes accreted at a rate of 3.7 mm/year on average (SF at 5.1 mm/year, SE at 2.1 mm/year, and CO at 3.9 mm/year) and the drop in sediment supply due to barrier closures translates, independently on the study area, into a 1.1 mm/year reduction (Figure 5.6a), which is about 45% of the relative sea-level rise rate experienced by the Venice Lagoon in the 20$^{th}$ century (2.5 mm/year) (Carbognin et al., 2004). Comparable absolute reduction of sedimentation among study areas suggests that flood regulation will have a more severe impact on marshes with lower sediment supply (Supporting Information).

We conclude that storm-surge barriers can heavily hinder sediment accumulation on coastal wetlands, thus increasing the fragility of their already precarious equilibrium and exacerbating the adverse effects of sea-level rise on their survival. While the analysis is performed on the specific Venice case, the outcomes have far-reaching

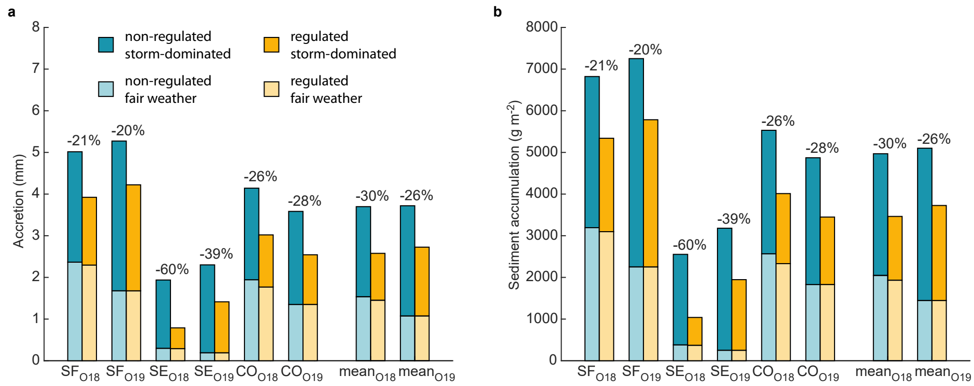


Figure 5.6: **Accretion and sediment accumulation on the salt marshes in the flood-regulated scenario. a,b,**, Change in accretion (**a**) and sediment accumulation (**b**) between the non-regulated (teal bars) and regulated scenario (yellow bars). Categories refer to the study areas (SF, SE and CO) or their mean. Subscripts indicate the beginning of the grouping period: O18, from October 2018 to October 2019, O19, from October 2019 to October 2020. Percentages indicate the relative change in the flood-regulated scenario with respect to the non-regulated one.

implications. In many coastal environments, with a small to negligible sediment supply from inland watersheds (Syvitski et al., 2005; Kirwan et al., 2011), marsh inorganic sediment deposition is largely controlled by settling of sediment resuspended from within the systems, especially by storm surges (Reed, 1995; FitzGerald and Hughes, 2019; Goodwin and Mudd, 2019) (Figure 5.5a). Hence, the reduction of water levels, associated with conventional engineering solutions planned to protect many coastal cities worldwide (Mooyaart and Jonkman, 2017), will change hydrodynamics and sediment transport in the nearby transitional areas. In particular, flood regulation will affect the upper intertidal zone, where only few surge events cause flooding and supply the sediment needed for marshes to offset increasing sea levels (Figure 5.5b).

The objectives of the conservation of the natural environment are thus in contrast with those of the protection of the built environment, revealing that the blanket is indeed short. The quantification of the negative environmental effects of storm-surge barriers offers the cue and the tools to reconcile these competing needs. This contrast can be for example mitigated by

i. coordinating complementary, diffuse measures and optimal operation strategies that enable barriers to be closed at higher activation thresholds (an activation threshold 20 cm higher limits the reduction in sedimentation to 10%, Figure 5.13);

ii. diversifying protection interventions for each marsh depending on the local impact of flood regulation on sedimentation;

iii. naturally or artificially increasing the sediment supply to coastal systems, e.g., in the case of Venice, diverting back the rivers once flowing into the lagoon.

In lack of coastal protection approaches that are inclusive of environmental conservation objectives, the reduction of storm-driven sedimentation associated with the numerous storm-surge barriers planned and being built around the world will result in an accelerated and more extended demise of the global coastal wetland area.

## 5.4 METHODS

### 5.4.1 Geomorphological setting

The Venice Lagoon, located along the north-eastern coast of Italy and connected with the Adriatic Sea through three inlets (Lido, Malamocco and Chioggia), is the largest lagoon of the Mediterranean basin, with an area of about 550 $km^2$ (Figure 5.1a,b). It is characterized by a mean water depth, excluding channels, of about 1.5 m and by a semidiurnal, microtidal regime, with a maximum tidal range of about 1.5 m (Defina et al., 2007; A. D'Alpaos et al., 2013). Due to its location, the Venice Lagoon can experience severe storm surges, mainly driven by the southeasterly Sirocco wind causing an increased water level at the north end of the Adriatic Sea (Figure 5.1c). Because of its elongated shape in the NE-SW direction, relatively large wind waves ($> 1$ m), as well as a relevant wind setup, can be generated in the central-southern basin of the Venice Lagoon by northeasterly Bora winds (Carniello et al., 2011; Mel et al., 2019) (Figure 5.1c).

Human interventions have been influencing hydrodynamic and sediment transport processes within the Venice Lagoon for centuries. All the major rivers flowing into the lagoon were diverted between the 15$^{th}$ and 17$^{th}$ century to prevent channel infilling and preserve navigation. This triggered a sediment-starved condition, further worsened by the construction of the jetties at the three inlets between 1872 and 1934, which hindered sediment flux from the sea and promoted sediment export (Tommasini et al., 2019). Hence, nowadays, the external fluvial and marine sources of sediment are negligible and hydrodynamic processes, such as tidal currents, wind waves and storm surges, mainly rework and redistribute intra-lagoonal sediments, as in many coastal transitional areas worldwide (Syvitski et al., 2005; Kirwan and Megonigal, 2013).

We established 27 permanent measurement stations grouped into three study sites: San Felice (SF, 12 stations), Sant'Erasmo (SE, 6 stations) and Conche (CO, 9 stations) salt marshes (Figure 5.1b). The SF salt marsh is close to the Lido inlet, directly facing one of the main channels dissecting the northern lagoon. The SE salt marsh is still in the northern lagoon adjacent to a shallow tidal flat and sheltered from the Lido inlet by the Sant'Erasmo island. The CO salt marsh is located in the southern lagoon and, thus, it is the most exposed to the action of the wind waves produced by Bora wind events.

Measurement stations are selected in order to be representative of the marsh study area and to cover its ecogeomorphic variability, considering different elevations, distances from the source of sediment, exposure to the dominant winds, and vegetation patterns. Once installed, the position of each station was surveyed with a total station Wild T2002 and its elevation was referred to the Italian Geographic Military Institute (IGM) reference datum.

### 5.4.2 Sediment sampling and analysis

Sediment accumulation is sampled at each station with two circular plastic sediment traps (diameter 0.18 m) designed to measure sediment accumulation with weekly to monthly time resolutions (Temmerman et al., 2003; Thomas and Ridd, 2004; Nolte et al., 2013). Sediment traps were fixed to the marsh surface using two steel claws. The sediment in the traps is collected with an approximate monthly frequency or immediately after a significant storm-surge event. From October 2018 to January 2021, we collected $n = 1446$ samples. Measurement stations are also equipped with a kaolinite horizon marker (diameter 0.20 m) cored yearly to measure vertical accretion rate, as an independent check (Nolte et al., 2013; Morris et al., 2016).

Once in the laboratory, sediment is rinsed with deionised water, oven-dried at 40°C for 48 hours or till no change in weight occurs and weighed to determine sediment accumulation. We estimated organic matter content with Loss-on-Ignition (LOI) procedure, crumbling 2 g of sediment in a ceramic mortar and combusting it in a muffle furnace at 375°C for 16 hours (Ball, 1964; Roner et al., 2016). The difference in weight between pre- and post-treatment provides organic matter content, as a percentage in weight.

Dividing sediment accumulation by bulk density, we can calculate vertical accretion (Morris et al., 2016). Bulk density can be estimated assuming porosity $p = 0.4$, mineral and organic sediment density equal to $\rho_i = 2400\ \mathrm{kg\,m^{-3}}$ and $\rho_o = 1200\ \mathrm{kg\,m^{-3}}$, respectively (Craft et al., 1993; Roner et al., 2016) and knowing inorganic sediment and organic matter percentage from LOI analysis. Accretion rates computed from sediment accumulation agree with kaolinite marker measurements, confirming that the adopted sediment traps offer a reliable measure of sedimentation (Figure 5.8).

### 5.4.3 Storm-dominated period classification

Water level and weather conditions at each study site were measured by three stations of the monitoring network of the Italian In-

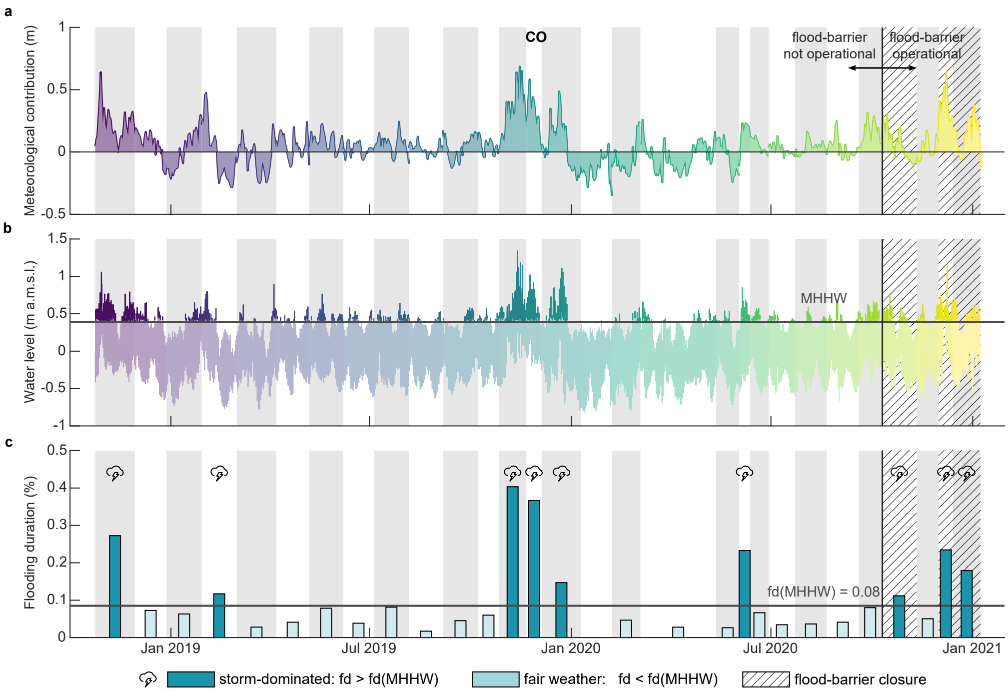


Figure 5.7: **Storm-dominated period classification** (example for CO study area). (**a**) meteorological contribution to the tide; (**b**) measured water level and MHHW (dark gray line); (**c**) comparison between the flooding duration of MHHW ($fd(MHHW) = 0.08$, dark gray line) and the flooding duration ($fd$) of each period. Alternate white and grey background indicates different observation periods, hatched background indicates periods with real closures of flood barriers.

stitute for Environmental Protection and Research (ISPRA) and are used to classify the tidal forcing and climatology of each observation period. Storm-surge conditions can qualitatively be detected considering the positive peaks in the meteorological contribution, computed subtracting the astronomical tide component from the measured water level (Figure 5.7a). However, a quantitative criterion is adopted herein. First, Mean Higher High Water (MHHW), which is defined as the arithmetic mean of the higher high water heights of the tide observed over a specific 19-year Metonic cycle, is computed. Storm-dominated periods are defined as observation periods in which measured water level remains above MHHW for more time than the average computed over the 19-years climatology

(Figure 5.7b-c). Using measured water levels, we implicitly account for the effect of wind and barometric pressure on generating storm surges.

The relative importance of sediment accumulation associated with storm surges clearly emerges when it is compared to the yearly total accumulation and we also considered different one-year-long periods, to avoid seasonal dependency (*O*18: October 2018 – October 2019, *J*19: January 2019-January 2020 and *O*19: October 2019 – October 2020, Figure 5.9).

### 5.4.4 Sedimentation-tide relationship

We investigated the relationship between sedimentation rate and water level considering different synthetic features of the tidal forcing, such as inundation intensity, time, and frequency for each observation period. We finally selected the Mean Inundation Depth (MID) as the most significant feature correlating with the sedimentation rate. MID is equal to the mean water depth that floods each station on the salt marsh and, implicitly, accounts for inundation intensity changes during the considered period, inherently related to the combined effect of astronomical and meteorological contribution. Sampling campaigns were planned to have hydrodynamic and meteorological conditions as uniform as possible within the same observation period, thus making MID representative of the water level time series. MID is negligibly affected by the different duration of periods when the latter is consistent with sediment trap temporal resolution, i.e., from weekly to monthly duration (Thomas and Ridd, 2004; Nolte et al., 2013).

The sedimentation rate exponentially increases with increasing MID. The exponential model is validated with a repeated 10-fold cross-validation scheme, confirming that model validity does not depend on the test set (see Table 5.1). Parameters are calibrated with a standard bootstrap resampling technique (see Table 5.2). The intercept of the exponential relationship can be interpreted as the typical organic matter accumulations when tidal forcing becomes negligible

(Figure 5.2 and parameter $a$ in Table 5.2).

Even though the considered marshes are differently exposed to the action of wind waves and tide, marsh-specific exponential models only slightly differ from one another (Figure 5.4). Wind waves can directly advect sediment onto marshes facing tidal flats, where resuspension occurs, or enhance suspended load subsequently redistributed by tidal currents also in different areas. However, both mechanisms result in increasing accumulation only if the marsh is flooded. Enhanced water levels are typically associated with high wind velocities, especially during storm surges. Therefore, relating sedimentation rate to MID, i.e., to measured water levels, and not just to the astronomical tide, implicitly encompasses the combined effect of wind-wave resuspension during storm surges and tidal-current redistribution.

### 5.4.5 Numerical simulations for the flood-regulated and non-regulated scenarios

Water levels for regulated and non-regulated scenarios are computed with a two-dimensional, finite-element model able to reproduce hydrodynamic processes in shallow water estuaries and lagoons (Carniello et al., 2011) (Supporting Information). In the flood-regulated scenario, the barriers at the inlets are raised whenever the maximum water level exceeds the safety threshold of 80 cm above mean sea level, to preserve all the lagoonal urban settlements from flooding (Mel et al., 2019). Whereas the non-regulated scenario is obtained by simulating the free propagation of the tide within the lagoon, i.e., not closing the inlets. Both simulations are run imposing as boundary conditions water levels measured 12 kilometers offshore in the Adriatic Sea at the platform of the Italian Research National Council (CNR) and wind velocities measured within the lagoon (Supporting Information).

## 5.5 SUPPORTING INFORMATION

**VERTICAL ACCRETION RATE.** The vertical accretion rate in each station is measured yearly through coring and measuring the layer deposited over the kaolinite horizon marker. Comparison between measured and computed accretion rate (Figure 5.8) confirms that the adopted sediment traps offer a reliable measure of sedimentation.

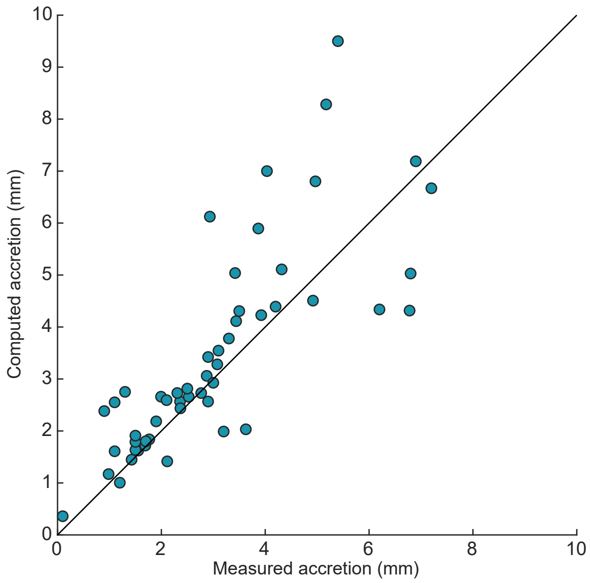


Figure 5.8: **Measured vs. computed vertical accretion.** Scatter plot of yearly vertical accretion measured with horizon marker and accretion computed with sediment accumulation data and bulk density

**STORM-RELATED SEDIMENTATION.** The relative importance of sediment accumulation associated with storm-dominant period and storm duration is considered for different one-year-long periods, to avoid seasonal dependency (*O*18: October 2018 – October 2019, *J*19: January 2019-January 2020 and *O*19: October 2019 – October 2020, Figure 5.9). It proves that storm surges account for more than 70% of the yearly sedimentation, although representing just 25% of the period duration on average. On the other hand, slight variation among

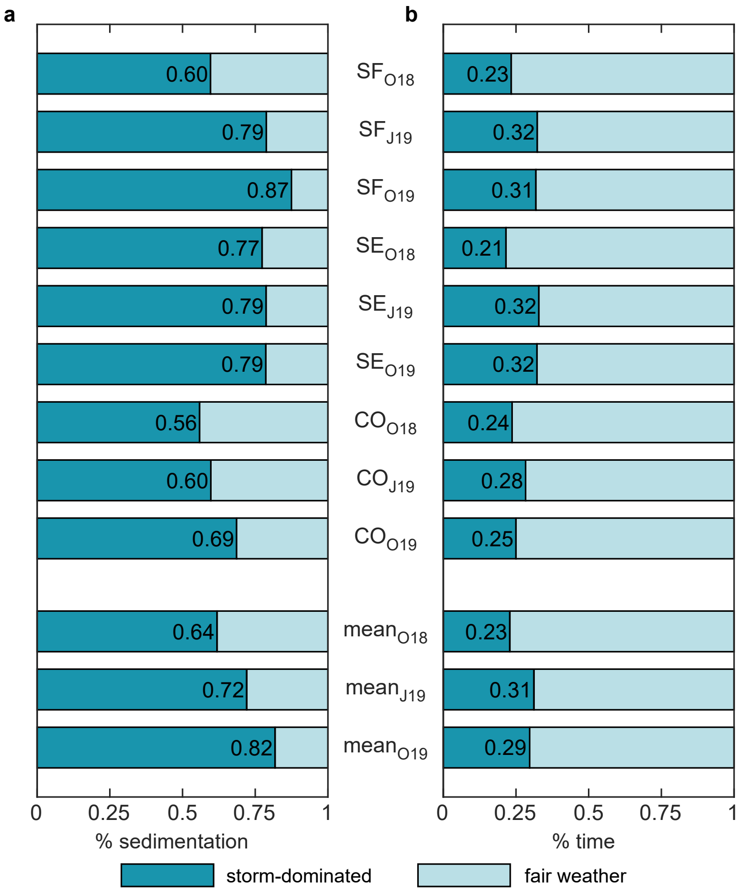


Figure 5.9: **Storm-related sedimentation.** Percentage of sedimentation (**a**) and percentage of time (**b**) related to storm events and to fair-weather conditions. Categories refer to the study areas (SF, SE and CO) and their mean (darker colour); subscripts indicate the beginning of the grouping period: *O*18, from October 2018 to October 2019, *J*19 from January 2019 to January 2020 and *O*19 from October 2019 to October 2020.

different yearly periods confirms that this two-year-long dataset can explain the main seasonal variations of the processes.

**RELATION WITH GEOMORPHOLOGICAL DRIVERS.** We report in Table 5.1 the results of the cross-validation analysis performed to test the model validity. Model parameters are computed with a standard bootstrap resampling technique (Methods) and results are shown in Table 5.2.

**Table 5.1: Cross-validation results.** Error indicators of the 10-fold cross-validation (repeated 100 times) for the whole lagoon and for each study area (SF, SE and CO): Mean Absolute Errors ($MAE$), Mean Squared Error ($MSE$) and Root Mean Squared Error (RMSE). Train errors have subscript t and validation errors have subscript v.

| Study area | MAEt ($g\,m^{-2}\,d^{-1}$) | MAEv ($g\,m^{-2}\,d^{-1}$) | MSEt ($g\,m^{-2}\,d^{-1})^2$ | MSEv ($g\,m^{-2}\,d^{-1})^2$ | RMSEt ($g\,m^{-2}\,d^{-1}$) | RMSEv ($g\,m^{-2}\,d^{-1}$) |
|---|---|---|---|---|---|---|
| Lagoon | 8.71 | 9.40 | 199.68 | 235.76 | 14.11 | 13.54 |
| SF | 9.52 | 12.62 | 194.98 | 492.25 | 13.85 | 15.81 |
| SE | 3.92 | 8.22 | 40.66 | 401.81 | 6.30 | 11.37 |
| CO | 7.95 | 10.47 | 133.49 | 302.43 | 11.44 | 12.84 |

**Table 5.2: Sedimentation rate – tide relationship.** Model parameter ($SR = a \cdot exp(b \cdot MID)$) for the whole lagoon and for each study area (SF, SE and CO). Standard errors are computed by a standard bootstrap technique.

| Study area | $a$ | $b$ | $R^2$ | $MAE$ | $p$-value |
|---|---|---|---|---|---|
| Lagoon | $1.95 \pm 0.56$ | $14.98 \pm 1.16$ | 0.71 | 8.63 | $\ll 0.001$ |
| SF | $3.39 \pm 1.56$ | $12.87 \pm 2.10$ | 0.68 | 9.96 | $\ll 0.001$ |
| SE | $0.09 \pm 0.05$ | $25.95 \pm 2.12$ | 0.96 | 3.92 | $\ll 0.001$ |
| CO | $3.40 \pm 1.53$ | $14.30 \pm 2.56$ | 0.64 | 7.64 | $\ll 0.001$ |

**THE EFFECT OF STORM-SURGE BARRIER OPERATION.** To quantify the effect of operating the storm-surge barrier system on salt-marsh sedimentation, we computed the water levels under non-regulated and flood-regulated scenarios from October 2018 to January 2021 using the two-dimensional, finite-element *Wind-Wave-Tidal-Model* (WWTM) (Carniello et al., 2005, 2011), which is based on a hydrodynamic module coupled with a wind-wave module.

The hydrodynamic module solves the 2D depth-integrated shallow water equations, suitably rewritten in order to reproduce wetting and drying processes in very shallow and irregular domains (Defina, 2000):

$$\frac{\partial q_x}{\partial t} + \frac{\partial}{\partial x}\left(\frac{q_x^2}{Y}\right) + \frac{\partial}{\partial y}\left(\frac{q_x q_y}{Y}\right) - \left(\frac{\partial R_{xx}}{\partial x} + \frac{\partial R_{xy}}{\partial y}\right) + \\ + \frac{\tau_{tx}}{\rho} - \frac{\tau_{wx}}{\rho} + gY\left(\frac{\partial h}{\partial x}\right) = 0 \quad (5.1)$$

$$\frac{\partial q_y}{\partial t} + \frac{\partial}{\partial x}\left(\frac{q_x q_y}{Y}\right) + \frac{\partial}{\partial y}\left(\frac{q_y^2}{Y}\right) - \left(\frac{\partial R_{xy}}{\partial x} + \frac{\partial R_{yy}}{\partial y}\right) + \\ + \frac{\tau_{ty}}{\rho} - \frac{\tau_{wy}}{\rho} + gY\left(\frac{\partial h}{\partial y}\right) = 0 \quad (5.2)$$

$$\eta\frac{\partial h}{\partial t} + \frac{\partial q_x}{\partial x}\frac{\partial q_y}{\partial y} = 0 \quad (5.3)$$

where t is time, the x,y subscripts represent the directions of a given variable in a Cartesian reference system, $\mathbf{q} = (q_x, q_y)$ is the flow rate per unit width, $R_{ij}$ stands for the depth-averaged Reynolds stresses ($i, j$ denoting either $x$ or $y$ coordinates), $\tau_{ti}$ and $\tau_{wi}$ are the bottom shear stress produced by tidal currents and wind-waves, respectively, $\rho$ indicates the fluid density, $g$ is the gravitational acceleration, $Y$ denotes the water volume per unit area (i.e., the equivalent water depth), $h$ is the free surface elevation, and $\eta$ is the wet fraction of the computational domain which accounts for surface irregularities during the wetting and drying processes (Defina, 2000). A semi-implicit staggered finite element method based on discontinuous Galerkin's approach is adopted to solve the governing equations (Defina, 2000).

The closure of the Reynolds stresses, which appear in the momentum equations along the two horizontal directions, is solved by introducing a suitable eddy viscosity, evaluated employing Smagorinsky's model (Smagorinsky, 1963). The horizontal components of the Reynolds stresses then read:

$$R_{xx} = 2\nu_e \frac{\partial q_x}{\partial x} \tag{5.4}$$

$$R_{xy} = \nu_e \left( \frac{\partial q_x}{\partial x} + \frac{\partial q_y}{\partial x} \right) \tag{5.5}$$

The eddy viscosity $\nu_e$ differs from the standard one as it also encloses the contribution from the stresses generated by the subgrid momentum exchange, which is yet difficult to evaluate due to its dependence on the full three-dimensional morphology of the bottom surface (Defina, 2000). The hydrodynamic module provides the wind-wave module with water levels and depth-averaged velocities that are used for calculating wave group celerity as well as for evaluating the influence of flow depth on wind-wave propagation.

The wind-wave module (Carniello et al., 2011), based on the same computational grid of the hydrodynamic model, solves the wave action conservation equation (Hasselmann et al., 1973). The latter is simplified by assuming that the direction of wave propagation instantaneously readjusts to match the wind direction (i.e., neglecting refraction). The wave action conservation equation describes the evolution of the wave action density ($N_0$ ) in the frequency domain and it reads (Carniello et al., 2011):

$$\frac{\partial N_0}{\partial t} + \frac{\partial}{\partial x} c'_{gx} N_0 + \frac{\partial}{\partial y} c'_{gy} N_0 = S_0 \tag{5.6}$$

where $c'_{gx}$ and $c'_{gy}$ represent the wave group celerity in the $x$ and $y$ direction respectively, and are used to approximate the propagation speed of $N_0$ (Holthuijsen et al., 1989; Carniello et al., 2011), while $S_0$ represents all source terms describing the external phenomena contributing to wave energy variations, which can be either positive (wind energy input) or negative (bottom friction, whitecapping and depth-induced breaking). Based on the relationship between peak-wave period and local wind speed and water depth (Young and Verhagen, 1996), the model is able to compute both the spatial and temporal distribution of the wave periods.

The WWTM model has been benchmarked against both hydrodynamic and wind-wave field data from the Venice Lagoon (Italy) (Carniello et al., 2005, 2011), Virginia Coast Reserve lagoons (USA) (Mariotti et al., 2010b), and Cadiz Bay (Spain) (Zarzuelo et al., 2018).

Once computed the water level time-series, MID is obtained, as for the measured water level, computing the mean of the water depth over the marsh when flooded. The site-specific exponential models (Figure 5.4) are then applied to compute sedimentation rate in the flood regulated and non-regulated scenarios.

In Figure 5.10, we show the measured sediment accumulation (grey bars) together with the modelled ones in the non-regulated (teal bars) and flood-regulated scenario (yellow bars) for each period. Before October 2020 the barrier system was not active and sedimentation modelled in the non-regulated scenario well reproduces the measurements. In addition, our analyses show that measured deposition during periods of barrier activation are also well reproduced by the proposed regression, confirming that the exponential relationship is not only able to capture sediment accumulation dynamics under unimpeded conditions, but also their changes due to the closure of the flood barriers. Accretion can be computed by combining sediment accumulation and bulk density (see Methods) and its changes through time in different scenarios are represented in Figure 5.11, together with the cumulative accretion (continuous lines) and compared with kaolinite horizon marker measurements (black dots). During

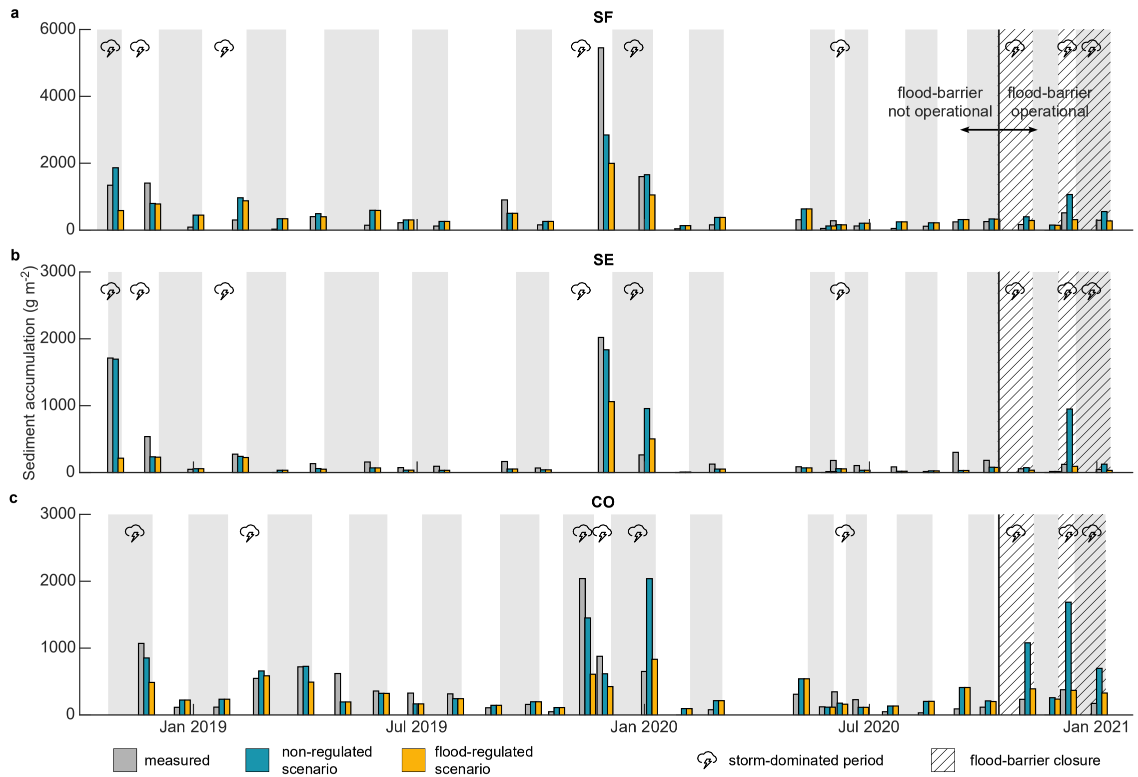


**Figure 5.10: Sediment accumulation changes in the flood regulated scenario.** Comparison between measured data (grey bars), sediment accumulation modelled in the non-regulated (teal bars) and regulated scenario (yellow bars) for each study area: SF (**a**), SE (**b**) and CO (**c**). Alternate white and grey background indicates different observation periods, hatched background indicates periods with actual closures of flood barriers. The cloud symbol indicates storm-dominated periods.

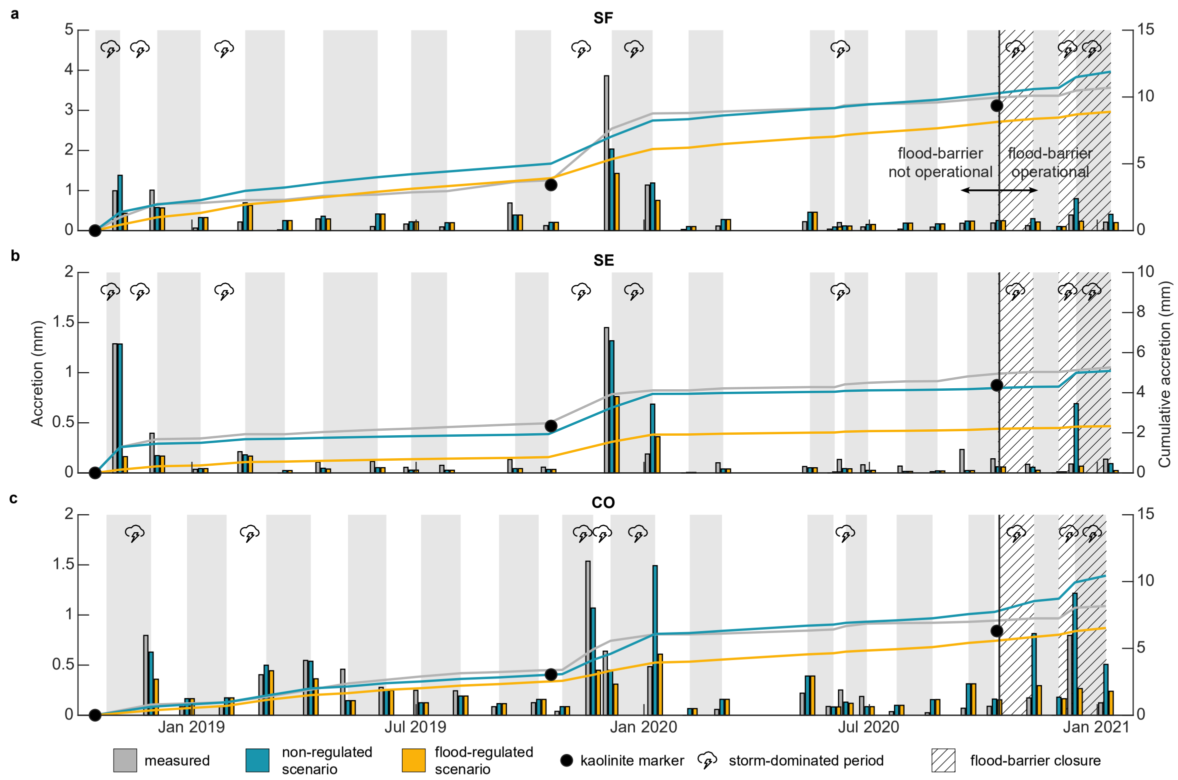


Figure 5.11: **Vertical accretion changes in the flood regulated scenario.** Comparison between measured data (grey bars), vertical accretion modelled in the non-regulated (teal bars) and regulated scenario (yellow bars) for each study area: SF (**a**), SE (**b**) and CO (**c**). Lines represent cumulative accretion rates and black solid circles are yearly horizon marker measurements. Alternate white and grey background indicates different observation periods, hatched background indicates periods with actual closures of flood barriers. The cloud symbol indicates storm-dominated periods.

fair-weather periods, accretion under natural and flood-regulated conditions closely resemble each other, and sediment supply drop due to flood regulation during storm-dominated periods is sufficient to severely reduce the accretion in this scenario.

Sediment accumulation can be summed over yearly periods separately for the two scenarios to understand sedimentation changes due to flood-regulation at the annual time scale (Figure 5.6b and Tables 5.3 and 5.4). On average, flood-regulation would have reduced sedimentation by more than 25% in the period October 2018-October 2020 (30% and 26% for the first and the second monitored year, respectively).

Interestingly, all sites would have been affected by comparable absolute reductions (between 1235 and 1514 $g\,m^{-2}$), although the total sedimentation in the non-regulated scenario is rather different among study areas. The SE salt marsh is characterized by the lowest total yearly sedimentation (2554 $g\,m^{-2}$ and 3183 $g\,m^{-2}$ for $O18$ and $O19$, respectively) due to its position far from the main channel network and facing a relatively sheltered tidal flat. Conversely, both the SF salt marsh, close to a major channel, and the CO salt marsh, exposed to the action of wind-waves propagating on a wide subtidal platform, display on average a sediment accumulation that is more than double than sediment accumulation in SE (6884 $g\,m^{-2}$ in $O18$ and 7309 $g\,m^{-2}$ in $O19$ for SF; 5741 $g\,m^{-2}$ in $O18$ and 5024 $g\,m^{-2}$ in $O19$ for CO). Consequently, sedimentation reduction due to flood-regulation will affect SE more severely than the other sites (-60% for $O18$ and -39% for $O19$ in SE; -21% for $O18$ and -20% for $O19$ in SF; -26% for $O18$ and -28% for $O19$ in CO - Figure 5.6). Our results suggest that the relative amount of sedimentation reduction will diversely affect the different marshes and, hence, their specific capability to keep pace with sea-level rise.

Data collected in autumn 2020, i.e., October 2020-December 2020 when the barrier system was operational, provide a direct quantification of sedimentation reduction due to flood regulation, that can be compared with the sedimentation of the corresponding period of

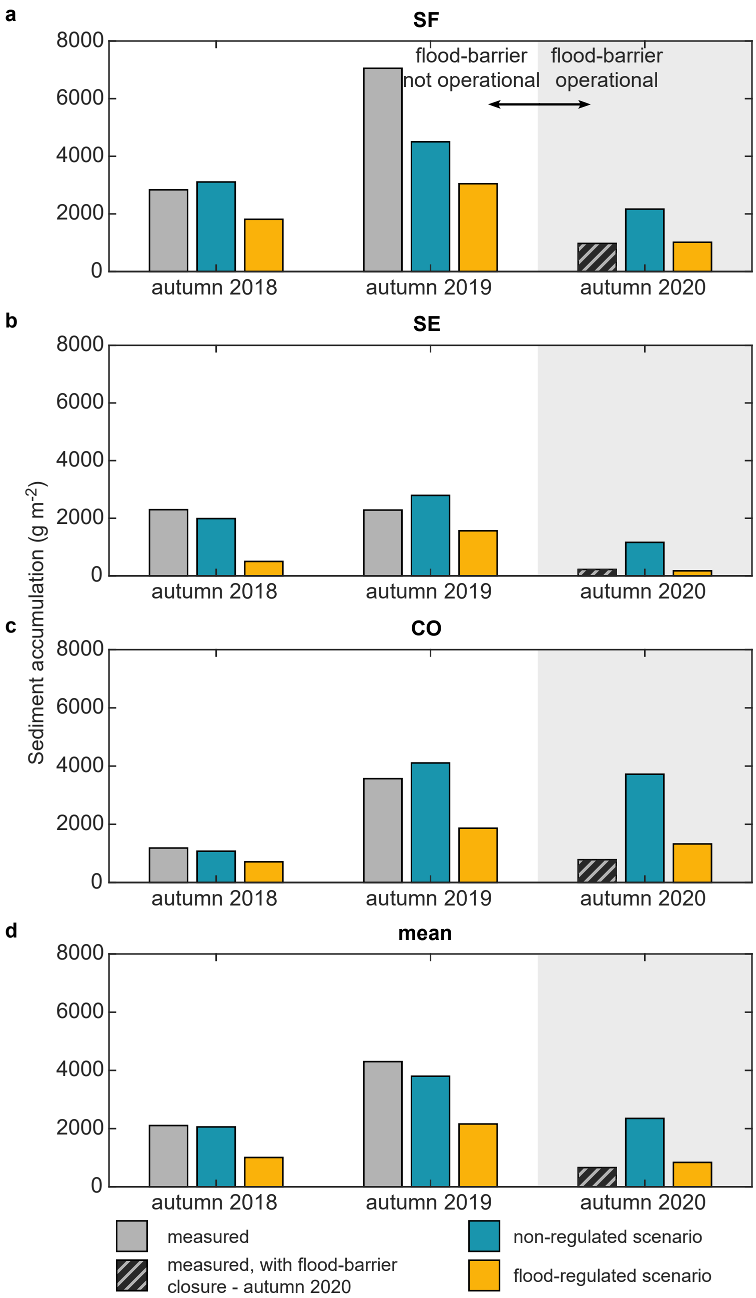


Figure 5.12: **Sedimentation changes due to flood-regulation during autumn.** Comparison between measured data (grey bars), modelled data in the non-regulated (teal bars) and regulated scenario (yellow bars) summed for autumnal months (October, November and December) for each study area: SF (**a**), SE (**b**), CO (**c**) and their mean (**d**). In autumn 2020 the flood barriers were used, so measurements refer to the flood-regulated condition.

2018 and 2019 (Figure 5.12). Measurements are well-reproduced by modelled data both in non-regulated (grey and teal bar in autumn 2018 and 2019) and flood-regulated conditions (hatched grey and yellow bars in autumn 2020).

Table 5.3: **Sediment accumulation changes from October 2018 to October 2019 (O18).** Sedimentation absolute change (3rd column) is computed as the difference between sedimentation in the regulated (2nd column) and non-regulated scenario (1st column).

| Study area | Sedimentation non-regulated scenario ($g\,m^{-2}$) | Sedimentation regulated scenario ($g\,m^{-2}$) | Absolute change ($g\,m^{-2}$) | Relative change % |
|---|---|---|---|---|
| $SF_{O18}$ | 6884.53 | 5411.03 | -1473.50 | -21% |
| $SE_{O18}$ | 2554.84 | 1040.82 | -1514.02 | -60% |
| $CO_{O18}$ | 5741.76 | 4240.01 | -1501.75 | -26% |
| $mean_{O18}$ | 5060.38 | 3563.95 | -1496.42 | -30% |

Table 5.4: **Sediment accumulation changes from October 2019 to October 2020 (O19).** Sedimentation absolute change (3rd column) is computed as the difference between sedimentation in the regulated (2nd column) and non-regulated scenario (1st column).

| Study area | Sedimentation non-regulated scenario ($g\,m^{-2}$) | Sedimentation regulated scenario ($g\,m^{-2}$) | Absolute change ($g\,m^{-2}$) | Relative change % |
|---|---|---|---|---|
| $SF_{O19}$ | 7309.86 | 5850.48 | -1473.50 | -20% |
| $SE_{O19}$ | 3183.73 | 1948.57 | -1514.02 | -39% |
| $CO_{O19}$ | 5024.30 | 3632.14 | -1501.75 | -28% |
| $mean_{O19}$ | 5172.63 | 3810.40 | -1496.42 | -26% |

**SENSITIVITY ANALYSIS OF DIFFERENT ACTIVATION THRESHOLDS.** Mobile flood barriers can be operated at different activation thresholds, which might be increased by adopting complementary conventional or ecosystem-based measures (Temmerman et al., 2013). In particular, for the Venice lagoon, the standard activation threshold is set at 110 cm above the local reference datum of Punta della Salute (ZPS) but the barriers can be activated also at lower levels to reduce flooding risk (up to 65 cm above ZPS, as it happened in October 2020). However, through additional local protection measures, the city might withstand higher water levels (reasonably up to 130 cm above ZPS). These changes in the activation thresholds would produce important differences in terms of marsh flooding and, hence, sedimentation, especially in the Venice lagoon where salt marshes occupy a relatively narrow range of elevations due to the microtidal regime (A. D'Alpaos et al., 2011; Goodwin and Mudd, 2019).

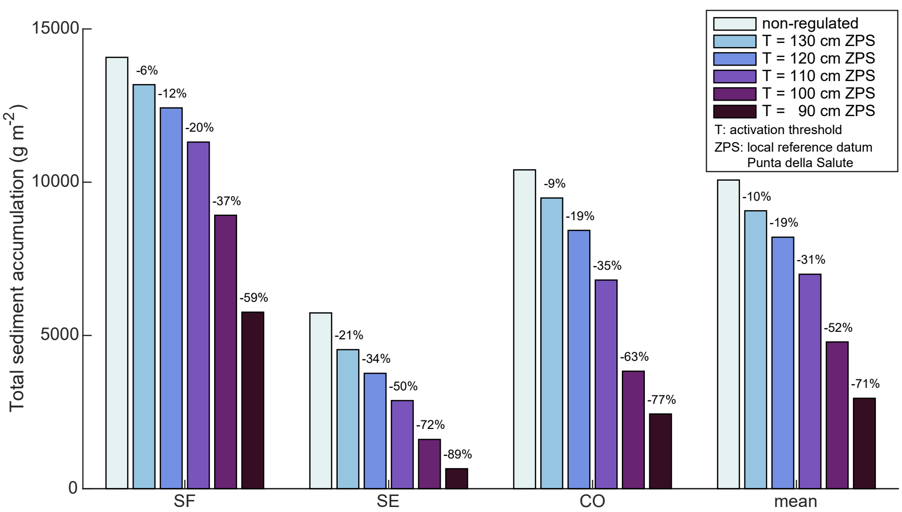


Figure 5.13: **Sedimentation changes due to flood-regulation during autumnal periods.** Comparison between measured data (grey bars), modelled data in the non-regulated (teal bars) and regulated scenario (yellow bars) summed for autumnal months (October, November and December) for each study area: SF (**a**), SE (**b**), CO (**c**) and their mean (**d**). In autumn 2020 the flood barriers were used, so measurements refer to the flood-regulated condition.

We performed a sensitivity analysis to assess the effect of different activation thresholds on sedimentation (Figure 5.13) using the methodology adopted in the present work. Different scenarios span from lower (i.e., 90 cm ZPS) to higher (i.e., 130 cm ZPS) activation thresholds, chosen in the reasonable activation range for the Venice lagoon. Lower activation thresholds dramatically reduce sediment accumulation on the marshes, up to 71% on average with the 90 cm ZPS activation threshold. Conversely, higher activation thresholds (i.e., 120 and 130 cm ZPS) only slightly affect sedimentation over the salt marshes.

In conclusion, although flood barriers negatively affect salt-marsh sedimentation, careful and integrated management can pave the way to a compromise between natural environment conservation and urban area protection.

# 6

# EFFECTS OF STORM-SURGE BARRIERS AT THE BASIN SCALE

This chapter is a manuscript accepted for publication in *Science Advances* and assesses the effects of the anthropogenic flood-regulation on the morphodynamic evolution of shallow tidal embayments by expanding at the basin scale some considerations introduced in the second part of Chapter 5. The first operations during Fall 2020 of the storm-surge barriers designed to avoid the flooding of the city of Venice give us the chance to compare the numerical modeling results with the first-ever measurements in a flood-regulated environment. The analysis carried out by comparing the numerical results obtained considering the scenario with the activation of the barriers to that without allows us to highlight the differences in the main hydrodynamic and morphodynamic parameters. Results can represent a useful tool for coastal managers to evaluate operational strategies of storm-surge barriers that account also for their morphological implications on the surrounding natural environment.

## LOSS OF GEOMORPHIC DIVERSITY IN SHALLOW TIDAL EMBAYMENTS PROMOTED BY STORM-SURGE BARRIERS

**Davide Tognin[1,2], Alvise Finotello[2,3], Andrea D'Alpaos[2,3], Daniele P. Viero[1], Mattia Pivato[2], Riccardo A. Mel[5], Andrea Defina[1,2], Enrico Bertuzzo[3], Marco Marani[1,2], and Luca Carniello[1,2]**

[1]Department of Civil, Environmental, and Architectural Engineering, University of Padova, Padova, Italy

[2]Center for Lagoon Hydrodynamics and Morphodynamics, University of Padova, Padova, Italy

[3]Department of Environmental Sciences, Informatics and Statistics, Ca' Foscari University of Venice, Mestre, Venice, Italy

[4]Department of Geosciences, University of Padova, Padova, Italy

[5]Department of Environmental Engineering, University of Calabria, Cosenza, Italy.

### 6.1 ABSTRACT

Coastal flooding prevention measures, such as storm-surge barriers, are being widely adopted globally due to the accelerating rise in sea levels. However, their impacts on the morphodynamics of shallow tidal embayments remain poorly understood. Here we combine field data and modelling results from the microtidal Venice Lagoon (Italy) to identify short- and long-term consequences of flood regulation on lagoonal landforms. Artificial reduction of water levels enhances wave-induced sediment resuspension from tidal flats, promoting in-channel deposition, at the expense of salt-marsh vertical accretion. In Venice, we estimate that the first 15 closures of the recently installed mobile floodgates operated between October 2020 and January 2021 contributed to a 12% reduction in marsh deposition, simultaneously promoting a generalized channel infilling. Therefore, suitable countermeasures need to be taken to offset these processes and prevent significant losses of geomorphic diversity due to repeated floodgate closures, whose frequency will increase as sea levels rise further.

## 6.2 INTRODUCTION

Low-lying coastal areas worldwide are threatened by the adverse consequences of flooding hazards related to climate change and rising sea levels (Nicholls et al., 2007; Kulp and Strauss, 2019; Kirezci et al., 2020; Nicholls et al., 2021). To mitigate flooding risk, many coastal cities supporting large populations and economies have adopted hard protection measures in the form of storm-surge barriers (Mooyaart and Jonkman, 2017; Vousdoukas et al., 2020). Significant examples are the barriers built to protect the Netherlands, the cities of London and Hull in the UK, St. Petersburg in Russia, New Orleans in Louisiana, and Venice in Italy. Surge barriers are also being proposed to protect Shanghai and New York, as well as Galveston Bay in the US.

Despite the rapidly increasing number of structures to defend coastal cities, the effects of flood regulation measures on the morphodynamic evolution of the tidal areas surrounding them still need to be fully understood (Eelkema et al., 2013; Orton et al., 2019). Storm-surge barriers may deeply affect the chief coastal land-forming processes, such as tides, surges, and waves (Green and Coco, 2014; Zhou et al., 2017; Haas et al., 2018), impacting sediment transport and the possible survival of many important transitional coastal environments as sea levels keep rising (Rodríguez et al., 2017). This is especially critical in sediment-supply limited, shallow embayments (Peteet et al., 2018), where morphodynamics is intimately related to wind-driven sediment resuspension and transport mechanisms and can be deeply affected by changes in water levels due to storm-surge barrier operations.

The Venice Lagoon, Italy, is one of the first examples of a sediment-starved, shallow back-barrier system protected by storm-surge barriers. The set of barriers, known as the Mo.S.E. system (the Italian acronym for *Experimental Electromechanical Module*), spans the three inlets - Lido, Malamocco, and Chioggia from North to South – that connect the Venice Lagoon to the Adriatic Sea (Figure 6.1). The mobile barriers are closed to avoid the flooding of Venice when the water

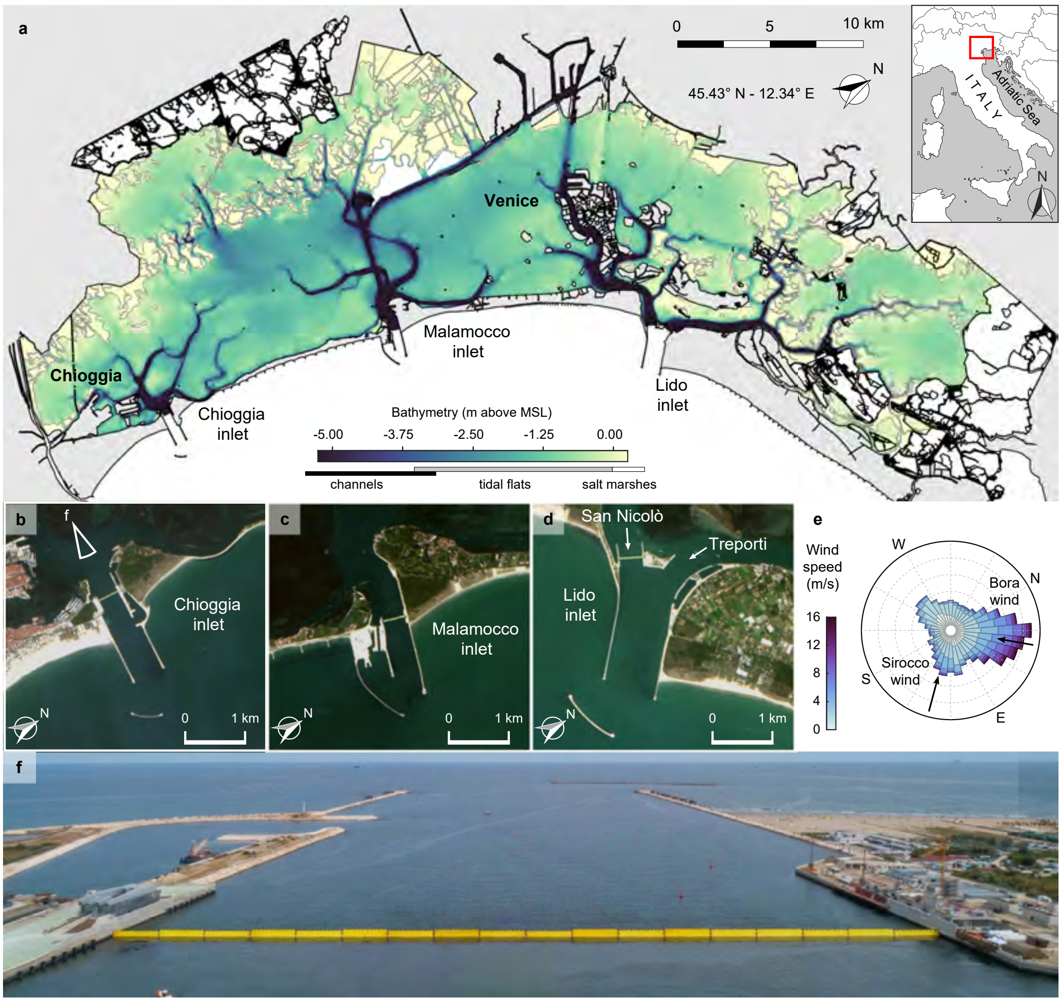


Figure 6.1: **Geomorphological setting and floodgates**. (**a**) Bathymetry of the Venice lagoon located in north-eastern Italy (inset). Salt marshes are indicated by the grey contour. Chioggia inlet (360 m wide, 12 m deep, 18 gates, **b**), Malamocco inlet (380 m wide, 14 m deep, 19 gates, **c**) and Lido inlet (**d**), divided into the San Nicolò barrier (400 m wide, 12 m deep, 20 gates) and the Treporti barrier (420 m wide, 6 m deep, 21 gates - still submerged during the test in the satellite image), during the closure test on 9 October 2020 10:00 UTC (Landsat 8 – NASA). (**e**) Wind rose for the period 2000-2019 measured in Chioggia, arrows highlight the two morphologically significant winds (Bora – NE, Sirocco – SE). (**f**) The Mo.S.E. barrier during a closure at the Chioggia inlet (Photo position indicated in panel **b**, photo credits https://www.mosevenezia.eu/).

level is predicted to exceed 1.10 m above the local reference datum of Punta della Salute (ZPS) (corresponding to 0.79 m above the current mean sea level) (Mel et al., 2021b). Each barrier is made by a series of flapgates (78 in total; Figure 6.1), which are hinged along a common horizontal axis and rest flush with the seabed under normal tidal levels to allow for the exchange of water and sediment fluxes, as well as regular ship traffic.

The construction of the Mo.S.E. system began in 2003 and the mobile floodgates were operated for the first time in October 2020, holding back high-tide waters outside the lagoon for the first time in history. Despite the heated public, technical, and scientific debate that have surrounded the Mo.S.E. since its conception in the 1970s (Ammerman and McClennen, 2000; Bras et al., 2002), the impacts that repeated closures of the lagoon inlets might have on the fate of the characteristic lagoonal landforms – i.e., salt marshes, tidal flats, and tidal channels (Figure 6.1a) – have not yet received the necessary attention. These landforms constitute the morphological backbone on which all the relevant morphodynamic and ecological processes rely. For instance, tide propagation and water residence time within the lagoon depend on the morphology of the tidal channel network, as well as on the relative extent and bed elevation of tidal-flat and salt-marsh areas (Aubrey and Speer, 1985). Salt marshes are also effective in limiting wind fetch, thereby reducing both wind-wave height and wind setup (Mariotti and Fagherazzi, 2013; Möller et al., 2014; Tommasini et al., 2019), with direct effects on water levels within the lagoon (L. D'Alpaos, 2010a; Silvestri et al., 2018). In addition, the morphological structure of the lagoon plays a key role in regulating the exchange of sediments, nutrients, and pollutants with the open sea, and provides diverse habitats for many plant and animal species which are also important for local economies (Costanza et al., 1997; Chmura et al., 2003; Barbier et al., 2011; Newton et al., 2018).

While there is no doubt that temporarily disconnecting the lagoon from the sea is key to preventing the flooding of Venice and other urban areas during severe storm-surge events (Bras et al., 2002), it is essential to fully understand the potentially cascading effects that repeated inlet closures might have on long-term lagoon morphodynamics. This becomes increasingly critical in view of the rise in the mean sea level expected over the next century (Oppenheimer et al., 2019; Kirezci et al., 2020), which will inevitably lead to more frequent closures (Mel et al., 2021a).

Here we use field data and numerical modelling of barrier activations from October 2020 to January 2021, focusing in particular on the first two closures that occurred on 3 and 15 October 2020, to understand the impacts of flood regulation on sediment transport within the lagoon and their possible implications for the morphological evolution of lagoonal landforms. We adopted a custom-built, extensively tested, 2-D finite-element numerical model able to reproduce morphodynamic processes within the Venice lagoon (Carniello et al., 2011, 2012; Mel et al., 2021b) (see Materials and Methods). To better understand the effects of Mo.S.E. operations, the results for the flood-regulated scenario are compared with those for non-regulated conditions, which would have occurred in the absence of the floodgate closures. Results of the simulations are then analysed in terms of differences in water levels, bottom shear stresses, suspended sediment concentrations, and salt-marsh flooding. Long-term effects of floodgate closures on the morphodynamics of the whole lagoon, as well as potential cascading effects due to the degradation of lagoonal landforms, are finally discussed together with possible mitigation solutions.

## 6.3 RESULTS

### 6.3.1 Effects on the lagoon hydrodynamics

The Mo.S.E. floodgates were raised to hold water levels within the lagoon below the safety threshold of 1.10 m above the local datum (ZPS), for both storm-surge events of 3 and 15 October 2020 (Figure 6.2, 6.8 and 6.9). Maximum measured water levels in the lagoon reached 0.80 ± 0.03 m (mean ± std. dev.) above ZPS during the

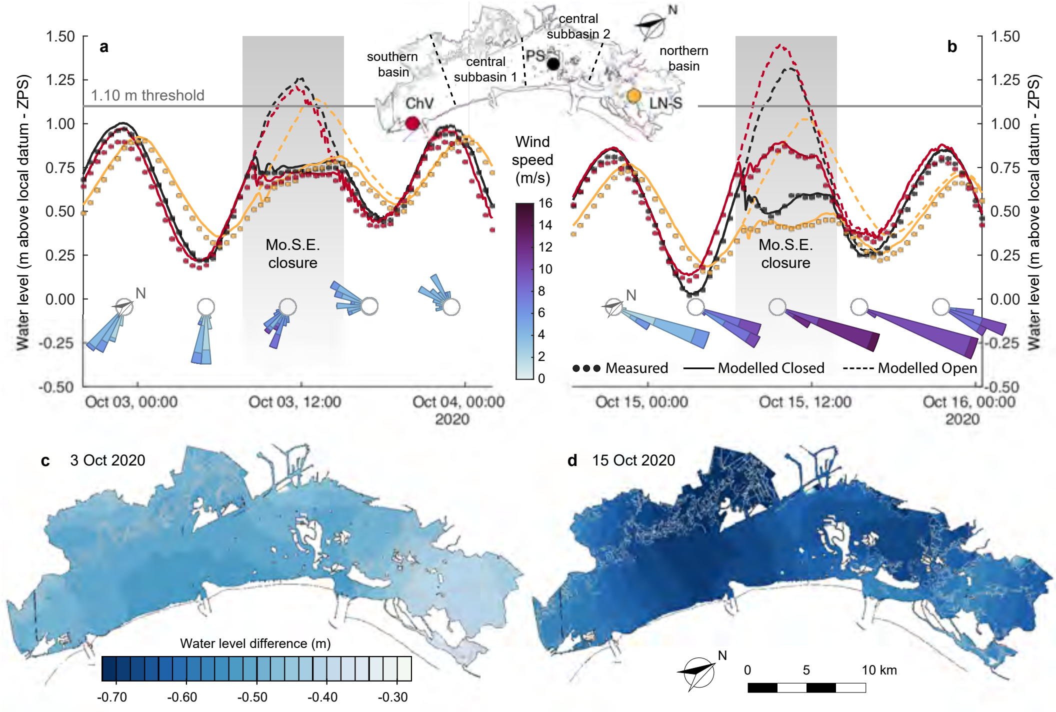


**Figure 6.2: Effect of floodgate closures on the lagoon hydrodynamics**. Water level and wind conditions for the 3 October (**a**) and 15 October 2020 (**b**) events. Solid circles represent water level measurements in three different stations (Punta della Salute (PS), Laguna Nord – Saline (LN-S) and Chioggia Vigo (ChV)) represented in the inset, solid and dashed lines represent water levels modelled in closed and open barrier scenarios, respectively. Wind roses show wind conditions grouped by 6-hour-long intervals and measured in the Laguna Nord – Saline station. Grey background indicates the timespan of Mo.S.E. closures. Difference between maximum modelled water level in the closed and open barrier scenarios, for 3 October (**c**) and 15 October 2020 (**d**) events.

storm-surge event of 3 October, characterized by a mild south-easterly Sirocco breeze (average and maximum wind speeds $v_{avg}$ =8.1 m/s and $v_{max}$ = 13.7 m/s, respectively; Figure 6.2a and 6.14a) and a reduced wind set-up equal to $\delta^{+}_{W_{avg}}$ =0.08 m between the western and eastern parts of the lagoon (Figure 6.2a,c and 6.14a). In contrast, on 15 October, although the maximum measured water levels in the lagoon were limited to 0.69 ± 0.17 m above ZPS, the strong north-easterly Bora wind ($v_{avg}$ = 14.8 m/s, $v_{max}$ = 22.8 m/s) blowing along the main axis of the lagoon generated a pronounced water set-up, with an average difference in the maximum observed water levels between the northern and southern part of the lagoon equal to $\delta^{+}_{W_{avg}} = 0.45$ m (Figure 6.2b,d and 6.14b).

Model results, which accurately reproduce observed water levels (Mean Absolute Error: 0.016 - 0.043 m, Nash-Sutcliffe Efficiency: 0.94 – 0.99; Figure 6.8 and 6.9, Table 6.1), indicate that water-level reduction with respect to the levels that would have occurred in the absence of the gate closure was not uniform within the lagoon (Figure 6.2c,d and 6.14). In particular, for the 3 October event, the reduction in maximum water levels is less pronounced in the northern lagoon ($0.36 \pm 0.05$ m, -38%), where the interplay between naturally preserved shallow tidal flats, deeply incised channels, and widespread salt marshes promotes natural damping of the tidal wave also when the floodgates are open. On the contrary, a larger water-level reduction, as high as $0.46 \pm 0.03$ m (-45%), is observed in the central and southern parts of the lagoon, as well as in the proximity of Venice. This is mainly dictated by the less significant dissipation of the tidal wave in these portions of the lagoon (Ferrarin et al., 2015), where marsh areas are less widespread and tidal flats are deeper (Carniello et al., 2009). In the case of strong Bora winds, as for the 15 October event, the largest water level reduction relative to the non-regulated scenario is again observed in the central lagoon ($0.69 \pm 0.04$ m, 57%). Although the northern and southern portions show the same value of the absolute reduction ($0.59 \pm 0.05$ m), the relative impact is different in the two cases. This absolute reduction represents a relative water level attenuation of 71% in the northern part, where the water level would have been relatively low even with open inlets, due to the enhanced wind set-up pushing the water in the south-eastern direction. In contrast, the relative water level attenuation in the southern basin, where stormwater levels would have been comparatively higher in the absence of flood-regulation, is about 46%.

### 6.3.2 Effects on tidal-flat and channel morphodynamics

Hydrodynamic changes due to Mo.S.E. operations can appreciably affect sediment transport in the lower-intertidal and subtidal zones, by modifying the local bottom shear stress $\tau_b$ (Fagherazzi et al., 2006; Defina et al., 2007) , which is primarily responsible for sediment resuspension.

On tidal flats, reduced water levels due to the closure of the inlets increase bottom friction and favour wave breaking. Model simulations of the open and closed scenario show that, as a result of this process, the maximum significant wave height ($H_s$) was reduced by 8% (mean reduction 0.02 m, max. 0.23 m) on 3 October, and by 20% (mean reduction 0.10 m, max. 0.45 m) on 15 October (Figure 6.3a,b and 6.15). Importantly, even though wave height is reduced, shallower water depths imposed by barrier closured determine larger values of $\tau_b$ across tidal-flat areas (Fagherazzi et al., 2006). Hence, the overall result of the reduced water levels during inlet closures is an increase in the maximum value of $\tau_b$ of about 5% (mean increase 0.02 Pa, max. 0.21 Pa) for the 3 October event and of 20% (mean increase 0.10 Pa, max. 0.52 Pa) for the 15 October event (Figure 6.3c,d and 6.16). In contrast, $\tau_b$ tends to decrease within the main channels close to the inlets, where the tidal currents, and hence the associated bed shear stresses, are largely reduced because of the gate closures (Figure 6.3c,d).

During both closure events, the increase in $\tau_b$ over tidal flats leads to a generalized increase in the suspended sediment concentration (SSC). Measured SSC shows peaks of $120\,\mathrm{mg\,l^{-1}}$ during the closures (Figure 6.10). Modelled SSC, thought not as closely as in the case of water levels, reasonably matches measurements, reproducing the magnitude and the modulation induced by tidal levels and wind waves (Mean Absolute Error: $1.16 - 8.91\ \mathrm{mg\,l^{-1}}$, Nash-Sutcliffe Efficiency: 0.49 – 0.64; Table 6.2), On 3 October, maximum modelled SSC was on average 4.5% higher than in the open lagoon scenario (mean increase $4.4\,\mathrm{mg\,l^{-1}}$, max $20.3\,\mathrm{mg\,l^{-1}}$; Figure 6.3e). In contrast, much higher wind speeds and, hence, $\tau_b$ resulted in an average increase in

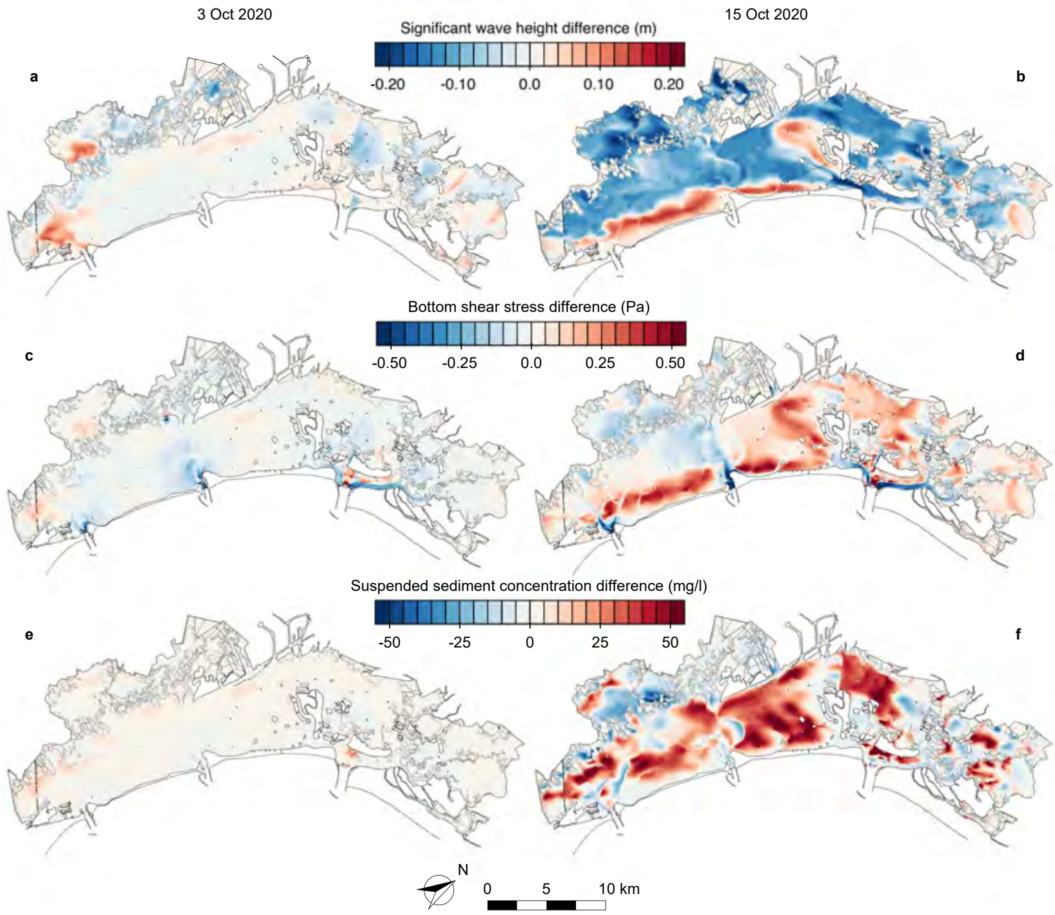


Figure 6.3: **Effect of floodgate closures on sediment resuspension within tidal flats and channels.** Difference between maximum modelled significant wave height in the closed and open barrier scenarios, for 3 October (**a**) and 15 October 2020 (**b**) events. Difference between maximum modelled bottom shear stress in the closed and open barrier scenarios, for 3 October (**c**) and 15 October 2020 (**d**) events. Difference between maximum modelled suspended sediment concentration in the closed and open barrier scenarios, for 3 October (**e**) and 15 October 2020 (**f**) events. All these maps were obtained by subtracting, for each of the parameters of interest, the maximum values observed in the closed and open barrier scenarios over the whole simulation horizon. Salt marshes are highlighted by grey lines.

the SSC maxima of 21% (mean increase 25.4 mg l$^{-1}$, max 71.6 mg l$^{-1}$) on 15 October, with extensive areas experiencing increments well above 50 mg l$^{-1}$ (Figure 6.3f and 6.17). Therefore, floodgate closures can significantly enhance the amount of sediment resuspended from the lagoon bed, especially if combined with strong winds that typically occur during storm-surge events (A. D'Alpaos et al., 2013). This circumstance might be further exacerbated by the fact that barrier closures are more likely in the late Fall and Winter when the biomass of both seagrass and benthic biofilm is reduced due to seasonal dynamics, thus offering relatively little protection against sediment erosion of the lagoon bottom (Carniello et al., 2014; Chen et al., 2017; Pivato et al., 2019).

### 6.3.3 Effects on salt-marsh morphodynamics

Changes in the hydrodynamic circulation and sediment dynamics due to inlet closures also have important effects on the evolution of salt marshes, which occupy the upper intertidal frame. First, by limiting high tides and storm surges, Mo.S.E. operations significantly reduce both the intensity and duration of salt-marsh flooding (Figure 6.4, 6.18 and 6.19). On 3 October 2020, the above-marsh water depth was reduced by $0.42 \pm 0.05$ m (64%, maximum value 0.52 m; Figure Figure 6.4a) and the flooding duration was reduced by 1.4 hours (30%) on average, with a maximum reduction of 6.3 hours (Figure 6.4c). Though salt-marsh areas in the central and southern lagoon suffered slightly more pronounced reductions, the above changes were approximately uniform in space during this event. In contrast, the stronger winds on 15 October pushed large amounts of water towards the southern end of the lagoon and almost half of the total salt-marsh area (46.5%) remained dry as a result, especially in the northern lagoon (Figure 6.4d). Numerical simulations suggest that all these marshes would have been otherwise flooded in the open lagoon scenario (Figure 6.18). The closure determined an average reduction in flooding depth of about $0.63 \pm 0.07$ m (73%, maximum 0.98 m; Figure 6.4b), while the flooding duration decreased by 2.8 hours (55%) on average (maximum value 7.28 hours; Figure 6.4d).

The reduction in marsh flooding duration and depth caused by gate closures has important implications, as periodic flooding is the only mechanism through which the suspended sediment carried by

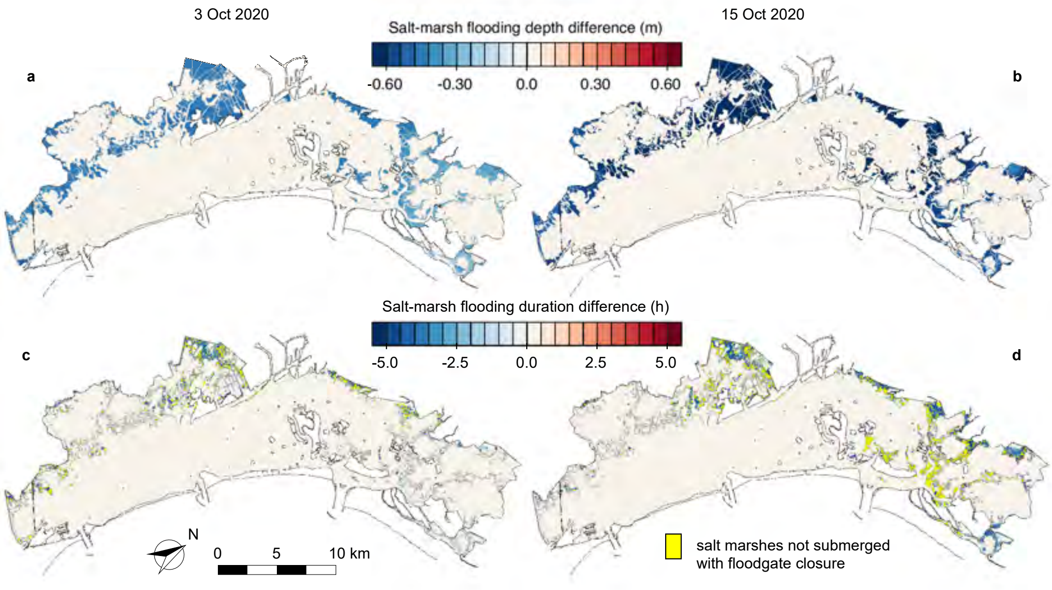


Figure 6.4: **Effect of floodgate closures on salt-marsh flooding.** Difference between maximum modelled salt-marsh flooding depth in the closed and open barrier scenario, for 3 October (**a**) and 15 October 2020 (**b**) events. Difference between maximum salt-marsh flooding duration in the closed and open barrier scenario, for 3 October (**c**) and 15 October 2020 (**d**) events. All these maps were obtained by subtracting, for each of the parameters of interest, the maximum values observed in the closed and open barrier scenarios over the whole simulation horizon. Salt marshes are highlighted by grey lines.

high waters can reach the marsh surface and contribute (together with organic sediment production by vegetation) to salt-marsh vertical accretion and to their ability to keep up with sea-level rise (Morris et al., 2002; Marani et al., 2010; A. D'Alpaos et al., 2011; Kirwan and Megonigal, 2013). While daily tidal inundations can only marginally contribute to salt-marsh vertical accretion, because of the reduced flooding duration and low SSC, surge-induced marsh flooding is typically in phase with peaks of SSC caused by intense wind-wave resuspension from tidal flats (Carniello et al., 2014), and it is characterized by higher water and longer durations, ultimately contributing to the deposition of larger sediment volumes (see Chapter 5). Recent field measurements of marsh sedimentation suggest that, although limited in time, flooding reduction related to floodgate closures critically influences the sustainability of salt marshes (see Chapter 5).

In contrast, floodgate closures only marginally affect marsh lateral erosion. Although the power of wind waves per unit length of marsh-margin can change due to wave height and water level modifications, these variations are typically smaller than 5% (absolute values $0.01 \pm 0.36$ W/m for the 3 October; $0.21 \pm 1.38$ W/m for the 15 October; Figure 6.20). Given the functional linear relationship between incoming mean wave power and marsh edge retreat rates (Marani et al., 2011; Leonardi et al., 2016), such changes are not likely to produce significant modifications in the rates at which marsh margins within the Venice Lagoon are currently being eroded (Tommasini et al., 2019; Finotello et al., 2020b).

### 6.3.4 Sediment budget at the basin scale

The primary effect of water-level reduction caused by inlet closures is to enhance sediment resuspension. In general, the fate of suspended sediments can be manifold, as they may settle on tidal flats, accumulate over salt marshes when these are flooded, deposit within the channels, or they may be transported through the channel network and the inlets to the open sea. To quantify each of these sediment fluxes, we track the temporal evolution of eroded and deposited sediment volumes for each of the different morphological units in each closure event (Figure 6.5a-d). We also quantify sediment budget changes on a longer time scale, accounting for all the 15 floodgate closures that occurred between October 2020 and January 2021 (Figure 6.5e,f).

Sediment export to the open sea is temporarily reduced by the floodgate closures by 30% (151 $m^3$) on 3 October, and by 51% (1740 $m^3$) on 15 October. Overall, we estimate that the Mo.S.E. closures have led to a 23% reduction (6630 $m^3$) in net sediment export (grey lines, Figure 6.5a,c,e) during the period October 2020 - January 2021. Floodgate closures only slightly increased erosion of tidal flats by +6% (49 $m^3$) and +1% (45 $m^3$) on 3 and 15 October, respectively (Figure 6.5b,d), though such erosion levels out at seasonal time scale (Figure 6.5f).

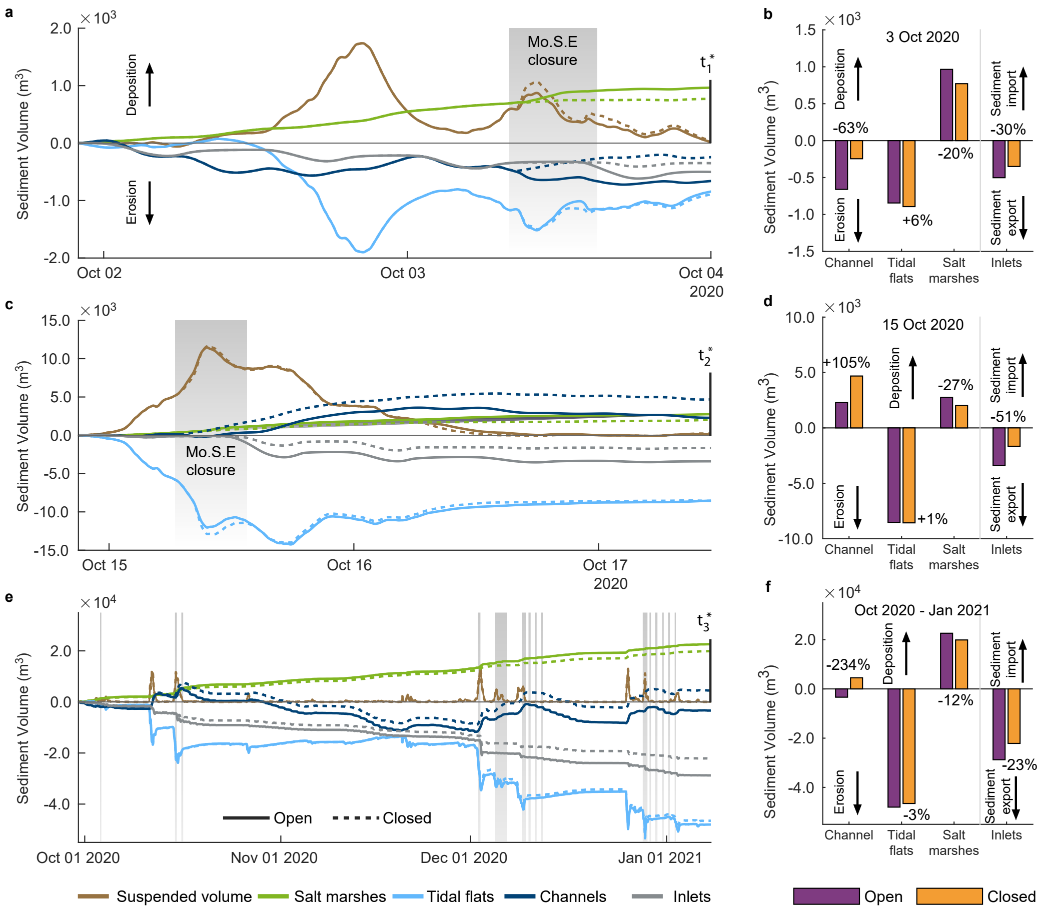


**Figure 6.5: Effect of floodgates closures on the sediment budget**. Sediment volume changes through time for different morphological units (salt marshes, tidal flats, channels), suspended sediment, and import/export through inlets for the 3 October event (**a**), 15 October event (**c**) and the period October 2020-January 2021 (**e**). Continuous lines refer to the open barrier scenario, dashed lines to the closed barrier one. Grey background indicates the timespan of Mo.S.E. closures. Net sediment volume change at the end of the events, when suspended sediment volume returns negligible (**b, d** and **f**). The time instants $t*$ considered for the net volume change represented are indicated in panels **a, c** and **e**. Percentages indicated the relative change in the closed barrier scenario with respect to the open barrier one.

Sediments reworked from tidal flats during closures are partially advected elsewhere by wind-induced secondary circulation and partially settle within the channel network, reducing channel erosion by 63% (415 $m^3$) on 3 October or increasing channel infilling by 105%

(2399 $m^3$) on 15 October compared to the open-lagoon scenario. On a seasonal time scale, repeated floodgate closures ultimately promote channel infilling through the deposition of sediment resuspended from tidal flats (Figure 6.5f). In contrast, water-level reduction due to inlet closures contributes to a substantial reduction of sediment volumes delivered to salt-marsh areas. This reduction equals 20% (193 $m^3$) for the 3 October event and 27% (737 $m^3$) on 15 October (Figure 6.5b,d), and occurs due to reduced flooding depths and durations (Figure 6.4), despite SSC being much higher than in the non-regulated scenario (Figure 6.3e,f). On a seasonal time scale, model estimates indicate a reduction of the volume deposited on salt-marsh surfaces of about 12% (2760 $m^3$) due to the 15 floodgate closures in October 2020-January 2021.

To better understand the mechanisms that lead to reduced sedimentation on the marshes, the fate of sediment resuspended from the lagoon bottom is analysed using a visualization technique based on Lagrangian particle tracking (see Materials and Methods). As an example, we have followed the paths of resuspended sediments in two different areas of the lagoon during the barrier operations of both 3 and 15 October, and compared them with the corresponding trajectories obtained by keeping the lagoon open to tidal fluxes (Figure 6.6). In the open lagoon scenario, the amount of resuspended sediment that reaches the marsh surface and settles therein is relevant, though variable in space depending on the directions of both tidal currents and wind waves (Figure 6.6). Specifically, on 3 October, about 20% of the sediment particles resuspended from the analysed tidal flats would have settled over the adjacent salt marshes in the open lagoon scenario (purple dots, Figure 6.6a,c), while on 15 October higher water levels and stronger winds would have further enhanced sediment settling up to 53%, especially on salt marshes located in the southern lagoon and exposed directly to the incoming Bora winds (purple dots, Figure 6.6d). Interestingly, the same wind setup strongly limits sedimentation over the marshes in the northern lagoon because of the local reduction in the water level (purple dots, Figure 6.6b).

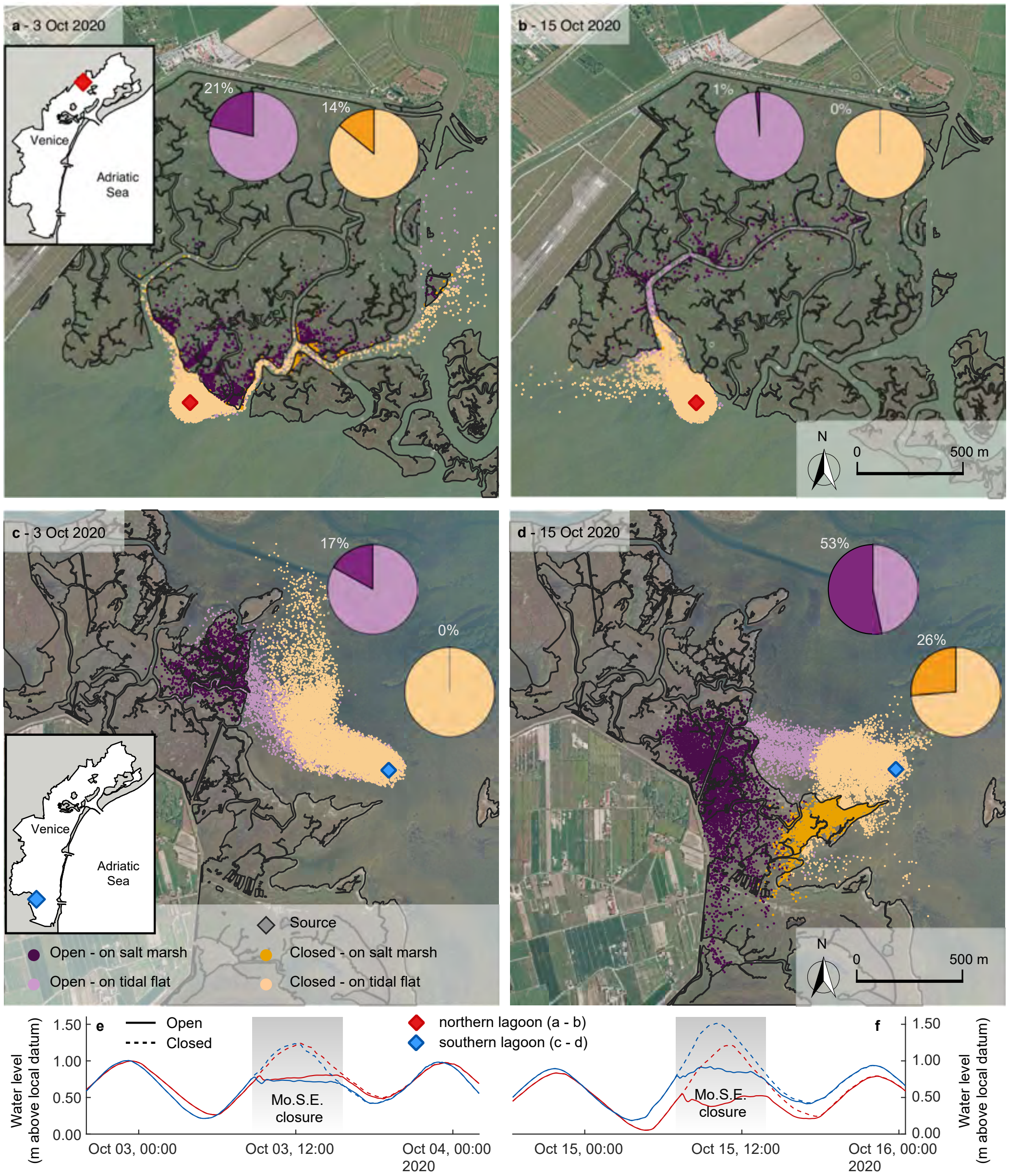


Figure 6.6: **Effect of floodgate closures on suspended sediment fate.** Particle position at the end of 3 October (**a**,**c**) and 15 October (**b**,**d**) events for two different salt-marsh areas, one in the northern lagoon (red diamond) and one in the southern lagoon (blue diamond). 10,000 particles are released at the source point (diamond) at the beginning of the closure in both open and closed barrier scenarios. Pie charts show the percentage of particle that reaches the salt marsh in the scenario with (darker yellow) and without (darker purple) barrier closure. Water levels modelled in front of the two marshes (**e**,**f**).

Conversely, when the Mo.S.E. is activated sediments remain confined within tidal channels and over tidal-flat areas due to reduced water levels and are not advected over marshes, where particle deposition is reduced by 30% to 100% compared to the non-regulated scenario (yellow dots, Figure 6.6). This effect can only be partially mitigated by local wind set-up. For instance, during the event of 15 October, water set-up generated by the north-easterly gale allowed for active sediment delivery to southern lagoon marshes, even though the total amount of deposited sediment particles was halved compared to the open-lagoon scenario (Figure 6.6d).

## 6.4 DISCUSSION

The temporary closure of a shallow tidal basin aimed at preventing urban flooding can deeply affect its morphodynamics and poses a major threat to tidal wetland sustainability, particularly under accelerating sea-level rise. Repeated floodgate closures promote sediment reworking on tidal flats and channel infilling, and hinder salt-marsh vertical accretion. The increased sediment retention caused by floodgate closures promotes a less-diverse geomorphological structure, rather than contributing to the preservation of tidal landforms.

Overall, when floodgates are operated, channels tend to be infilled by the increased resuspension on tidal flats, reduced sediment delivery to marshes, and the additional volume of sediment retained within the basin. However, the pattern of channel bed evolution depends on both the temporal scale considered and the local morphodynamic. In channel networks dissecting the inner portions of the lagoon, sediments can hardly be remobilized by weak tidal currents. The deposited sediments thus actively contribute to permanent channel infill and increase dredging costs to maintain the navigability of waterways. Conversely, within the major channels and closer to the inlets, sediments are temporarily accumulated during barrier closures but, on a longer time scale, they can be remobilized by the higher tidal velocities and eventually will be slowly flushed out to the open sea due to the general ebb-dominated character of tidal currents in the Venice Lagoon (Ferrarin et al., 2015; Finotello et al., 2019). Although it might partially counterbalance the increased in-channel deposition, the sediment export induced by ebb-currents represents a net loss for the sediment budget at the basin scale. Therefore, both permanent channel infill and sediment export by ebb-dominated tidal currents bear negative implications for the sediment budget and the maintenance of the lagoon geomorphic diversity.

Moreover, artificially lowered water levels reduce the volume of suspended sediment advected over salt marshes, thus depriving them of a critical sediment source. Even though floodgate closures can temporarily increase the volume of sediment available in suspension, due to enhanced sediment resuspension from tidal flats, the reduced marsh inundation causes a substantial decrease in the volume of sediment delivered to salt marshes. This mechanism is confirmed by field data showing that marsh sedimentation increases exponentially with inundation depth (Chapter 5), with water levels capped by floodgate closures determining much lower sediment accumulation. This might ultimately lead to extensive marsh drowning, which, together with the ongoing lateral erosion, will further accelerate the rate at which salt marshes are lost in the Venice Lagoon during the last four centuries (Carniello et al., 2009; Tommasini et al., 2019). Additional salt-marsh losses might have critical implications not only from an ecosystem perspective (Barbier et al., 2011), because of the loss in biodiversity and ecosystem services that it would signify, but also for flood-risk mitigation. Indeed, further loss of salt-marsh surfaces can potentially trigger positive morphodynamic feedbacks (A. D'Alpaos et al., 2012), with detrimental cascading effects for the whole lagoon basin. Decreasing marsh areas favour an inertially-dominated tidal propagation and increase wind fetch, and thus wave height. Stronger tidal currents and higher wind waves would further exacerbate the ongoing erosive processes within the lagoon, paving the way to the transition from a tidal lagoon to a bay environment (Carniello et al., 2009). Moreover, less significant dissipation of tides leads to local increases in the mean high water level (Silvestri et al., 2018), and larger wind fetches can induce stronger water-level setups, in this way potentially offsetting, at least partially, the benefits of flood protection measures.

On the one hand, we emphasize that the effect of flood-regulation on the morphodynamics depends exclusively on the reduced water level within the lagoon and it is not strictly related to the type of floodgates adopted. On the other hand, our analysis suggests that environmental sustainability should have a high priority for designing and managing storm-surge barriers. Trade-offs between the safeguarding of urban areas from flooding and the preservation of tidal ecosystem needs will be essential to ensure adequate resilience against climate change to shallow tidal embayments where flood barriers operate. In the specific case of the Venice Lagoon, many complementary solutions could be exploited by coastal managers to mitigate the detrimental morphodynamic effects of repeated inlet closures. These solutions, none of which suffice on their own to compensate for the loss of geomorphic diversity, include:

i. the artificial raising of sidewalk elevation in the major urban settlements within the lagoon, aimed to increase the current safety water level and reduce the frequency with which floodgates have to be closed;

ii. the reintroduction of fluvial-sediment to compensate for the loss of inorganic sediment, both over tidal flats and salt marshes;

iii. the extensive building and restoration of salt marshes, especially adopting nature-based techniques (Temmerman et al., 2013; Temmerman and Kirwan, 2015; Baptist et al., 2019; Fairchild et al., 2021);

iv. the protection of tidal flats and salt marshes against erosion by preserving and improving the ecological conditions that promote the colonization by benthic vegetation, seagrasses, and halophytes, and through the realization of eco-engineering solutions to mitigate sediment erosion, such as oyster reefs and mussel beds (Temmerman et al., 2013; Chowdhury et al., 2019), able to limit wind fetch, dissipate wave energy, and act as breakwaters for high water levels.

These interventions, together with careful management of the floodgate operations and improved weather-forecasting tools, would make it possible to ensure flood protection of Venice and other inhabited lagoonal settlements while preserving the lagoon ecosystem as a whole.

## 6.5 MATERIALS AND METHODS

### 6.5.1 Geomorphological setting

The Venice Lagoon, Italy (Figure 6.1a) is the largest brackish tidal basin of the Mediterranean Sea, with an area of about 550 $km^2$ . It is a shallow microtidal basin, characterized by a semidiurnal tidal regime with an average range of 1.0 m and a mean water depth over the tidal flats of about 1.5 m. It is connected to the Adriatic Sea through 3 inlets: Lido, Malamocco, and Chioggia from North to South (Figure 6.1b-d). The main, morphologically significant winds are represented by the north-easterly Bora wind and the south-easterly Sirocco wind (Figure 6.1e). Due to the NE-SW elongated shape of the Venice Lagoon, the Bora wind can generate relatively large waves ($\tilde{1}$ m), especially in the southern sector of the lagoon.

Human interventions have been modifying the Venice Lagoon for centuries (L. D'Alpaos, 2010a). To prevent the lagoon from infilling with fluvial sediment and, therefore, preserve navigability, the Venetian Republic diverted all large rivers to the sea. This process started in 1457 and changed the sediment balance of the basin, triggering sediment starvation and a generalized deepening of the lagoon (Carniello et al., 2009). From the end of the 19$^{th}$ century to the mid of the 20$^{th}$ century, sediment export toward the sea was further exacerbated by the construction of the jetties at the inlets (Lido 1882-1892, Malamocco

1813-1872, Chioggia 1910-1934) (Carniello et al., 2009; L. D'Alpaos, 2010a; Finotello et al., 2019).

Between 1930 and 1970, intense groundwater exploitation for industrial purposes enhanced loss of relative elevation, resulting in an overall relative sea-level rise equal to 25 cm (Carbognin et al., 2004). Because of subsidence and eustatic sea-level rise, the city of Venice started experiencing even more frequent flooding during storm surges. The solution proposed after the catastrophic flooding event of 4 November 1966 (maximum water level of 1.94 m above the local Punta della Salute datum) was the Mo.S.E. project (Figure 6.1b-d,f).

### 6.5.2 Hydro-morphodynamic model

We adopted a two-dimensional (2D) model that consists of three modules, namely the hydrodynamic module coupled with the wind-wave module (WWTM) (Carniello et al., 2011) and the sediment transport and bed evolution module (STABEM) (Carniello et al., 2012) suitable for reproducing sediment dynamics governing the morphodynamic evolution of shallow micro-tidal basins.

The hydrodynamic module solves the 2D depth-integrated shallow water equations (SWEs), phase-averaged over a representative elementary area of irregular topography to deal with very shallow flows, wetting, and drying (Defina, 2000). Projected on a Cartesian frame $(x, y)$, the SWEs read:

$$\vartheta(\eta)\frac{\partial \eta}{\partial t} + \nabla \cdot \mathbf{q} = 0 \tag{6.1}$$

$$\frac{\mathrm{D}}{\mathrm{D}t}\left(\frac{\mathbf{q}}{Y}\right) + \frac{1}{Y}\nabla \cdot \mathbf{Re} + \frac{\boldsymbol{\tau}_t}{Y\rho} - \frac{\boldsymbol{\tau}_s}{Y\rho} + g\nabla h = 0 \tag{6.2}$$

where $t$ is time, $\eta$ is is the free surface elevation over a datum, $\mathbf{q} = (q_x, q_y)$ is the depth-integrated velocity (i.e., discharge per unit width), $\nabla$ and $\nabla\cdot$ denote the 2D gradient and divergence operators.

The term $\vartheta$ is the wet fraction of the computational domain that depends on the water depth and on the local topographic unevenness (Defina, 2000). In the momentum equation (6.2), $\mathrm{D}/\mathrm{D}t$ is the material (or Lagrangian) time derivative, $Y$ is the water volume per unit area (i.e., the equivalent water depth), $\boldsymbol{\tau}_t$ and $\boldsymbol{\tau}_s$ are the shear stresses at the bottom (due to tidal currents) and at the free surface (due to wind drag), respectively, $\rho$ is the water density, and $g$ is gravity. The Reynolds stresses are computed using a depth-averaged version of Smagorinsky's model (Smagorinsky, 1963). In tensor index notation, they read:

$$\mathbf{Re} = R_{ij} = \nu_e Y(u_{i,j} + u_{j,i}) \tag{6.3}$$

$$\nu_e = 2C_s^2 A_e \sqrt{2(u_{xx}^2 + (u_{x,y} + u_{y,x})^2 + 2(u_{y,y})^2} \tag{6.4}$$

with $i, j$ in eq. 6.4 denoting either the x or y coordinates and $\mathbf{u} = \mathbf{q}/Y$. The eddy viscosity, $\nu_e$, is proportional to the strain rate, with $A_e$ the area of the computational element and $C_s = 0.2$ the Smagorinsky coefficient.

In the numerical scheme, the material derivative in eq. 6.2 is expressed as the finite difference in time and solved with the method of characteristics. This mixed Eulerian-Lagrangian approach allows solving the continuity equation (6.1) with a semi-implicit scheme, which leads to a self-adjoint spatial operator. It is solved on a staggered triangular grid with the finite element method of Galerkin (Defina, 2003) and the flow rates are obtained by back-substitution.

The wind-wave module (Carniello et al., 2011) solves the wave action conservation equation (Hasselmann et al., 1973) using the same computational grid of the hydrodynamic module, that provides water depths and depth-averaged flow velocities, used to propagate the wind-wave field. The wave action density ($N_0$) in the frequency domain evolves according to Carniello et al. (2011):

$$\frac{\partial N_0}{\partial t} + \frac{\partial}{\partial x} c'_{gx} N_0 + \frac{\partial}{\partial y} c'_{gy} N_0 = S_0 \tag{6.5}$$

where $c'_{gx}$ and $c'_{gy}$ are the group celerity components of wave used to approximate the propagation speed of $N_0$ (Holthuijsen et al., 1989; Carniello et al., 2011). The wind-wave source terms, grouped in the term $S_0$, account for positive (wind energy input) and negative (bottom friction, whitecapping and depth-induced breaking) contributions to wave energy. The model computes the spatial and temporal distribution of the wave periods based on the relationship between peak-wave period, local wind speed, and water depth (Young and Verhagen, 1996). As the lagoon margins are almost vertical and jagged, refraction is neglected and waves are assumed to propagate in the wind direction. The horizontal orbital velocity at the bottom, which is obtained from the significant wave height through the linear wave theory, provide the additional component of the bottom shear stress, $\tau_w$, induced by the wind-wave field. The nonlinear interactions between $\tau_w$ and the current-induced bottom shear stress ($\tau_t$) are accounted for by means of the empirical formulation by Soulsby (Soulsby, 1995), which increases the value of the total bottom shear stress, $\tau_b$, beyond the mere sum of $\tau_t$ and $\tau_w$.

Using the same computational grid, the STABEM module (Carniello et al., 2012) solves the advection-diffusion equation for suspended sediment with a conservative, second-order in space scheme and the Exner's equation:

$$\frac{\partial C_i Y}{\partial t} + \nabla \cdot (\mathbf{q} C_i) - \nabla \cdot (\mathbf{D}_h \nabla C_i) = E_i - D_i \quad i = s, m \tag{6.6}$$

$$(1 - n)\frac{\partial z_b}{\partial t} = \sum_i (D_i - E_i) \tag{6.7}$$

where $C$ is the depth-averaged sediment concentration, $\mathbf{D}_h(x, y, t)$ is space- and time-dependent two-dimensional diffusivity tensor, assumed equal to the eddy viscosity computed by the hydrodynamic module (Viero and Defina, 2016), $E$ and $D$ represent the entrainment and deposition of bed sediment, $z_b$ is the bed elevation and n the bed porosity, assumed equal to 0.4. The subscript $i$ refers to the non-cohesive (sand, $s$) and cohesive (mud, $m$) sediment classes that typically characterize the bed of tidal lagoons. The relative content of mud, which represents the sum of clay and silt, is assumed to vary both in time and space; it determines the cohesive or non-cohesive behaviour of the mixture and the critical value of the bottom shear stress. The threshold value of mud content $p_{mc} = 10\%$ is assumed to discriminate between non-cohesive and cohesive behavior (van Ledden et al., 2004). Based on measurements in the Venice Lagoon, the median diameters $D_{50}$ adopted in the simulations to describe cohesive and non-cohesive sediments are 20 $\mu$m and 200 $\mu$m, respectively (Carniello et al., 2011).

The deposition rate of sand, $D_s$, is computed as:

$$D_s = w_s r_0 C_s \tag{6.8}$$

where $w_s$ is the absolute value of the sand settling velocity and $r_0$ is the ratio of near-bed to depth-averaged concentration which is here assumed constant and equal to 1.4 (Parker et al., 1987).

The deposition rate of pure cohesive mud, $D_m$, is given by Krone's formula

$$D_m = w_m C_m \max\{0; 1 - \tau_b/\tau_d\} \tag{6.9}$$

where $w_m$ is the absolute value of the mud settling velocity, $\tau_b$ the bottom shear stress computed by the hydrodynamic module, and $\tau_d$ the critical shear stress for deposition ($\tau_d = 1.0$ Pa). The settling velocities, $w_s$ and $w_m$, are computed using the van Rijn formulation (van Rijn, 1984) for solitary particles in clear and still water, thus not incorporating flocculation effects which are negligible for particle diameter larger than 20 $\mu$m (Mehta et al., 1989).

The erosion rate strongly depends on the degree of cohesion of the mixture. For non-cohesive mixtures ($p_m < p_{mc}$), the erosion rate of sand, $E_s$, is described by the van Rijn formulation (van Rijn, 1984), whereas the erosion rate of mud, $E_m$, can be computed through the formulation proposed by van Ledden et al. (2004) as follows:

$$\begin{aligned} E_s &= (1-p_m)w_s \cdot 1.5\left(\frac{D_{50}/Y}{D_*^{0.3}}\right)T^{1.5} \\ E_m &= \frac{p_m}{1-p_m}M_{nc}T \end{aligned} \quad \text{for} \quad p_m < p_{mc} \tag{6.10}$$

For cohesive mixtures ($p_m > p_{mc}$), both sand and mud erosion rates can be computed using the Partheniades's formula

$$\begin{aligned} E_s &= (1-p_m)\cdot M_c T \\ E_m &= p_m M_c T \end{aligned} \quad \text{for} \quad p_m > p_{mc} \tag{6.11}$$

In equations (6.10) and (6.11), $D_*$ is the dimensionless grain size ($D_* = D_{50}[(s-1)g/\nu^2]^{1/3}$, being $s$ the sediment specific density and $\nu$ the water kinematic viscosity), $T$ is the transport parameter, $M_{nc}$ and $M_c$ are the specific entrainment for non-cohesive and cohesive mixtures respectively (van Ledden et al., 2004)

$$M_{nc} = \alpha\frac{\sqrt{(s-1)gD_{50}}}{D_*^{0.9}}, \quad M_c = \left(\frac{M_{nc}}{M_m}\cdot\frac{1}{1-p_{mc}}\right)^{\frac{1-p_m}{1-p_{mc}}}\cdot M_m \tag{6.12}$$

where $M_m$ is the specific entrainment for pure mud ($M_m = 5\cdot 10^{-2}$ g m/s ) and $\alpha$ is set equal to $1\cdot 10^{-5}$. The transport parameter is usually defined as $T = \max\{0; \tau_b/\tau_c - 1\}$, describing a sharp transition between $T = 0$ and $T = \tau_b/\tau_c - 1$, where $\tau_b$ is the local bottom shear stress and $\tau_c$ is the critical shear stress for erosion. However, in real tidal systems, both $\tau_b$ and $\tau_c$ are not constant in space, thus we assume that they are both random variables, following a log-normal distribution (Carniello et al., 2012). The result of this stochastic approach is a smooth transition between $T = 0$ and $T = \tau_b/\tau_c - 1$.

All parameters are within the range of variability of similar deposition and erosion formulations (Temmerman et al., 2005b; Breda et al., 2021). In particular, erosion is set equal to zero on salt marshes because vegetation reduces velocity and dampens waves, protecting sediment from erosion (Möller et al., 1999; Temmerman et al., 2005b). The result of erosion and deposition fluxes of sand and mud is a variation in bed level through time, which is computed according to eq. (6.7).

The model has been widely benchmarked against hydrodynamic, wind-wave, and turbidity field- and satellite-data from the Venice Lagoon (Italy) (Carniello et al., 2011, 2014), Virginia Coast Reserve lagoons (USA) (Mariotti et al., 2010b), and Cadiz Bay (Spain) (Zarzuelo et al., 2018).

The computational domain representing the Venice Lagoon (Figure 6.7) consists of 51'084 nodes and 96'751 triangular elements. The model is forced with water levels measured at the three inlets, as well as with wind directions and velocities measured in three different zones of the lagoon by the Venice Municipality *"Centro Previsioni e Segnalazioni Maree"* (CPSM) monitoring network (Figure 6.7). The 3 October event simulation starts 80 hours before the floodgates closure and ends 32 hours after barrier opening. The 15 October event simulation starts 54 hours before the floodgates closure and ends 59 hours after the subsequent opening. Moreover, to evaluate the effects of the barrier closures on the sediment budget at a seasonal timescale, we simulated the whole period between 30 September 2020 and 10 January 2021 to cover all the first 15 barrier operations.

Finally, a Lagrangian particle tracking scheme has been set up to visualize the fate of sediments that are suspended at a given location and time instant (see Figure 6.6), according to the actual sediment dynamics computed by the Eulerian scheme implemented in STABEM. We release a large number of non-inertial particles at a given location and move them according to the velocity field computed by the hydrodynamic module adding a stochastic component, with the local eddy viscosity to measure the diffusivity, to simulate a random walk process (Visser, 1997). To account for deposition, at each time step and for each cell of the mesh we compute the number of particles within the cell, $n_j$, and the ratio of deposited to the total suspended material, $R_D = dt \cdot D/(CY)$, with $dt$ the time step, $D$ and $C$ the total (sand plus mud) deposition rate and vertically-averaged concentration, respectively. Given that $R_D$ expresses the probability of deposition of suspended particles in the cell according to STABEM computations, in the Lagrangian particle tracking scheme $n_{stop} = R_D \cdot n_j$ particles

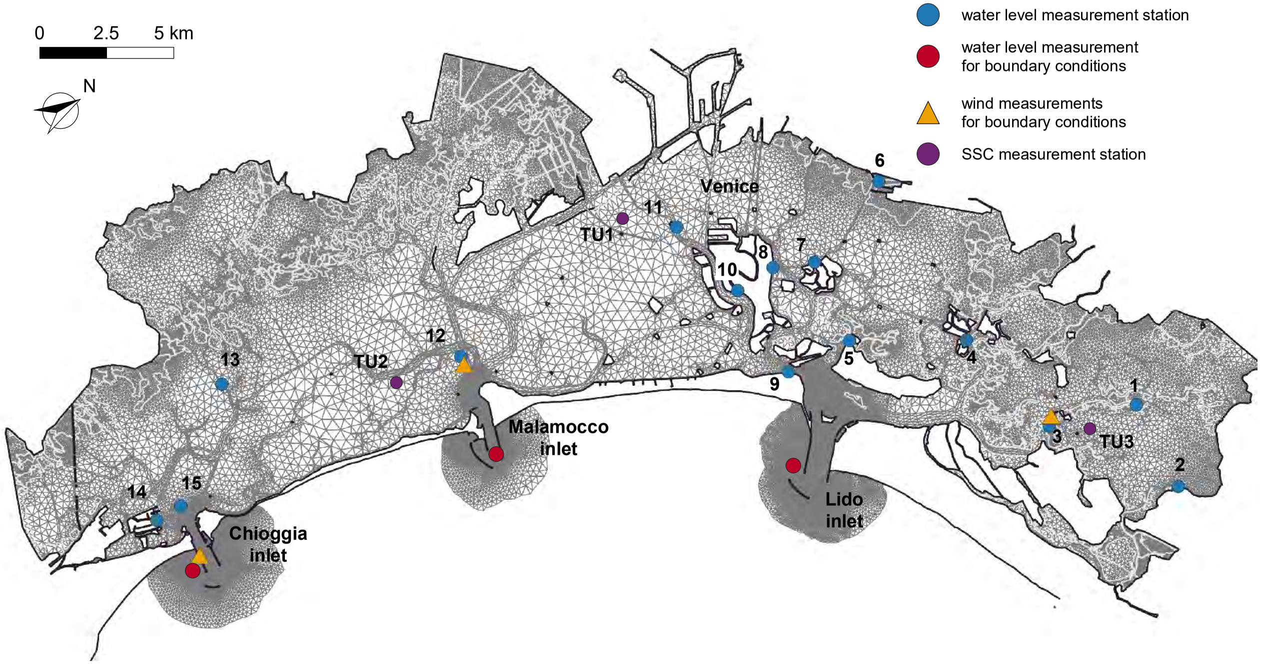


**Figure 6.7: Computational grid.** Blue circles indicate water level stations, whose measurements are used to test model results in Supplementary Figures 2 and 3. Red circles indicate water level measurement stations adopted as boundary conditions. Orange triangles indicate wind measurement stations adopted as boundary conditions. Purple circles indicate suspended sediment concentration (SSC) measurement stations.

are permanently stopped at each time step. To account for the fractional part of $n_{stop}$, denoted as $frac(n_{stop})$, we generate a random number $r \in [0, 1]$ and stop an additional particle if $r < frac(n_{stop})$. The number of released particles, $N_p = 10,000$, is large enough to make the percentages of particles deposited on the marsh (Figure 6.6) independent of $N_p$.

## 6.6 SUPPORTING INFORMATION

### 6.6.1 Reliability of the hydrodynamic model

The comparison between measured and modelled water levels is displayed in Figure 6.8 for the 3 October closure and in Figure 6.9 for the 15 October closure for 15 different stations within the Venice Lagoon (location shown in Figure 6.7). The hydrodynamic model accurately reproduces observed water levels, also under flood-regulated conditions.

Model reliability is quantified by means of standard statistical parameters, namely the Mean Absolute Error (MAE), Root Mean Squared Error (RMSE), and Nash-Sutcliffe Efficiency (NSE) (Table 6.1). MAE ranges between 0.016 and 0.043 m, RMSE is between 0.021 and 0.054 m. NSE is always higher than 0.94, thus the model performance is classified as "excellent" following the classification proposed by J. I. Allen et al. (2007).

### 6.6.2 Reliability of the sediment transport model

The ability of the model to reproduce sediment transport processes and the related bed evolution is evaluated by comparing field measurements and model results in terms of suspended sediment concentration (SSC), as well as salt-marsh vertical accretion and tidal-flat bed elevation changes. Figure 6.10 compares measured and modelled SSC during the 3 and 15 October closures at three different gauging stations within the lagoon (location shown in Figure 6.7), and the parameters to quantify model reliability are listed in Table 6.2. MAE is lower than 8.9 mg l$^{-1}$ and RMSE is lower than 15.8 mg l$^{-1}$. The model efficiency is classified as "very good" based on NSE larger than 0.52 (J. I. Allen et al., 2007). Therefore, despite not begin as accurate as simulated water levels, modelled SSC values reasonably match measurements, reproducing the magnitude and the modulation of SSC induced by the combined action of tidal levels and wind waves.

Salt-marsh accretion measurements are available for 27 sites grouped in three marshes (locations shown in the upper panel of Figure 6.11). Accretion was measured through kaolinite horizon markers and yearly accretion rates are available for the period 2019-2020 (Tognin et al., 2021). To compare field measurements and model results, ad hoc numerical simulations were performed using water levels and wind climate measured during the observation period as boundary conditions. The comparison between field measurements and model results is performed both at the scale of individual marshes and for the whole lagoon (Figure 6.11). The mean absolute error between measured and modelled accretion rates is equal to $0.56 \pm 2.80$ mm/year. In addition, we performed the non-parametric Kolgomorov-Smirnov test to quantitatively compare the distributions of measured and modelled accretion rates and it confirms that they do not significantly differ (significance level $\alpha = 0.01$) for each considered study site as well as for the whole lagoon (Table 6.3).

Although direct measurements of bed elevation change on tidal flats are not available, estimates of erosion and deposition rates can be obtained from periodic bathymetric surveys available at the scale of the entire lagoon. In particular, we computed the mean annual bed elevation change experienced by tidal flats of the Venice Lagoon by subtracting the digital elevation model derived from the two most recent bathymetries available (i.e., 1970 and 2003) and by computing the mean rate of change. We then compared the results with the annual bed elevation change computed through the numerical model using water levels and wind climate measured in 2005 and 2020 as boundary conditions. The year 2005 is selected because probability distributions of water levels and wind conditions are closest to median values for the period 2000-2020, and thus morphological changes obtained with these forcing factors are deemed to be similar to those experienced by the lagoon over decadal timescales and captured by bathymetric surveys. Despite being characterized by water levels and wind conditions different from the average, numerical simulations are performed for the year 2020 as well, as it represents the year in which the Mo.S.E. barrier system became operational.

Modelled and observed bed elevation changes are compared for 20 tidal-flat sites (circular areas with radius equal to 1 km) distributed all over the Venice Lagoon (locations shown in the upper panel of Figure 6.12). Boxplots in Figure 6.12 show that bed elevation changes retrieved from bathymetric data are comparable with those computed using the numerical model, both for the 2005 and 2020 simulations. The mean absolute error between measured and modelled bed elevation changes is equal to 7.9 $\pm$ 18.3 mm/year for the 2005 simulation and to 7.6 $\pm$ 18.1 mm/year for the 2020 simulation. Kolmogorov-Smirnov tests show that model results of the 2005 simulation do not significantly differ from bathymetric measurements in any case (significance level $\alpha = 0.01$, Table 6.4). In addition, bed elevation changes resulting from the 2020 simulation do not significantly differ from field data in 16 out of the 20 study sites $\alpha = 0.01$, Table 6.4). The statistical comparison between field measurements and model results in terms of SSC, salt-marsh accretion, and bed elevation changes of tidal flats shows that erosional and depositional fluxes, together with the resulting elevation changes of different morphological units, are reasonably captured by the numerical model.

### 6.6.3 Statistical characterization of water level and wind conditions associated with flooding events

In addition to representing the first-ever closures of the Mo.S.E. barriers to avoid the flooding of the city of Venice, the operations of the 3 and 15 October 2020 were characterized by hydrodynamic and meteorological conditions that are typical to events that lead to extensive flooding of Venice city and other inhabited settlements within the lagoon (Figure 6.13). To demonstrate this, we analyzed water level and wind data measured from 1983 to 2020 and retain all data corresponding to water levels exceeding the safety threshold of 110 cm above the local datum of “Punta della Salute”. Water levels were measured at the “Diga Lido Sud” gauging station, which is located just outside of the Lido inlet and therefore is not affected by barrier operations (Figure 6.7). Wind velocities and directions were retrieved from the “Chioggia Diga Sud” anemometric station, which is representative of wind conditions across the whole Lagoon (Carniello et al., 2005).

The 3 October 2020 event is very close to the median of the distribution, because water levels and wind velocities are characterized by a cumulative exceedance probability of 0.55 and 0.52, respectively. On the contrary, the 15 October event is characterized by higher water levels and wind velocities, with values of cumulative exceedance probability equal to 0.90 and 0.88, respectively.

Based on the above analysis, the two selected events can be considered representative of both average (3 October) and quite intense (15 October) tide and wind conditions among those typically leading to flooding events.

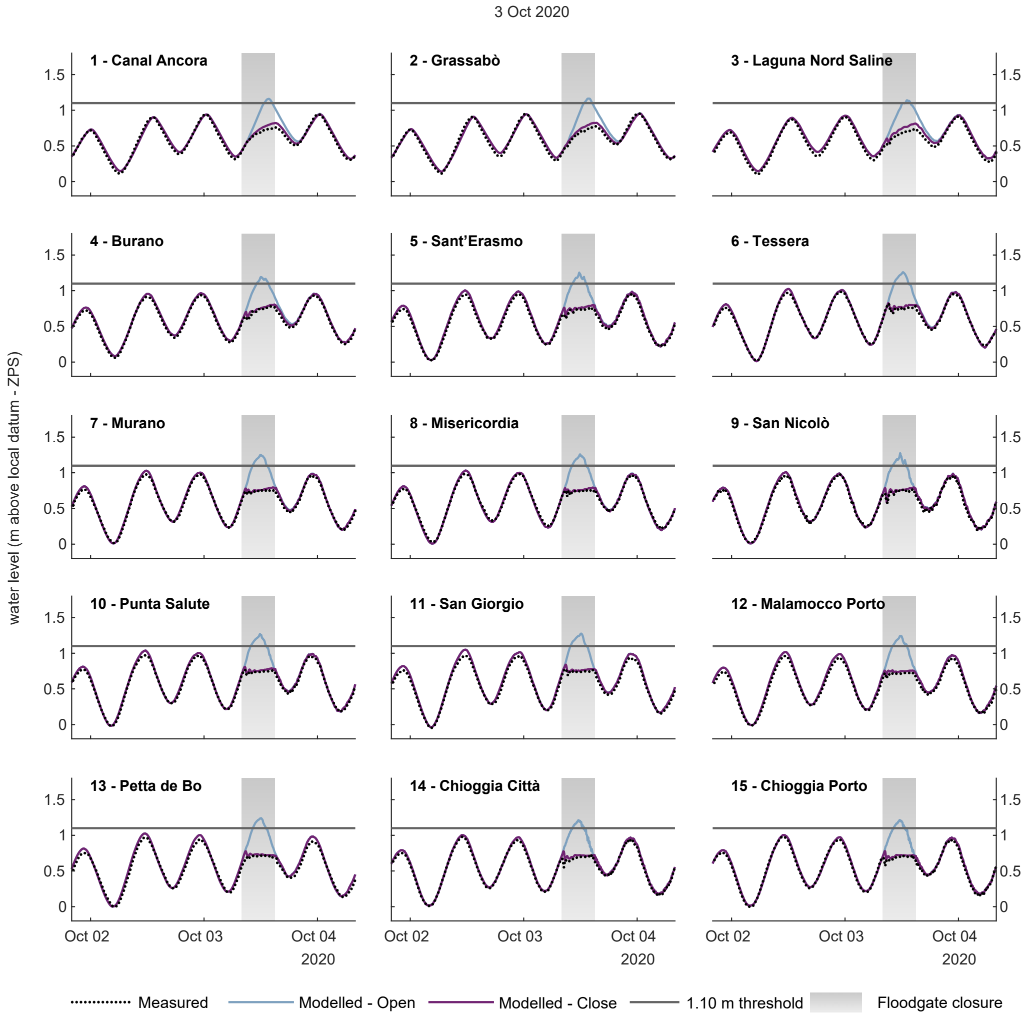


**Figure 6.8: Water level for the 3 October event.** Comparison between measured water level (black dots), modelled water level in the open barrier scenario (light blue), and modelled water level in the closed barrier scenario (purple). Measurement station positions are indicated in Figure 6.7.

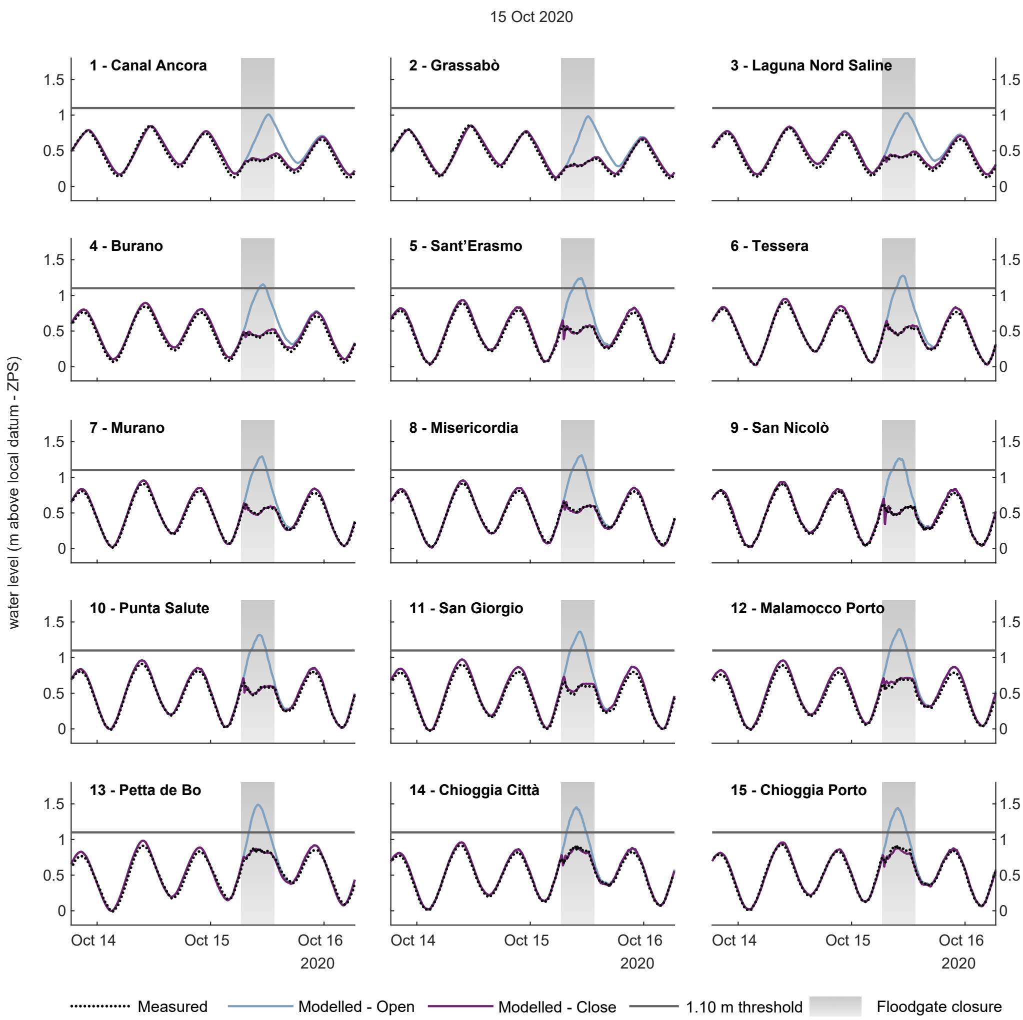


**Figure 6.9: Water level for the 15 October event.** Comparison between measured water level (black dots), modelled water level in the open barrier scenario (light blue), and modelled water level in the closed barrier scenario (purple). Measurement station positions are indicated in Figure 6.7.

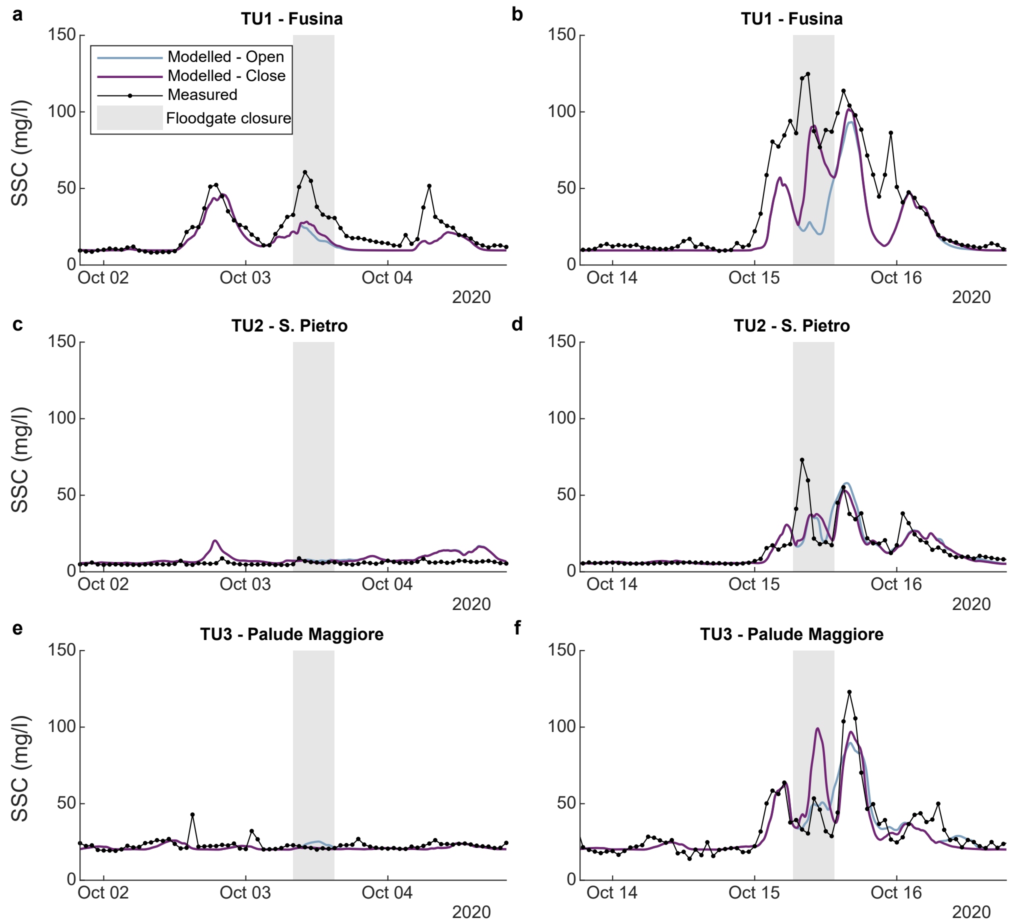


**Figure 6.10: Suspended sediment concentration (SSC).** Comparison between measured SSC (black line), modelled SSC in the open barrier scenario (light blue) and modelled SSC in the closed barrier scenario (purple). Measurement station positions are indicated in Figure 6.7. Notably the model accurately predicts not only the magnitude of the SSC but also its modulation induced by tidal-level and wind-wave variations.

**Table 6.1: Model efficiency on water level.** Model efficiency for water level computed in the 15 measurement stations shown in Figure 6.7 estimated through Mean Absolute Error ($MAE$), Root Mean Squared Error ($RMSE$) and Nash-Sutcliff Efficiency ($NSE$), defined as $1 - \sum(d-m)/\sum(d-D)$, where $d$ are the measured data, $m$ is the corresponding model estimate, and $D$ is the mean of the measured data. Performance categories can be defined as follows (J. I. Allen et al., 2007): $NSE > 0.65$ excellent (***); $ME = 0.65 - 0.5$ very good (**); $ME = 0.5 - 0.2$ good (**); $ME < 0.2$ poor (*).

| | Study area | *MAE* | | *RMSE* | | *NSE* | |
|---|---|---|---|---|---|---|---|
| | | 3/10/2020 | 15/10/2020 | 3/10/2020 | 15/10/2020 | 3/10/2020 | 15/10/2020 |
| 1 | Canal Ancora | 0.035 | 0.035 | 0.050 | 0.050 | 0.952*** | 0.942*** |
| 2 | Grassabò | 0.037 | 0.034 | 0.053 | 0.054 | 0.946*** | 0.938*** |
| 3 | Laguna Nord | 0.042 | 0.038 | 0.050 | 0.046 | 0.950*** | 0.949*** |
| 4 | Burano | 0.029 | 0.036 | 0.036 | 0.040 | 0.979*** | 0.970*** |
| 5 | Sant'Erasmo | 0.033 | 0.029 | 0.037 | 0.034 | 0.980*** | 0.982*** |
| 6 | Tessera | 0.021 | 0.020 | 0.029 | 0.027 | 0.988*** | 0.989*** |
| 7 | Murano | 0.026 | 0.022 | 0.032 | 0.027 | 0.986*** | 0.989*** |
| 8 | Misericordia | 0.021 | 0.018 | 0.028 | 0.023 | 0.989*** | 0.992*** |
| 9 | San Nicolò | 0.024 | 0.023 | 0.030 | 0.031 | 0.988*** | 0.986*** |
| 10 | Punta Salute | 0.027 | 0.023 | 0.032 | 0.027 | 0.988*** | 0.990*** |
| 11 | San Giorgio | 0.038 | 0.037 | 0.044 | 0.042 | 0.977*** | 0.978*** |
| 12 | Malamocco Porto | 0.037 | 0.042 | 0.043 | 0.047 | 0.976*** | 0.970*** |
| 13 | Petta de Bo | 0.043 | 0.038 | 0.050 | 0.045 | 0.965*** | 0.977*** |
| 14 | Chioggia Città | 0.022 | 0.021 | 0.029 | 0.026 | 0.988*** | 0.991*** |
| 15 | Chioggia Porto | 0.022 | 0.017 | 0.028 | 0.021 | 0.988*** | 0.995*** |

**Table 6.2**: **Model efficiency for suspended sediment concentration (SSC)**. Model efficiency for SSC computed in the 3 measurement stations shown in Figure 6.7 estimated through Mean Absolute Error ($MAE$), Root Mean Squared Error ($RMSE$) and Nash-Sutcliff Efficiency ($NSE$), defined as $1 - \sum(d-m)/\sum(d-D)$, where $d$ are the measured data, $m$ is the corresponding model estimate, and $D$ is the mean of the measured data. Performance categories can be defined as follows (J. I. Allen et al., 2007): $NSE > 0.65$ excellent (***); $ME = 0.65 - 0.5$ very good (**); $ME = 0.5 - 0.2$ good (**); $ME < 0.2$ poor (*).

| | Study area | $MAE$ | | $RMSE$ | | $NSE$ | |
|---|---|---|---|---|---|---|---|
| | | 3/10/2020 | 15/10/2020 | 3/10/2020 | 15/10/2020 | 3/10/2020 | 15/10/2020 |
| 1 | TU1 - Fusina | 4.790 | 8.914 | 6.526 | 15.879 | 0.525** | 0.638** |
| 2 | TU2 – S.Pietro | 1.162 | 3.466 | 1.537 | 7.238 | 0.557** | 0.607** |
| 3 | TU3 – Palude Maggiore | 1.598 | 6.039 | 1.957 | 11.389 | 0.535** | 0.542** |

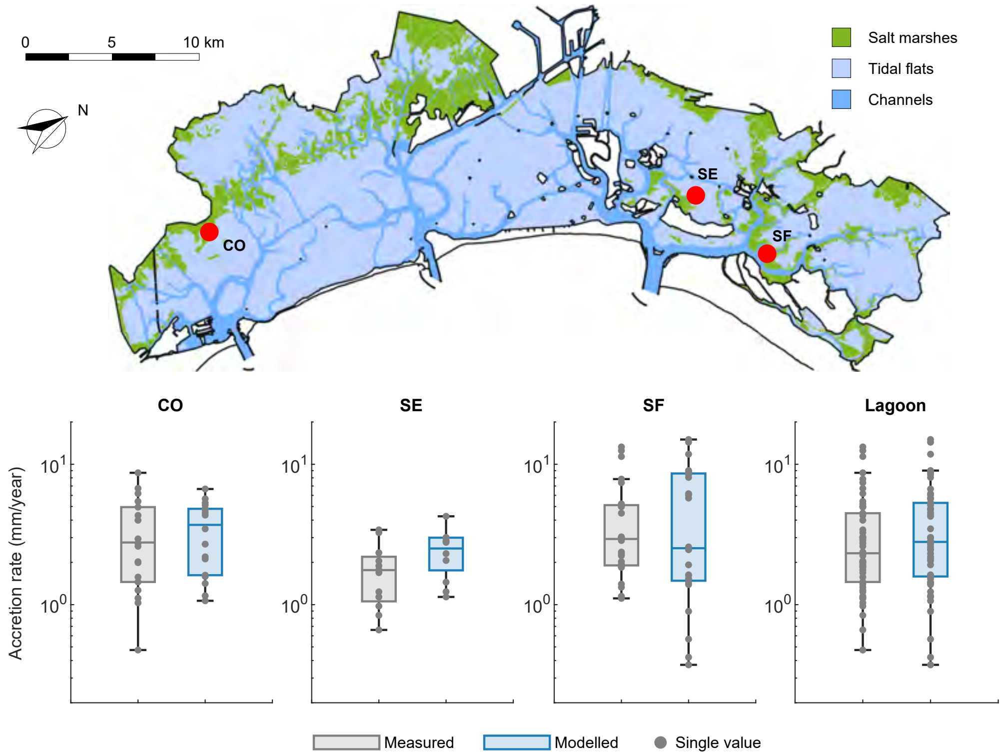


Figure 6.11: **Comparison between measured and modelled salt-marsh accretion.** Comparison between measured (grey) and modelled (blue) accretion rates on salt marshes. Data refer to years 2019 and 2020. Locations of the marsh study sites are shown by red dots in the upper panel. All y-axes in the lower panels are on a logarithmic scale.

Table 6.3: **Statistical test on salt-marsh accretion.** Results of the Kolmogorov-Smirnov test performed to test the null hypothesis that measured and modelled salt-marsh accretion rate (Figure 6.11) are from the same distribution. h = 0 indicates that the test does not reject the null hypothesis, and h = 1 otherwise. Significance level $\alpha = 0.01$.

| | Study area | h | p-value |
|---|---|---|---|
| 1 | CO | 0 | 0.708 |
| 2 | SE | 0 | 0.065 |
| 3 | SF | 0 | 0.387 |
| 4 | Lagoon | 0 | 0.724 |

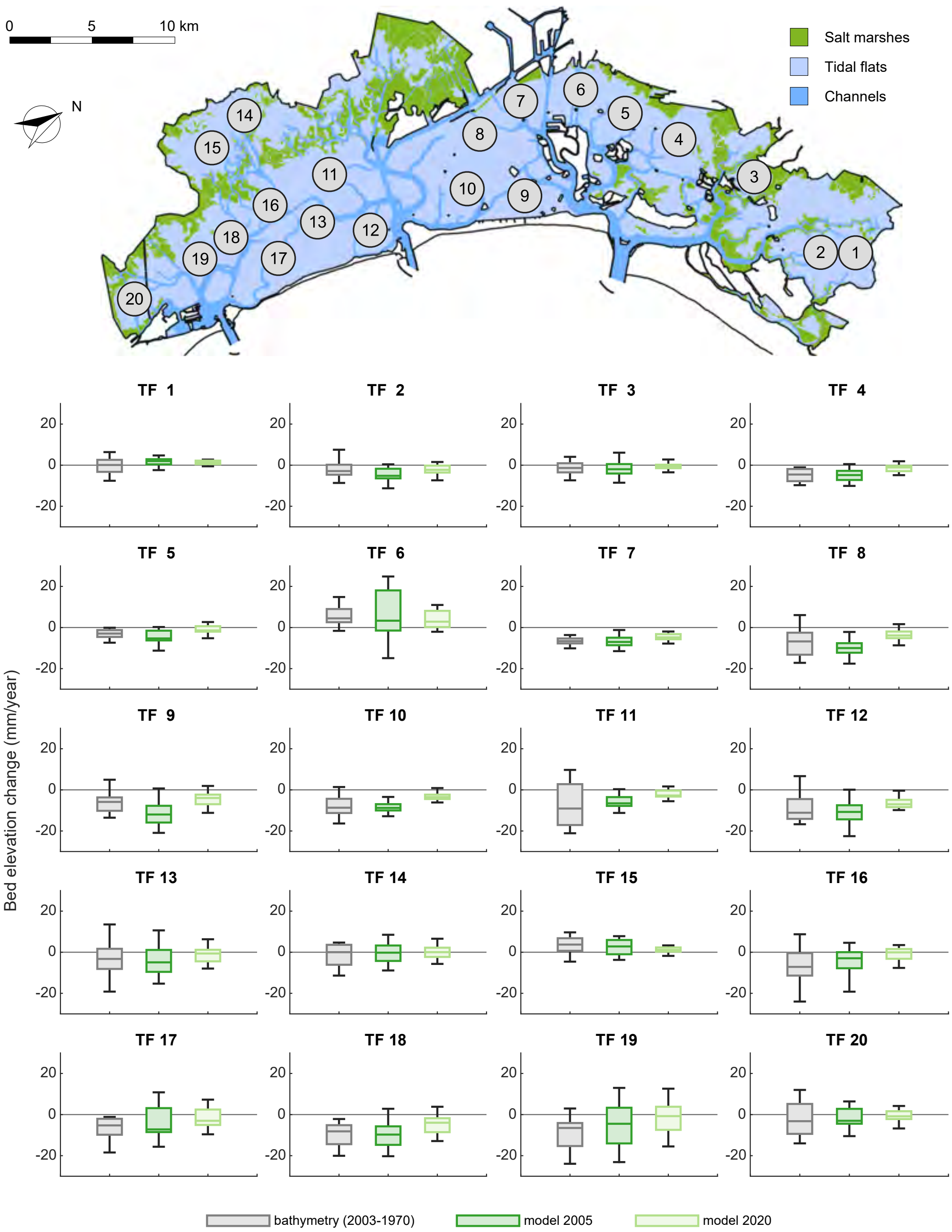


Figure 6.12: **Comparison between measured and modelled bed elevation change on tidal flats.** Comparison between bed elevation change obtained from bathymetric surveys (grey) and modelled using as boundary conditions water levels and wind climate measured in 2005 (dark green) and 2020 (light green). Locations of the studied tidal flat areas are shown in the upper panel.

Table 6.4: **Statistical test on tidal-flat bed elevation change.** Results of the Kolmogorov-Smirnov test performed to test the null hypothesis that measured and modelled tidal-flat bed elevation change (Figure 6.12) are from the same distribution. The test compares the bed elevation change obtained from bathymetric surveys with model results obtained using as boundary conditions water level and wind climate measured in 2005 ($3^{rd}$ and $4^{th}$ columns) and 2020 ($5^{th}$ and $6^{th}$ columns). h = 0 indicates that the test does not reject the null hypothesis, and h = 1 otherwise. Significance level $\alpha = 0.01$.

| | Study area | Bathymetry - Mod. 2005 | | Bathymetry - Mod. 2020 | |
|---|---|---|---|---|---|
| | | h | p-value | h | p-value |
| 1 | TF 1 | 0 | 0.247 | 0 | 0.116 |
| 2 | TF 2 | 0 | 0.218 | 0 | 0.709 |
| 3 | TF 3 | 0 | 0.999 | 0 | 0.247 |
| 4 | TF 4 | 0 | 0.018 | 1 | 0.002 |
| 5 | TF 5 | 0 | 0.190 | 0 | 0.031 |
| 6 | TF 6 | 0 | 0.247 | 0 | 0.247 |
| 7 | TF 7 | 0 | 0.012 | 1 | 0.001 |
| 8 | TF 8 | 0 | 0.116 | 0 | 0.049 |
| 9 | TF 9 | 0 | 0.018 | 0 | 0.116 |
| 10 | TF 10 | 0 | 0.060 | 1 | 4.22E-06 |
| 11 | TF 11 | 0 | 0.059 | 1 | 1.83E-04 |
| 12 | TF 12 | 0 | 0.742 | 1 | 0.006 |
| 13 | TF 13 | 0 | 0.956 | 0 | 0.462 |
| 14 | TF 14 | 0 | 0.945 | 0 | 0.425 |
| 15 | TF 15 | 0 | 0.425 | 1 | 0.001 |
| 16 | TF 16 | 0 | 0.387 | 0 | 0.031 |
| 17 | TF 17 | 0 | 0.673 | 0 | 0.190 |
| 18 | TF 18 | 0 | 0.965 | 0 | 0.059 |
| 19 | TF 19 | 0 | 0.425 | 0 | 0.014 |
| 20 | TF 20 | 0 | 0.010 | 0 | 0.010 |

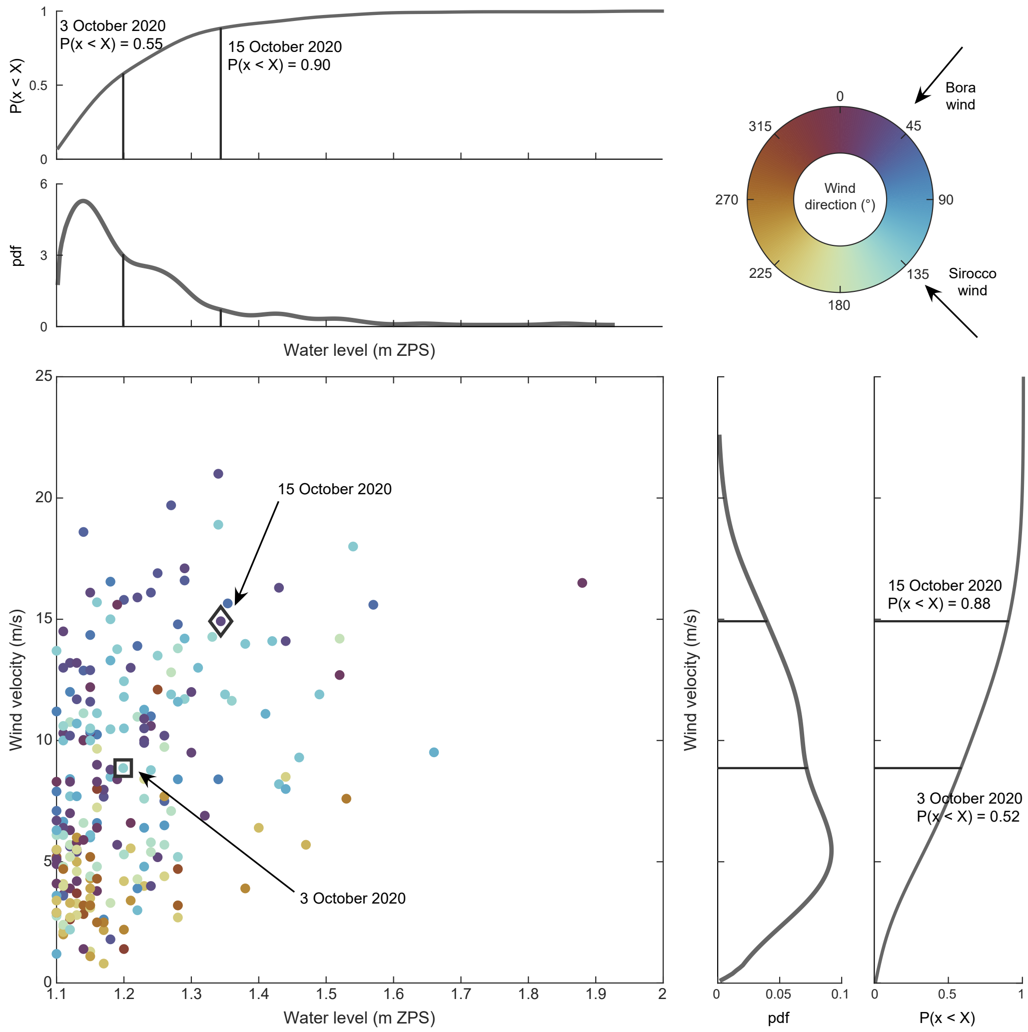


**Figure 6.13: Statistical characterization of tide and wind conditions associated with the flooding of lagoonal settlements.** Scatterplot of water levels and wind conditions associated with flooding events, i.e., water level higher than 1.10 m above the local datum of "Punta della Salute" (ZPS), based on data recorded from 1983 to 2020. Water levels are measured at the "Lido Diga Sud" gauging station, whereas wind data are derived from the "Chioggia Diga Sud" anemometric station. Colors indicate wind direction. Square and diamond highlight the 3 October and 15 October 2020 events, respectively. Probability density estimates and cumulative probability of water level and wind velocity are shown in the upper and right panels, respectively.

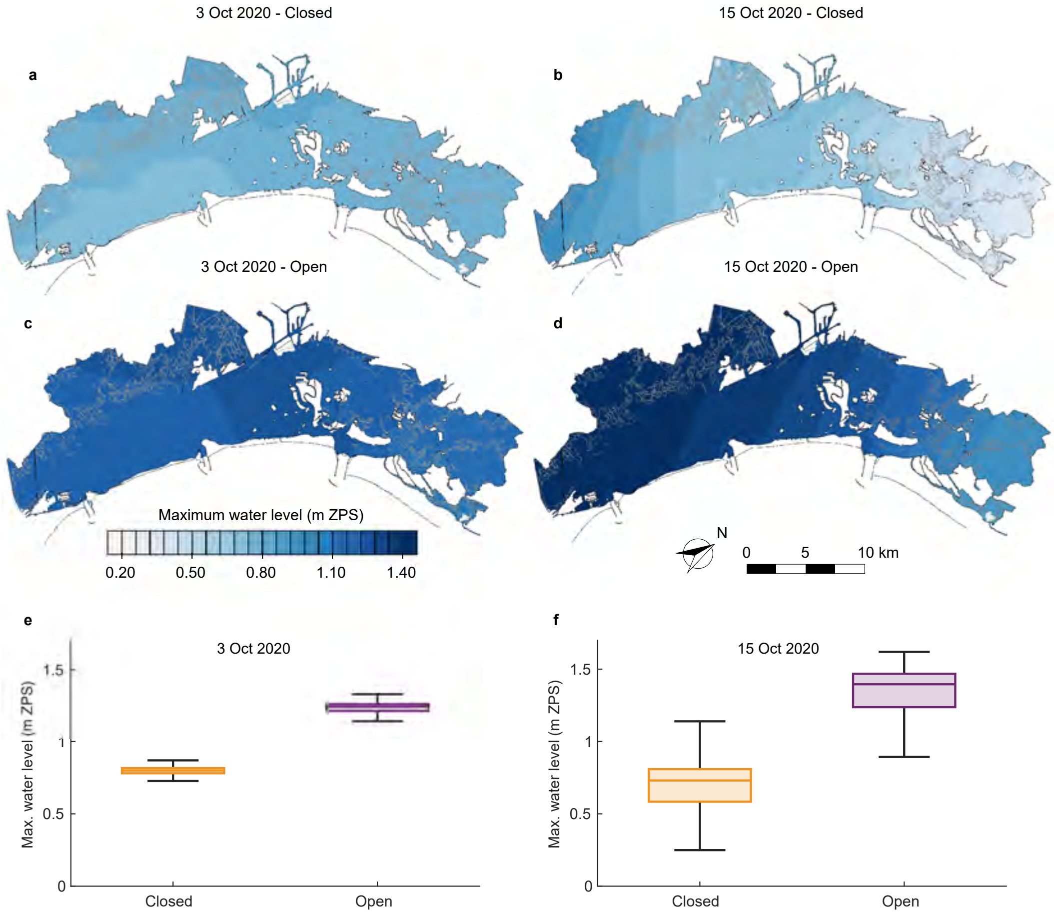


**Figure 6.14: Maximum water level.** Maximum water level in the closed barrier scenario, for the 3 October (**a**) and 15 October 2020 (**b**) operations, and in the open barrier scenario, for the 3 October (**c**) and 15 October 2020 (**d**) events. Boxplots of the maximum water level within the lagoon, considering both the closed (yellow) and open (purple) barrier scenario, for the 3 October (**e**) and 15 October (**f**) events.

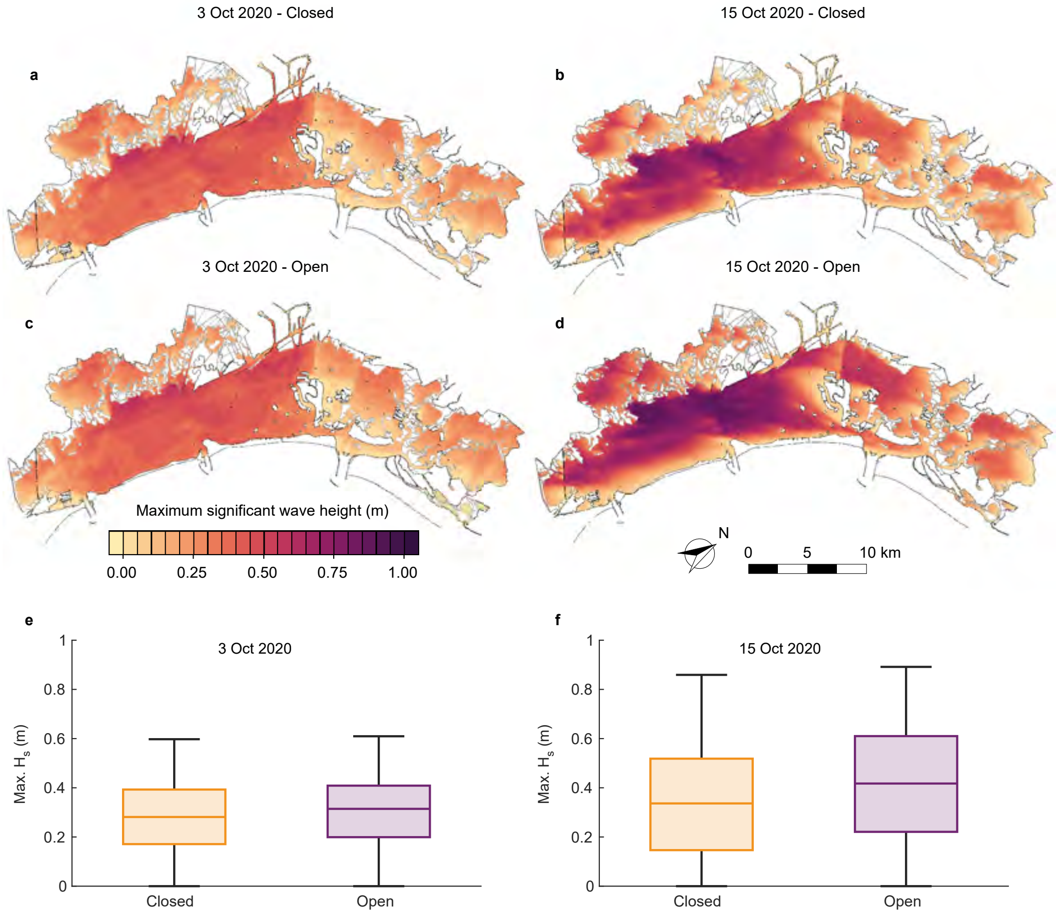


**Figure 6.15:** **Maximum significant wave height $H_s$**. Maximum significant wave height in the closed barrier scenario, for the 3 October (**a**) and 15 October 2020 (**b**) operations, and in the open barrier scenario, for the 3 October (**c**) and 15 October 2020 (**d**) events. Boxplots of the maximum water level within the lagoon, considering both the closed (yellow) and open (purple) barrier scenario, for the 3 October (**e**) and 15 October (**f**) events.

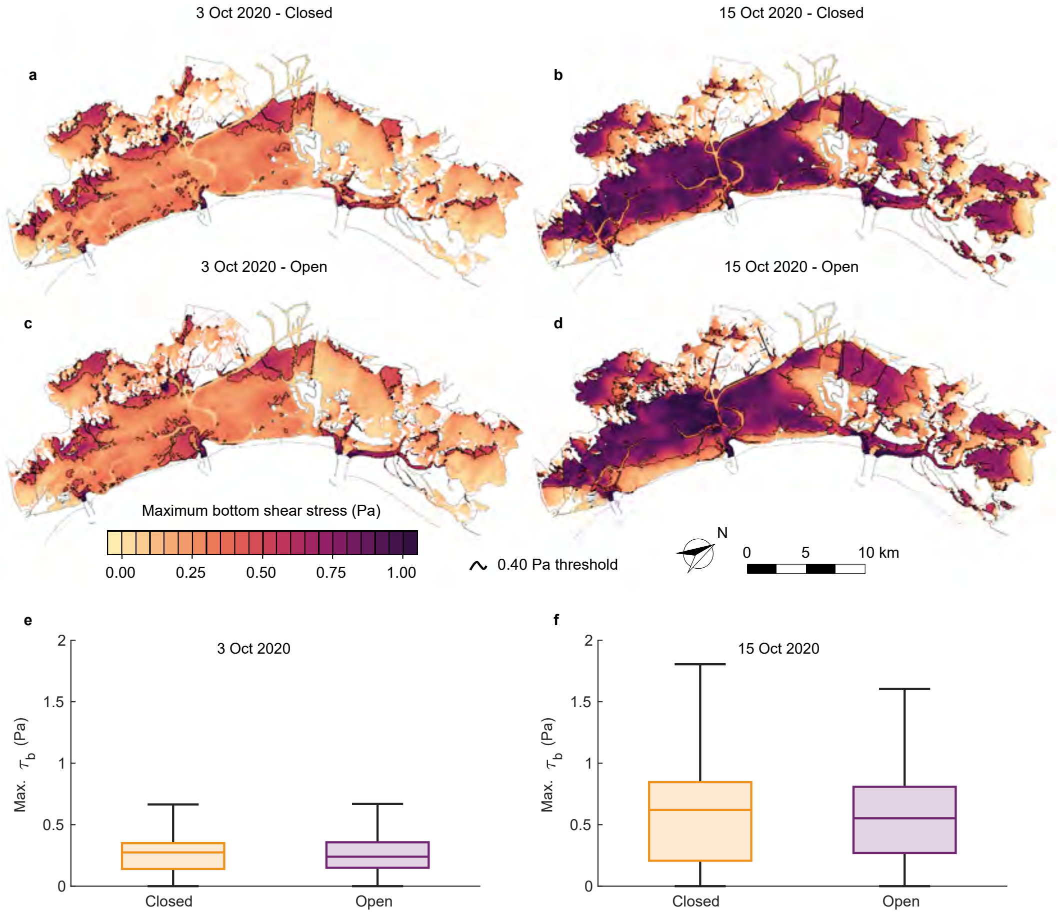


**Figure 6.16: Maximum bottom shear stress $\tau_b$.** Maximum bottom shear stress in the closed barrier scenario, for the 3 October (**a**) and 15 October 2020 (**b**) operations, and in the open barrier scenario, for the 3 October (**c**) and 15 October 2020 (**d**) events. Boxplots of the maximum water level within the lagoon, considering both the closed (yellow) and open (purple) barrier scenario, for the 3 October (**e**) and 15 October (**f**) events.

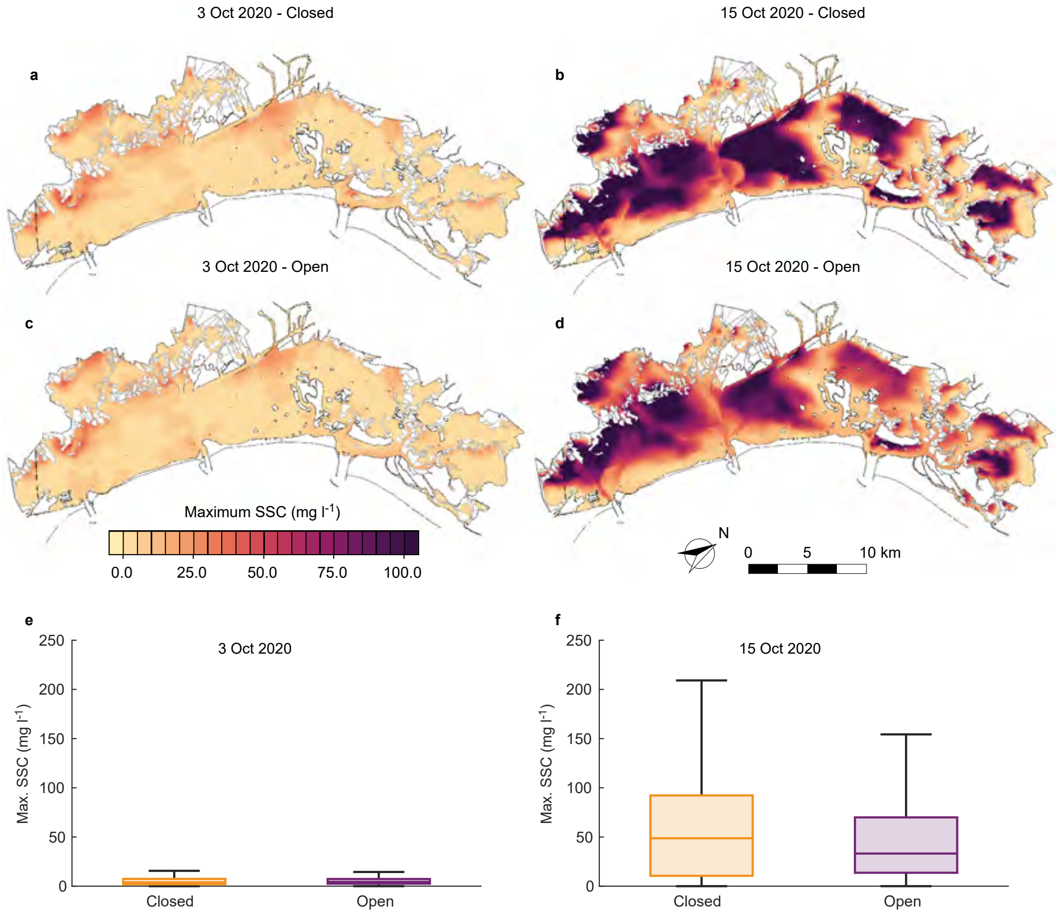


**Figure 6.17: Maximum suspended sediment concentration (SSC).** Maximum suspended sediment concentration in the closed barrier scenario, for the 3 October (**a**) and 15 October 2020 (**b**) operations, and in the open barrier scenario, for the 3 October (**c**) and 15 October 2020 (**d**) events. Boxplots of the maximum water level within the lagoon, considering both the closed (yellow) and open (purple) barrier scenario, for the 3 October (**e**) and 15 October (**f**) events.

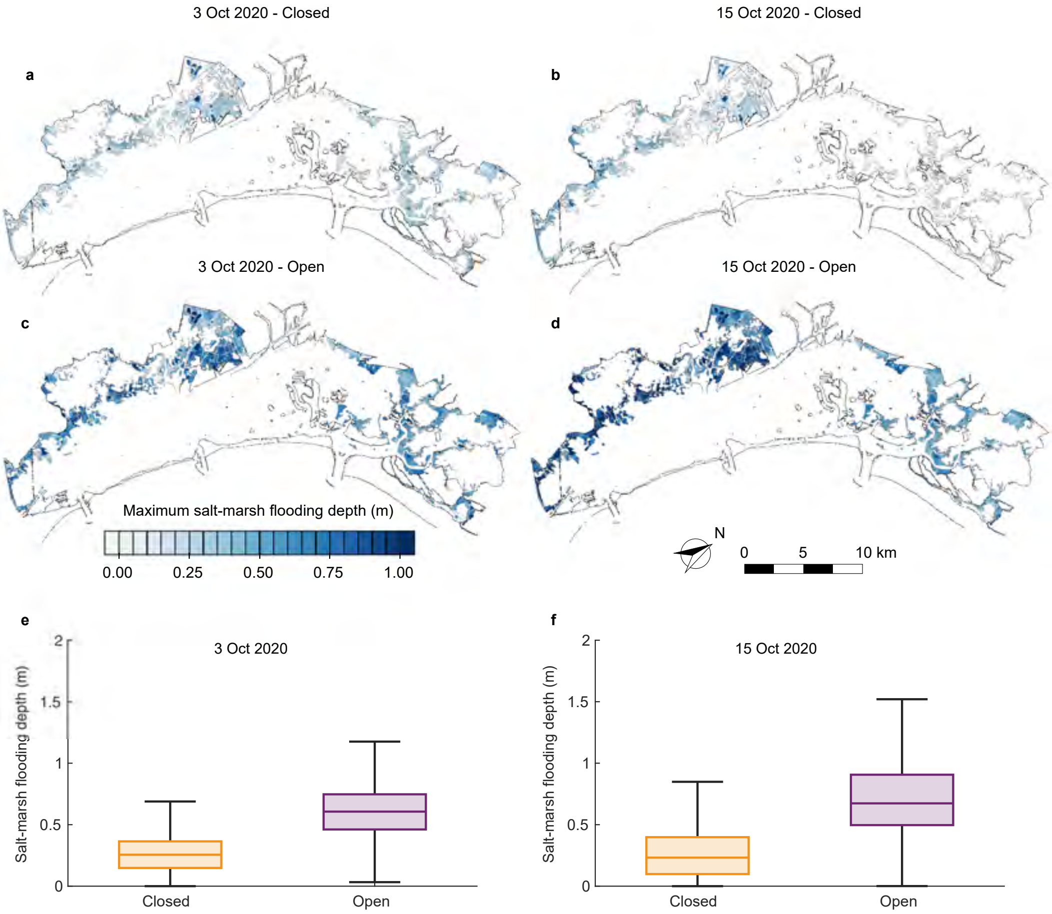


Figure 6.18: **Maximum salt-marsh flooding depth.** Maximum salt-marsh flooding depth in the closed barrier scenario, for the 3 October (**a**) and 15 October 2020 (**b**) operations, and in the open barrier scenario, for the 3 October (**c**) and 15 October 2020 (**d**) events. Boxplots of the maximum water level within the lagoon, considering both the closed (yellow) and open (purple) barrier scenario, for the 3 October (**e**) and 15 October (**f**) events.

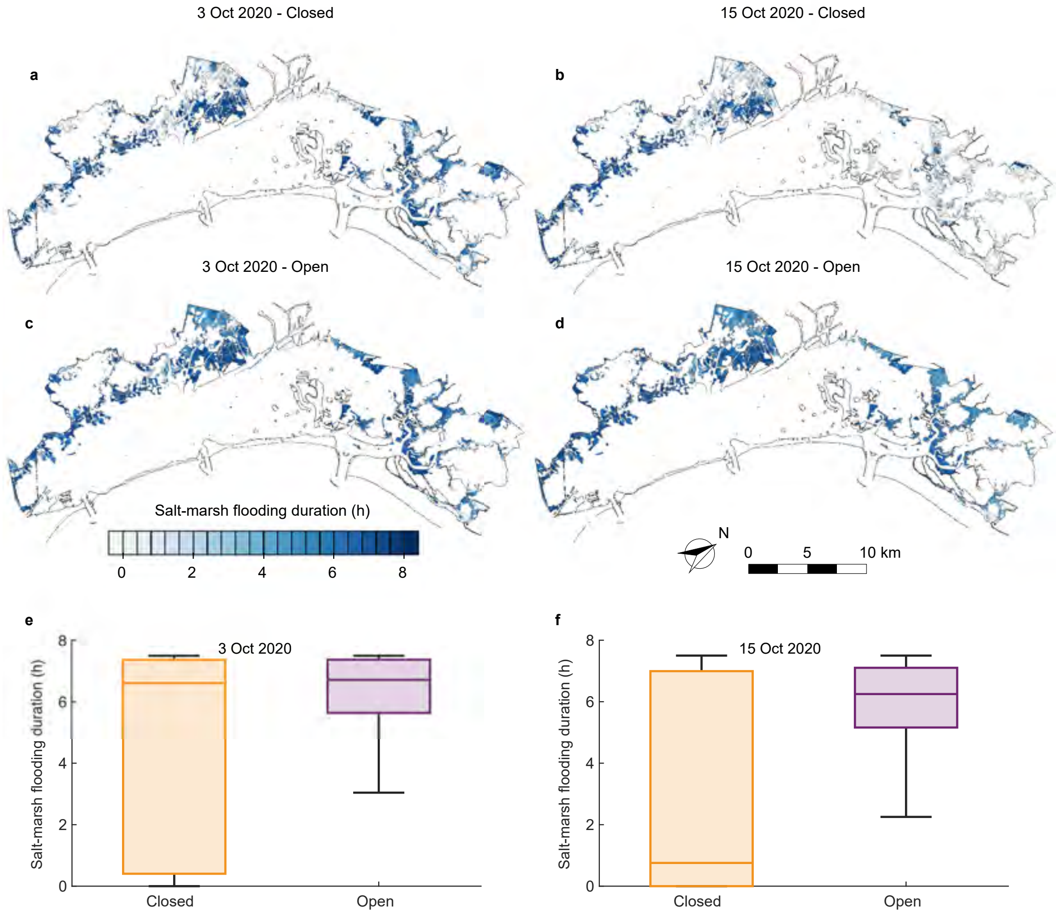


**Figure 6.19: Maximum salt-marsh flooding duration.** Maximum salt-marsh flooding duration in the closed barrier scenario, for the 3 October (**a**) and 15 October 2020 (**b**) operations, and in the open barrier scenario, for the 3 October (**c**) and 15 October 2020 (**d**) events. Boxplots of the maximum water level within the lagoon, considering both the closed (yellow) and open (purple) barrier scenario, for the 3 October (**e**) and 15 October (**f**) events.

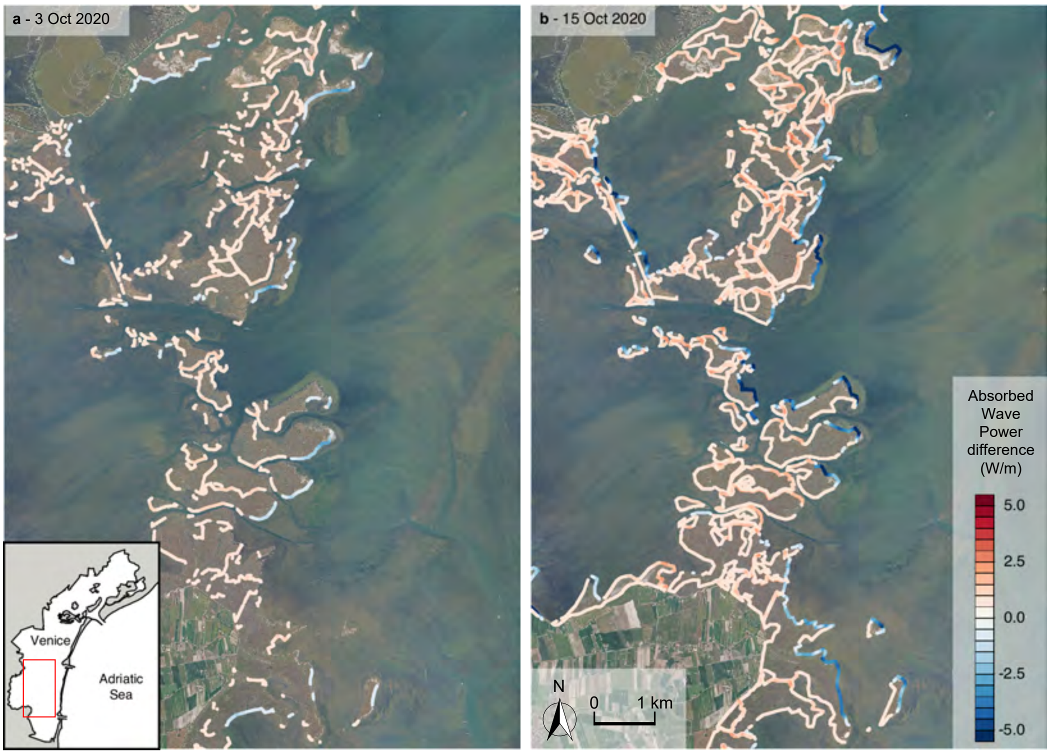


**Figure 6.20: Absorbed wave power difference.** Difference of the mean wave power absorbed by salt-mash margins in the central-southern lagoon between the flood-regulated and non-regulated scenarios, for the 3 October (**a**) and 15 October 2020 (**b**) events.

# 7

# CONCLUSIONS

Using a multidisciplinary approach, that combines numerical modelling, statistical analyses, field observations, and laboratory techniques, the present study deals with erosional and depositional dynamics in shallow tidal systems and how they are affected by natural and anthropogenic drivers. In particular, sediment erosion and transport dynamics were statistically characterized by analysing spatially-explicit time series of bottom shear stresses and suspended sediment concentrations computed using a calibrated and widely tested finite-element numerical model. Spatial and temporal sedimentation patterns on salt marshes were investigated considering short-term sedimentation observations measured in the Venice Lagoon from October 2018 to October 2021. Finally, the impacts on tidal basins and, in particular, on salt marshes of anthropogenic flood-regulation were evaluated combining field data and numerical modelling of the first-ever operations of the storm-surge barriers in the Venice Lagoon during Fall 2020.

The main results stemmed out from this research can be summarized answering the questions posed in Section 1.5 as follows:

i. *Can the stochastic effects of high-energy, wave-driven events on sediment erosion and transport be considered in a synthetic, but reliable,* *modelling framework for the long-term evolution of shallow tidal environments?*

Erosion and sediment transport dynamics can both be modelled as marked Poisson processes, because interarrival times of over-threshold events of bottom shear stress and suspended sediment concentration are exponentially distributed. This confirms the possibility of set-up a synthetic, statistically-based framework for the long-term biomorphodynamic evolution of shallow tidal systems.

In the specific case of the Venice Lagoon, its morphological evolution, shaped by both natural processes and anthropogenic interventions in the last four centuries, results generally in an increase of interarrival times, durations and intensities of over-threshold events, thus leading to less frequent but longer and more intense erosion and suspended sediment concentration events (Chapters 2 and 3).

ii. *Which is the relative contribution of storm-dominated and fair-weather periods to salt-marsh sedimentation?*

Field observations from the salt marshes of the microtidal Venice Lagoon show that about 70% of the yearly total sediment accumulation occurs during storm-dominated periods, despite their short duration. Hence, sediment accumulation on salt marshes appears to be supplied by intense, episodic storm surges, rather than by the mild, rhythmic tidal flooding (Chapter 4 and 5).

iii. *How do tides and wind waves affect spatial sedimentation patterns on salt marshes?*

Comparing sedimentation measurements and marsh topographic profiles, we show how tide, wind waves and their mutual combination during storm surges influences spatial sedimentation patterns on salt marshes. Surge enhanced water levels can promote wind-wave driven sediment fluxes directly across the mudflat-marsh transition. These fluxes alter purely tidal sedimentation patterns resulting from creek-driven gradual flooding and, thus, affect marsh topographic elevation and morphology (Chapter 4). These results challenge the conventional view of salt-marsh sedimentation as an essentially tide-driven process and provide further insight into the relative importance of the different hydrodynamic and sediment transport mechanisms that shape marsh platforms.

iv. *How do storm-surge barriers affect sediment transport at the basin scale? In particular, how is salt-marsh sedimentation affected by flood regulation?*

Flood-regulation using storm-surge barriers tends to promote channel infilling and hinder salt-marsh sediment accumulation. Even though barrier closures can temporarily reduce sediment loss from the system, they promote a less-diverse geomorphological structure, rather than contributing to the preservation of tidal landforms (Chapter 6).

Flood regulation will affect particularly the upper intertidal zone, where only few surge events cause flooding and supply the sediment needed for marshes to offset increasing sea levels. We prove that the large yet episodic, storm-driven sediment supply is seriously reduced by temporally limited capping of water levels by storm-surge barrier operations, thus casting doubt on marsh resilience to sea-level rise (Chapter 5).

The temporary closure of storm-surge barriers to avoid flooding of urban areas can deeply affect the morphodynamic processes and poses further pressures on the surrounding tidal environment. The quantification of the environmental effects of storm-surge barriers offers the cue and the tools to develop management strategies that can reconcile the objectives of the protection of the built environment and those of preservation of natural tidal ecosystems.

# BIBLIOGRAPHY


Adam, Paul (1990). *Saltmarsh Ecology*. Cambridge Studies in Ecology. Cambridge: Cambridge University Press, pp. i–iv. DOI: 10.1017/CBO9780511565328.

Allen, J. I., P. J. Somerfield, and F. J. Gilbert (2007). "Quantifying uncertainty in high-resolution coupled hydrodynamic-ecosystem models". *Journal of Marine Systems* 64.1-4, pp. 3–14. DOI: 10.1016/j.jmarsys.2006.02.010.

Allen, J. R. L. and M J Duffy (1998). "Medium-term sedimentation on high intertidal mudflats and salt marshes in the Severn Estuary, SW Britain: the role of wind and tide". *Marine Geology* 150.1, pp. 1–27. DOI: https://doi.org/10.1016/S0025-3227(98)00051-6.

Allen, J. R. L. (2000). "Morphodynamics of Holocene salt marshes: a review sketch from the Atlantic and Southern North Sea coasts of Europe". *Quaternary Science Reviews* 19.12, pp. 1155–1231. DOI: 10.1016/S0277-3791(99)00034-7.

Allen, J. R. L. (1995). "Salt-marsh growth and fluctuating sea level: implications of a simulation model for Flandrian coastal stratigraphy and peat-based sea-level curves". *Sedimentary Geology* 100.1, pp. 21–45. DOI: https://doi.org/10.1016/0037-0738(95)00101-8.

Ammerman, Albert J. and Charles E. McClennen (2000). "Saving Venice". *Science* 289.5483, pp. 1301–1302. DOI: 10.1126/science.289.5483.1301.

Amos, C. L., A. Bergamasco, Georg Umgiesser, S. Cappucci, D. Cloutier, L. Denat, M. Flindt, M. Bonardi, and S. Cristante (2004). "The stability of tidal flats in Venice Lagoon - The results of in-situ measurements using two benthic, annular flumes". *Journal of Marine Systems*. DOI: 10.1016/j.jmarsys.2004.05.013.

Anderson, Franz E. (1972). "Resuspension of estuarine sediments by small amplitude waves". *Journal of Sedimentary Research* 42.3, pp. 602–607.

Aubrey, D. G. and P. E. Speer (1985). "A study of non-linear tidal propagation in shallow inlet/estuarine systems Part I: Observations". *Estuarine, Coastal and Shelf Science* 21.2, pp. 185–205. DOI: https://doi.org/10.1016/0272-7714(85)90096-4.

Balkema, A. A. and L. de Haan (1974). "Residual Life Time at Great Age". *The Annals of Probability*. DOI: 10.1214/aop/1176996548.

Ball, D. F. (1964). "Loss-on-Ignition As an Estimate of Organic Matter and Organic Carbon in Non-Calcareous Soils". *Journal of Soil Science* 15.1, pp. 84–92. DOI: 10.1111/j.1365-2389.1964.tb00247.x.

Baptist, Martin J., T. Gerkema, B. C. van Prooijen, D. S. van Maren, M. van Regteren, K. Schulz, I. Colosimo, J. Vroom, T. van Kessel, B. Grasmeijer, P. Willemsen, K. Elschot, A. V. de Groot, J. Cleveringa, E. M.M. van Eekelen, F. Schuurman, H. J. de Lange, and M. E.B. van Puijenbroek (2019). "Beneficial use of dredged sediment to enhance salt marsh development by applying a 'Mud Motor'". *Ecological Engineering* 127.May 2018, pp. 312–323. DOI: 10.1016/j.ecoleng.2018.11.019.

Barbier, Edward B., Sally D. Hacker, Chris Kennedy, Evamaria W. Koch, Adrian C. Stier, and Brian R. Silliman (2011). *The value of estuarine and coastal ecosystem services*. DOI: 10.1890/10-1510.1.

Belliard, Jean-Philippe, Alexandra Silinski, Dieter Meire, Gerasimos Kolokythas, Yaïr Levy, Alexander Van Braeckel, Tjeerd J. Bouma, and Stijn Temmerman (2019). "High-resolution bed level changes in relation to tidal and wave forcing on a narrow fringing macrotidal flat: Bridging intra-tidal, daily and seasonal sediment dynamics". *Marine Geology* 412.January, pp. 123–138. DOI: 10.1016/j.margeo.2019.03.001.

Bendoni, M., Riccardo A. Mel, Luca Solari, Stefano Lanzoni, Simona Francalanci, and Hocine Oumeraci (2016). "Insights into lateral marsh retreat mechanism through localized field measurements". *Water Resources Research*. DOI: 10.1002/2015WR017966.

Bertassello, Leonardo Enrico, P. Suresh C. Rao, Jeryang Park, James W. Jawitz, and Gianluca Botter (2018). "Stochastic modeling of wetland-groundwater systems". *Advances in Water Resources* 112.December 2017, pp. 214–223. DOI: 10.1016/j.advwatres.2017.12.007.

Bertness, Mark D. and Aaron M. Ellison (1987). "Determinants of Pattern in a New England Salt Marsh Plant Community". *Ecological Monographs* 57.2, pp. 129–147. DOI: 10.2307/1942621.

Blum, Michael D. and Harry H. Roberts (2009). "Drowning of the Mississippi Delta due to insufficient sediment supply and global sea-level rise". *Nature Geoscience* 2.7, pp. 488–491. DOI: 10.1038/ngeo553.

Botter, Gianluca, A. Porporato, I. Rodriguez-Iturbe, and Andrea Rinaldo (2007). "Basin-scale soil moisture dynamics and the probabilistic characterization of carrier hydrologic flows: Slow, leaching-prone components of the hydrologic response". *Water Resources Research*. DOI: 10.1029/2006 WR005043.

Botter, Gianluca, S. Basso, I. Rodriguez-Iturbe, and Andrea Rinaldo (2013). "Resilience of river flow regimes". *Proceedings of the National Academy of Sciences* 110.32, pp. 12925–12930. DOI: 10.1073/pnas.1311920110.

Bras, Rafael L., Donald R. F. Harleman, Andrea Rinaldo, and Paolo Rizzoli (2002). "[Reply to "Did the Italian Government approve an obsolete project to save Venice?" by P.A. Pirazzoli] Obsolete? No. Necessary? Yes.

The gates will save Venice". *Eos, Transactions American Geophysical Union* 83.20, p. 217. DOI: 10.1029/2002EO000149.

Brand, Evelien, Margaret Chen, and Anne-Lise Montreuil (2020). "Optimizing measurements of sediment transport in the intertidal zone". *Earth-Science Reviews* 200, p. 103029. DOI: 10.1016/j.earscirev.2019.103029.

Breugem, W. A. and L. H. Holthuijsen (2007). "Generalized Shallow Water Wave Growth from Lake George". *Journal of Waterway, Port, Coastal, and Ocean Engineering*. DOI: 10.1061/(asce)0733-950x(2007)133:3(173).

Breda, Angelo, Patricia M Saco, Steven G Sandi, Neil Saintilan, Gerardo Riccardi, and José F. Rodríguez (2021). "Accretion, retreat and transgression of coastal wetlands experiencing sea-level rise". *Hydrology and Earth System Sciences* 25.2, pp. 769–786. DOI: 10.5194/hess-25-769-2021.

Brooks, Helen, Iris Möller, Simon J. Carr, Clementine Chirol, Elizabeth Christie, Ben R. Evans, Kate L. Spencer, Thomas Spencer, and Katherine R. Royse (2021). "Resistance of salt marsh substrates to near-instantaneous hydrodynamic forcing". *Earth Surface Processes and Landforms* 46.1, pp. 67–88. DOI: 10.1002/esp.4912.

Cahoon, Donald R., Denise J. Reed, John W Day, Gregory D. Steyer, Roelof M. Boumans, James C. Lynch, David McNally, and Numair Latif (1995). "The Influence of Hurricane Andrew on Sediment Distribution in Louisiana Coastal Marshes". *Journal of Coastal Research*, pp. 280–294.

Cahoon, Donald R. (2006). "A review of major storm impacts on coastal wetland elevations". *Estuaries and Coasts* 29.6, pp. 889–898. DOI: 10.1007/BF02798648.

Carbognin, Laura, Pietro Teatini, and Luigi Tosi (2004). "Eustacy and land subsidence in the Venice Lagoon at the beginning of the new millennium". *Journal of Marine Systems*. DOI: 10.1016/j.jmarsys.2004.05.021.

Carniello, Luca, Andrea Defina, Sergio Fagherazzi, and Luigi D'Alpaos (2005). "A combined wind wave-tidal model for the Venice lagoon, Italy".

*Journal of Geophysical Research: Earth Surface* 110.4, pp. 1–15. DOI: 10.1029/2004JF000232.

Carniello, Luca, Andrea Defina, and Luigi D'Alpaos (2009). "Morphological evolution of the Venice lagoon: Evidence from the past and trend for the future". *Journal of Geophysical Research* 114.F4, F04002. DOI: 10.1029/2008JF001157.

Carr, Joel A., Paolo D'Odorico, Karen J. McGlathery, and Patricia L. Wiberg (2010). "Stability and bistability of seagrass ecosystems in shallow coastal lagoons: Role of feedbacks with sediment resuspension and light attenuation". *Journal of Geophysical Research: Biogeosciences* 115.G3. DOI: 10.1029/2009JG001103.

Carniello, Luca, Andrea D'Alpaos, and Andrea Defina (2011). "Modeling wind waves and tidal flows in shallow micro-tidal basins". *Estuarine, Coastal and Shelf Science* 92.2, pp. 263–276. DOI: 10.1016/j.ecss.2011.01.001.

Carniello, Luca, Andrea Defina, and Luigi D'Alpaos (2012). "Modeling sand-mud transport induced by tidal currents and wind waves in shallow microtidal basins: Application to the Venice Lagoon (Italy)". *Estuarine, Coastal and Shelf Science* 102-103, pp. 105–115. DOI: 10.1016/j.ecss.2012.03.016.

Carniello, Luca, Sonia Silvestri, Marco Marani, Andrea D'Alpaos, V. Volpe, and Andrea Defina (2014). "Sediment dynamics in shallow tidal basins: In situ observations, satellite retrievals, and numerical modeling in the Venice Lagoon". *Journal of Geophysical Research: Earth Surface* 119.4, pp. 802–815. DOI: 10.1002/2013JF003015.

Carniello, Luca, Andrea D'Alpaos, Gianluca Botter, and Andrea Rinaldo (2016). "Statistical characterization of spatiotemporal sediment dynamics in the Venice lagoon". *Journal of Geophysical Research: Earth Surface*, pp. 1049–1064. DOI: 10.1002/2015JF003793.

Carr, Joel A., Paolo. D'Odorico, Karen J. McGlathery, and Patricia L. Wiberg (2016). "Spatially explicit feedbacks between seagrass meadow structure, sediment and light: Habitat suitability for seagrass growth". *Advances in Water Resources* 93, pp. 315–325. DOI: https://doi.org/10.1016/j.advwatres.2015.09.001.

Carling, P. A. (1982). "Temporal and spatial variation in intertidal sedimentation rates". *Sedimentology* 29.1, pp. 17–23. DOI: 10.1111/j.1365-3091.1982.tb01705.x.

Castagno, Katherine A., Alfonso M. Jiménez-Robles, Jeffrey P. Donnelly, Patricia L. Wiberg, Michael S. Fenster, and Sergio Fagherazzi (2018). "Intense Storms Increase the Stability of Tidal Bays". *Geophysical Research Letters* 45.11, pp. 5491–5500. DOI: 10.1029/2018GL078208.

Chapman, Valentine Jackson (1974). *Salt Marshes and Salt Deserts of the World*. Lehre, Germany: J. Cramer, p. 392.

Chen, Xindi, Changkuan Zhang, Zeng Zhou, Zheng Gong, J. J. Zhou, J. F. Tao, David M. Paterson, and Qian Feng (2017). "Stabilizing Effects of Bacterial Biofilms: EPS Penetration and Redistribution of Bed Stability Down the Sediment Profile". *Journal of Geophysical Research: Biogeosciences*. DOI: 10.1002/2017JG004050.

Chen, Xindi, Changkuan Zhang, David M. Paterson, Ian Townend, Chuang Jin, Zeng Zhou, Zheng Gong, and Qian Feng (2019). "The effect of cyclic variation of shear stress on non-cohesive sediment stabilization by microbial biofilms: the role of 'biofilm precursors'". *Earth Surface Processes and Landforms* 44.7, pp. 1471–1481. DOI: 10.1002/esp.4573.

Chirol, Clementine, Kate L. Spencer, Simon J. Carr, Iris Möller, Ben Evans, Jason Lynch, Helen Brooks, and Katherine R. Royse (2021). "Effect of vegetation cover and sediment type on 3D subsurface structure and shear strength in saltmarshes". *Earth Surface Processes and Landforms* 46.11, pp. 2279–2297. DOI: 10.1002/esp.5174.

Chmura, Gail L., Shimon C. Anisfeld, Donald R. Cahoon, and James C. Lynch (2003). "Global carbon sequestration in tidal, saline wetland soils". *Global Biogeochemical Cycles*. DOI: 10.1029/2002GB001917.

Chowdhury, Mohammed Shah Nawaz, Brenda Walles, Sm Sharifuzzaman, M. Shahadat Hossain, Tom Ysebaert, and Aad C. Smaal (2019). "Oyster breakwater reefs promote adjacent mudflat stability and salt marsh growth in a monsoon dominated subtropical coast". *Scientific Reports* 9.1, p. 8549. DOI: 10.1038/s41598-019-44925-6.

Christiansen, T., Patricia L. Wiberg, and T. G. Milligan (2000). "Flow and Sediment Transport on a Tidal Salt Marsh Surface". *Estuarine, Coastal and Shelf Science* 50.3, pp. 315–331. DOI: 10.1006/ecss.2000.0548.

Coco, Giovanni, Zeng Zhou, B. van Maanen, Maitane Olabarrieta, Rafael O. Tinoco, and Ian Townend (2013). "Morphodynamics of tidal networks: Advances and challenges". *Marine Geology* 346, pp. 1–16. DOI: 10.1016/j.margeo.2013.08.005.

Costanza, Robert, Ralph D'Arge, Rudolf de Groot, Stephen C. Farber, Monica Grasso, Bruce Hannon, Karin Limburg, Shahid Naeem, Robert V. O'Neill, Jose Paruelo, Robert G. Raskin, Paul Sutton, and Marjan van den Belt (1997). "The value of the world's ecosystem services and natural capital". *Nature* 387.6630, pp. 253–260. DOI: 10.1038/387253a0.

Cramér, Harald and M R Leadbetter (1967). *Stationary and related stochastic processes*. New York: John Wiley & Sons, Ltd, p. 348.

Craft, C.B., E.D. Seneca, and S.W. Broome (1993). "Vertical accretion in microtidal regularly and irregularly flooded estuarine marshes". *Estuarine, Coastal and Shelf Science*. DOI: 10.1006/ecss.1993.1062.

Da Lio, Cristina, Andrea D'Alpaos, and Marco Marani (2013). "The secret gardener: vegetation and the emergence of biogeomorphic patterns in tidal environments." *Philosophical transactions. Series A, Mathematical,* *physical, and engineering sciences* 371.2004, p. 20120367. DOI: 10.1098/rsta.2012.0367.

D'Alpaos, Andrea, Stefano Lanzoni, Marco Marani, Sergio Fagherazzi, and Andrea Rinaldo (2005). "Tidal network ontogeny: Channel initiation and early development". *Journal of Geophysical Research: Earth Surface* 110.F2. DOI: https://doi.org/10.1029/2004JF000182.

D'Alpaos, Luigi and Paolo Martini (2005). "The influence of inlet configuration on sediment loss in the Venice lagoon". In: *Flooding and Environmental Challenges for Venice and its Lagoon: State of Knowledge*. Ed. by C. A. Fletcher and Tom Spencer. Cambridge: Cambridge University Press, pp. 419–430.

D'Alpaos, Andrea, Stefano Lanzoni, Marco Marani, and Andrea Rinaldo (2007). "Landscape evolution in tidal embayments: Modeling the interplay of erosion, sedimentation, and vegetation dynamics". *Journal of Geophysical Research* 112.F1, F01008. DOI: 10.1029/2006JF000537.

D'Alpaos, Luigi and Andrea Defina (2007). "Mathematical modeling of tidal hydrodynamics in shallow lagoons: A review of open issues and applications to the Venice lagoon". *Computers and Geosciences* 33.4, pp. 476–496. DOI: https://doi.org/10.1016/j.cageo.2006.07.009.

D'Alpaos, Andrea, Stefano Lanzoni, Marco Marani, and Andrea Rinaldo (2009). "On the O'Brien-Jarrett-Marchi law". *Rendiconti Lincei* 20.3, pp. 225–236. DOI: 10.1007/s12210-009-0052-x.

D'Alpaos, Andrea, Stefano Lanzoni, Marco Marani, and Andrea Rinaldo (2010). "On the tidal prism-channel area relations". *Journal of Geophysical Research: Earth Surface*. DOI: 10.1029/2008JF001243.

D'Alpaos, Andrea, Simon M. Mudd, and Luca Carniello (2011). "Dynamic response of marshes to perturbations in suspended sediment concentrations and rates of relative sea level rise". *Journal of Geophysical Research: Earth Surface* 116.4, pp. 1–13. DOI: 10.1029/2011JF002093.

D'Alpaos, Andrea, Cristina Da Lio, and Marco Marani (2012). "Biogeomorphology of tidal landforms : physical and biological processes shaping the tidal landscape". *Ecohydrology* 5.5, pp. 550–562. DOI: 10.1002/eco.279.

D'Alpaos, Andrea, Luca Carniello, and Andrea Rinaldo (2013). "Statistical mechanics of wind wave-induced erosion in shallow tidal basins: Inferences from the Venice Lagoon". *Geophysical Research Letters*. DOI: 10.1002/grl.50666.

D'Alpaos, Andrea and Marco Marani (2016). "Reading the signatures of biologic-geomorphic feedbacks in salt-marsh landscapes". *Advances in Water Resources* 93, pp. 265–275. DOI: 10.1016/j.advwatres.2015.09.004.

D'Alpaos, Luigi (2010a). *Fatti e misfatti di idraulica lagunare. La laguna di Venezia dalla diversione dei fiumi alle nuove opere delle bocche di porto*. Venice: Istituto Veneto di Scienze, Lettere e Arti, p. 329.

D'Alpaos, Luigi (2010b). *L'evoluzione morfologica della laguna di Venezia attraverso la lettura di alcune mappe storiche e delle sue mappe idrografiche*. Istituto Veneto di Scienze, Lettere e Arti, 105 pp.

Davidson-Arnott, Robin G. D., Danika Van Proosdij, Jeff Ollerhead, and Laura Schostak (2002). "Hydrodynamics and sedimentation in salt marshes: Examples from a macrotidal marsh, Bay of Fundy". *Geomorphology* 48.1-3, pp. 209–231. DOI: 10.1016/S0169-555X(02)00182-4.

Day, J. W., J. Rybczyk, F. Scarton, A. Rismondo, D. Are, and G. Cecconi (1999). "Soil Accretionary Dynamics, Sea-Level Rise and the Survival of Wetlands in Venice Lagoon: A Field and Modelling Approach". *Estuarine, Coastal and Shelf Science* 49.5, pp. 607–628. DOI: https://doi.org/10.1006/ecss.1999.0522.

Defina, Andrea, Luca Carniello, Sergio Fagherazzi, and Luigi D'Alpaos (2007). "Self-organization of shallow basins in tidal flats and salt marshes". *Journal of Geophysical Research: Earth Surface* 112.3, pp. 1–11. DOI: 10.1029/2006JF000550.

Defendi, V., V. Kovačević, F. Arena, and L. Zaggia (2010). "Estimating sediment transport from acoustic measurements in the Venice Lagoon inlets". *Continental Shelf Research* 30.8, pp. 883–893. DOI: 10.1016/j.csr.2009.12.004.

Defina, Andrea (2000). "Two-dimensional shallow flow equations for partially dry areas". *Water Resources Research* 36.11, pp. 3251–3264. DOI: 10.1029/2000WR900167.

Defina, Andrea (2003). "Numerical experiments on bar growth". *Water Resources Research* 39.4. DOI: https://doi.org/10.1029/2002WR001455.

D'Odorico, Paolo and Sergio Fagherazzi (2003). "A probabilistic model of rainfall-triggered shallow landslides in hollows: A long-term analysis". *Water Resources Research*. DOI: 10.1029/2002WR001595.

Du, Jiabi, Kyeong Park, Timothy M. Dellapenna, and Jacinta M. Clay (2019). "Dramatic hydrodynamic and sedimentary responses in Galveston Bay and adjacent inner shelf to Hurricane Harvey". *Science of The Total Environment* 653, pp. 554–564. DOI: https://doi.org/10.1016/j.scitotenv.2018.10.403.

Duarte, Carlos M., J. J. Middelburg, and N. Caraco (2005). "Major role of marine vegetation on the oceanic carbon cycle". *Biogeosciences* 2.1, pp. 1–8. DOI: 10.5194/bg-2-1-2005.

Duvall, Melissa S., Patricia L. Wiberg, and Matthew L. Kirwan (2019). "Controls on Sediment Suspension, Flux, and Marsh Deposition near a Bay-Marsh Boundary". *Estuaries and Coasts* 42.2, pp. 403–424. DOI: 10.1007/s12237-018-0478-4.

Dyer, K. R., M. C. Christie, N. Feates, M. J. Fennessy, M. Pejrup, and W. van der Lee (2000). "An Investigation into Processes Influencing the Morphodynamics of an Intertidal Mudflat, the Dollard Estuary, The Netherlands: I. Hydrodynamics and Suspended Sediment". *Estuarine, Coastal and Shelf Science* 50.5, pp. 607–625. DOI: 10.1006/ecss.1999.0596.

Dyer, K. R. (1989). “Sediment processes in estuaries: Future research requirements”. *Journal of Geophysical Research* 94.C10, p. 14327. DOI: 10.1029/JC094iC10p14327.

Dyer, K. R. (1998). “The typology of intertidal mudflats”. *Geological Society, London, Special Publications* 139.1, pp. 11–24. DOI: 10.1144/GSL.SP.1998.139.01.02.

Eelkema, Menno, Zheng Bing Wang, Anneke Hibma, and Marcel J. F. Stive (2013). “Morphological Effects of the Eastern Scheldt Storm Surge Barrier on the Ebb-Tidal Delta”. *Coastal Engineering Journal* 55.3, pp. 1350010–1350026. DOI: 10.1142/S0578563413500101.

Eprim, Y. (2005). “Venice mobile barriers project: Barrier caissons construction details”. In: *Flooding and Environmental Challenges for Venice and its Lagoon: State of Knowledge*. Ed. by C. A. Fletcher and Tom Spencer. Cambridge: Cambridge University Press, pp. 257–262.

Evans, Ben R., Iris Möller, Thomas Spencer, and Geoff Smith (2019). “Dynamics of salt marsh margins are related to their three-dimensional functional form”. *Earth Surface Processes and Landforms* 44.9, esp.4614. DOI: 10.1002/esp.4614.

Fagherazzi, Sergio, Luca Carniello, Luigi D’Alpaos, and Andrea Defina (2006). “Critical bifurcation of shallow microtidal landforms in tidal flats and salt marshes”. *Proceedings of the National Academy of Sciences* 103.22, pp. 8337–8341. DOI: 10.1073/pnas.0508379103.

Fagherazzi, Sergio and Patricia L. Wiberg (2009). “Importance of wind conditions, fetch, and water levels on wave-generated shear stresses in shallow intertidal basins”. *Journal of Geophysical Research: Earth Surface*. DOI: 10.1029/2008JF001139.

Fagherazzi, Sergio, Matthew L. Kirwan, Simon M. Mudd, Glenn R. Guntenspergen, Stijn Temmerman, Andrea D’Alpaos, Johan Van De Koppel, John M. Rybczyk, Enrique Reyes, Chris Craft, and Jonathan Clough

(2012). "Numerical models of salt marsh evolution: Ecological, geomorphic, and climatic factors". *Reviews of Geophysics*. DOI: 10.1029/2011RG000359.

Fairchild, Tom P., William G. Bennett, Greg Smith, Brett Day, Martin W. Skov, Iris Möller, Nicola Beaumont, Harshinie Karunarathna, and John N. Griffin (2021). "Coastal wetlands mitigate storm flooding and associated costs in estuaries". *Environmental Research Letters* 16.7, p. 074034. DOI: 10.1088/1748-9326/ac0c45.

Feagin, R. A., S. M. Lozada-Bernard, T. M. Ravens, Iris Möller, K. M. Yeager, and A. H. Baird (2009). "Does vegetation prevent wave erosion of salt marsh edges?" *Proceedings of the National Academy of Sciences* 106.25, pp. 10109–10113. DOI: 10.1073/pnas.0901297106.

Ferrarin, Christian, Alberto Tomasin, Marco Bajo, Antonio Petrizzo, and Georg Umgiesser (2015). "Tidal changes in a heavily modified coastal wetland". *Continental Shelf Research* 101, pp. 22–33. DOI: 10.1016/j.csr.2015.04.002.

Finotello, Alvise, Stefano Lanzoni, Massimiliano Ghinassi, Marco Marani, Andrea Rinaldo, and Andrea D'Alpaos (2018). "Field migration rates of tidal meanders recapitulate fluvial morphodynamics". *Proceedings of the National Academy of Sciences* 115.7, pp. 1463–1468. DOI: 10.1073/pnas.1711330115.

Finotello, Alvise, Alberto Canestrelli, Luca Carniello, Massimiliano Ghinassi, and Andrea D'Alpaos (2019). "Tidal Flow Asymmetry and Discharge of Lateral Tributaries Drive the Evolution of a Microtidal Meander in the Venice Lagoon (Italy)". *Journal of Geophysical Research: Earth Surface* 124.12, pp. 3043–3066. DOI: 10.1029/2019JF005193.

Finotello, Alvise, Andrea D'Alpaos, Manuel Bogoni, Massimiliano Ghinassi, and Stefano Lanzoni (2020a). "Remotely-sensed planform morphologies reveal fluvial and tidal nature of meandering channels". *Scientific Reports* 10.1, pp. 1–13. DOI: 10.1038/s41598-019-56992-w.

Finotello, Alvise, Marco Marani, Luca Carniello, Mattia Pivato, Marcella Roner, Laura Tommasini, and Andrea D'alpaos (2020b). "Control of wind-wave power on morphological shape of salt marsh margins". *Water Science and Engineering* 13.1, pp. 45–56. DOI: 10.1016/j.wse.2020.03.006.

FitzGerald, Duncan M. and Zoe J. Hughes (2019). "Marsh Processes and Their Response to Climate Change and Sea-Level Rise". *Annual Review of Earth and Planetary Sciences*. DOI: 10.1146/annurev-earth-082517-010255.

French, J. R. and D. R. Stoddart (1992). "Hydrodynamics of salt marsh creek systems: Implications for marsh morphological development and material exchange". *Earth Surface Processes and Landforms* 17.3, pp. 235–252. DOI: 10.1002/esp.3290170304.

French, J. R. and Tom Spencer (1993). "Dynamics of sedimentation in a tide-dominated backbarrier salt marsh, Norfolk, UK". *Marine Geology* 110.3-4, pp. 315–331. DOI: 10.1016/0025-3227(93)90091-9.

French, J. R., T. Spencer, A. L. Murray, and N. S. Arnold (1995). "Geostatistical Analysis of Sediment Deposition in Two Small Tidal Wetlands, Norfolk, U.K." *Journal of Coastal Research* 11.2, pp. 308–321.

Friedrichs, Carl T. and James E. Perry (2001). "Tidal Salt Marsh Morphodynamics: A Synthesis". *Journal of Coastal Research* 27, pp. 7–37.

Friedrichs, Carl T. and Ole S. Madsen (1992). "Nonlinear diffusion of the tidal signal in frictionally dominated embayments". *Journal of Geophysical Research* 97.C4, p. 5637. DOI: 10.1029/92jc00354.

Friedrichs, Carl T. (2011). "Tidal Flat Morphodynamics". In: *Treatise on Estuarine and Coastal Science*. Vol. 3. Elsevier, pp. 137–170. DOI: 10.1016/B978-0-12-374711-2.00307-7.

Gartner, Jeffrey W. (2004). "Estimating suspended solids concentrations from backscatter intensity measured by acoustic Doppler current profiler in San Francisco Bay, California". *Marine Geology* 211.3-4, pp. 169–187. DOI: 10.1016/j.margeo.2004.07.001.

Gedan, K. Bromberg, Brian R. Silliman, and M. D. Bertness (2009). "Centuries of Human-Driven Change in Salt Marsh Ecosystems". *Annual Review of Marine Science* 1.1, pp. 117–141. DOI: 10.1146/annurev.marine.010908.163930.

Goodwin, Guillaume C. H. and Simon M. Mudd (2019). "High platform elevations highlight the role of storms and spring tides in salt marsh evolution". *Frontiers in Environmental Science* 7.5, pp. 1–14. DOI: 10.3389/fenvs.2019.00062.

Goodwin, Guillaume C. H., Luca Carniello, Andrea D'Alpaos, Marco Marani, and Sonia Silvestri (2021). "Long-term seasonal dynamics of seagrass extent in a Mediterranean Lagoon (Venice, Italy) from public satellite data". In: *EGU General Assembly Conference*. Copernicus Meetings. DOI: https://doi.org/10.5194/egusphere-egu21-8837.

Goodbred Steven L., Jr. and Albert C. Hine (1995). "Coastal storm deposition: Salt-marsh response to a severe extratropical storm, March 1993, west-central Florida". *Geology* 23.8, pp. 679–682. DOI: 10.1130/0091-7613(1995)023<0679:CSDSMR>2.3.CO;2.

Grass, Anthony J. (1970). "Initial Instability of Fine Bed Sand". *Journal of the Hydraulics Division* 96.3, pp. 619–632. DOI: 10.1061/JYCEAJ.0002369.

Green, Malcolm O. and Giovanni Coco (2007). "Sediment transport on an estuarine intertidal flat: Measurements and conceptual model of waves, rainfall and exchanges with a tidal creek". *Estuarine, Coastal and Shelf Science*. DOI: 10.1016/j.ecss.2006.11.006.

Green, Malcolm O. and Giovanni Coco (2014). "Review of wave-driven sediment resuspension and transport in estuaries". *Reviews of Geophysics* 52.1, pp. 77–117. DOI: 10.1002/2013RG000437.

Green, Malcolm O., Kerry P. Black, and Carl L. Amos (1997). "Control of estuarine sediment dynamics by interactions between currents and waves at several scales". *Marine Geology* 144.1-3, pp. 97–116. DOI: 10.1016/S0025-3227(97)00065-0.

Green, Malcolm O. (2011). "Very small waves and associated sediment resuspension on an estuarine intertidal flat". *Estuarine, Coastal and Shelf Science* 93.4, pp. 449–459. DOI: 10.1016/j.ecss.2011.05.021.

Haas, T. de, H. J. Pierik, A. J. F. F van der Spek, K. M. Cohen, B. van Maanen, and Maarten G. Kleinhans (2018). "Holocene evolution of tidal systems in The Netherlands: Effects of rivers, coastal boundary conditions, eco-engineering species, inherited relief and human interference". *Earth-Science Reviews* 177.September 2017, pp. 139–163. DOI: 10.1016/j.earscirev.2017.10.006.

Hasselmann, Klaus F., Tim P. Barnett, E. Bouws, H. Carlson, David E. Cartwright, K. Eake, J. A. Euring, A. Gicnapp, D. E. Hasselmann, and P. Kruseman (1973). "Measurements of wind-wave growth and swell decay during the Joint North Sea Wave Project (JONSWAP)." *Ergaenzungsheft zur Deutschen Hydrographischen Zeitschrift, Reihe A*.

Holthuijsen, L. H., N. Booij, and T. H. C. Herbers (1989). "A prediction model for stationary, short-crested waves in shallow water with ambient currents". *Coastal Engineering* 13.1, pp. 23–54. DOI: https://doi.org/10.1016/0378-3839(89)90031-8.

Hu, Zhan, Peng Yao, Daphne van der Wal, and Tjeerd J. Bouma (2017). "Patterns and drivers of daily bed-level dynamics on two tidal flats with contrasting wave exposure". *Scientific Reports* 7.1, p. 7088. DOI: 10.1038/s41598-017-07515-y.

Hughes, Zoe J. (2012). "Tidal Channels on Tidal Flats and Marshes". In: *Principles of Tidal Sedimentology*. Ed. by R.A. Davis and R.W. Dalrymple. Chap. 11, pp. 1–621. DOI: 10.1007/978-94-007-0123-6.

Jones, Clive G., John H. Lawton, and Moshe Shachak (1994). "Organisms as Ecosystem Engineers". *Oikos* 69.3, p. 373. DOI: 10.2307/3545850.

Kirwan, Matthew L. and A. Brad Murray (2007). "A coupled geomorphic and ecological model of tidal marsh evolution". *Proceedings of the National Academy of Sciences of the United States of America* 104.15, pp. 6118–6122. DOI: 10.1073/pnas.0700958104.

Kirwan, Matthew L., Glenn R. Guntenspergen, Andrea D'Alpaos, James T. Morris, Simon M. Mudd, and Stijn Temmerman (2010). "Limits on the adaptability of coastal marshes to rising sea level". *Geophysical Research Letters* 37.23, pp. 1–5. DOI: 10.1029/2010GL045489.

Kirwan, Matthew L., A. Brad Murray, Jeffrey P. Donnelly, and D. Reide Corbett (2011). "Rapid wetland expansion during European settlement and its implication for marsh survival under modern sediment delivery rates". *Geology* 39.5, pp. 507–510. DOI: 10.1130/G31789.1.

Kirwan, Matthew L. and Simon M. Mudd (2012). "Response of salt-marsh carbon accumulation to climate change". *Nature* 489.7417, pp. 550–553. DOI: 10.1038/nature11440.

Kirwan, Matthew L. and J. Patrick Megonigal (2013). "Tidal wetland stability in the face of human impacts and sea-level rise". *Nature* 504.7478, pp. 53–60. DOI: 10.1038/nature12856.

Kirezci, Ebru, Ian R. Young, Roshanka Ranasinghe, Sanne Muis, Robert J. Nicholls, Daniel Lincke, and Jochen Hinkel (2020). "Projections of global-scale extreme sea levels and resulting episodic coastal flooding over the 21st Century". *Scientific Reports* 10.1, pp. 1–12. DOI: 10.1038/s41598-020-67736-6.

Kulp, Scott A. and Benjamin H. Strauss (2019). "New elevation data triple estimates of global vulnerability to sea-level rise and coastal flooding". *Nature Communications* 10.1, p. 4844. DOI: 10.1038/s41467-019-12808-z.

Lacy, Jessica R., Madeline R. Foster-Martinez, Rachel M. Allen, Matthew C. Ferner, and John C. Callaway (2020). "Seasonal Variation in Sediment Delivery Across the Bay-Marsh Interface of an Estuarine Salt Marsh".

*Journal of Geophysical Research: Oceans* 125.1, pp. 1–21. DOI: 10.1029/2019JC015268.

Lawson, S. E., Patricia L. Wiberg, Karen J. McGlathery, and D. C. Fugate (2007). “Wind-driven sediment suspension controls light availability in a shallow coastal lagoon”. *Estuaries and Coasts* 30.1, pp. 102–112. DOI: 10.1007/BF02782971.

Le Hir, P., W. Roberts, O. Cazaillet, M.C. Christie, P. Bassoullet, and C. Bacher (2000). “Characterization of intertidal flat hydrodynamics”. *Continental Shelf Research* 20.12-13, pp. 1433–1459. DOI: 10.1016/S0278-4343(00)00031-5.

Le Hir, P., Y. Monbet, and F. Orvain (2007). “Sediment erodability in sediment transport modelling: Can we account for biota effects?” *Continental Shelf Research* 27.8, pp. 1116–1142. DOI: 10.1016/j.csr.2005.11.016.

Lee, Hee J., Hyung R. Jo, Yong S. Chu, and Kyung S. Bahk (2004). “Sediment transport on macrotidal flats in Garolim Bay, west coast of Korea: significance of wind waves and asymmetry of tidal currents”. *Continental Shelf Research* 24.7-8, pp. 821–832. DOI: 10.1016/j.csr.2004.01.005.

Leonardi, Nicoletta, Neil Kamal Ganju, and Sergio Fagherazzi (2016). “A linear relationship between wave power and erosion determines salt-marsh resilience to violent storms and hurricanes”. *Proceedings of the National Academy of Sciences of the United States of America* 113.1, pp. 64–68. DOI: 10.1073/pnas.1510095112.

Leonardi, Nicoletta, Iacopo Carnacina, Carmine Donatelli, Neil Kamal Ganju, Andrew James Plater, Mark Schuerch, and Stijn Temmerman (2018). “Dynamic interactions between coastal storms and salt marshes: A review”. *Geomorphology* 301, pp. 92–107. DOI: 10.1016/j.geomorph.2017.11.001.

Leonard, Lynn A. and Mark E. Luther (1995). "Flow hydrodynamics in tidal marsh canopies". *Limnology and Oceanography* 40.8, pp. 1474–1484. DOI: 10.4319/lo.1995.40.8.1474.

MacKenzie, R. A. and M. Dionne (2008). "Habitat heterogeneity: importance of salt marsh pools and high marsh surfaces to fish production in two Gulf of Maine salt marshes". *Marine Ecology Progress Series* 368, pp. 217–230. DOI: 10.3354/meps07560.

Maciel, Fernanda P., Pablo E. Santoro, and Francisco Pedocchi (2021). "Spatio-temporal dynamics of the Río de la Plata turbidity front; combining remote sensing with in-situ measurements and numerical modeling". *Continental Shelf Research* 213, p. 104301. DOI: https://doi.org/10.1016/j.csr.2020.104301.

Marani, Marco, Enrica Belluco, Andrea D'Alpaos, Andrea Defina, Stefano Lanzoni, and Andrea Rinaldo (2003). "On the drainage density of tidal networks". *Water Resources Research* 39.2, pp. 1–11. DOI: 10.1029/2001WR001051.

Martini, Paolo, Luca Carniello, and C. Avanzi (2004). "Two dimensional modelling of flood flows and suspended sedimenttransport: the case of the Brenta River, Veneto (Italy)". *Natural Hazards and Earth System Sciences* 4.1, pp. 165–181. DOI: 10.5194/nhess-4-165-2004.

Marani, Marco, Andrea D'Alpaos, Stefano Lanzoni, Luca Carniello, and Andrea Rinaldo (2007). "Biologically-controlled multiple equilibria of tidal landforms and the fate of the Venice lagoon". *Geophysical Research Letters* 34.11, pp. 1–5. DOI: 10.1029/2007GL030178.

Marani, Marco, Andrea D'Alpaos, Stefano Lanzoni, Luca Carniello, and Andrea Rinaldo (2010). "The importance of being coupled: Stable states and catastrophic shifts in tidal biomorphodynamics". *Journal of Geophysical Research: Earth Surface* 115.4, pp. 1–15. DOI: 10.1029/2009JF001600.

Mariotti, Giulio and Sergio Fagherazzi (2010). "A numerical model for the coupled long-term evolution of salt marshes and tidal flats". *Journal of Geophysical Research: Earth Surface* 115.F1. DOI: 10.1029/2009JF001326.

Mariotti, Giulio, Sergio Fagherazzi, Patricia L. Wiberg, Karen J. McGlathery, Luca Carniello, and Andrea Defina (2010a). "Influence of storm surges and sea level on shallow tidal basin erosive processes". *Journal of Geophysical Research: Oceans* 115.C11, p. C11012. DOI: 10.1029/2009JC005892.

Mariotti, Giulio, Sergio Fagherazzi, Patricia L. Wiberg, Karen J. McGlathery, Luca Carniello, and Andrea Defina (2010b). "Influence of storm surges and sea level on shallow tidal basin erosive processes". *Journal of Geophysical Research* 115.C11, p. C11012. DOI: 10.1029/2009JC005892.

Marani, Marco, Andrea D'Alpaos, Stefano Lanzoni, and M. Santalucia (2011). "Understanding and predicting wave erosion of marsh edges". *Geophysical Research Letters* 38.21. DOI: 10.1029/2011GL048995.

Mariotti, Giulio and Sergio Fagherazzi (2012). "Modeling the effect of tides and waves on benthic biofilms". *Journal of Geophysical Research: Biogeosciences* 117.G4. DOI: 10.1029/2012JG002064.

Marani, Marco, Cristina Da Lio, and Andrea D'Alpaos (2013). "Vegetation engineers marsh morphology through multiple competing stable states". *Proceedings of the National Academy of Sciences*. DOI: 10.1073/pnas.1218327 110.

Mariotti, Giulio and Sergio Fagherazzi (2013). "Wind waves on a mudflat: The influence of fetch and depth on bed shear stresses". *Continental Shelf Research* 60, S99–S110. DOI: 10.1016/j.csr.2012.03.001.

Mariotti, Giulio and Joel A. Carr (2014). "Dual role of salt marsh retreat: Long-term loss and short-term resilience". *Water Resources Research* 50.4, pp. 2963–2974. DOI: 10.1002/2013WR014676.

Masselink, Gerd, Michael Hughes, and Jasper Knight (2014). *Introduction to Coastal Processes and Geomorphology*. Routledge. DOI: 10.4324/9780203785461.

Mcleod, Elizabeth, Gail L. Chmura, Steven Bouillon, Rodney Salm, Mats Björk, Carlos M. Duarte, Catherine E. Lovelock, William H. Schlesinger, and Brian R. Silliman (2011). "A blueprint for blue carbon: toward an improved understanding of the role of vegetated coastal habitats in sequestering CO 2". *Frontiers in Ecology and the Environment* 9.10, pp. 552–560. DOI: 10.1890/110004.

Mcowen, Chris, Lauren Weatherdon, Jan-Willem Bochove, Emma Sullivan, Simon Blyth, Christoph Zockler, Damon Stanwell-Smith, Naomi Kingston, Corinne Martin, Mark Spalding, and Steven Fletcher (2017). "A global map of saltmarshes". *Biodiversity Data Journal* 5, e11764. DOI: 10.3897/BDJ.5.e11764.

McSweeney, Jacqueline M., Robert J. Chant, John L. Wilkin, and Christopher K. Sommerfield (2017). "Suspended-Sediment Impacts on Light-Limited Productivity in the Delaware Estuary". *Estuaries and Coasts* 40.4, pp. 977–993. DOI: 10.1007/s12237-016-0200-3.

Mehta, A.J., Earl J. Hayter, W. Reginald Parker, Ray B. Krone, and Allen M. Teeter (1989). "Cohesive sediment transport. I: Process description". *Journal of Hydraulic Engineering* 115.8, pp. 1076–1093.

Meier, Dirk (2004). "Man and environment in the marsh area of Schleswig – Holstein from Roman until late Medieval times". *Quaternary International* 112.1, pp. 55–69. DOI: 10.1016/S1040-6182(03)00065-X.

Mel, Riccardo A., Luca Carniello, and Luigi D'Alpaos (2019). "Addressing the effect of the Mo.S.E. barriers closure on wind setup within the Venice lagoon". *Estuarine, Coastal and Shelf Science* 225, p. 106249. DOI: https://doi.org/10.1016/j.ecss.2019.106249.

Mel, Riccardo A., Luca Carniello, and Luigi D'Alpaos (2021a). "How long the Mo.S.E. barriers will be effective in protecting all the urban settlements in the Venice lagoon? The wind setup constraint". *Coastal Engineering* 168.January, p. 103923. DOI: 10.1016/j.coastaleng.2021.103923.

Mel, Riccardo A., Daniele Pietro Viero, Luca Carniello, Andrea Defina, and Luigi D'Alpaos (2021b). "The first operations of Mo.S.E. system to prevent the flooding of Venice: Insights on the hydrodynamics of a regulated lagoon". *Estuarine, Coastal and Shelf Science* 261.August, p. 107547. DOI: 10.1016/j.ecss.2021.107547.

Miller, Richard L. and Brent A. McKee (2004). "Using MODIS Terra 250 m imagery to map concentrations of total suspended matter in coastal waters". *Remote Sensing of Environment* 93.1, pp. 259–266. DOI: https://doi.org/10.1016/j.rse.2004.07.012.

Mitsch, W. J. and J. G. Gosselink (2015). *Wetlands*. John Wiley & Sons, Ltd, p. 752.

Molinaroli, Emanuela, Stefano Guerzoni, Alessandro Sarretta, Mauro Masiol, and Mario Pistolato (2009). "Thirty-year changes (1970 to 2000) in bathymetry and sediment texture recorded in the Lagoon of Venice sub-basins, Italy". *Marine Geology* 258.1, pp. 115–125. DOI: https://doi.org/10.1016/j.margeo.2008.12.001.

Möller, Iris, Matthias Kudella, Franziska Rupprecht, Thomas Spencer, Maike Paul, Bregje K. van Wesenbeeck, Guido Wolters, Kai Jensen, Tjeerd J. Bouma, Martin Miranda-Lange, and Stefan Schimmels (2014). "Wave attenuation over coastal salt marshes under storm surge conditions". *Nature Geoscience* 7.10, pp. 727–731. DOI: 10.1038/ngeo2251.

Möller, Iris, Tom Spencer, Mike Best, William Austin, and Annette Burden (2021). "Saltmarsh Restoration: An introduction". In: *Saltmarsh Restoration Handbook: UK and Ireland*. Ed. by R. Hudson, J. Kenworthy, and M. Best. Bristol, UK: Environment Agency, pp. 1–16.

Möller, Iris, Tom Spencer, and J. R. French (1996). "Wind wave attenuation over saltmarsh surfaces: Preliminary results from Norfolk, England". *Journal of Coastal Research* 12.4, pp. 1009–1016.

Möller, Iris, Thomas Spencer, Jonathan R. French, D. J. Leggett, and M. Dixon (1999). "Wave transformation over salt marshes: A field and numerical modelling study from north Norfolk, England". *Estuarine, Coastal and Shelf Science*. DOI: 10.1006/ecss.1999.0509.

Moore, Kenneth A. and Richard L. Wetzel (2000). "Seasonal variations in eelgrass (Zostera marina L.) responses to nutrient enrichment and reduced light availability in experimental ecosystems". *Journal of Experimental Marine Biology and Ecology* 244.1, pp. 1–28. DOI: https://doi.org/10.1016/S0022-0981(99)00135-5.

Mooyaart, L. F. and S. N. Jonkman (2017). "Overview and Design Considerations of Storm Surge Barriers". *Journal of Waterway, Port, Coastal, and Ocean Engineering* 143.4, p. 06017001. DOI: 10.1061/(ASCE)WW.1943-5460.0000383.

Morris, James T., P. V. Sundareshwar, Christopher T. Nietch, Björn Kjerfve, and Donald R. Cahoon (2002). "Responses of coastal wetlands to rising sea level". *Ecology* 83.10, pp. 2869–2877. DOI: 10.1890/0012-9658(2002)083[2869:ROCWTR]2.0.CO;2.

Morris, James T., Donald .C Barber, John C. Callaway, Randy Chambers, Scott C. Hagen, Charles S. Hopkinson, Beverly J. Johnson, Patrick Megonigal, Scott C. Neubauer, Tiffany Troxler, and Cathleen Wigand (2016). "Contributions of organic and inorganic matter to sediment volume and accretion in tidal wetlands at steady state". *Earth's Future* 4.4, pp. 110–121. DOI: 10.1002/2015EF000334.

Murray, A. Brad (2007). "Reducing model complexity for explanation and prediction". *Geomorphology* 90.3-4, pp. 178–191. DOI: 10.1016/j.geomorph.2006.10.020.

Nepf, Heidi M. (1999). "Drag, turbulence, and diffusion in flow through emergent vegetation". *Water Resources Research* 35.2, pp. 479–489. DOI: 10.1029/1998WR900069.

Newton, Alice et al. (2018). "Assessing, quantifying and valuing the ecosystem services of coastal lagoons". *Journal for Nature Conservation* 44.March 2017, pp. 50–65. DOI: 10.1016/j.jnc.2018.02.009.

Nicholls, Robert J., P. P. Wong, V. R. Burkett, J. O. Codignotto, J. E. Hay, R. F. McLean, S. Ragoonaden, and Colin D. Woodroffe (2007). "Coastal systems and low-lying areas." In: *Climate Change 2007: Impacts, Adaptation and Vulnerability. Contribution of Working Group II to the Fourth Assessment Report of the Intergovernmental Panel on Climate Change*. Ed. by M. L. Parry, O. F. Canziani, J. P. Palutikof, P. J. van der Linden, and C. E. Hanson. Cambridge University Press, pp. 315–356.

Nicholls, Robert J., Daniel Lincke, Jochen Hinkel, Sally Brown, Athanasios T. Vafeidis, Benoit Meyssignac, Susan E. Hanson, Jan-Ludolf Merkens, and Jiayi Fang (2021). "A global analysis of subsidence, relative sea-level change and coastal flood exposure". *Nature Climate Change* 11.4, pp. 338–342. DOI: 10.1038/s41558-021-00993-z.

Nichols, Maynard M. and John D. Boon (1994). "Sediment Transport Processes in Coastal Lagoons". In: *Coastal Lagoon Processes*. Ed. by Björn Kjerfve. Vol. 60. C. Chap. 7, pp. 157–219. DOI: 10.1016/S0422-9894(08)70012-6.

Nolte, S., E. C. Koppenaal, P. Esselink, K. S. Dijkema, Mark Schuerch, A. V. De Groot, J. P. Bakker, and Stijn Temmerman (2013). "Measuring sedimentation in tidal marshes: A review on methods and their applicability in biogeomorphological studies". *Journal of Coastal Conservation* 17.3, pp. 301–325. DOI: 10.1007/s11852-013-0238-3.

Oenema, Oene and Ronald D. DeLaune (1988). "Accretion rates in salt marshes in the Eastern Scheldt, South-west Netherlands". *Estuarine,* *Coastal and Shelf Science* 26.4, pp. 379–394. DOI: 10.1016/0272-7714(88)90019-4.

Oppenheimer, M., B.C. Glavovic, J. Hinkel, R. van de Wal, A.K. Magnan, A. Abd-Elgawad, R. Cai, M. CifuentesJara, R.M. DeConto, T. Ghosh, J. Hay, F. Isla, B. Marzeion, B. Meyssignac, and Z. Sebesvari (2019). "Sea Level Rise and Implications for Low-Lying Islands, Coasts and Communities". In: *IPCC Special Report on the Ocean and Cryosphere in a Changing Climate*.

Orton, Philip, Sarah Fernald, Kristin Marcell, Bennett Brooks, Bram Van Prooijen, and Ziyu Chen (2019). *Surge Barrier Environmental Effects and Empirical Experience Workshop Report*. Tech. rep., p. 31.

Ouillon, S., P. Douillet, and S. Andréfouët (2004). "Coupling satellite data with in situ measurements and numerical modeling to study fine suspended sediment transport: a study for the lagoon of New Caledonia". *Coral Reefs* 23.1, pp. 109–122. DOI: 10.1007/s00338-003-0352-z.

Park, Jeryang, Gianluca Botter, James W. Jawitz, and P. Suresh C. Rao (2014). "Stochastic modeling of hydrologic variability of geographically isolated wetlands: Effects of hydro-climatic forcing and wetland bathymetry". *Advances in Water Resources*. DOI: 10.1016/j.advwatres.2014.03.007.

Parsons, Daniel R., Robert J. Schindler, Julie A. Hope, Jonathan Malarkey, Jaco H. Baas, Jeffrey Peakall, Andrew J. Manning, Leiping Ye, Steve Simmons, David M. Paterson, Rebecca J. Aspden, Sarah J. Bass, Alan G. Davies, Ian D. Lichtman, and Peter D. Thorne (2016). "The role of biophysical cohesion on subaqueous bed form size". *Geophysical Research Letters* 43.4, pp. 1566–1573. DOI: 10.1002/2016GL067667.

Parker, G., M. Garcia, Y. Fukushima, and W. Yu (1987). "Experiments on turbidity currents over an erodible bed". *Journal of Hydraulic Research* 25.1, pp. 123–147. DOI: 10.1080/00221688709499292.

Peteet, Dorothy M., Jonathan Nichols, Timothy Kenna, Clara Chang, James Browne, Mohammad Reza, Stephen Kovari, Louisa Liberman, and Stephanie

Stern-Protz (2018). "Sediment starvation destroys New York City marshes' resistance to sea level rise". *Proceedings of the National Academy of Sciences of the United States of America* 115.41, pp. 10281–10286. DOI: 10.1073/pnas.1715392115.

Pethick, J. S. (1974). "The Distribution of Salt Pans on Tidal Salt Marshes". *Journal of Biogeography* 1.1, p. 57. DOI: 10.2307/3038068.

Pethick, J. S. (1981). "Long-term Accretion Rates on Tidal Salt Marshes". *SEPM Journal of Sedimentary Research* Vol. 51.2, pp. 571–577. DOI: 10.1306/212F7CDE-2B24-11D7-8648000102C1865D.

Pinder, David A and Michael E Witherick (1990). "Port industrialization, urbanization and wetland loss". In: *Wetlands: A Threatened Landscape*. Ed. by Michael Williams. Oxford, United Kingdom: Wiley-Blackwell, pp. 235–266.

Pivato, Mattia, Luca Carniello, Isabella Moro, and Paolo D'Odorico (2019). "On the feedback between water turbidity and microphytobenthos growth in shallow tidal environments". *Earth Surface Processes and Landforms* 44.5, pp. 1192–1206. DOI: 10.1002/esp.4567.

Ralston, David K. and Mark T. Stacey (2007). "Tidal and meteorological forcing of sediment transport in tributary mudflat channels". *Continental Shelf Research* 27.10-11, pp. 1510–1527. DOI: 10.1016/j.csr.2007.01.010.

Reed, Denise J., Thomas Spencer, Anne L. Murray, Jonathan R. French, and Lynn A. Leonard (1999). "Marsh surface sediment deposition and the role of tidal creeks: Implications for created and managed coastal marshes". *Journal of Coastal Conservation* 5.1, pp. 81–90. DOI: 10.1007/BF02802742.

Reed, Denise J. (1988). "Sediment dynamics and deposition in a retreating coastal salt marsh". *Estuarine, Coastal and Shelf Science* 26.1, pp. 67–79. DOI: 10.1016/0272-7714(88)90012-1.

Reed, Denise J. (1989). "Patterns of sediment deposition in subsiding coastal salt marshes, Terrebonne Bay, Louisiana: The role of winter storms". *Estuaries* 12.4, pp. 222–227. DOI: 10.2307/1351901.

Reed, Denise J. (1995). "The response of coastal marshes to sea-level rise: Survival or submergence?" *Earth Surface Processes and Landforms* 20.1, pp. 39–48. DOI: 10.1002/esp.3290200105.

Rodríguez, José F., Patricia M Saco, Steven G Sandi, Neil Saintilan, and Gerardo Riccardi (2017). "Potential increase in coastal wetland vulnerability to sea-level rise suggested by considering hydrodynamic attenuation effects". *Nature Communications* 8.1, p. 16094. DOI: 10.1038/ncomms16094.

Rodriguez-Iturbe, I., D. R. Cox, and V. Isham (1987). "Some models for rainfall based on stochastic point processes". *Proceedings of the Royal Society of London. A. Mathematical and Physical Sciences* 410.1839, pp. 269–288. DOI: 10.1098/rspa.1987.0039.

Rogers, Kerrylee and Colin D. Woodroffe (2015). "Tidal Flats and Salt Marshes". In: *Coastal Environments and Global Change*. Wiley Online Books. Chichester, UK: John Wiley & Sons, Ltd, pp. 227–250. DOI: 10.1002/9781119117261.ch10.

Roner, Marcella, Andrea D'Alpaos, Massimiliano Ghinassi, Marco Marani, Sonia Silvestri, Erica Franceschinis, and Nicola Realdon (2016). "Spatial variation of salt-marsh organic and inorganic deposition and organic carbon accumulation: Inferences from the Venice lagoon, Italy". *Advances in Water Resources*. DOI: 10.1016/j.advwatres.2015.11.011.

Roner, Marcella, Massimiliano Ghinassi, Mariaelena Fedi, Lucia Liccioli, Luca Giorgio Bellucci, Lara Brivio, and Andrea D'Alpaos (2017). "Latest Holocene depositional history of the southern Venice Lagoon, Italy". *The Holocene* 27.11, pp. 1731–1744. DOI: 10.1177/0959683617708450.

Ruhl, C. A., D. H. Schoellhamer, Richard P. Stumpf, and C. L. Lindsay (2001). "Combined Use of Remote Sensing and Continuous Monitoring to Analyse the Variability of Suspended-Sediment Concentrations in San Francisco Bay, California". *Estuarine, Coastal and Shelf Science* 53.6, pp. 801–812. DOI: 10.1006/ecss.2000.0730.

Sandi, Steven G., José F. Rodríguez, Neil Saintilan, Gerardo Riccardi, and Patricia M. Saco (2018). "Rising tides, rising gates: The complex ecogeomorphic response of coastal wetlands to sea-level rise and human interventions". *Advances in Water Resources* 114, pp. 135–148. DOI: https://doi.org/10.1016/j.advwatres.2018.02.006.

Sanford, Lawrence P. (1994). "Wave-Forced Resuspension of Upper Chesapeake Bay Muds". *Estuaries* 17.1, p. 148. DOI: 10.2307/1352564.

Sarretta, A., S. Pillon, E. Molinaroli, Stefano Guerzoni, and G. Fontolan (2010). "Sediment budget in the Lagoon of Venice, Italy". *Continental Shelf Research* 30.8, pp. 934–949. DOI: 10.1016/j.csr.2009.07.002.

Schuerch, Mark, Thomas Spencer, Stijn Temmerman, Matthew L. Kirwan, Claudia Wolff, Daniel Lincke, Chris J. McOwen, Mark D. Pickering, Ruth Reef, Athanasios T. Vafeidis, Jochen Hinkel, Robert J. Nicholls, and Sally Brown (2018). "Future response of global coastal wetlands to sea-level rise". *Nature* 561.7722, pp. 231–234. DOI: 10.1038/s41586-018-0476-5.

Schuerch, Mark, Thomas Spencer, and Ben R. Evans (2019). "Coupling between tidal mudflats and salt marshes affects marsh morphology". *Marine Geology* 412.November 2018, pp. 95–106. DOI: 10.1016/j.margeo.2019.03.008.

Schlesinger, William H. and Emily S. Bernhardt (2020). *Biogeochemistry*. Elsevier, p. 749. DOI: 10.1016/C2017-0-00311-7.

Schwimmer, Reed A. (2001). *Rates and Processes of Marsh Shoreline Erosion in Rehoboth Bay, Delaware, U.S.A.* Tech. rep., pp. 672–683.

Silvestri, Sonia, Andrea D'Alpaos, Giovanna Nordio, and Luca Carniello (2018). "Anthropogenic Modifications Can Significantly Influence the Local Mean Sea Level and Affect the Survival of Salt Marshes in Shallow Tidal Systems". *Journal of Geophysical Research: Earth Surface* 123.5, pp. 996–1012. DOI: 10.1029/2017JF004503.

Smagorinsky, J. (1963). "General circulation experiments with the primitive equations: I. the basic experiment". *Monthly Weather Review* 91.3, pp. 99–164. DOI: 10.1175/1520-0493(1963)091<0099:GCEWTP>2.3.CO;2.

Soulsby, R. L. (1995). "Bed shear-stresses due to combined waves and currents". In: *Advances in Coastal Morphodynamics*. Ed. by M. J. F. Stive. Delft Hydraul., Delft, Netherlands, pp. 420–423.

Soulsby, R. L. (1997). *Dynamics of Marine Sands: A Manual for Practical Applications*. Thomas Telford, London.

Spalding, Mark D., Anna L. McIvor, Michael W. Beck, Evamaria W. Koch, Iris Möller, Denise J. Reed, Pamela Rubinoff, Tom Spencer, Trevor J. Tolhurst, Ty V. Wamsley, Bregje K. Wesenbeeck, Eric Wolanski, and Colin D. Woodroffe (2014). "Coastal Ecosystems: A Critical Element of Risk Reduction". *Conservation Letters* 7.3, pp. 293–301. DOI: 10.1111/conl.12074.

Stefanon, Luana, Luca Carniello, Andrea D'Alpaos, and Andrea Rinaldo (2012). "Signatures of sea level changes on tidal geomorphology: Experiments on network incision and retreat". *Geophysical Research Letters*. DOI: 10.1029/2012GL051953.

Stumpf, Richard P. (1983). "The process of sedimentation on the surface of a salt marsh". *Estuarine, Coastal and Shelf Science* 17.5, pp. 495–508. DOI: 10.1016/0272-7714(83)90002-1.

Syvitski, James P. M., Charles J. Vörösmarty, Albert J. Kettner, and Pamela Green (2005). "Impact of Humans on the Flux of Terrestrial Sediment to the Global Coastal Ocean". *Science* 308.5720, pp. 376–380. DOI: 10.1126/science.1109454.

Syvitski, James P. M., Albert J. Kettner, Irina Overeem, Eric W. H. Hutton, Mark T. Hannon, G Robert Brakenridge, John Day, Charles Vörösmarty, Yoshiki Saito, Liviu Giosan, and Robert J. Nicholls (2009). "Sinking deltas due to human activities". *Nature Geoscience* 2.10, pp. 681–686. DOI: 10.1038/ngeo629.

Tambroni, N., J. Figueiredo da Silva, R. W. Duck, S. J. McLelland, Chiara Venier, and Stefano Lanzoni (2016). "Experimental investigation of the impact of macroalgal mats on the wave and current dynamics". *Advances in Water Resources* 93, pp. 326–335. DOI: 10.1016/j.advwatres.2015.09.010.

Temmerman, Stijn, G. Govers, S. Wartel, and Patrick Meire (2003). "Spatial and temporal factors controlling short-term sedimentation in a salt and freshwater tidal marsh, Scheldt estuary, Belgium, SW Netherlands". *Earth Surface Processes and Landforms* 28.7, pp. 739–755. DOI: 10.1002/esp.495.

Temmerman, Stijn, Tjeerd J. Bouma, G. Govers, and D. Lauwaet (2005a). "Flow paths of water and sediment in a tidal marsh: Relations with marsh developmental stage and tidal inundation height". *Estuaries* 28.3, pp. 338–352. DOI: 10.1007/BF02693917.

Temmerman, Stijn, Tjeerd J. Bouma, G. Govers, Zheng Bing Wang, Mindert B. de Vries, and Peter M.J. Herman (2005b). "Impact of vegetation on flow routing and sedimentation patterns: Three-dimensional modeling for a tidal marsh". *Journal of Geophysical Research: Earth Surface* 110.F4. DOI: 10.1029/2005JF000301.

Temmerman, Stijn, Tjeerd J. Bouma, Johan Van De Koppel, Daphne van der Wal, Mindert B. de Vries, and Peter M. J. Herman (2007). "Vegetation causes channel erosion in a tidal landscape". *Geology* 35.7, pp. 631–634. DOI: 10.1130/G23502A.1.

Temmerman, Stijn, Patrick Meire, Tjeerd J. Bouma, Peter M.J. Herman, Tom Ysebaert, and Huib J. De Vriend (2013). "Ecosystem-based coastal defence in the face of global change". *Nature* 504.7478, pp. 79–83. DOI: 10.1038/nature12859.

Temmerman, Stijn and Matthew L. Kirwan (2015). "Building land with a rising sea". *Science* 349.6248, pp. 588–589. DOI: 10.1126/science.aac8312.

Thomas, Séverine and Peter V. Ridd (2004). "Review of methods to measure short time scale sediment accumulation". *Marine Geology* 207.1-4, pp. 95–114. DOI: 10.1016/j.margeo.2004.03.011.

Tinoco, Rafael O. and Giovanni Coco (2016). "A laboratory study on sediment resuspension within arrays of rigid cylinders". *Advances in Water Resources* 92, pp. 1–9. DOI: 10.1016/j.advwatres.2016.04.003.

Tognin, Davide, Andrea D'Alpaos, Marco Marani, and Luca Carniello (2021). "Marsh resilience to sea-level rise reduced by storm-surge barriers in the Venice Lagoon". *Nature Geoscience*. DOI: 10.1038/s41561-021-00853-7.

Tommasini, Laura, Andrea D'Alpaos, Luca Carniello, Luigi D'Alpaos, and Andrea Rinaldo (2017). "Ricostruzione morfologica della Laguna di Venezia ai tempi dell'Alberti (1611)". In: *La laguna di Venezia e le nuove opere alle bocche*.

Tommasini, Laura, Luca Carniello, Massimiliano Ghinassi, Marcella Roner, and Andrea D'Alpaos (2019). "Changes in the wind-wave field and related salt-marsh lateral erosion: inferences from the evolution of the Venice Lagoon in the last four centuries". *Earth Surface Processes and Landforms* 44.8, pp. 1633–1646. DOI: doi:10.1002/esp.4599.

Tweel, Andrew W. and R. Eugene Turner (2014). "Contribution of tropical cyclones to the sediment budget for coastal wetlands in Louisiana, USA". *Landscape Ecology* 29.6, pp. 1083–1094. DOI: 10.1007/s10980-014-0047-6.

Umgiesser, G., M. Sclavo, S. Carniel, and A. Bergamasco (2004). "Exploring the bottom stress variability in the Venice Lagoon". *Journal of Marine Systems*. DOI: 10.1016/j.jmarsys.2004.05.023.

Valiela, Ivan (2009). *Global coastal change*. Oxford: John Wiley & Sons, p. 376.

van Ledden, Mathijs, Zheng Bing Wang, Han Winterwerp, and Huib J. De Vriend (2004). "Sand-mud morphodynamics in a short tidal basin". In: *Ocean Dynamics*. DOI: 10.1007/s10236-003-0050-y.

van Rijn, Leo C. (1984). "Sediment transport, part II: suspended load transport". *Journal of hydraulic engineering* 110.11, pp. 1613–1641.

Venier, Chiara, Andrea D'Alpaos, and Marco Marani (2014). "Evaluation of sediment properties using wind and turbidity observations in the shallow tidal areas of the Venice Lagoon". *Journal of Geophysical Research: Earth Surface*. DOI: 10.1002/2013JF003019.

Viero, Daniele Pietro and Andrea Defina (2016). "Water age, exposure time, and local flushing time in semi-enclosed, tidal basins with negligible freshwater inflow". *Journal of Marine Systems* 156, pp. 16–29. DOI: 10.1016/j.jmarsys.2015.11.006.

Visser, André W. (1997). "Using random walk models to simulate the vertical distribution of particles in a turbulent water column". *Marine Ecology Progress Series* 158, pp. 275–281. DOI: 10.3354/meps158275.

Volpe, V., Sonia Silvestri, and Marco Marani (2011). "Remote sensing retrieval of suspended sediment concentration in shallow waters". *Remote Sensing of Environment* 115.1, pp. 44–54. DOI: 10.1016/j.rse.2010.07.013.

Vousdoukas, Michalis I., Lorenzo Mentaschi, Jochen Hinkel, Philip J. Ward, Ignazio Mongelli, Juan-Carlos Ciscar, and Luc Feyen (2020). "Economic motivation for raising coastal flood defenses in Europe". *Nature Communications* 11.1, p. 2119. DOI: 10.1038/s41467-020-15665-3.

Vu, Huy D., Kazimierz Więski, and Steven C. Pennings (2017). "Ecosystem engineers drive creek formation in salt marshes". *Ecology* 98.1, pp. 162–174. DOI: 10.1002/ecy.1628.

Wang, Ping (2012). "Principles of Sediment Transport Applicable in Tidal Environments". In: *Principles of Tidal Sedimentology*. Ed. by Richard A.

Davis and Robert W. Dalrymple. Vol. c. Dordrecht: Springer Netherlands, pp. 1–621. DOI: 10.1007/978-94-007-0123-6.

Wells, John T., Charles E. Adams, Yong-Ahn Park, and Eben W. Frankenberg (1990). “Morphology, sedimentology and tidal channel processes on a high-tide-range mudflat, west coast of South Korea”. *Marine Geology* 95.2, pp. 111–130. DOI: 10.1016/0025-3227(90)90044-K.

Widdows, John and Mary Brinsley (2002). “Impact of biotic and abiotic processes on sediment dynamics and the consequences to the structure and functioning of the intertidal zone”. *Journal of Sea Research* 48.2, pp. 143–156. DOI: 10.1016/S1385-1101(02)00148-X.

Williams, Michael (1990). “Agricultural impacts in temperate wetlands”. In: *Wetlands: A Threatened Landscape.* Ed. by Michael Williams. Vol. 181-216. Oxford, United Kingdom: Wiley-Blackwell.

Wolman, M. Gordon and John P. Miller (1960). “Magnitude and frequency of forces in geomorphic processes”. *The Journal of Geology* 68.1, pp. 54–74.

Woodroffe, Colin D. (2002). *Coasts*. Cambridge: Cambridge University Press. DOI: 10.1017/CBO9781316036518.

Wren, D. G., B. D. Barkdoll, R. A. Kuhnle, and R. W. Derrow (2000). “Field Techniques for Suspended-Sediment Measurement”. *Journal of Hydraulic Engineering* 126.2, pp. 97–104. DOI: 10.1061/(ASCE)0733-9429(2000)126:2(97).

Wright, L. D. and B. G. Thom (1977). “Coastal depositional landforms”. *Progress in Physical Geography: Earth and Environment* 1.3, pp. 412–459. DOI: 10.1177/030913337700100302.

Young, Ian R. and L. A. Verhagen (1996). “The growth of fetch limited waves in water of finite depth. Part 1. Total energy and peak frequency”. *Coastal Engineering*. DOI: 10.1016/S0378-3839(96)00006-3.

Zarzuelo, Carmen, Alejandro López-Ruiz, Andrea D'Alpaos, Luca Carniello, and Miguel Ortega-Sánchez (2018). "Assessing the morphodynamic response of human-altered tidal embayments". *Geomorphology*. DOI: 10.1016/j.geomorph.2018.08.014.

Zarzuelo, Carmen, Andrea D'Alpaos, Luca Carniello, Alejandro López-Ruiz, Manuel Díez-Minguito, and Miguel Ortega-Sánchez (2019). "Natural and Human-Induced Flow and Sediment Transport within Tidal Creek Networks Influenced by Ocean-Bay Tides". *Water* 11.7. DOI: 10.3390/w11071493.

Zhou, Zeng, Giovanni Coco, Ian Townend, Maitane Olabarrieta, Mick van der Wegen, Zheng Gong, Andrea D'Alpaos, Shu Gao, Bruce E. Jaffe, Guy Gelfenbaum, Qing He, Yaping Wang, Stefano Lanzoni, Zheng Bing Wang, Han Winterwerp, and Changkuan Zhang (2017). "Is "Morphodynamic Equilibrium" an oxymoron?" *Earth-Science Reviews* 165, pp. 257–267. DOI: 10.1016/j.earscirev.2016.12.002.